MONITORING AND MODELLING
THE PROPERTIES OF SOIL
AS POROUS MEDIUM

EDITED BY
WOJCIECH SKIERUCHA, RYSZARD T. WALCZAK

Centre of Excellence for Applied Physics in Sustainable Agriculture AGROPHYSICS

Institute of Agrophysics Polish Academy of Sciences

EU 5th Framework Program QLAM-2001-00428

Monitoring and Modelling the Properties of Soil as Porous Medium

EDITORS:
Wojciech Skierucha
Ryszard Walczak

Lublin 2005

PREFACE

The monograph contains 23 publications about different scientific aspects of porous media. The majority of the papers were presented in the International Conference: "Monitoring and Modelling the Properties of Soil as Porous Medium: The Role of Soil Use" that took place in the Centre of Excellence for Applied Physics in Sustainable Agriculture AGROPHYSICS (contract No. QLAM-2001-00428) located in the Institute of Agrophysics in Lublin, Poland, during the period February 13-16, 2005.

Monitoring and modelling of natural, industrial and social objects and processes are complementary activities necessary for the decision making, *eg* defining the direction of further research, making predictions or drawing conclusions. These both elements cannot be treated separately. Monitoring is used for validation purposes and as a source of input data for the models. Modelling determines whether the trends in specific attributes can be successfully detected with monitoring and identifies key components of system behaviour that can be measured in a monitoring program.

Modelling refers to the processes or objects in artificial and limited conditions, where research tools can be successfully applied, but still close enough to the real process or object under consideration. Modelling is applied when the analyzed object is too small or too big, the process is too fast or too slow or it is impossible to conduct research because of technical or economical reasons.

Soil as a porous object and concerned processes taking place in it are particularly difficult for monitoring and modelling because of their spatial and temporal diversity, different dimensional and temporal scale of appearance. The experience, research methods and instrumentation developed in monitoring and modelling of agricultural porous media like soil, food products and granular materials can be implemented in building industry, transportation or environmental engineering. Also, the same applies to the other direction for the benefit of agricultural sciences.

The Institute of Agrophysics, Polish Academy of Sciences in Lublin has been permanently conducting investigation on development of methods and equipment for monitoring physical and chemical parameters of the soil-canopy-atmosphere system as well as hydrophysical and thermophysical processes in granular agricultural materials, like soil and food products. Our fields of interest include the theory, design, fabrication, manufacturing and application of devices for sensing and transducing physical as well as chemical phenomena. Special attention is put on sensitivity, selectivity, noise, dynamic range, interfering effects

and the development of laboratory and field measurement systems. The examples of sensor research conducted in IAPAN are:

- − development of advanced systems and sensors working Time Domain Reflectometry technique for the simultaneous measurement of water content, salinity and temperature of porous materials, especially soil,
- − adaptation of measurement systems and sensors from other field of research in the agrophysical application, including ion selective electrodes, widely used in liquids for selected anions and cations activity,
- − application of chosen sensors for determination of mass and energy transport coefficient in porous bodies by monitoring mass and energy in non-stationary transport processes,
- − modelling the processes of mass and energy transport in porous media and the models experimental verification,
- − networks of distributed smart sensor with the implementation of wireless communication and Internet access.

The Conference, supported by the EC Center of Excellence AGROPHYSICS and the Institute of Agrophysics Polish Academy of Sciences in Lublin, served for the exchange of information between interdisciplinary scientists in the field of porous materials monitoring and modelling, with the special concern to soil and its use. The Conference was also a part of the programme World Year of Physics 2005 in Poland.

We hope to contribute in the studies of porous materials, which have similar importance for humans as air and water. The development of monitoring techniques and modelling methods of porous materials have and will have a great impact on the application of physics in sustainable industry and agriculture.

Ryszard Walczak
Director of IAPAS, Lublin, Poland
Director of CoE AGROPHYSICS

Wojciech Skierucha
Secretary of the Conference

CONTENTS

APPLICATION OF THERMOGRAPHY FOR EVALUATION OF PARAMETERS CHARACTERIZING SEED AND FRUIT QUALITY

Baranowski Piotr, Mazurek Wojciech, Walczak Ryszard T.

Institute of Agrophysics, Polish Academy of Sciences, Lublin, Poland
pbaranow@demeter.ipan.lublin.pl

Abstract

In the Institute of Agrophysics Polish Academy of Sciences the investigations have been performed to apply thermography for determination of quality of plant materials. This paper presents the methodology of the radiation temperature measurement of the chosen fruit and seed material. The results of the studies of germination capacity of leguminous plant seeds and laboratory studies on the use of fruit surface temperature for determination of transpiration rate are presented. Furthermore the application of thermal imaging for detection of apple bruises is described.

K e y w o r d s : Thermography, porous media, seed germination, apple transpiration, fruit bruises

Introduction

The extensive research on finding new methods of investigation of the seed germination capacity is awaited because germination tests used these days require long time of waiting for the result and in case of rare species cannot be used at all because a representative number of seeds has to be at disposal [7,9]. The proposed in this paper use of the thermographic method for the evaluation of germination capacity of leguminous plant seeds enables to shorten the time of the selection process and can be performed on individual seeds.

The mechanism of water uptake in the process of swelling is different in case of healthy, dead and sick seeds. This fact has its representation in the energy balance of the seed surface. The created method is based on monitoring the heat conversion in the early stages of water absorption in the seed, which has its representation in the changes of radiation temperature of seed surface during the swelling process [2].

Thermal properties of fruits (thermal diffusivity) are strongly influenced by the composition of its tissue and in case of any disturbance caused by mechanical or physiological factors they are considerably modified in some parts of fruit [1,2,4]. These changes of thermal properties have impact on the rate of temperature changes under temperature gradient occurring between the

7

surrounding and the fruit. It was confirmed that thermography is a good tool for detecting apple bruises as well as translucence (glassiness) of the fruit flesh.

The seed material included some varieties of soya bean, vetch, pea, navy bean, snap bean and broad bean coming from different years of harvest, so that the seed material was characteristic for different storage periods, including the time after which seeds lose their germination capacity. During the experiment a standard method of testing the germination capacity was applied for the seeds of the investigated varieties, to be compared with the new method based on thermography measurement. The measurements were performed in settled and controlled external conditions. This required thermostabilisation of laboratory and installation of the sensors of air temperature humidity and pressure.

The rapid development of infrared technology and its increasing availability for users, let us think, that methodical and practical results of the initialised studies in the form of ready measurement procedures and determination of the relation between radiation temperature of seed or fruit material and the parameters of their quality evaluation, will find use in plant material storage and breeding [1,10,11].

Studies of the seed germination capacity with the use of thermography

Both, standard method of germination capacity determination (ISTA, 1999) [7] and a method based on the measurement of radiation temperature of the seeds in different stages the swelling process were used and compared.

During the measurements air temperature and air humidity were controlled and registered. The system of registration and processing of infrared and visible range images consisted of AGEMA 880 LWB and a CCD camera. The measurements were performed on the seeds of some varieties of soya bean, pea, navy bean, snap bean and broad bean coming from different years of harvest, so that the seed material was characteristic for different storage periods, including the time after which seeds lose their germination capacity.

From the point of view of evaluation of seed germination capacity, it is very important to compare the temperature changes in those seeds in which radicles and sprouts appeared during the swelling process and those seeds that did not germinate.

Results presented here are restricted to beans (cv 'Eureka'). It was assumed in the study that the rate of water uptake during the swelling process would differ in seeds in case of dissimilarity of their germination capacity. Accordingly, differentiation of evaporation rate from seeds surface should be reflected by differences of the radiation temperature of their surface.

8
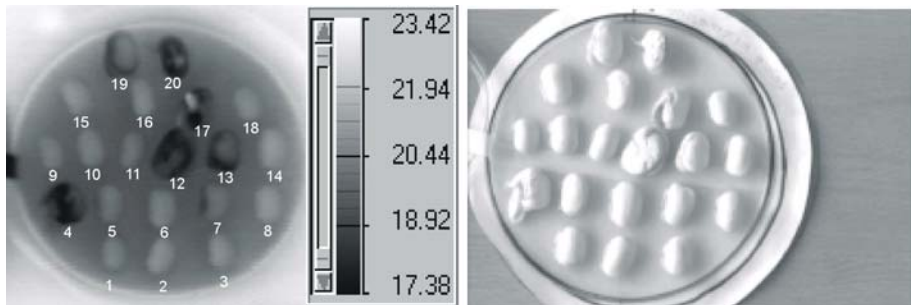
Fig. 1. Thermal image (left) and visible image (right) of bean seeds; radiation temperature changes of the numbered seeds that germinated in the first 4 days and that did not germinate at all are presented in **Fig. 2**

In **Fig. 1**, a thermal image and a visible image, taken after the first 3 days of the swelling of bean seeds are presented. Each dish in this experiment contained 20 seeds. Considerable differences were noticed in average temperature of seeds at the initial stage of the swelling process depending on the storage time and germination energy. The courses of temperature changes in time of viable bean seeds showed a considerable decrease in the radiation temperature (more than 2.5°C) during the first 3 days of the swelling process (left part of **Fig. 2**). The magnitude of this decrease as well as the time period in which it is observed, are characteristic for particular varieties. For instance, in the studied pea cultivars ('Sześciotygodniowy' and 'Piast'), the decrease of radiation temperature of more than 1^0C was observed in the first 12 hours of the swelling process [2].

Another characteristic feature of the radiation temperature distribution on the seed surface in the swelling process is that after the period of decrease, the temperatures of the viable seeds remain in the specific range. For bean seeds, starting from 4320 minutes of the swelling to its end, seed surface temperature changes from 18.3°C to 20.1°C (left part of **Fig. 2**). Analogically, after the 1440 minutes of swelling, the temperatures of pea seeds remain in the range of 19.1 – 19.4°C [2].

The changes in radiation temperature of selected seeds in right part of **Fig. 2** refer to the bean seeds that did not germinate until the end of the swelling process. It is characteristic that decreases in the radiation temperature of seeds in the period of first 3 days of swelling did not exceed 1°C. Further on, radiation temperature remains in the range of 20.3 - 22°C. The numbers of the curves correspond to the respective numbers in **Fig. 1**.
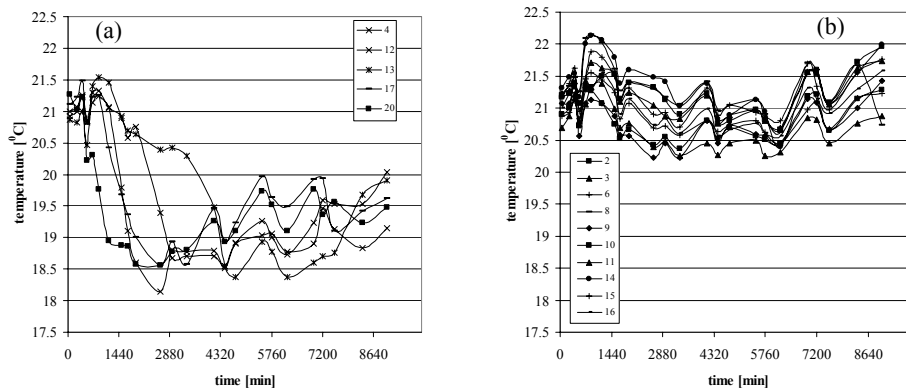
Fig. 2. Changes in radiation temperature of: (a) - seeds that formed radicle after the first 4 days of the swelling process, (b) - seeds that did not germinate

The rapid development of infrared technology and its increasing availability for the users let us think that methodical and practical results of the initialised studies in the form of ready measurement procedures and determination of the relation between radiation temperature of seed or fruit material and the parameters of their quality evaluation, will find use in plant material storage and breeding [6].

Laboratory studies on the use of fruit surface temperature for determination of transpiration

Transpiration plays an important role in the water balance of fruit. In the conditions of transport and fruit storing, even a short term changes of ambient temperature influence the intensity of transpiration and in consequence the fruit quality [5,8]. Thermography was applied for determination of transpiration intensity of fruits. The object of the study were apples of three varieties: `Jonagold`, `Ligol` and `Gloster` and plums of three varieties: `Top`, `Bluefre` and `President`. The measurement of radiation temperature was performed for three values of ambient temperature, *ie* 11, 18 and 23°C during the successive three days. To register the distribution of radiation temperature of fruit surface the system was used, consisting of thermographic AGEMA 880 LWB (8-13 μm) camera and CCD camera working in the range of visible light. In the conditions of the experiment, the differences between radiation temperature of the apple fruit surface and the air temperature were noticed reaching up to 2.3°C.

For three investigated ranges of ambient temperature, the range of transpiration change for apples is from 1.3 do 6.6 x 10^{-7} kg·m^{-2}·s^{-1}, whereas for plums it is from 2 to 36 x 10^{-7} kg·m^{-2}·s^{-1}. Both for apples and plums, the highest observed values of

10

transpiration for all investigated fruits was stated at the ambient temperature 23°C and the lowest at 11°C.
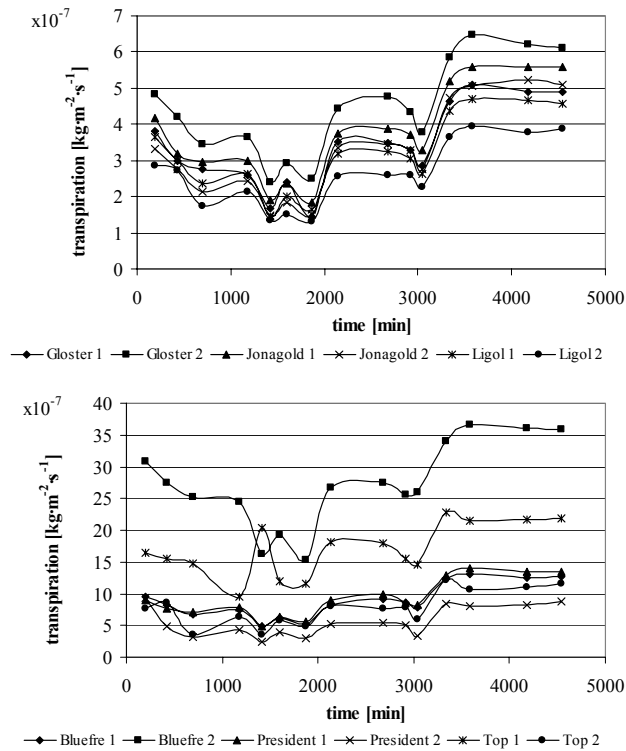
Fig. 3. Transpiration changes in time for investigated varieties of apples and plums for three levels of ambient temperature

Apples of `Ligol` variety and plums of `President` variety were characterized by the lowest values of transpiration. The highest differences of transpiration between particular fruits occured under ambient temperature of 23°C. Some of plum fruits (two highest courses in **Fig. 3**) had several times higher values of transpiration than the others. The leakage of fruit juice was observed from them.

Transpiration coefficients of apples and plums of the investigated varieties for three various ambient temperatures (11, 18 and 23°C), differ significantly. For apples they contain in the range $0 - 10^{-6}$ m·s^{-1} and for plums from 0 to $7 \cdot 10^{-6}$ m·s^{-1}.

Detection of apple bruises with the use of thermography

Three varieties of apples were studied: 'Jonagold', 'Ligol' and 'Gloster'. Apples were bruised by dropping them from 0.25 m onto a smooth, ceramic surface. Before and after the measurement of radiation temperature, apples were stored in temperature 1.5^0C. Thermal images of apple surface with bruise were obtained with the use of AGEMA 880 LWB system during 12-minute session of heating of apples in ambient temperature 25^0C. The thermograms in **Fig. 4** present a 'Jonagold' apple in three stages after bruising.
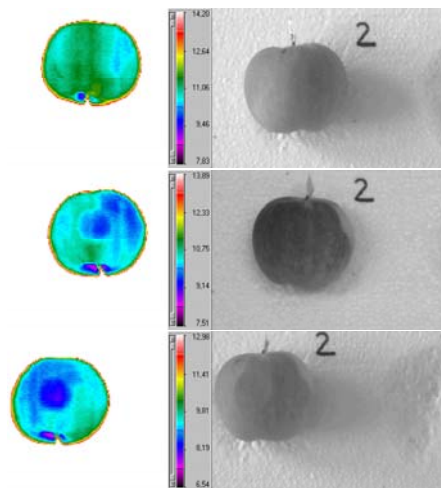
Fig. 4. Thermograms (left) and visible light images (right) of bruised apple 'Jonagold', two, twenty six and fifty hours after bruising (from upper side to the bottom)

In each thermogram two surfaces were selected, first covering the bruised surface of the fruit and second, the surface of sound tissue. The obtained courses of temperature changes of both surfaces during the heating process showed for all the studied varieties the occurrence of temperature differences between bruised and sound parts in the range 0.5-1.5°C. The highest differences of radiation temperature were noticed for 'Jonagold' variety and the lowest for 'Gloster' variety, which were determined by highest differences of firmness between these two varieties.

It was stated that independently from the studied variety and the time after bruising the mean temperatures of the bruised parts of apples were lower than the parts of apples with sound tissues. Whiskers in the plots of temperature courses of two areas (**Fig. 5**), representing bruised and sound tissues, show the ranges of temperature changes within these areas.
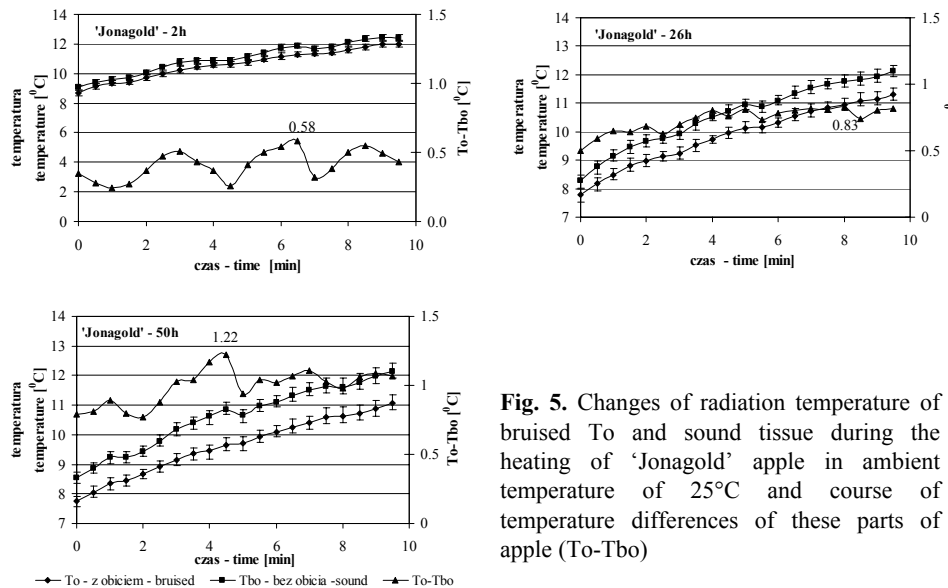
Fig. 5. Changes of radiation temperature of bruised To and sound tissue during the heating of 'Jonagold' apple in ambient temperature of 25°C and course of temperature differences of these parts of apple (To-Tbo)

In many cases, the temperature differences between bruised and sound tissues were so large that common ranges of temperature between these areas did not occur and therefore it was not necessary to use detail statistical analysis and the methods of image processing to identify bruises.

References

1. **Baranowski P., Mazurek W., Walczak R.T.:** Zastosowanie termografii do badania stresu wodnego roślin i ewapotranspiracji rzeczywistej. Acta Agrophysica, 21, 1999.
2. **Baranowski, P., Mazurek, W. and Walczak R.T.:** Thermographic observation of seeds in early stage of swelling (in Polish). V-th Conference of Infrared Termography and Thermometry Ustroń: 349-352, 2002.
3. **Chaerle L., Van Der Straeten D.:** Seeing is believing: imaging techniques to monitor plant health. Biochemica et Biophysica Acta, 1519, 153-166, 2001.
4. **Chaerle, L. and Van der Straeten, D.:** Seeing is believing: imaging techniques to monitor plant health. Biochimica et Biophysica Acta, 1519:153-166, 2001.
5. **Chen H., De Baerdemaeker J.:** Optimization of Impact Parameters for Reliable Excitation of Apples During Firmness Monitoring. J.agric. Engng Res., 61, 275-285, 1995.
6. **Hellebrand, H.J., Linke M., Beuche H., Herold B. and Geyer M.:** Horticular products evaluated by thermography. Ag. Eng. University of Warwick, UK. Abstracts Part 2, Paper No. 00-PH-003: 26-27, 2000.
7. **International Seed Testing Assotiation:** International Rules for Seed Testing. Seed Sci. & Technol. 27 Suplement, 1999.

8. **Leonardi C., Baille A., Guichard S.:** Predicting transpiration of shaded and non-shaded tomato fruits under greenhouse environments. Scientia Horticulturae, 84, 297-307, 2000.
9. **Lombardi, T., Fochetti, T., Bertacchi, A. and Onnis, A.:** Germination requirements in a population of Typha latifolia Aquatic Botany 56:1-10,1997.
10. **Walczak R.T., Baranowski P. Mazurek W.:** Application of thermography in agrophysics, Training Course for Young Research Workers "Physicochemical and Physical Methods of Studies of Soil and Plant Materials. Theory and Practice", IAPAS, Lublin, 27.11-2.12.2003.
11. **Walczak R.T., Baranowski P., Mazurek W., Lamorski K.:** The analysis of infrared images to evaluate energetic status of agricultural porous media. 2nd International Workshop Applied Physics in Life Science, Czech University of Agriculture Prague, Technical Faculty, Department of Physics, Prague, 25th September 2003.

14

SOIL DEHYDROGENASE ACTIVITY AS INFLUENCED BY SOME PHYSICAL FACTORS

Brzezińska[1] Małgorzata, Stępniewska[2] Zofia, Stępniewski[3] Witold,
Włodarczyk[1] Teresa

[1]Institute of Agrophysics, Polish Academy of Sciences, Lublin, Poland
mbrzez@demeter.ipan.lublin.pl
[2]Catholic University of Lublin, Poland
[3]Technical University of Lublin, Poland

Abstract

The aim of the paper was to study the effect of soil physical factors such as bulk density, moisture content and temperature on soil dehydrogenase activity. The studies were performed on soils from Ap horizons of 11 Orthic Luvisols and 10 Haplic Phaeozems developed from loess. The soil samples were subjected to 14-day pre-incubation on soil moisture tension plates (0; 5; and 15.9 kPa) at 10, 20 and $30^{o}C$ in 30 cm^3 plastic cylinders at bulk density of 1.1 to 1.4 Mg m^{-3}. After pre-incubation, the measurements of oxygen diffusion rate (*ODR*), redox potential (*Eh*), and the concentration of reduced Fe were performed. The dehydrogenase activity under standard conditions (20 hours of flood incubation at $30^{o}C$) by the method of TTC reduction to formazan was assayed. The increase in moisture and temperature caused significant stimulation of the dehydrogenase activity. The highest effect was exerted by soil water content. Flooding the soil caused an increase of the soil dehydrogenase activity by a factor of about 15 as compared to the 15.9 kPa treatment. The enzyme activity increased 2.6 – and 4.6 – times for the 15.9 kPa treatment and soil flooding, respectively, with the increase of soil temperature by 10 ^{o}C. The enzyme activity in the Phaeozems was in average about 3 times higher than that of Luvisols. The increase of soil water content and the incubation at higher temperature caused in general deterioration of the soil aeration status. It has been concluded that soil dehydrogenase activity is influenced by the oxygenation status of the soil as expressed by its redox potential and - but to smaller extent - by *ODR*. Physical parameters tested, being essential environmental variables, influence the dehydrogenase activity indirectly by affecting soil oxidation-reduction status. Thus their effect can be explained by changes of redox potential.

K e y w o r d s : soil dehydrogenase activity, redox potential, temperature, soil bulk density, soil water content

Introduction

Soil dehydrogenase activity is commonly used as an indicator of the biological activity in the soil [6]. Dehydrogenase enzymes play a significant role in the biological oxidation of soil organic matter by transferring protons and electrons from substrates to acceptors. Numerous soil dehydrogenases are assumed to function only intracellularly, exclusively with intact, living cells. Dehydrogenase activity has been used as a general index of soil biological activity because of the involvement of these enzymes in the oxidative energy-transfer sequences [20]. Numerous studies reveal correlations of the activity with several parameters of soil biological activity such as microbial numbers, biomass, soil respiratory activity, ATP content, soil organic matter and fertility, respiration, denitrification, carbon and nitrogen cycling and other soil enzyme activities [2,3,4,8,10,11,13,18,19,21,27].

These processes, being a part of respiration pathways of soil microorganisms, are closely related to the air-water conditions of the soil porous system [14,23,24,25,26,27]. The objectives of present study was to (i) evaluate the influence of physical factors such as water content, temperature and bulk density on dehydrogenase activity and (ii) determine the relationship between dehydrogenase activity and soil aeration parameters.

Materials and methods

The studies were performed on soils from Ap horizons of 11 Orthic Luvisols and 10 Haplic Phaeozems developed from loess. Organic carbon of soils was in the range 0.65 - 2.10%; pH between 5.58 and 7.71. Air-dry, sieved through 1 mm sieve, soils placed in 30 cm^3 plastic cylinders (29 mm in diameter and 45 mm in height) were subjected to 14-day pre-incubation at three levels of water content corresponding to 0 kPa (capillary saturation); 5 kPa and 15.9 kPa on soil moisture tension plates at 10; 20 and 30^oC. Soils were compacted to a bulk density of 1.1; 1.2; 1.3 and 1.4 Mg m^{-3} prior to the pre-incubation under different water and temperature conditions.

After pre-incubation, the measurements of oxygen diffusion rate (*ODR*), redox potential (*Eh*) and the concentration of reduced Fe were performed [1,14]. Dehydrogenase activity was assayed under standard conditions (20 hours of flooded incubation at 30^oC) by the method of reduction of 2,3,5-triphenyltetrazolium chloride (TTC) to formazan, according to Casida *et al.* [7].

Results and discussion

Soil water content, temperature and compaction are physical parameters influencing the natural habitat of field soil porous system. Two-week pre-incubation of the soils developed from loess, performed under different water and temperature conditions caused significant changes of dehydrogenase activity as well as of soil aeration status. **Table 1** illustrates the influence of water conditions (from water saturation to soil moisture tension of 15.9 kPa) on the dehydrogenase activity and aeration status.

Table 1. Influence of water conditions on dehydrogenase activity, air-filled porosity (*Eg*), oxygen diffusion rate (*ODR*), redox potential (*Eh*) and reduced Fe content. Average values of 21 loess soils pre-incubated at 0; 5 and 15.9 kPa; at 10; 20 and 30°C; bulk density of 1.3 Mg m^{-3}. (DHA – dehydrogenase activity)

Soil water tension [hPa]	DHA [μg TPF g^{-1} 20h^{-1}]	*Eg* [m^{3}m^{-3}]	*ODR* [μg m^{-2}s^{-1}]	*Eh* [mV]	Fe^{+2} [mg kg^{-1}]
0.0	401.0^a	0.012^a	6.64^a	56^a	692^a
5.0	119.0^b	0.079^b	15.70^b	199^b	332^b
15.9	26.7^b	0.117^c	24.80^c	334^c	103^c

Dehydrogenase activity was highest in water saturated soils and decreased significantly in soils pre-incubated at 5 and 15.9 kPa. The increase of soil moisture tension was evidently connected with the increase of values of aeration parameters such as air-filled porosity (calculated from water content, bulk density and particle density), oxygen diffusion rate, redox potential and with the decrease of concentration of reduced Fe.

Table 2 presents the influence of temperature during 14-day pre-incubation on dehydrogenase activity, *Eh* and Fe (II) content. Higher temperature caused an increase of dehydrogenase activity and increase of reduced Fe content as well as a drop of *Eh* values.

Table 2. Influence of temperature on dehydrogenase activity, redox potential and reduced Fe content. Average values of 21 loess soils pre-incubated at 10; 20 and 30°C at 0, 5 and 15.9 kPa; bulk density of 1.3 Mg m^{-3}

Temperature [°C]	Dehydrogenase activity [μg TPF g^{-1} 20h^{-1}]	*Eh* [mV]	Fe^{+2} [mg kg^{-1}]
10	48.5^a	249^a	100^a
20	126^a	216^a	287^b
30	454^b	121^b	912^c

The influence of bulk density on air-filled porosity of soils pre-incubated under differentiated water and temperature conditions was significant (**Table 3**). The experiment showed no statistically significant differences for dehydrogenase activity and other aeration parameters in the bulk density range under consideration.

The highest effect on dehydrogenase activity was exerted by soil moisture content. Flooding the soil caused an increase of the soil dehydrogenase activity by a factor of about 15 as compared to the 15.9 kPa treatment. The enzyme activity increased by a factor of 2.6 for the 15.9 kPa treatment and by a factor of 4.6 for the flood treatment with the increase of temperature by 10 $^{\circ}$C in the range 10-30°C (factors calculated for soils pre-incubated at density of 1.3 Mg m^{-3}). Intensity of the influence of temperature on dehydrogenase activity depended on soil water content. An increase of the dehydrogenase activity in flooded soil was observed for other soils under both field and laboratory conditions [9,15,16,22,23,26].

Table 3. Influence of bulk density (1.1-1.4 Mg m^{-3}) on air-filled porosity; average values of loess soils pre-incubated at 10; 20 and 30 $^{\circ}$C at 0; 5 and 15.9 kPa

Bulk density [Mg m^{-3}]	Eg [m^{3}m^{-3}]
1.10	0.155^a
1.20	0.110^b
1.30	0.057^c
1.40	0.011^c

Analysis of the results showed a close relationship between dehydrogenase activity and soil oxygen status. **Fig. 1** illustrates this relation obtained after pre-incubation of soils in the entire range of water content, temperature and bulk density used. It should be noted, that this pattern includes the data of 21 soils originating of the same parent material, but different in their organic matter content and pH. The activity of the Phaeozems was in average about 3 times as high as that of Luvisols. Despite of such variability of the tested soils, the relationship was significant.

The incubation of the soils in the entire range of water tensions and temperature differentiated the aeration parameters. Air-filled porosity (**Fig. 1a**) varied from 0.24 m^{3}m^{-3} to nearly zero, *ODR* values (**Fig. 1b**) - from 80 to 0.5 μgm^{-2}s^{-1}. These two parameters correlated with dehydrogenase activity (for exponential model r= -0.61*** and r= -0.57***, respectively).

The increase of soil moisture content and temperature caused the deterioration of the soil aeration status expressed also by soil redox potential. Redox potential

changed from +600 mV to below -160 mV (**Fig. 1c**). A decrease of Eh was accompanied by an increase of reduced iron content from about 10 even to over 2000 mg per kg of soil (**Fig. 1d**).
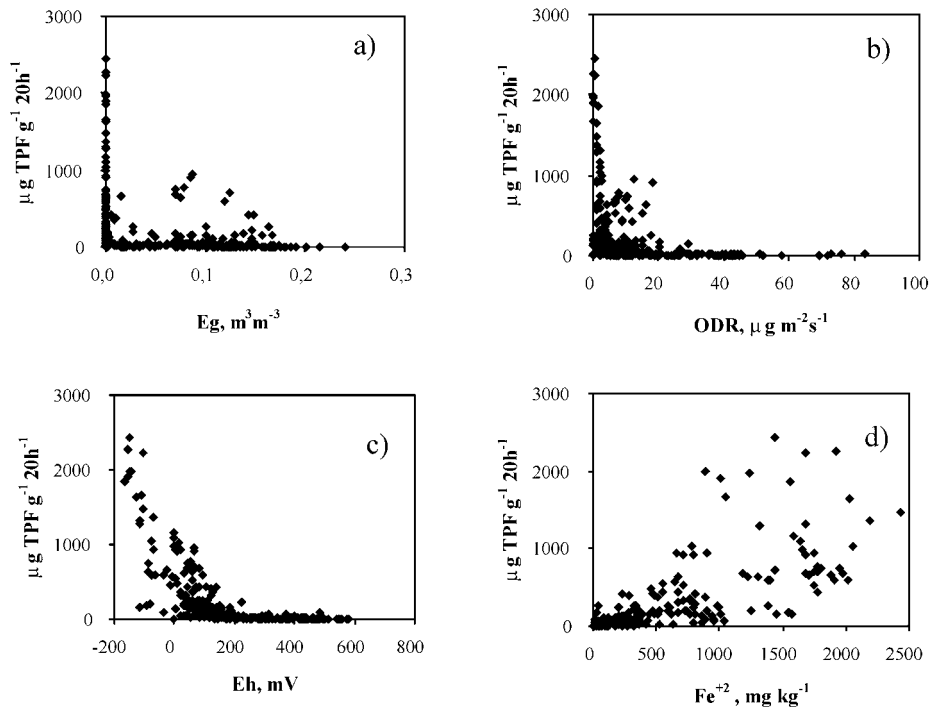
Fig. 1. Relationship between dehydrogenase activity and soil aeration parameters: a) air-filled porosity; b) oxygen diffusion rate; c) redox potential; d) Fe(II) content; results of 21 soils pre-incubated under entire range of water tension and temperature

Redox potential is a very useful parameter in the describing of the dynamic changes in the soil after its flooding or drying and gives an information about the rate of redox reactions taking place in the soil [14,17]. These redox transformations are closely connected with respiration activity of soil microorganisms. The relationship between dehydrogenase activity and Eh as well as Fe^{+2} content illustrates reaction of soil microorganisms to the changes in soil environment. The lack of oxygen implicates facultative anaerobes to initiate such metabolic processes, which supply sufficient amount of energy, necessary to their normal activity. One of the stages of

anaerobic respiration, taking place in soil, is the use of Fe(III) forms as terminal electron acceptors. These processes involve activity of dehydrogenases [5,12].

Dehydrogenase activity of 21 tested soils (developed from loess) incubated under controlled air-water and temperature conditions showed a very good relationship with redox potential and Fe^{+2} content (for exponential model r=-0.83*** and r=0.77***, respectively).

It should be kept in mind that both the soil types were developed from the same parent material, which, to some extent, approximates their properties. The differences between the Phaeozems and the Luvisols can be explained in terms of the differences in their redox potentials during incubation. Similar explanations can also be given for the differences in dehydrogenase activity caused by changes of soil water tension and temperature. The lowest redox potential values (down to -150 mV) observed in the Phaeozems at the highest temperature (30^oC) were accompanied by maximal dehydrogenase activity. The Luvisols were not as active at 30^oC and their redox potential did not drop below -100 mV.

Soil physical factors, being essential environmental variables, have such a strong indirect influence on soil dehydrogenase activity through the changes in soil aeration status (as expressed by *Eh, ODR*, or - but to smaller extent - by Fe(II) content and *Eg*). This should be taken into consideration during sampling, transportation and storage of soil samples before their dehydrogenase activities are assayed.

References

1. **Aleksandrova L.J. and Naidenova O.A.:** Laboratory measurements in soil science (in Russian) Kolos, Leningrad, 1967.
2. **Aon M.A., Cabello M.N., Sarena D.E., Colaneri A.C., Franco M.G., Burgos J.L., Cortassa S.:** I. Spatio-temporal patterns of soil microbial and enzymatic activities in an agricultural soil. Appl. Soil Ecol. 18, 239-254, 2001. **Garcia** C., Hernandez T., Costa F.: Microbial activity In soils under Mediterranean environmental conditions. Soil Biol. Biochem. 26, 1185-1191, 1994.
3. **Bandick A.K., Dick R.P.:** Field management effects on soil enzyme activities. Soil Biol. Biochem. 31, 1471-1479, 1999.
4. **Baran S., Bielińska J.E., Oleszczuk P.:** Enzymatic activity in an airfield soil polluted with polycyclic aromatic hydrocarbons. Geoderma 118, 221-232, 2004.
5. **Bromfield S.M.:** Reduction of ferric compounds by soil bacteria. J. General Microbiol. 11, 1-6, 1954.
6. **Burns R.G**.: Soil Enzymes. Acad. Press Inc., (London) LTD, 1978.
7. **Casida L.E., Klein D.A. and Santoro T**.: Soil dehydrogenase activity. Soil Sci. 98, 371-376, 1964.

8. **Chander** K., Brookes P.C., Harding S.A.: Microbial biomass dynamics following addition of metal-enrinched sewage sludges to a sandy loam. Soil Biol. Biochem. 27, 1409-1421, 1995.

9. **Chendrayan K., Adhya T.K. and Sethunathan N**.: Dehydrogenase and invertase activities of flooded soils. Soil Biol. Biochem. 12, 271-273, 1980.

10. **Curl E.A., Harper J.D.** Fauna-microflora interactions. In: The Rhizosphere (Ed. J.M. Lynch). Wiley-Inter-science, New York, 369-388, 1990.

11. **Frankenberger, W.T.Jr., Dick W.A.:** Relationship between enzyme activities and microbial growth and activity indices in soil. Soil Sci. Soc. Am. J. 47, 945-951, 1983.

12. **Galstian A.S. and Awungian Z.S**.: Significance of the enzymes in oxidation of Fe and Mn oxides in soil (in Russian). Trans. 10th Intern. Congress Soil Sci. III. Nauka Publishing House, Moscov, 130-135, 1974.

13. **Garcia-**Gil J.C., Plaza C., Sensie N., Brunetki, Polo A.: Effects of sewage sludge amendment on humin acids and microbiological properties of a semiarid Mediterranean soil. Biol. Fertil. Soils 39, 320-328, 2004.

14. **Gliński J. and Stępniewski W**.: Soil Aeration and its Role for Plants. CRC Press, Boca Raton, Florida, 1985.

15. **Gliński J., Stępniewska Z. and Brzezińska M**.: Characterization of dehydrogenase and catalase activity of the soils of the two natural sites with respect to the soil oxygenation status. Polish J. Soil Sci. 19, 47-52, 1986.

16. **Gliński J., Stępniewska Z. and Kasiak A**.: Changes of soil enzyme activity under different conditions of oxygen content and moisture (in Polish). Roczn. Glebozn. 34, 53-59, 1983.

17. **Gunnison D., Engler R.M., Patrick W.H.Jr**.: Chemistry and microbiology of newly flooded soils: relationship to reservoir - water quality. Microbial Processes in Reservoirs. Chapt. 3, 39-57, 1985.

18. **Januszek K**.: Aktywność enzymatyczna wybranych gleb leśnych Polski południowej w świetle badań polowych i laboratoryjnych. Zeszyty Naukowe AR w Krakowie, Rozprawy nr 250, Kraków 1999.

19. **Kucharski** J.: Relacje między aktywnością enzymów a żyznością gleby. W: Drobnoustroje w środowisku. Występowanie, aktywność i znaczenie (Red. W. Barabasz). AR Kraków, 327-347, 1997.

20. **Ladd J.N., Foster R.C., Nannipieri P., Oades J.M.:** Soil structure and biological activity. In: Soil Biochemistry, Vol. 9 (Eds G. Stocky, J.M. Bollag). Marcel Dekker Inc, New York, Basel, Hong Kong, Chapter 2, 23-78, 1996.

21. **Myśków W., Stachyra A., Zięba S., Masiak D.:** Biological activity as index of soil fertility (In Polish). Roczn. Gleb. 47, 1/2, 88-99, 1996.

22. **Okazaki M., Hirata E. and Tensho K**.: TTC reduction in submerged soils. Soil Sci. Plant Nutr. 29, 489-497, 1983.

23. **Pedrazzini F.R. and McKee K.L**.: Effect of flooding on activities of soil dehydrogenases and alcohol dehydrogenase in rice (*Oryza sativa L.*) roots. Sci. Plant Nutr. 30, 359-366, 1984.

24. **Stępniewska Z., Gliński J., Włodarczyk T., Brzezińska M., Blum W.E.H., Rampazzo N. and Wimmer B**.: Soil aeration status of some Austrian soils. Int. Agrophysics 11, 199-206, 1997.

25. **Stępniewski W., Stępniewska Z., Gliński J., Brzezińska M., Włodarczyk T., Przywara G., Vàrallyay G., Rajkai K.**: Dehydrogenase activity of some Hungarian soils as related to their water and aeration status. Int. Agrophysics 14, 341-354, 2000.

26. **Stępniewski W., Stępniewska Z., Włodarczyk T., Dabek-Szreniawska M., Brzezińska M., Słowińska-Jurkiewicz A., Przywara G.:** Aeration related properties and their influence on soil biological parameters. Int. Agrophysics 7, 163-173, 1993.
27. **Włodarczyk T., Stępniewski W., Brzezińska M.:** Dehydrogenase activity, redox potential, and emission of carbon dioxide and nitrous oxide from Cambisols under flooding conditions. Biol. Fertil. Soils 36, 200-206, 2002b.

PORE-SHAPE COMPONENT OF SOIL WETTABILITY
Czachor Henryk

Institute of Agrophysics, Polish Academy of Sciences Lublin, Poland
hczachor@demeter.ipan.lublin.pl

Introduction

Matric potential of soil water is a result of wettability of solid phase by soil solution. It is a common opinion that the wettability or repellency of soils depends on surface properties of soil particles, type of organic matter and associated contact angle [1,3,4,7,17,18]. There is no direct method of its measurement in porous media. One way of porous media- water reppelency/wettability quantification is the application of indices like water drop penetration time (WDPT) or the ethanol probe (EP), which are applied in soil science. In the first method a soil –water interaction is characterized via time of water drop percolation, in second one –the lowest ethanol content of water – ethanol solution that wets the soil [10,11,15,20].

Among the indirect methods the wetting front displacement following a horizontal infiltration and a capillary rise experiments are applied to determine the contact angle [12,14,19]. Their theoretical background is described by Washburn equation. In principle these methods are valid under assumption that the pore shape can be modelled by cylindrical tube, while the real pores in soils have at least three different features: they are either cylindrical or straight and they are interconnected. The consequences of non-cylindrical shape of pores on capillary rise are examined in this paper.

Capillary pressure in non-cylindrical pores

A cross section through a real grain porous body shows frequently the image similar to **Fig. 1**, which concerns to a virtual packed aggregate composed of spherical uniform particles [5]. The geometrical radius of the pore is changing along the path and its shape is far from straight line.

Axis symmetrical, sinusoidal shaped capillary has been applied to model the soil pores. For the reason of simplicity and symmetry the equation for the geometrical radius of the capillary $r_g(x)$ being a periodic function of coo-ordinate x is applied [2,6]

$$r_g(x) = r_1 + r_2 \sin(\pi / hx) \tag{1}$$

where: $r_1 > r_2$
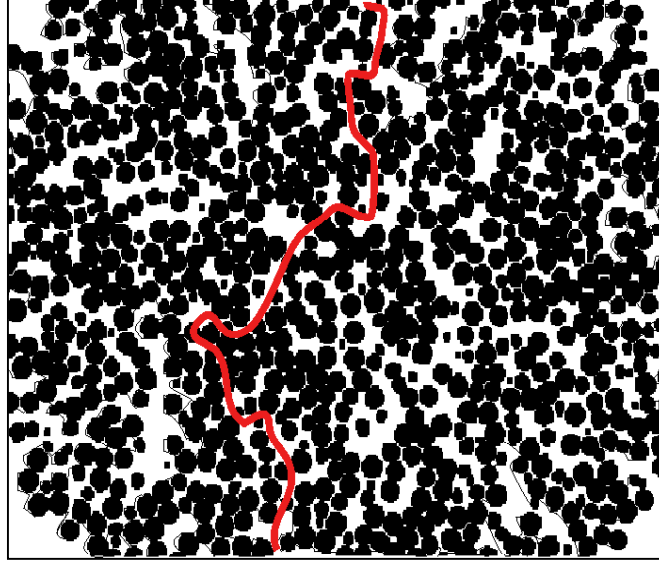
Fig. 1. Cross section through a granular porous body [5]; gray line shows a possible path of a single meniscus during the capillary rise movement

Meniscus in such capillary has a shape of concave mazer (see **Fig. 2**). Its curvature radius can be expressed as

$$r_k(\theta,x) = \frac{r1(1 + d\sin(\pi/hx))\sqrt{(1 + (\pi r_2 / h\cos(\pi/hx))^2)}}{((\cos(\theta) - \pi d\sin(\theta)\cos(\pi/hx))} \tag{2}$$

where: $d = r_2/r_1$ - wall waveness.

The ratio

$$A(x,\theta) = Pcs/Pcc \tag{3}$$

where: $P_{cc} = 2*\sigma_L/r_1$ - capillary pressure in cylindrical capillary, $P_{cs} = 2*\sigma_L/r_k$ - capillary pressure in sinusoidal capillary shows the difference between both approaches

$$A(x,\theta) = \frac{\cos(\theta) - \pi d\sin(\theta)\cos(\pi/hx)}{(1 + d\sin(\pi/hx))\sqrt{[1 + [\pi r_2 / h\cos(\pi/hx_m)]^2]}} \tag{4}$$

24
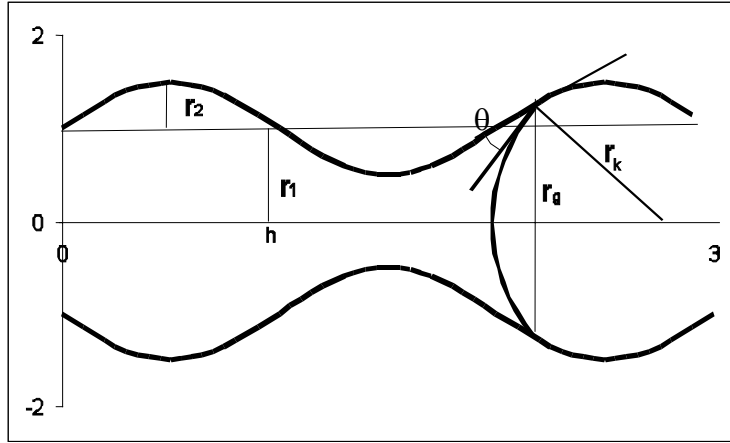
Fig. 2.   Meniscus in a sinusoidal capillary domain

Analysis of the capillary pressure formula (Eq. 4) shows that the water repellency in such a capillary should occur at the contact angle much lower than 90^0. The critical contact angle θ_c value, showing the limit between repellency and wettability, depends on the shape of the pores according to the equation

$$ctg(\theta_c) = \pi \cdot d \tag{5}$$

Capillary rise in sinusoidal capillaries

The general equation describing the liquid movement is done by Poiseuille's equation

$$\frac{dV}{dt} = \frac{\pi [r_g(x)]^4}{8\eta} \frac{dP}{dx} \tag{6}$$

where: V - volume flow rate, t - time, η - liquid viscosity, P - pressure difference, $r_g(x)$ - tube radius. For an incompressible liquid in circular tube the volume flow rate is independent on x nevertheless if it is combined with the average linear rate of the liquid dx/dt by

$$\frac{dV}{dt} = \pi [r_g(x)]^2 \frac{dx}{dt} \tag{7}$$

Let suppose a vertical sinusoidal capillary of radius done by Eq. 1 with the meniscus at the height x_m. Flow rate dV/dt for $x <= x_m$ is independent on x, so the pressure difference P at this level can be calculated as [16]:

$$P = \frac{8\eta(dV/dt)}{\pi}\int_0^{x_m}\frac{dx}{[r_g(x)]^4}$$

(8)

or as

$$P = P_{cs} - \rho g x_m$$

(9)

If $h << x_m$ the calculation of the integral in Eq. 14 can be done in the analytical form:

$$\int_0^{x_m}\frac{dx}{[r_g(x)]^4} = x_m/(2h)\int_0^{2h}\frac{dx}{[r_g(x)]^4} = x_m * \frac{r_1(2r_1^2 + 3r_2^2)}{2(r_1^2 - r_2^2)^{3.5}}$$

(10)

Equations 12 and 13 are valid for any x including the meniscus position x_m. Substituting Eq. 8 into Eq. 15 and combining Eqs. 12-16 after some basic transformations one can get the analytical expression for meniscus rate dx_m/dt

$$\frac{dx_m}{dt} = \frac{\sigma r_1[1-d^2]^{3.5}}{2\eta[2+3d^2]} * \frac{\cos\theta - \pi d\sin\theta * \cos(\pi/hx_m)}{x_m[1+d\sin(\pi/hx_m)]^3\sqrt{[1+[\pi d\cos(\pi/hx_m)]^2]}}$$
$$- \frac{\rho g r_1^2[1-d^2]^{3.5}]}{4\eta[2+3d^2]} * \frac{1}{[1+d\sin(\pi/hx_m)]^2};$$

(11)

Complexity of Eq. 17 is apparent in fact. If the capillary waveness $d=0$ one obtains a well known formula for rising in cylindrical capillary

$$\frac{dx_m}{dt} = \frac{\sigma r_1\cos\theta}{4\eta x_m} - \frac{\rho g r_1^2}{8\eta}$$

(12)

which after integration can be presented in the form

$$t(x_m) = -\frac{x_m}{B} - \frac{A}{B^2}\ln(1 - \frac{B}{A}x_m)$$

(13)

where: $A = \sigma r\cos(\theta)/(4\eta)$; $B = r^2\rho g/(8\eta)$;

Analytical integration of Eq. 11 is not possible. However the numerical one can be done as fallows: for a chosen values of r_1, r_2, h and θ the meniscus rate v_m

26

can be calculated for any height x by means of Eq. 11. The relationship $v_m = f(x)$ has been calculated for $x_i \in (\Delta x, x_{max})$ where $\Delta x = x_i - x_{i-1}$ and $\Delta x = 0.1h$. The time Δt_{i-1} related to the displacement between the height x_{i-1} and x_i was calculated as a ratio of displacement and the mean harmonic rate of v_{i-1} and v_i

$$\Delta t_{i-1} = \frac{\dfrac{x_i - x_{i-1}}{2}}{\dfrac{1}{v_i} + \dfrac{1}{v_{i-1}}} \tag{14}$$

where: x_i - height related to the rate v_i.

Than the time T of rising to the height x_i can be done as

$$T(x_i) = \sum_{j=2}^{i} \Delta t_{j-1}; \tag{15}$$
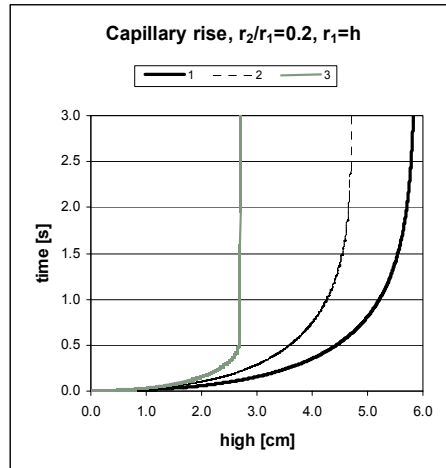
Fig.4. Kinetics of capillary rise in cylindrical (CC) and sinusoidal (CS) tubes

Some examples of calculated kinetics shows **Fig. 4**. Line 1 corresponds to a cylindrical capillary and $\theta=0^0$, 2- sinusoidal one $r_2/r_1=0.2$, $\theta=0^0$, 3- sinusoidal one $r_2/r_1=0.2$, $\theta=30^0$. The influence of wall wavness and contact angle is evident. The curves corresponding to the sinusoidal capillaries are not smooth one but composed of small steps like a staircase [9]. Several other calculations have been done to find out the influence of capillary shape and contact angle on capillary rise kinetics $T(x)$. Than the Eq. 13 was applied to the obtained data. Application of non-linear estimation (Statistica 5 package) made possible to calculate the values of A and B parameters from Eq. 13, which contains two unknown values:

27

the pore and radius the contact angle. Both of them concern to the cylindrical pore model while Eq.1 characterizes the examined case. It is worth to mention that it is a common situation when a soil or other porous media are investigated by means of such method. For this reason the calculated values have been named the apparent ones.

The results obtained are shown at **Fig. 5** and **Fig. 6**. Calculated contact angle is a strongly increasing function of wall wavness while the calculated pore radius is even smaller than the neck radius [8].
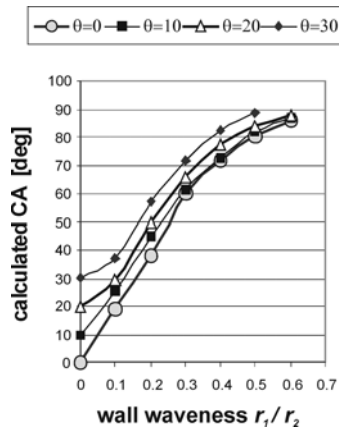
Fig.5. Apparent CA calculated from cylindrical model– wall waveness relationship (true CA –parameter)
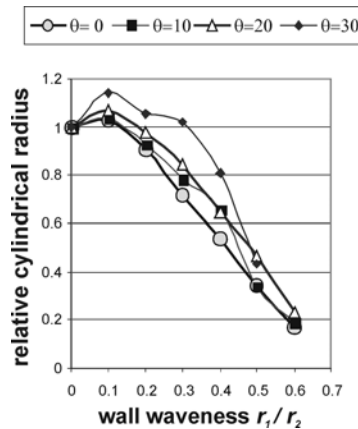
Fig.6. Apparent pore radius calculated from cylindrical model– wall waveness relationship (true CA –parameter)

.

Presented results show that the geometry of pores and contact angle are or can be very important characteristics for capillary driven liquid in porous media. Experimental verification of the presented model can be done when the true CA characterizing by liquid – solid porous body interaction is known. However in the case of granular materials the true CA is unknown. Difficulties with a true contact angle measurement in grain materials have been solved in the following way: 50x100 mm glass plate has been wash carefully by means of distillate water and dried in room conditions. Five distillate water drops of equal volume (0.01 cm^3) have been placed at the glass surface by mean of pipette. As the glass surface was clean the drop shapes were far from circular. Their images have been saved and than analysed by means of image analysis to determine the drop geometry i.e. the liquid-solid surface area S_{wet} and associated radius a (Eq. 16). Supposing spherical shape of the drop mazer of known volume V_d one can calculate the drop height h (Eq. 17), sphere radius R (Eq. 18) and than, from the Eq. 19, a solid-liquid contact angle θ.

$$a = \sqrt{S_{wet} / \pi} \qquad (16)$$

$$V_d = 1/6\pi h(3a^2 + h^2) \qquad (17)$$

$$R = (h^2 + a^2)/(2h) \qquad (18)$$

$$\theta = 90 - \arccos[a / R] \qquad (19)$$

Average value of static contact angle θ between glass and water calculated from five measurements was 27.4°. Than the same glass material broken into 1cm pieces has been powdered by means of agate mill. The fraction 90 –1000 micrometer has been separated for farther experiments. Glass powder was packed into a glass column of 30 mm in diameter and 420 mm height. After filing the column the 50 Hz vertical oscillations have been applied to the column wall which compacted the powder to the needed bulk density. The oscillation amplitude was about 1- 1.5 mm. The bottom of the column was covered by means of highly permeable textile. Than the standard capillary rise procedure has been applied to follow the kinetics of wetting front in vertical column of glass bead [12].

Tab.1. The apparent contact angle and the pore radius for glass beads and soils calculated from capillary rise experiments

Medium particle radius r [10^{-6} m]	Porosity [v/v]	Apparent pore radius [10^{-6} m]	Apparent contact angle [deg]	True contact angle [deg]
glass beads 45<r<157	0.326	8.79	77.6	-
glass beads 45<r<157	0.367	9.44	76.2	-
glass beads 45<r<157	0.33	6.8	75.2	-
glass beads 45<r<157	0.38	7.67	79.1	-
glass powder 45<r<500	0.30	33.7	80.3	27.4
glass powder 45<r<500	0.35	42.1	79.5	27.4
glass powder 45<r<500	0.39	49.6	79.4	27.4
moorsh [14]	-	-	72.8[1]/88.2[2]	-
reed peat [14]	-	-	71.1[1]/87.6[2]	-
alder peat [14]	-	-	74.1[1]/88.8[2]	-
loamy sand	0.38	-	69-72	-

(1)   equilibrium method [11], (2)- dynamic method [12]

It worth to mention that the wetting front during the capillary rise process was not flat and its shape became more and more irregular. In some cases at the end of raising the difference of capillary rise heights observed at the column perimeter reached 2-3 cm. So the position of wetting front has been calculated as the

average value of four readings taken from four sides of the column. To find out the value of A and B parameters from Eq. 20 the fitting procedure of non linear estimation using Rosenbrock - quasi Newton method (Statistica 5 package) was applied to the experimental data: rising time T and capillary rise height x. Than the values of apparent CA and pore radius have been calculated for all investigated media. The results are shown in **Table 1.**

Conclusions

Variable cross-section area is a common feature of soil pores. Capillary movement of water in them is depended not only on size but on shape of the pores as well. Simple axis- symmetrical sinusoidal model of inter-grain micro channels has been applied to quantify the influence of non-cylindrical pore shape on capillary rise movement of liquid. Analytical form of capillary pressure and of liquid conductivity has been found what allowed simulating the meniscus rising in such capillaries for a range of true contact angles and of different shapes of them. Application of the cylindrical capillary model to the results obtained from sinusoidal one gave the possibilities to estimate the influence of the pore shape (waveness) on the capillary rise movement of liquid. The contact angle and the pore radius values have been calculated for a range of capillary shapes. It was found that both are highly depended on capillary shape. The values of such CA are strongly increasing function of wall wavenees and of true CA. In contrast the calculated radius is decreasing function of capillary wavenees and its values can be even smaller than the neck size (r_2 - r_1).

Above conclusions have been qualitatively confirmed by the experiments curried out on glass beads and soils. The CA values calculated from capillary rise experiments data and cylindrical model give the CA values in the range 70-85 degrees for glass beads and even higher for peat soil, while the experimentally determined true CA value for a glass plate was 27.4 degrees while the calculated one related to glass powder was about 80. The range of CA values presented in **Table 1** is rather small taking into account the origin of the materials. This fact can be treated as the confirmation of the our opinion that in the case of porous media the CA calculated from cylindrical model is/(can be) more depended on pore structure than on true CA [13].

Liquid-solid contact angle in soil based on the Washburn equation is some times called the apparent one. Presented results explain the meanings of this term – for porous media like soils its value is depended not only on interface tensions between soil phases and organic matter content but on the pore geometry as well.

30

The above results can be summarized as fallow: the pore topology is an important factor determining the wettability and the repellency of soils.

References

1. **Bautersa T.W.J., Steenhuisa T.S., DiCarlob D.A., Nieberc J.L., Dekker L.W, Ritsemad C.J., Parlangea J.-Y., Haverkampe R.:** Physics of water repellent soils. Journal of Hydrology, 231–232, pp. 233–243, 2000.
2. **Bayramili E., van der Ven T.G.M., Mason S.G.:** Tensiometric studies on wetting. I. Some effects of surface roughness (theoretical). Can . J. Chem. 59, pp.1954-1961, 1981.
3. **Buchmann J., Ellies A., Hartge K.H.:** Development and application of a new sessile drop contact angle method to assess soil water repellency. Journal of Hydrology, 231-232, pp. 66-75.2000.
4. **Buczko U., Bens O., Fischer H., Huttl R.F.:** Water repellency in sandy luvisols under differe nt forest transformation stages in northeast Germany. Geoderma 109, pp. 1– 18, 2002.
5. **Czachor H., Gozdz A.:** Modelling of granular and cellular materials. Transaction of the ASAE., 44 2, pp.439-445, 2001.
6. **Czachor H.:** Essais sur modele de l'influence d'hydrophobisation de surface et de geometrie de la phase solide du milieux poreux sur la tension capillaire. Zesz. Probl. Post. Nauk Rol. z. 312, 1986.
7. **Doerr S.H., Shakesby., R.A., Walsh R.P.D.:** Soil water repellency: its causes, characteristics and hydro-geomorphological significance. Earth-Science Reviews 51, pp. 33–65, 2000.
8. **Dullien F.A.L., El-Sayed M.S., Batra V.K.: J.:** Colloid Sci., 60, 3, pp.497-506, 1977.
9. **Haines W.B.:** J. Agric. Sci. 17, 264, 1927.
10. **Jaramillo D.F., Dekker L.W., Ritsema J. C.J., Hendrickx M.H.:** Occurrence of soil water repellency in arid and humid climates, Journal of Hydrology 231–232, pp. 105–111, 2000.
11. **Letey J., Carrillo M.L.K., Pang X.P.:** Approaches to characterize the degree of water repellency. Journal of Hydrology 231–232, pp. 61–65, 2000.
12. **Malik R.S., Kumar S., Danhiya I.S.:** An approach to quick determination of some water transmission characteristics of porous media. Soil Sci., 137(6), pp.395-400, 1984.
13. **Philip J.R.:** Limitations on scaling by contact angle. Soil Sci. Amer. Proc. 34, pp. 507-509, 1971.
14. **Scott D.F.:** Soil wettability in forested catchments in South Africa as measured by different methods and as affected by vegetation cover and soil characteristics. Journal of Hydrology 231–232, pp. 87–104, 2000.
15. **Siebold A., Nardin M., Schultz J., Walliser A., Oppliger M.:** Effect of dynamic contact angle on capillary rise phenomena. Colloids and Surfaces A: Physicochemical and Engineering Aspects, 161 (1), pp. 81 – 87, 2000.
16. **Staples T. L., Shaffer D.G.:** Wicking flow in irregular capillaries Colloids and Surfaces A: Physicochemical and Engineering Aspects 204, pp. 239–250, 2002.
17. **Tschapek M.:** Criteria for determining the hydrophilicity–hydropobicity of soils. Zeitschrift fur Pflanzenernaehrung und Bodenkunde 147, pp.137–149, 1984.

18. **Wang Z., Wu L., Wu Q.J.:** Water-entry value as an alternative indicator of soil water-repellency and wettability. Journal of Hydrology 231–232, pp.76–83, 2000.
19. **Waniek E., Szytałowicz J., Brandyk T.:** Determination of soil-water contact angle in peat-moorsh soils by capillry rise experiments. Suoseura –Finnish Peatland Society, 51(3), pp. 149-154, 2000.
28. **Watson C.L., Letey J., Mustafa M.A.:** The influence of liquid surface tension and liquid-solid contact angle on liquid entry into porous media. Soil Sci. 112, 3, 1971.

ON SOME THERMAL CHARACTERISTICS OF THREE COMMON SOILS IN BULGARIA

Doneva[1] Katerina, Ilieva[1] Vesselina, Marinova[2] Tania

[1] Institute of Soil Science, Sofia, Bulgaria
caeruleus2001@yahoo.com
[2]National Institute of Meteorology and Hydrology, Sofia, Bulgaria

Abstract

The thermal diffusivity and thermal field of three common soils in Bulgaria were investigated in this study. The thermal diffusivity was determined by indirect method on the basis of data from standard soil temperature measurements in meteorological stations of the National Institute of Meteorology and Hydrology. For this purpose theoretical model based on the heat conduction equation was used. The type of the studied soils, their mechanical composition and chemical properties were determined in laboratories of the Institute of Soil Science. The influence of the soil type, mechanical composition and amount of humus and hygroscopic moisture on the thermal diffusivity was investigated.

K e y w o r d s *:* thermal characteristics of soil, thermal diffusivity, soil temperature, mechanical composition and chemical properties of soil.

Nomencluture

λ – thermal conductivity, J m^{-1} s^{-1} °C^{-1};

C – heat capacity per unit volume, J m^{-3} °C^{-1};

c – specific heat capacity, J kg^{-1} °C^{-1};

ρ – density, kg m^{-3};

a – thermal diffusivity, m^2 s^{-1};

T – soil temperature, °C;

$\overline{T}$ – mean annual temperature of the soil surface, °C;

A_0 – amplitude of the soil surface temperature variations, °C;

z – vertical coordinate, m;

τ – period of soil temperature variations;

ω – cyclic frequency of the temperature variations, s^{-1};

$A(z_i)$ – amplitude of the soil temperature variations at depth z_i, °C

Introduction

Mass and heat flows in soil are dynamic processes. This situation is due to the soil itself, as it is a dispersive multi–component medium, and to the plants and climate. Specific physical conditions of soil depend to a considerable extent, on its physical properties [10]. The thermal conductivity λ and the heat capacity per unit volume, $C = c\rho$ (c is specific heat capacity and ρ – density) are the basic thermal characteristics of the soil. A secondary parameter is the thermal diffusivity a of the soil.

Heat capacity per unit volume of soil depends on the heat capacity of the individual components of the soil and is equal to the sum of such component capacities, while thermal conductivity of the soil is not directly related to the values of thermal conductivity of the individual soil components, but depends also on the distribution of soil particles in space [2,9].

The thermal conductivity of the soil depends primarily on the soil moisture. In the initial range of moisture content it increases only slightly, since water put in dry soil is first absorbed on the surface of mineral particles [8].

The thermal diffusivity of the soil is the quotient of the thermal conductivity and the heat capacity per unit volume of the soil

$$a = \frac{\lambda}{C} \tag{1}$$

It determines the capability of the soil to equalize the temperature at all the points of the object under study, and in terms of numbers equals the rate of temperature change at a given point in the soil, caused by a unit change in the temperature gradient. The thermal diffusivity is related primarily to the soil moisture. The relationship is a complex as when wetting dry soil the increase in the thermal conductivity is faster than the increase in the heat capacity. Further wetting of the soil results in smaller and smaller increases in the thermal conductivity, while the heat capacity increases steadily at an unchangeable rate. When the rate of increase in the heat capacity with increasing soil moisture is greater than the rate of increase in the thermal conductivity, a decrease in the thermal diffusivity is observed. Therefore, the thermal diffusivity reaches its maximum at soil moisture and density levels typical for a given soil. At such soil moisture and density values the rate of "temperature wave" propagation in the soil is the highest [1,9].

Material and methods

In this study the thermal diffusivity and the thermal field of three common soils in Bulgaria – Leached Smolnitza, Leached Chernozem, and Calcareous Alluvial Meadow soil, were investigated. For this purpose data from the standard measurements of soil temperature at depths of 0.02 m and 0.20 m in three meteorological stations of the National Institute of Meteorology and Hydrology (NIMH) of Bulgaria, were used: Sofia–CMS, General Toshevo and Ivailo. Also soil samples from the layer 0.05 − 0.10 m were taken in the vicinity of the soil thermometers, positioned on the grassed ground of the meteorological stations. The type of the studied soils was determined as follows:

Sofia–CMS: Leached Smolnitza, (*Eutric Vertisol* [3])
General Toshevo: Leached Chernozem, (*Luvic Chernozem* [3])
Ivailo: Calcareous Alluvial Meadow soil (*Calcaric Fluvisol* [3])

Particle size distribution, $pH_{(H_2O)}$, $pH_{(Kll)}$, hygroscopic moisture, and chemical composition: soil organic matter (humus), amount of carbonates, mineral forms of Nitrogen, P_2O_5, K_2O of the soil samples were also determined. The data are presented in **Table 1** and **Table 2**.

Table 1. Mechanical composition in % (particle size distribution data) in dry matter

Sample location and depth in m NIMH	Loss at reaction with HCl							
		Sum >1	1.00– 0.25	0.25– 0.05	0.05– 0.01	0.01– 0.005	0.005– 0.001	<0.001	Sum <0.01
Sofia–CMS 0.05–0.10	0	0.0	5.5	14.2	20.6	12.2	9.9	37.6	59.7
G. Toshevo 0.05–0.10	0	0.0	0.3	7.1	42.4	19.4	11.8	19.0	50.2
Ivailo 0.05–0.10	0	3.2	16.1	35.2	18.1	12.4	7.4	7.6	27.4

The thermal diffusivity a was calculated for the different soils included in this study, by using the temperature wave method and soil temperature data on the basis of the theoretical model, developed in [6] and based on the heat conduction equation:

$$\frac{\partial T}{\partial t} = a \frac{\partial^2 T}{\partial z^2} \tag{1}$$

where T is the soil temperature, t is the time and z – the vertical coordinate.

Table 2a. Chemical properties of the soils

Sample location and depth [m]		Hygroscopic moisture [%]	Humus [%]	pH (H₂O)	pH (KCL)
NIMH					
Sofia–CMS	0.05–0.10	7.48	6.86	6.3	5.5
G. Toshevo	0.05–0.10	4.54	5.17	6.7	5.7
Ivailo	0.05–0.10	2.62	4.45	7.1	6.2

Table 2b. Chemical properties of the soils

Sample location and depth [m]		Carbonates [%]	Mineral forms of Nitrogen [mg/kg]		P_2O_5 [mg/100g]	K_2O [mg/100g]
NIMH			NH_4^+	NO_3^-		
Sofia–CMS	0.05–0.10	0.0	9.05	1.34	2.4	41.5
G. Toshevo	0.05–0.10	0.0	11.73	4.02	3.3	47.1
Ivailo	0.05–0.10	0.77	8.38	2.34	5.2	45.8

The solution of Eq. 1 was obtained at constant thermal diffusivity and without initial condition as the soil surface temperature was accepted as a simply periodic function of time:

$$T = \overline{T} + A_0 \cos \frac{2\pi}{\tau} t$$

where: $\overline{T}$ is the mean annual temperature of the soil surface, τ – the period of the temperature variations (in this case one year), A_0 – the amplitude of the temperature variations. Furthermore it was accepted that the annual variations of temperature abate at some depth in the soil. At these boundary conditions the solution of (1) has the form:

$$T(z,t) = \overline{T} - \frac{A_0}{2} e^{-\sqrt{\omega/2a}z} \cos(\sqrt{\omega/2a}z - \omega t) \tag{2}$$

where: $\omega = \frac{2\pi}{\tau}$ is the cyclic frequency of the temperature variations.

The procedure for determining the thermal diffusivity by using the soil temperature data is described in details in [4,5]. On the basis of (2) a formula for calculating the thermal diffusivity of soil was obtained in the form:

$$a = \frac{\omega(z_{i+1} - z_i)^2}{2\ln^2 \dfrac{A(z_{i+1})}{A(z_i)}} \tag{3}$$

where: $A(z_i)$ and $A(z_{i+1})$ are the amplitudes of the annual soil temperature variations on two consecutive depths z_i and z_{i+1}.

In this work the thermal diffusivity of different soils was calculated by formula (3) for the soil layer $0.02 - 0.20$ m. The amplitudes of the annual variations of soil temperature at depths of 0.02 and 0.20 m were determined on the basis of daily values of soil temperature, measured in the meteorological stations Sofia–CMS, General Toshevo and Ivailo in the period 1993–2002.

Results and discussion

In order to calculate the thermal diffusivity, the annual course of soil temperature is graphically presented for every station and every depth in **Fig. 1**–**Fig. 3** by the corresponding mean daily long-term values, approximated with polynomial of 5th degree by the method of least squares.

To make the calculations easier the consecutive days of the year (from 1 to 365), divided by 10^2 are plotted along the abscissa of the graphs in **Fig. 1**–**Fig. 3**. Also the interpolation curves (the smooth curves) and corresponding equations are presented.

By the interpolation curves in figures 1–3 the mean long-term amplitudes of the annual soil temperature variations were determined for each of the stations at depths of 0.02 and 0.20 m, which were used to calculate the thermal diffusivity applying formula (3). Thus, mean values of the thermal diffusivity for the layer $0.02 - 0.20$ m of the studied soils were calculated, and the results are shown in **Table 3**.

Table 3. Thermal diffusivity of the studied soils

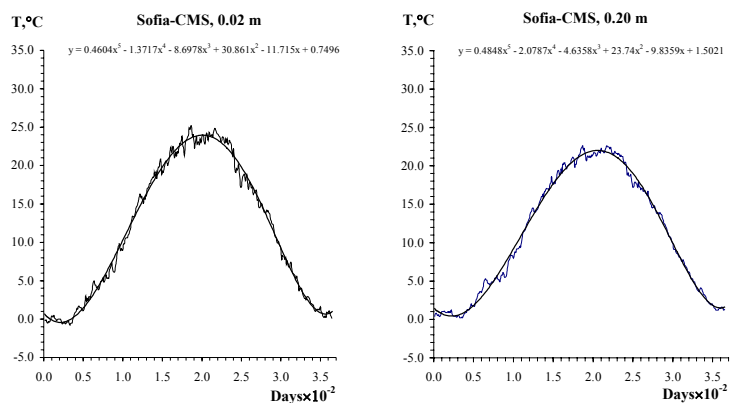| Meteorological station	Type of the soils	Thermal diffusivity [$m^2\,s^{-1}$]
Sofia– CMS	Leached Smolnitza	2.13×10^{-7}
General Toshevo	Leached Chernozem	3.86×10^{-7}
Ivailo	Calcareous Alluvial Meadow soil	2.25×10^{-7}

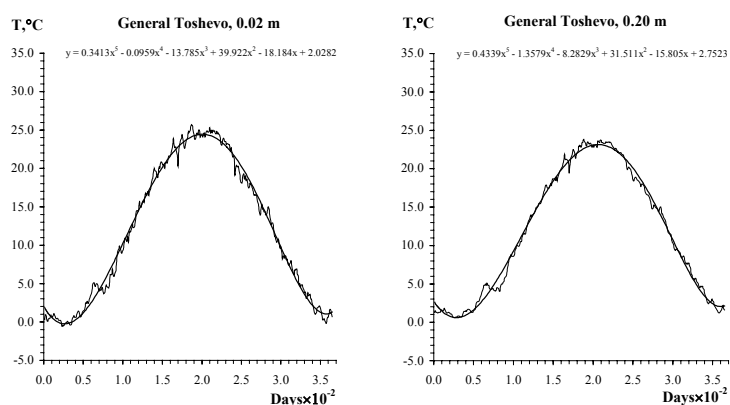**Fig.1.** Annual course of soil temperature in Leached Smolnitza

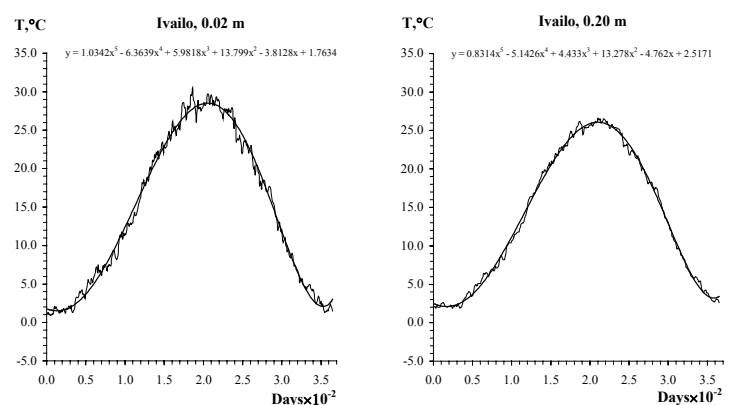**Fig.2.** Annual course of soil temperature in Leached Chernozem

Fig.3. Annual course of soil temperature in Calcareous Alluvial Meadow soil

It can be seen that the value of the thermal diffusivity for Leached Chernozem is the highest, followed by that of the Calcareous Alluvial Meadow soil. The value of a is the lowest for the Leached Smolnitza. The results obtained in the present study are similar to the results of other authors, which studied the influence of soil type on the thermal diffusivity [5,7].

By its mechanical composition the Leached Chernozem (with the highest value of the thermal diffusivity) is characterized with the highest percent of particles with size of 0.05 – 0.01 mm, coarse silt (**Tab. 1**), followed by the amount of particles with size of 0.01 – 0.005 mm, which is medium silt. The sum of the particles with size less than 0.01 mm is 50.2%. The soil with the lowest value of the thermal diffusivity is the Leached Smolnitza, which has the highest content of particles with size less than 0.001 mm (**Tab. 1**), after it is the fraction with particle size of 0.05 – 0.01 mm, the coarse silt. Sum of the particles with size less than 0.01 mm is 59.7%.

Humus amount is the highest in the Leached Smolnitza, followed by those in the Leached Chernozem and Calcareous Alluvial Meadow soil (**Tab. 2a**). The values of the thermal diffusivity are 2.13×10^{-7}, 3.86×10^{-7} and $2.25 \times 10^{-7} \text{m}^2\text{s}^{-1}$ respectively. It was found that the thermal diffusivity decreases with increasing of the humus amount. The same tendency is observed with the hygroscopic moisture percentage.

Conclusions

Mean values of the thermal diffusivity were obtained for three broadly distributed soils in Bulgaria: Leached Chernozem, Calcareous Alluvial Meadow soil and Leached Smolnitza, by indirect method. For this purpose theoretical model based on heat conduction equation with constant thermal diffusivity and soil temperature data for the decade 1993-2002 were used.

Also the mechanical composition and chemical properties, $pH_{(H_2O)}$, $pH_{(Kll)}$, hygroscopic moisture, humus amount, carbonates, mineral forms of Nitrogen, P_2O_5, and K_2O were determined for each of the studied soil types. It was found that the Leached Smolnitza was characterized with the lowest thermal diffusivity and the highest content of particles with size less than 0.001 mm. The Leached Chernozem (with the highest value of the thermal diffusivity) has the highest percent of particles with size of 0.05 – 0.01 mm. Thermal diffusivity decreases with increasing of the humus amount. The same tendency is observed with the hygroscopic moisture percentage.

References

1. **Chudnovski A. F.:** Heat transfer in dispersion media (in Russian). Gostehizdat, M-L, 1964.
2. **De Vries D. A.:** Thermal properties of soils. Physics of Plant Environment (Ed. W. R. van Wijk) North-Holland, Amsterdam, 210–235, 1963.
3. **FAO**, Revised Legend, Rome, 1991.
4. **Marinova T.K., Sharov V.G., Slavov N.S.:** On the Modelling of the Soil Temperature Variations (in Russian). Bulgarian Journal of Meteorology & Hydrology, 1, 44–47, 1990.
5. **Marinova T.K.:** On Determination of Conductivity Coefficient of the Main Soils in Bulgaria (in Russian). Bulgarian Journal of Meteorology & Hydrology, 4, No 2, 65–69, 1993.
6. **Slavov N., Sharov V., Marinova T.:** Study of the Variation of Temperature with Soil Depth (in Bulgarian). Problems of Meteorology and Hydrology, 6, 46–55, 1989.
7. **Stanev S., Tanov E.:** On the thermal diffusivity of some soil types in Bulgaria (in Bulgarian). Proceedings of the Institute of Hydrology and Meteorology, 4, 131–147, 1965.
8. **Usowicz B.:** Studies on the dependence of soil temperature on its moisture in field (in Polish). Ph. D. Thesis, University of Agriculture, Lublin, Poland, 1991.
9. **Usowicz B.:** A method for the estimation of thermal properties of soil. Int. Agrophysics, 7, 27–34, 1993.
10. **Walczak R., Usowicz B.:** Variability of moisture, temperature and thermal properties in bare soil and in crop field. Int. Agrophysics 8, 161–168, 1994.

AGROPHYSICAL METHODS AND MICROCOMPUTER SYSTEMS FOR EVALUATION AND MANAGEMENT OF PROPERTIES OF THE SOIL-PLANT-ATMOSPHERE SYSTEM IN THE AGRICULTURAL FIELD
Kolev Nikola

Institute of Soil Science "Nikola Poushkarov", Sofia, Bulgaria
nvkolev@mail.bg

Introduction

The modern agricultural research and practice need quantitative information about the main soil properties of the open field. Many of the processes essential to soil and to plant growth, such as transpiration, evapotranspiration, exchange of heat and moisture, depend significantly on the soil surface and canopy foliage.

Numbers of authors (Ludlow and Fisher, 1976; Bazza et al., 1988) illustrate by field data, the influence of canopy structure, leaf orientation, and height of canopy on the soil surface temperature. It also depends on the soil moisture and solar radiation. Drying of the soil can elevate soil surface temperature, causing an increase of moisture and temperature gradients in the soil profile.

The practice of the irrigation control in Bulgaria has to be changed radically to meet the requirements of the new economical and ecological situation caused by the restitution of the private ownership of the land and the free market orientation of the whole Bulgarian economy during the last few years. The proper irrigation could be done effectively only on the basis of a reliable information on the "soil - plants - atmosphere" continuum by measuring soil moisture, soil temperature, wind velocity, solar radiation and some other variables.

Having an evaluation of surface energy balance components in the fields and calculated evapotranspiration is not difficult to organise an automated control of irrigation. The use of automated irrigation systems becomes optimal and their economic justification is the increased production resulting from the high quality water application.

A number of authors describe different methods and instruments to estimate the evapotranspiration based on the measurement of energy balance components. Kalma and Jupp (1990) describe a field evaluation of the sensible heat flux, latent heat flux and the flux density of water vapour.

Brunel (1989), Vogt and Jaeger (1990), Pieri and Fuchs (1990) use the aerodynamic method and method of thermal infrared emission of natural surface to estimate latent heat flux and evapotranspiration.

Sanoyan (1982), Ashktorab *et al.* (1989), *Ham et al.* (1990), Pieri and Fuchs (1990) determine evapotranspiration by measuring the surface energy balance of the field using the Bowen ratio method.

Each of the authors gives an account of different instruments to measure temperature, humidity, wind velocity and other meteorological elements. These instruments do not work as a complete measurement system.

Chudnovski (1966) and Sanoyan (1982) describe automatic systems measuring meteorological elements and calculating the evapotranspiration based on the surface energy balance of the field. It is important that all measurements are carried out consecutively in time. When it is necessary to calculate temperature and water vapour differences the process of measurement should be fast. The major difficulty associated with the approach is that the instrumentation must detect small changes of the magnitude.

It is important to irrigate when the agrometeorological conditions are appropriate. Many authors pointed out that sprinkling is effective only when the wind velocity is less than 6-7 ms^{-1} or the solar radiation is not more than 800-900 W/m^{-2}, to prevent the risk of plant diseases. From the other hand many crops (wheat, potato, tomato, maize, *etc*) need refreshing sprinkling when the air temperature is high and the relative humidity is very low.

The present paper describes a possibility to use agrophysical methods and microcomputer agrometeorological systems for evaluation of main properties of the soil - plant - atmosphere system in the field.

Theoretical considerations

The soil properties have different values in different zones of the agricultural field. No effective method for evaluating one or other property distribution is established, but there is an opportunity to use a pattern for an ordered set of closed isolines. In other words, it is possible to consider the unhomogeneous field as numerical homogeneous zones displaying these with tree-root structure (**Fig. 1**), a concept first suggested by Uchitomi and Mine (1988).

Out of the soil properties, let us consider only the soil moisture, W_S; the conclusions will be referred to soil temperature, salinity, etc.

In the agricultural field we can find regions, H_i, with high moisture, W_{si}^1, and regions, L_i, with low moisture, W_{si}^2. Then:

$$H_i \in S_o \text{ and } L_i \in S_o \tag{1}$$
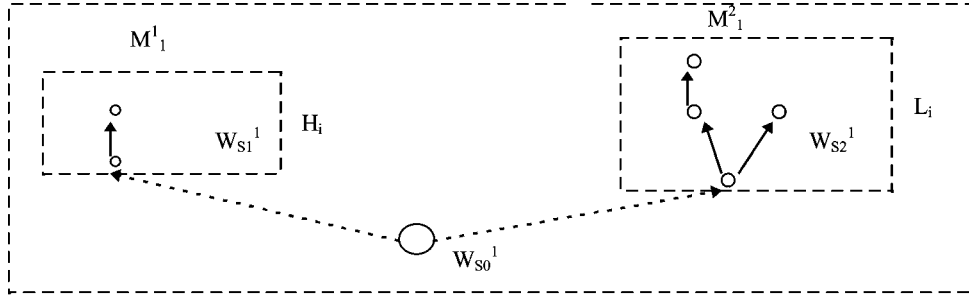
Fig.1. Soil moisture picture of unhomogeneous field with homogeneous zones M_1^1 and M_2^1.

Getting the patterns; M_o of the region S_o, M_i^1 of the region H_i, M_2^1 of the region L_i, we can write:

$$M_o = \{C_k(W_S) \mid W_S^1 < W_S < W_S^2, k = 1, 2, 3, ..., \} \qquad (2)$$

$$M_i^1 = \{C_k(W_S) \mid W_S^0 < W_S < W_S^2, k = 1, 2, 3, ..., \} \qquad (3)$$

$$M_i^2 = \{C_k(W_S) \mid W_S^1 < W_S < W_S^0, k = 1, 2, 3, ..., \} \qquad (4)$$

where: $C(W_S)$ are the isomoisture closed lines at a moisture W_S, W_S^1 is the maximum of the moisture W_S, W_S^2 is the minimum moisture and W_S^0 is the background moisture at the S_0 region. M_i^1 is high moisture pattern set and M_i^2 is low moisture pattern set and

$$M_i^1 \in M_0 \text{ and } M_i^2 \in M_0. \qquad (5)$$

The values of the soil moisture W_S for high and low moisture regions (W_S^1 and W_S^2) and the whole set W_S^0 can be presented in tree-root structures as shown for W_S^1 in **Fig. 1**.

We can write:

$$W_S^0 = f(W_S^1, W_S^2) \qquad (6)$$

Canopy structure is another factor setting restrictions on the homogenity of the soil properties. The soil moisture and the soil temperature, for example, differ under the plants and between the rows of row-crop canopies, and depend on the fraction of soil surface exposed to direct sunlight. We can calculate the area of this fraction based on the relationship between the sunlight transpiration, leaf area index and leaf angle distribution. The concept of this relationship first has been suggested by Monsi and Saeki (1953) and can be approximated by Beer's Low.

Based on the reliable estimation of homogeneous areas and sunlit and shadowed fractions in these areas, a scheme for spatial distribution of sensors for

contact electronic measurements in a single representative area of row-crop canopy can be arranged.

Measurement methods and instrumentation

Independent measurement of the surface energy balance components in the agricultural fields helps to calculate the soil evaporation and canopy transpiration. This operating mode requires reliable estimates of evapotranspiration based on relatively simple measurements under field conditions. It concerns both continuous measurement of the basic variables of the agrometeorological condition in the field, and supplying information for irrigation control on the base of the estimated conditions.

The sensors and electronic devices used for measurements have been designed to operate long time in field conditions. Gypsum-type blocks PVGTV-3, made in "N.Poushkarov" Institute (Kirkova Y., 1984), were used for soil moisture measurements. Semiconductor diodes sealed in the gypsum blocks as soil temperature sensors produce junction electrical resistance proportional to the temperatures of the soil profile. A sensor consisting of two-metal electrode system joined with temperature sensible microdiode, all in a ceramic body, has been designed to monitor the soil salinity in the field.

An alternating current digital bridge, battery supplied, and made in "Nikola Poushkarov" Institute of Soil Science and Agroecology (Kolev *et al.*, 1985), was used with the specifically calibrated sensors of soil moisture, temperature and salinity. Temperature measurements of the soil surface were obtained by an infrared distant thermometer, Raynger II-AG type. A portable pH-meter, Metrohm type, was used for evaluation of pH of the soil solution in the field. The soil and air temperature and the humidity were measured by "Grant" Squirrel meter/logger.

After comparative analysis of the energy balance method and the aerodynamic method for estimation of the evapotranspiration under field conditions Sanoyan (1982) recommends the energy balance method.

Many authors (Ashktorab, 1989, Kalma, 1990, Ham, 1990) use a set of sensors and portable devices for measurement of the soil heat flux, soil and air temperature and humidity, wind velocity, net radiation. Other (Chudnovski, 1966, Sanoyan, 1982, Kolev *et al.*, 1988, Pieri, 1990, Abramov *et al.*, 1990) use special designed measurement systems for these purposes. The devices and systems mentioned here cannot measure simultaneously all of the parameters which are necessary for calculation of evapotranspiration. The readout from each sensor is

obtained in contiguous moments of time. That introduces a truncation error in estimation of the evapotranspiration.

For avoiding the indicated above disadvantages of measurement we organized a microcomputer system with parallel interface of the measurement channels (Kolev *et al.*, 1988). The system gives simultaneous readings of the energy balance elements. The block-diagram of the system is shown in **Fig. 2**.

```
┌─────────────────────────────┐      ┌─────────────────────────────┐
│  GROUP OF SOIL SENSORS      │      │                             │
│  W_S1, W_S2, T_S1, T_S2     │      │  GROUP OF  AIR SENSORS      │
└─────────────────────────────┘      └─────────────────────────────┘
         ↓ ↓ ↓ ↓                          ↓ ↓ ↓ ↓ ↓ ↓
┌─────────────────────────────┐      ┌─────────────────────────────┐
│  MEASUREMENT CHANNELS       │      │  MEASUREMENT CHANNELS       │
│          FOR                │      │          FOR                │
│  W_S1, W_S2, T_S1, T_S2, G  │      │  R, Q, Q_0, e_a1, e_a2, T_a1, T_a2 │
└─────────────────────────────┘      └─────────────────────────────┘
              ↓                                   ↓
┌──────────────────────────────────────────────────────────────────┐
│        MULTICHANNEL PARALLEL ADC WITH MEMORY                      │
└──────────────────────────────────────────────────────────────────┘
        ↓         DATA              ADDRESS        ↑
                  BUS                 BUS
┌──────────────────────────────────────────────────────────────────┐
│                  PERSONAL MICROCOMPUTER                           │
└──────────────────────────────────────────────────────────────────┘
```
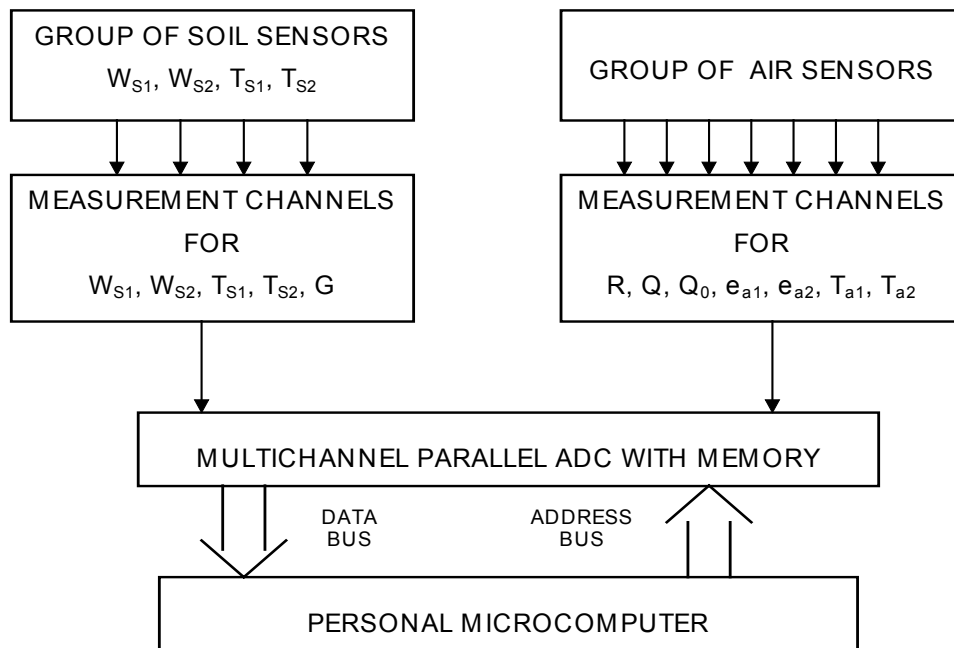
Fig.2. Block diagram of the microcomputer system with parallel interface of the measurement channels

The measurements of the air temperature, and humidity at two levels and over the soil surface or canopy, net radiation, soil heat flux and wind velocity are carried out. The instantaneous values are converted simultaneously by a multichannel AD converter and memorised. Then the data gathered is read-out in continuous moments of the time.

All sensors are designed in the Institute of Agrophysics in Leningrad USSR. The aspirate psychrometers are Balansomer BM-2 type. The soil heat flux is measured by a Toplomer heat flux plate.

The lower psychrometer was at 0.5 m above the soil surface or the canopy. The higher psychrometer was at 1.5 m above the first. The humidity at both heights and is calculated from the dry and wet temperatures obtained by the

psychrometers with vertical aspiration. The ventilation speed of the psychrometers is in the range of 3 - 5 m.s^{-1}. The radiometer was located at 1 m above the soil surface or canopy. The wind velocity sensor was at 3 m above the soil surface. The flux plate was positioned at 0.05 m below the soil surface.

The measurements are taken over a 1-minute period followed by 3 in pause. After calculation of the evapotranspiration and the heat flux the results are memorised by the computer. The evapotranspiration from the field is determined every 3 min. Every hour the average data of evapotranspiration is obtained from the microcomputer.

Results and discussion

Maize and cotton fields were selected where systematic electronic measurements of soil moisture, temperature, electrical conductivity and pH, were carried out during the period from May to September, 1995. The sites for the study were a pilot field of the National Aeronautic Research Centre near the city of Plovdiv, and a pilot field of the Cotton Institute in the city of Chirpan, both located in South Bulgaria. The soils are classified as tipic halpoxererts (near Plovdiv) and tipic calsixererts (near Chirpan), and contain 6 - 7% clay, 2.5 - 3% humus and with 1.2 - 1.3 gcm^{-3} density (Kolev *et al.*, 1995).

On 28 June 1995 the maize and cotton canopy had LAI near 0.7. These canopies contain lives oriented mostly at oblique angle of near 50°. On 28 June 1995, the solar zenith angle θ was 72° and the angle δ was 20°.

The gypsum blocks were buried at 20, 40, 60 and 80 cm depth, the gypsum temperature blocks were installed at 5, 10, 20 and 40 cm depth and the salinity ceramic blocks at 20 and 40 cm depth. The sensors were situated in the soil profile after drilling holes.

Soil moisture was measured within ±1% accuracy and soil temperature was measured within ±0.1°C accuracy.

Series of measurements were taken periodically in the beginning of every new phenophase during the vegetation of maize and cotton, and started after the sprout of the plants.

Soil moisture and temperature measurements were carried out in representative single areas of the fields at 9:00, 12:00 and 15:00 o'clock on the day and then were coupled with simple microclimatic evaluation of solar radiation, humidity, air temperature, wind velocity and cloudiness of the plot-fields based on standard climatic methods and equipment. Soil salinity and pH measurements were made one time a day.

Results of every day measurements of soil moisture, temperature, salinity and pH were computed for obtaining W_S^0, T_S^0, C_S^0 and pH^0 based on the above stated tree-root method.

A series of profiles of soil moisture in and between rows is presented in **Table 1** as a result of data obtained on 28 June 1995.

Table 1. Results of soil moisture W_S^0 of one-day measurements (28 June 1995) obtained by tree-root method

Site	Depth [cm]	W_S^0 [%] in a row	W_S^0 [%] between rows	Field capacity, [%]
Maize field near Plovdiv	soil surface	12.0	10.1	
	20	24.0	22.0	
	40	25.2	24.8	29
	60	26.1	25.9	
	80	26.0	26.0	
Cotton field near Chirpan	soil surface	18.2	16.0	
	20	25.6	19.4	
	40	27.0	25.2	35
	60	28.8	29.6	
	80	33.2	33.0	

The results of soil temperature measurements obtained on the same day are shown in **Table 2**.

Table 2. Results of soil temperature T_S^0 of one-day measurements (28 June 1995)

Site	Depth, [cm]	9:00 h T_S [^{0}C] in row	9:00 h T_S [^{0}C] between rows	12:00 h T_S [^{0}C] in row	12:00 h T_S [^{0}C] between rows	15:00 h T_S [^{0}C] in row	15:00 h T_S [^{0}C] between rows
Maize	soil surf.	25.2	26.6	33.0	37.0	36.0	39.1
field	5	24.6	25.7	30.0	33.1	30.3	33.0
near	10	23.0	25.0	27.5	29.5	29.0	29.5
Plovdiv	20	22.0	23.0	26.0	27.5	26.7	27.0
Cotton	soil surf.	26.3	30.1	40.0	44.6	40.2	42.6
field	5	25.4	27..9	32.5	35.0	33.0	35.1
near	10	25.0	27.0	27.4	31.9	27.3	28.3
Chirpan	20	23.2	25.0	25.1	25.2	26.0	26.3

The values of W_S^0 correspond to microclimatic conditions and they decrease systematically near the soil surface due to the intensive evapotranspiration. The maize canopy was in a phase of 6 - 7 leaves with LAI = 0.70, and the cotton was in a phase of 7 - 8 leaves with LAI = 0.65. The soil moisture content under the surface layer of the cotton field was high because of 8-litre rainfall the day before.

Table 3 contains data of microclimatic elements evaluated on this day.

Table 3. Results of microclimatic measurements on 28 June, 1995

Microclimatic elements	Dimension	9:00 h		12:00 h		15:00 h	
		Maize field	Cotton field	Maize field	Cotton field	Maize field	Cotton field
Solar radiation	W.m^{-2}	620	650	980	1000	960	950
Relative humidity	%	52.0	68.5	28.0	35.0	26.0	26.5
Air Tem-perature	°C	25.1	25.6	30.0	31.8	30.3	32.0
Wind velocity	m.s^{-1}	0.5	0.5	0.5	0.5	0	0
Cloudness	-	clear sky	clear sky	clear sky	clear sky	clear sky	clear sky

As can be seen, the air temperature for a sunny day is less than the temperature of the soil surface. The profiles of the soil temperature show the way it decreased with depth. The reduction rate depends on solar radiation, LAI and soil moisture content.

The results of electrical conductivity of the soil (EC) and pH of the soil solutions, obtained by the measurements on 28 June 1995, are shown in **Table 4**.

Table 4. Result of soil electrical conductivity and pH measurements on 28 June 1995

Site	Depth, cm	Electrical conduct. EC (dS/m)	PH
Maize field	20	0.32	6.7
near Plovdiv	40	0.16	6.9
Cotton field	20	0.70	7.5
near Chirpan	40	0.30	8.0

Table 4 shows that the soil salinity of these unirrigated fields is nearly nominal throughout the growing season since no fertilizers had been applied to neither maize nor cotton.

The electrical conductivity of the soil is depending on the weather condition during the season.

Under conditions of water shortage in Bulgaria it is necessary to look for criteria and techniques for the most rational using of irrigation water. Thus information on the basic agrometeorological parameters (soil moisture, soil temperature, humidity and air temperature, solar radiation, rain/snowfall, etc.) within a growing area will be of great importance for the agronomists to come to correct decisions.

Several agrometeorological systems such as ARAX (Sampey, 1986), ALCYON DATA (ALD - manual, 1984) and systems developed in the Department of Agrophysics of the Poushkarov Institute of Soil Science and Agroecology (Kolev *et al.*, 1988), as shown in **Fig. 2**, have been installed in different regions in Bulgaria. These systems provide continuous measurements of 10 to 17 basic parameters characterising the state of the soil-plants-surface-air continuum.

The question is how such information should be structured and used for the purposes of the irrigation control.

The microcomputer systems used can be set up to collect the data at time intervals of 3 minutes to 4 hours. The more frequent is the data measured the more reliable is the information. But the frequent measurements need more power and reasonable compromise could be achieved.

An agrometeorological system with 6 satellite stations was montage in the agricultural field near Plovdiv in the South Bulgaria.

Table 5 shows a typical printout of one satellite station of the system in an apple orchard at 2:00 p.m. on 30 May, 1997.

Table 5. Typical printout of one satellite station of the system in an apple orchard at 2:00 p. m. on 30 May, 1997

ARAX satellite Station No2			
Channels	Parameters	Current report at 02:00 p.m.	Trend report average per hour
1	air temperature (z_1)	23°C	2.4 ^{o}C
2	air temperature (z_2)	25 ^{o}C	-
3	solar radiation	0.9 kW.h.m^{-2}	0.8 kW.h.m^{-2}
4	rel. humidity (z_{11})	43%	44%
5	rel. humidity (z_{12})	45%	-
6	wind velocity	1 m.s^{-1}	1 m.s^{-1}
7	rainfall	0 cm	0 cm
8	soil moisture (z_{01})	85%	85%
9	soil moisture (z_{02})	87%	-
10	soil temperature (z_{01})	18 ^{o}C	16 ^{o}C
11	soil temperature (z_{02})	15 ^{o}C	-

The soil moisture and the soil temperature are measured at different levels (*eg* at 20 cm and at 40 cm below the surface) according to the root zone of the given crop. The air temperature is measured at two levels above the soil surface.

Table 5 shows the so-called trend report about the hour information stored in the personal computer memory during the day.

Table 6 gives the trend report of the daily information of the first decade of March 1987 stored for the current month period in the memory.

Table 6. Trend report of the daily information of the first decade of March 1987

			ARAX satellite Station No 2				
May 1988 Days	Solar rad. [kW]	Air temp. [°C]	Rel.hum [%]	Soil moist. [%]	Soil temp. [°C]	Wind velosity [m,s⁻¹]	Rain fall [cm]
1	0.7	8	62	88	2	2.0	0.0
2	0.5	1	81	90	2	3.0	1.5
3	3.6	-9	59	88	1	0.5	0.0
4	4.7	8	50	88	1	1.5	0.0
5	3.4	-8	64	88	0	1.5	0.0
6	3.7	-8	66	88	0	0.5	0.0
7	3.8	-9	61	87	1	2.0	0.2
8	1.6	-6	76	85	0	1.5	0.0
9	3.6	-4	69	87	-1	4.5	0.0
10	4.3	-4	52	87	-1	4.5	0.0

The information about the basic agrometeorological parameters shown in **Table 5** helps the agronomist to estimate the current moisture and the temperature in the soil layer controlled. When the soil moisture is under the critical for the given crop he may take the decision to irrigate the crop area. The other parameters, which affect the decision such as the wind velocity, solar radiation and air temperature are of the great importance too.

In the case of sprinkler irrigation the agronomist should give attention to the critical values of the wind velocity because of the possible irregularity in water distribution over the area. The air temperature and humidity and the solar radiation will help to choose the moment to start the irrigation without danger of plant diseases.

Using the data in **Table 5** the agronomist can experimentally find the reasons for developing of certain disease or monitor various species of insect activity allowing more cost effective insecticide applications. Again air temperature and thermal summation can be used to increase awareness as to when pests occur, and

in this fashion help determine when to initiate looking for the insects in the field (the so called degree days method).

The computer agrometeorological systems measure a number of different parameters for which an alert condition can be implemented. That is to say, that for any one given sensor measurement a high and/or low limit can be set. Once set, the computer will initiate an alert message identifying a particular sensor that has exceeded its present limit.

An agronomist with a great professional experience using the daily averages given in **Table 6** can forecast the water needs of a growing area and to control the irrigation. Thermal summation, total solar radiation and precipitation's play an important role in forecasting crop growth, fertilization schedules and crop yield. So the computer meteorological systems can be strategically located within a growing area to accurately monitor pertinent growing information.

Conclusions

A way to manage electronic measurements for evaluation of soil properties at unhomogeneous fields based on tree-root method and a single representative area has been presented. Gypsum blocks for soil moisture and temperature, and salinity sensors, interfaced to alternating current bridge made at "Nikola Poushkarov" Institute, proved to be useful in soil profile measurements and in determination of the soil heat and water fluxes following rain or irrigation. These measurements combined with soil surface measurements done by an infrared thermometer can be widely used to evaluate the main components of the energy budget of the agricultural field.

The structure of the microcomputer measurement system with parallel interface of the measurement channels submitted above suggests a direct and correct estimation of the evapotranspiration from the field. The determination of the evapotranspiration by the energy balance method using the Bowen ratio allows measuring only some of the agrometeorological components. That's why the method and the measurement systems described are useful for the agricultural practice.

A number of the agrometeorological computer systems have been developed recently in the USA, Bulgaria and other countries. The structure of the information discussed helps the agronomists to forecast the water conditions in the field and to make right decisions for irrigation control. For practical application of the systems an estimation of the soil moisture in a representative spot in the is sufficient.

Since the systems monitor the weather conditions all the year round it's possible to create big databases, which characterize the agrometeorological situation in the field.

Results of the measurements indicate that the electronic devices and microcomputer systems described in the paper are functioning correctly and they are capable of measuring the properties and energy budget fluxes of the soil - plant - atmosphere system.

Analysis of the sensitivity of the means revealed just how necessary it is to use accurate values of the properties for their management in the field.

References

1. **Abramov V.G. Vichev N.:** Automated system for information retrieval and processing "IVK - agrometeorolog", Proceedings of the Symp., Leningrad, 1990.
2. **Alcyon Data** - Manual, Switzerland, 1985.
3. **Ashktorab H., Pruitt W. O., Paw K. T., George W. V.:** Energy balance determination close to the soil surface using a micro-Bowen ratio system, Agricultural and Forest Meteorology, 46, 259-274, 1989.
4. **Bazza M., Shumway H., Nielsen D.R.:** Two-dimensional Spectral Analysis of Soil Surface Temperature. Hilgardia, 56:1-28, 1988.
5. **Brunel J. P.:** Estimation of sensible heat flux from measurements of surface radiative temperature at two meters: application to determine actual evaporation rate, Agricultural and Forest Meteorology, 46, 179-193, 1989.
6. **Chudnovski A. F., Shlimovich B. M.:** Semi-conductors, radioelectronics and cybernetics in the agrometeorology, Gidrometeoizdat, Leningrad, 1966.
7. **Ham J. M., Heilman G., Lascano R. J.:** Determination of Soil Water Evaporation and Transpiration from Energy Balance and Stem Flow Measurements, Agricultural and Forest Meteorology, 52, 287-301, 1990.
8. **Kalma J. D., Jupp D. L. B.:** Estimation evaporation from pasture using infrared thermometer: evaluation of a one layer resistance model, Agricultural and Forest Meteorology, 51, 223-246, 1990.
9. **Kirkova Y.:** Development and Study of Sorption Soilmoisture Transducers. PhD thesis, Sofia. 1984.
10. **Kolev N.,** *et al*: Electronic Devices for Assessment of Soilmoisture. X World Congress of the IMEKO, Prague, 1985.
11. **Kolev N.V.,** *et al*: Mobile Microcomputer System for Agrobiological Parameters. Symp. Biotechnology and Biotechnics, Razgrad, Bulgaria. 1988.
12. **Kolev N.V**., *et al.* Space Distributed Land Surface Electronic Measurements for Evaluation of Soil Temperature. J. of Agricultural Eng., 6-8, 1995.
13. **Ludlow M.M. Fisher M.J.:** Influence of Soil Surface Litter on Frost Damage. Aust. Inst. Agric. Sci. J. 42:134-136, 1976.
14. **Monsi M., Saeki T.:** Uber den Lichtfaktor in den Pflanzengesell Schaten und Deine Beteuntung fue die Stoff Production,. Jpn J. Bot., 14:22-52, 1953.

15. **Pieri P. Fuchs M.:** Comparison of Bowen Ratio and Aerodynamic Estimates of Evapotranspiration, Agricultural and Forest Meteorology, 49, 243- 256, 1990.
16. **Sampey H.:** Installation and Operation ARAX Series: KD-4000, KD-2000. Hardware Vol.1. ARAX International Corporation, Vanderbilt, PA, USA, 1986.
17. **Sanoyan M. G.:** Agrometeorological and agrophysical principles and methods of the irrigation control, Gidrometeoizdat, Leningrad, 1982.
18. **Uchitomi S. Mine K.:** Intermittent Diagnostics of the Thermal Process by Means of Attention Subset Diagnosis Based on the Tree-Root Structure. Proceedings of the XI World Congress of IMEKO, Theory, Calibration, Houston, 271-278, 1988.
19. **Vogt R., Jaeger L.:** Evapotranspiration from a pine forest - using the Aerodynamic Methods and Bowen Ratio Method. Agricultural and Forest Meteorology, 50, 39-54, 1990.

SOIL SURFACE AND FOLIAGE TEMPERATURE MAPS O FA COTTON FIELD FROM SPATIAL INFRARED MEASUREMENTS

Kolev[1] Nikola, Ovcharova[2] Antonia

[1]Institute of Soil Science " N. Poushkarov", Sofia, Bulgaria
nvkolev@mail.bg
[2]Agricultural University, Plovdiv, Bulgaria

Introduction

A success of crop growing management in agriculture, connected with evaluation of basic soil-plant system properties in the field, depends on how well will be organised representative spatial distributed electronic field measurements. Data, collected by these measurements will help us to discover homogeneous zones of the properties in a nonhomogeneous agricultural field. Well-known is that the soil –plant system is a mixed class (Mishev, 1986, 1991; Thurnholm, 1990) and it is difficult to separate its individual elements. For a more complete interpretation of data of discrete temperature measurements, it is better to transform point discrete data to the soil–plant continuum (Nielsen *et al*., 1973; Webster, 1985; Kutilek and Nielsen, 1994) obtaining temperature maps, based on geostatistical methods.

The objective of this study is to obtain and to analyse soil surface and folliage temperature maps of a cotton field in South Bulgaria, based on results of space distributed measurements in 1998 and 2000.

Materials and Methods

Throughout the summer of 1998 and 2000 an experimental plot of cotton was grown on an agricultural field in South Bulgaria and area around the plot is a wide, flat plain. The vegetation period of the cotton is from 10-15 of April to the 10-15 of September and first one or two months canopy does not complitely cover the soil (LAI<1).

Measurements of soil surface and plant folliage temperature by infrared thermometer type Raynger II have been made in 80 measurement points along every measurement line (**Fig. 1**) expeditionally in the beginning of the basic cotton growing phases. Additionally, the soil profile temperature and moisture was measured with soilmoisture meter-thermometer with gypsum blocks at depths

of 10, 20 and 40 cm. Measurements of microclimatic variables have been made at a representative place of the plot by standard meteorological devices.
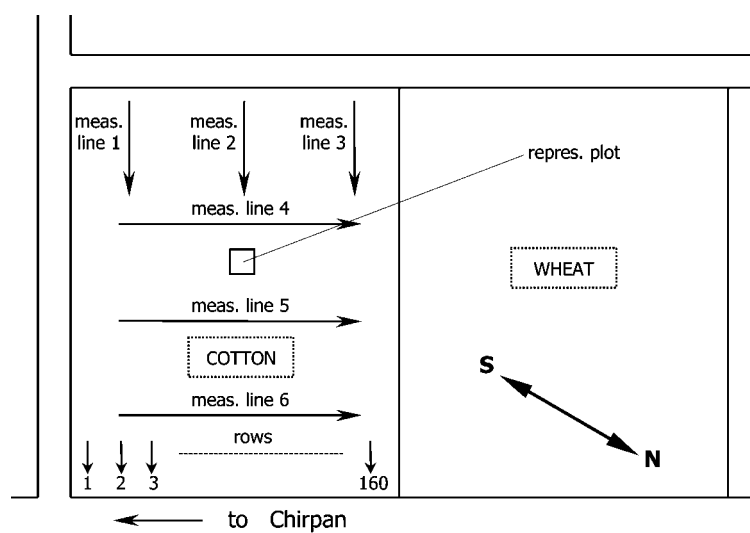

Fig. 1. A draft of the cotton field with measurement lines

Results and Discussion

The soil type identified on the agricultural field is powerful Chernozem-smolnitza. It has 68-70% physical clay in the surface horizon. Humus content is from 3.0 to 3.5%, decreasing in depth. Soil reaction is slightly alkaline, with pH from 6.5 to 7.0% in KCl. The ultimate field soil moisture capacity curs at 33-35 weight percent and volume dencity is 1.2-1.3 g/cm^3.

Table 1. Soilmoisture (% of FC) and temperature measurement results in 11:00 on the expedition days of 1998 and 2000

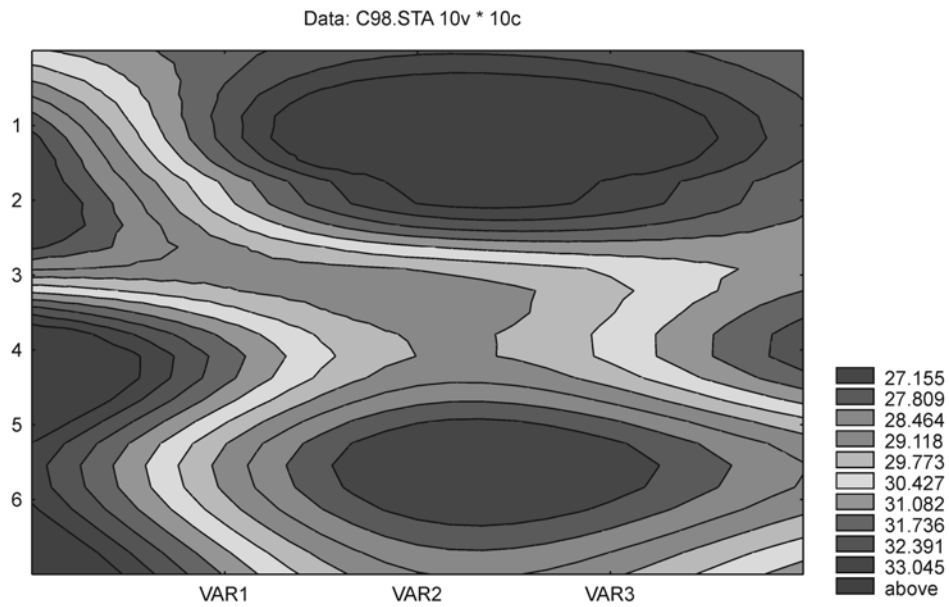| Depth	1998								2000			
	5.06.		18.06.		7.08.		4.09.		21.06.		1.08.	
	Ws	^{0}C	Ws	^{0}C	Ws	^{0}C	Ws	^{0}C	Ws	^{0}C	Ws	^{0}C
Soil surf.		50.1		48.8		43.8		44.5		54.2		60.5
3 cm		35.0		32.3		33.0		32.6		31.4		28.8
5 cm		33.4		30.6		32.3		30.0		30.2		28.0
10 cm	74	23.8	60	20.0	57	31.8	<60	25.6	75	24.4	82	25.7
20 cm	74	22.0	68	20.0	60	29.2	<60	23.2	81	22.2	85	24.2
40 cm	91	19.0	79	18.0	60	21.0	<60	19.0	85	18.6	85	19.5

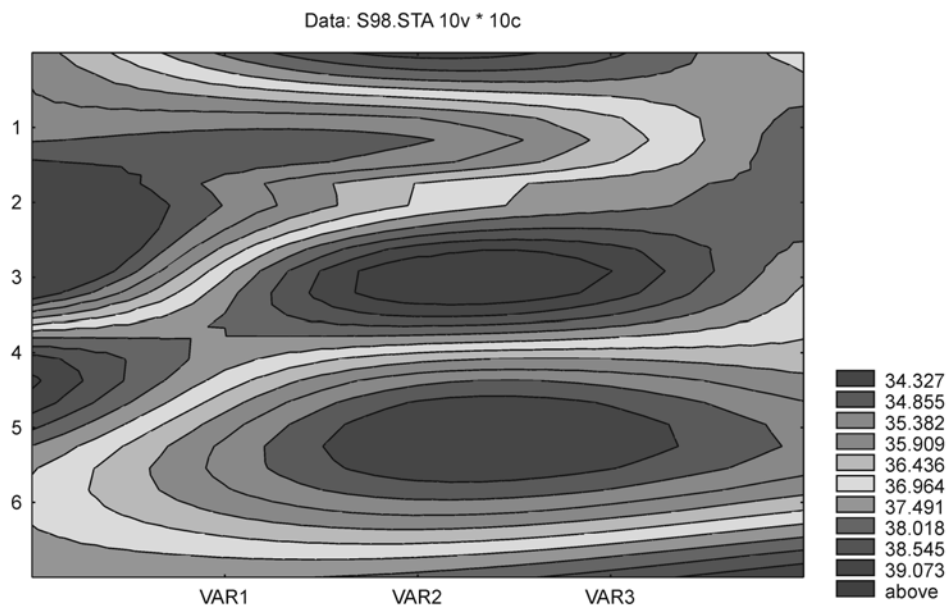**Fig.2.** Cotton canopy temperature map in 11:00 on 07.08.1998

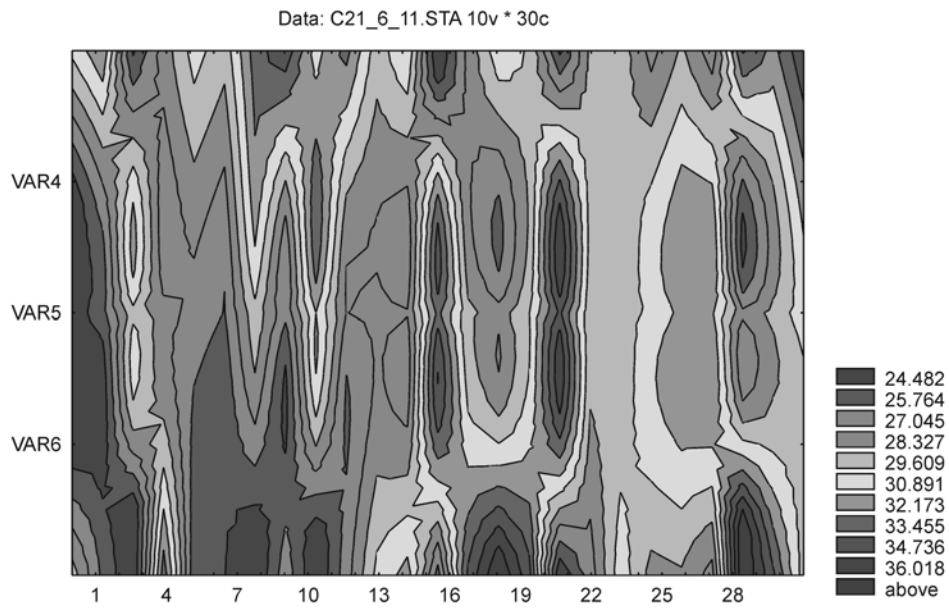**Fig. 3.** Soil surface temperature map of the field in 11: 00 on 07.08.1998

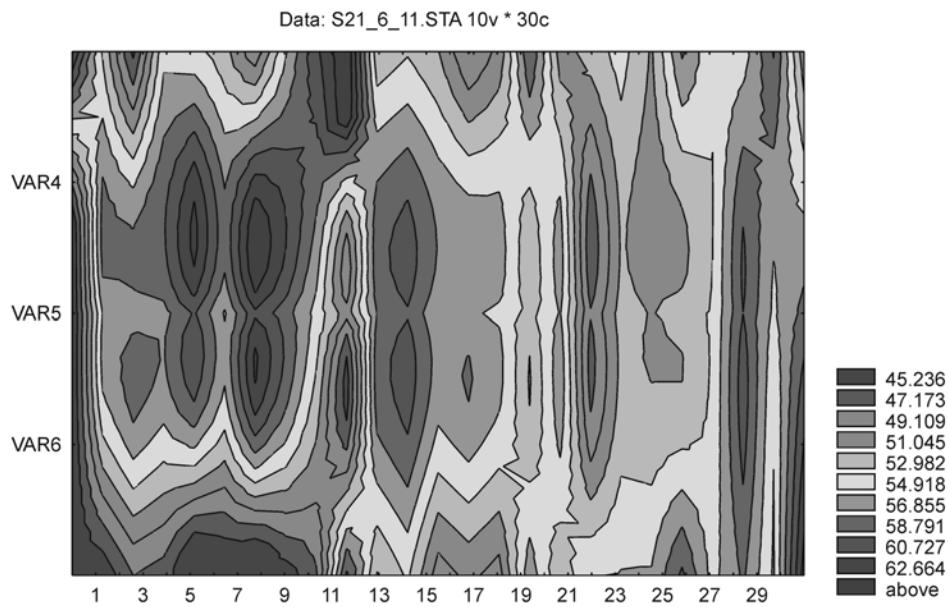**Fig. 4.** Cotton canopy temperature map in 11:00 on 21.06.2000

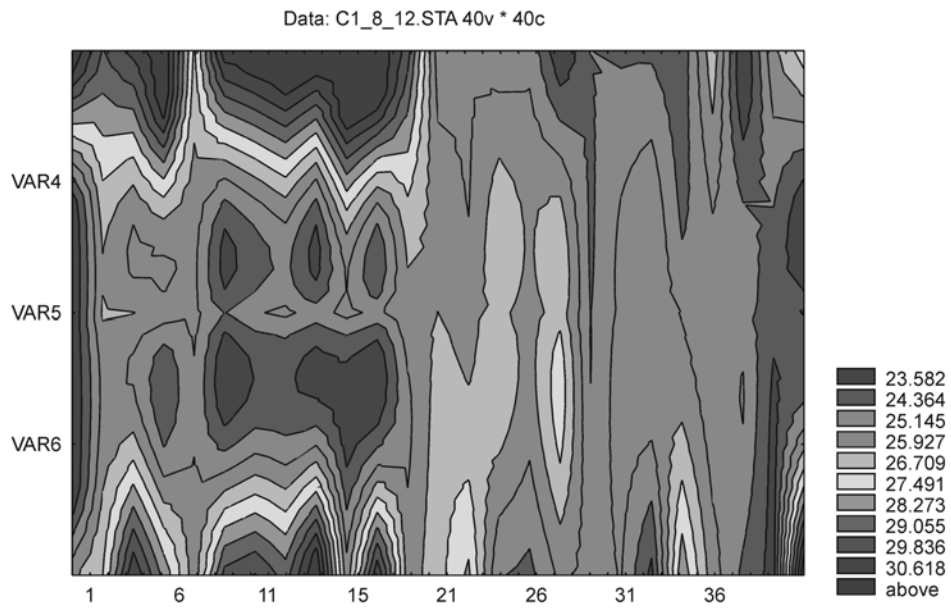**Fig. 5.** Soil surface temperature map of the field in 11:00 on 21.06.2000

Data: C1_8_12.STA 40v * 40c

	23.582
	24.364
	25.145
	25.927
	26.709
	27.491
	28.273
	29.055
	29.836
	30.618
	above

Fig. 6. Cotton canopy temperature map in 11:00 on 01.08.2000

Data: S1_8_13.STA 80v * 80c

	27.814
	29.363
	30.912
	32.460
	34.009
	35.557
	37.106
	38.654
	40.203
	41.751
	above
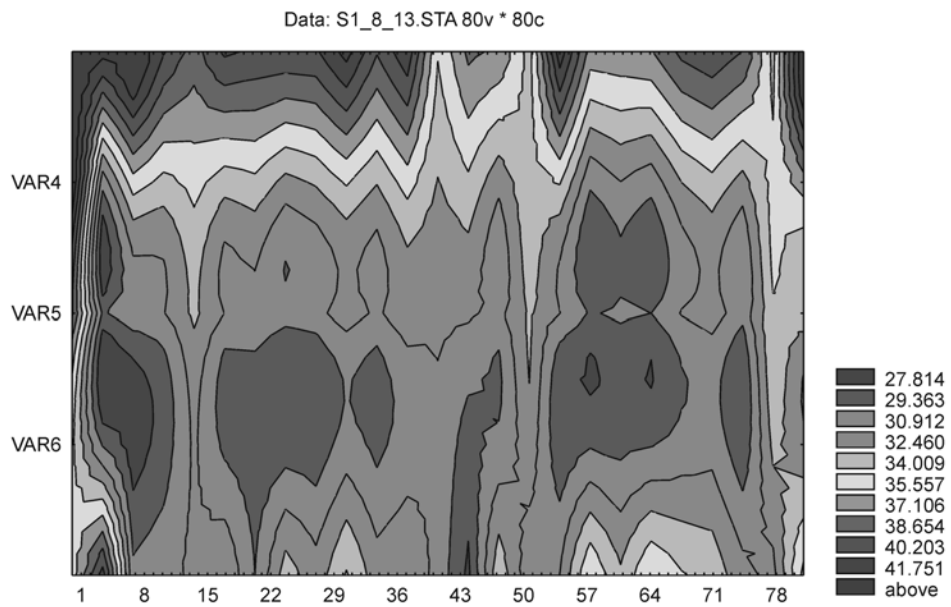
Fig. 7. Soil surface temperature map of the field in 11:00 on 01.08.2000

There were 4 measurement expedition days in 1998 and 2 - in 2000. Spurious effects of mutual leaf shading and small-scale variations in soil moisture and temperature were largely ignored.

There were large database for the period of expeditions that's why we will select some days measurement results for showing map structures. Table 1 includes soilmoisture and soil temperature measurement results during the expedition days. **Fig. 2** and **Fig. 3** show cotton canopy and soil surface temperature maps, based on the results of space-distributed measurements by infrared thermometer on 7 August 1998. **Fig. 4** – **Fig. 7** show temperature maps on 21 June and 1 August 2000. The weather had been sunny and quiet on 7 August 1998, 21 June and 1 August 2000.

The information analysis of the maps points out that the canopy temperature distribution zones are similar in different growing days including different years.

For cotton field conditions there are relationship between canopy and soil temperature maps that's why it is easy to measure remotely only canopy temperature and to predict soil moisture and temperature distribution on the field.

Conclusion

Soil surface and canopy temperature maps of a cotton field are obtained using geostatistics and microcomputer programs. There is relationship between canopy and soil surface temperature zones with similar thermal conditions. Based on the maps we can minimise the temperature measurement points in the field with preservation of the necessary useful information.

References

1. **Kutilek M., Nielsen D.:** Soil Hydrology. Catena-Verlag., p.246, 1994.
2. **Mishev D.:** Spectral Characteristics of Natural Formations, Publishing House of Bulgarian Academy of Sciences, Sofia, , p.150 1986.
3. **Mishev D.:** Spectral Characteristics of Mixed Classes of Natural Formations, Acta Astronautica,V.25, Pergamon Press plc., pp.443-446, 1991.
4. **Nielsen D.J., Biggar J., Erh K.:** Spatial Variability of Field-Measured Soil-Water Properties. Hilgardia 42, pp.215-259, 1973.
5. **Thurnhold B.:** A comparison of measured and simulated soil temperature using air temperature and soil surface energy balance as boundary conditions. Agric. and Forest Meteorology, 53, pp.59-73, 1990.
6. **Webster R.:** Quantitative Spatial Analysis of Soil in the Field. Advances in Soil Science, vol.3, Springler Verlag, New York, pp.1-70, 1985.

HYDRAULIC FUNCTIONS IN BI-MODAL SOILS WITH LOGNORMAL PORE SIZE DISTRIBUTION

Kutílek Miroslav and Jendele Libor

Prague, Czech Republic
kutilek@ecn.cz

Abstract

Soil water retention curve together with saturated and unsaturated hydraulic conductivity are basic soil hydraulic functions used in the solution of transport processes in soils. We modified the relevant equations based on lognormal pore size distribution to bi-modal soils. We used the measured data from A and B-horizons of four soil profiles to test the proposed theory. Bi-modal soils are characterized by the existence of matrix and structural domains of capillary pores. The pressure head separating them is not constant and it varies in a broad range of values. The classification of soil pores into various categories with fixed boundaries of pore radii lacks therefore objectivity. The structural porosity is lower than the matrix porosity and their ratio decreases in the B horizon. Parameters of the pore size distribution obtained by optimization differ in the two domains. They were used for plotting the separate soil water retention curves of matrix and structural domains. Parameters characterizing the unsaturated conductivity function differ substantially when the matrix and structural domains are compared. Our assumption on different configuration of soil porous systems in matrix and structural domains was proved. We obtained a good agreement between computed and measured data when the optimized parameters entered into equations of soil water retention and the unsaturated conductivity function. The proposed equations and restrictive conditions are therefore well applicable to bi-modal soils.

K e y w o r d s : Pore size distribution; hydraulic functions; unsaturated conductivity; soil water retention curve

Introduction

The term soil hydraulic function contains soil water retention curve together with saturated and unsaturated hydraulic conductivity. Their knowledge is required for modelling of transport processes in soils. Pore size distribution and the configuration of the soil porous system are basic factors influencing soil hydraulic functions. E.g. the recently used model of unsaturated hydraulic conductivity $K(h) = K_S$ (Portion of the porous system saturated by water as function of h)/(The whole porous system saturated by water, $h = 0$). K_S is saturated hydraulic conductivity and h is the pressure head (potential). The degree

of saturation of the soil porous system by water is formulated as the soil water retention curve $h(\theta)$, where θ is the volumetric soil water content. Soil water retention curve has been described by the empirical equations, the most frequent ones are that of Brooks and Corey (1964) and equation of van Genuchten (1980). They have been broadly applied in numerous simulation models. The evidence on the unbalance of approaches is clear, since empirical equation enters into a physically based relationship. The lack of correspondence between the measured and modeled data is frequently defined and it is balanced by introduction of various attempts, as e.g. the concept of mobile and immobile water or by various types of fitting parameters. We expect the elimination of this imbalance by introduction of results of a detailed research on soil porous systém resulting in a physical description of the soil water retention curve. We expect then a more exact description of transport processes in soils, especially of the preferential flow. The first step in the research is the introduction of the appropriate description of the pore size distribution.

Brutsaert (1966) studied four models of pore size distribution, among them the lognormal distribution in relation to soil water retention curve. We can conclude from his research that the lognormal distribution looks at least as an acceptable approximation. This assumption is supported by Walczak et al. (1982). A more detailed analysis was presented by Pachepsky et al. (1992) and Kosugi (1994), who formulated the lognormal pore size distribution function $g(r) = d\theta/dr$

$$g(r) = \frac{\theta_S - \theta_R}{\sigma r \sqrt{2\pi}} \exp\left\{ -\frac{[\ln(r/r_2)]^2}{2\sigma^2} \right\} \qquad (1)$$

where: r is the pore radius, r_m is the geometric mean radius, σ is the standard deviation, θ_R is the residual soil water content when the liquid flow is essentially zero. The value of θ_R is usually not measured but it is found as a fitting parameter, and θ_S is the soil water content at saturation, ie at $h = 0$. Soil water retention curve is expressed as a cumulative function to Eq. (1) with $h = a/r$, where h is [cm], a is the coefficient dependent upon the geometry of pore section we use in the model. For a cylindrical pore of radius r [μm] and water at 20^oC is $a = 1490$. The equation describing soil water retention curve is (Pachepsky, 1992, Kosugi, 1994)

$$S = \frac{1}{2} erfc \left[\frac{\ln(h/h_m)}{\sigma \sqrt{2}} \right] \qquad (2)$$

with S the relative saturation, or parametric soil water content [dimensionless]

$$S = \frac{\theta - \theta_R}{\theta_S - \theta_R} \tag{3}$$

h_m is the pressure head related to r_m and *erfc* is the complementary error function.

The equation of relative unsaturated conductivity $K_R = K/K_S$ was gradually improved (Childs and Collis George, 1950, Fatt and Dijkstra, 1951, Burdine, 1953, Mualem, 1976) up to the recent general form

$$K_R = S^\alpha \left[\frac{\int_0^r r^\beta g(r) dr}{\int_0^\infty r^\beta g(r) dr} \right]^\gamma \tag{4}$$

The interpretation of parameters α, β, γ was discussed in detail by Mualem (1992) and Mualem and Dagan (1978). With a certain simplification α represents the macroscopic description of tortuosity, when the pore is partially drained, then the flow path copies the irregular surface of the pore and the tortuosity increases. Parameter β is related to microscopic tortuosity, to pore radius, and it increases with the decrease of pore radius. Correlation between the pores is expressed by γ.

Kosugi (1999) introduced $g(r)$ from Eq. (1) into Eq. (4) to get the equation of the relative unsaturated hydraulic conductivity K_R (h). We obtain after rearrangement of his equations (Kutílek, 2004)

$$K_R = S^\alpha \left\{ \frac{1}{2} erfc \left[(\ln \frac{h}{h_m}) \frac{1}{\sigma\sqrt{2}} + \frac{\beta\sigma}{\sqrt{2}} \right] \right\}^\gamma \tag{5}$$

Applicability of equations have been experimentally checked by their authors and e.g. in publications of Leij *et al* (2002), Vervoort and Cattle (2003) for mono-modal soils where the derivative curve to soil water retention curve has one peak only. The derivative curve can be identified with the pore size distribution curve, see Eq. (1).

However, we find frequently (Durner, 1992) two or even three peaks on the derivative curve to the soil water retention curve and then we speak on bi-modal or tri-modal soils. Othmer *et al.* (1991) demonstrated the bi-modality of Gleyic Hapludalf loamy soil. They applied the van Genuchten (1980) and Mualem (1976) description of soil hydraulic functions to the bi-modal model and they obtained a substantial improvement of unsaturated conductivity function *K(h)*,

when the measured data were considered as a standard. The prediction of water content in the field soil was improved for time interval of four months by the use of bi-modal model, too, when the data were compared to results obtained with mono-modal simulation model.

The aim of this paper is to apply the theory on hydraulic functions of lognormal pore size distribution to bi-modal soils.

Theory

Lognormal Model of Hydraulic Functions in Bi-Modal Soils

We assume that two peaks on the pore size distribution function appear due to the existence of two porous systems within the domain of capillary pores. Further on, we use the classification of soil pores based on the laws of hydrostatics and hydrodynamics (Kutílek and Nielsen, 1994) with the terminology of micropores slightly modified in accordance with proposal of Tuller and Or (2002):

1. Submicroscopic pores where the clusters of water molecules do not allow the existence of continuous water flow paths due to the small size of pores.
2. Micropores, or capillary pores where the shape of air-water interface is determined by the configuration of pores and by the forces on the interface (capillary forces). The unsaturated flow of water is described by Darcy-Buckingham and Richards equations. The category of micropores is further subdivided into two subcategories in bi-modal soils:
    2.1. Matrix (intra-aggregate, intra-pedal, textural) pores within soil aggregates or soil blocks. The arrangement of the soil skeleton, coating of aggregates, cutans and nodules typical for each soil taxon have main influence upon the soil water hydrostatics and hydrodynamics in the matrix domain. Saturated hydraulic conductivity is strongly reduced when compared to conductivity of the whole soil (Horn, 1994).
    2.2. Structural (inter-aggregate, inter-pedal) pores between the aggregates, or eventually between the soil blocks. Their morphology and interconnection depends upon the shape, size and stability of aggregates and blocks, or, generally upon the soil genesis and the type of soil use.
3. Macropores (non-capillary) pores of such a size that capillary menisci across the pores are not formed. A more detailed classification of macropores is related to their origine, shape, stability and persistence in time.

We are dealing with subcategories of matrix and structural pores in this study. The boundary between the domains of matrix and structural pores is denoted h_A. It is the air entry value of the matrix domain, too. It is determined as the minimum

value between two peaks on the derivative curve to the retention curve, illustrative example is in **Fig. 1**.
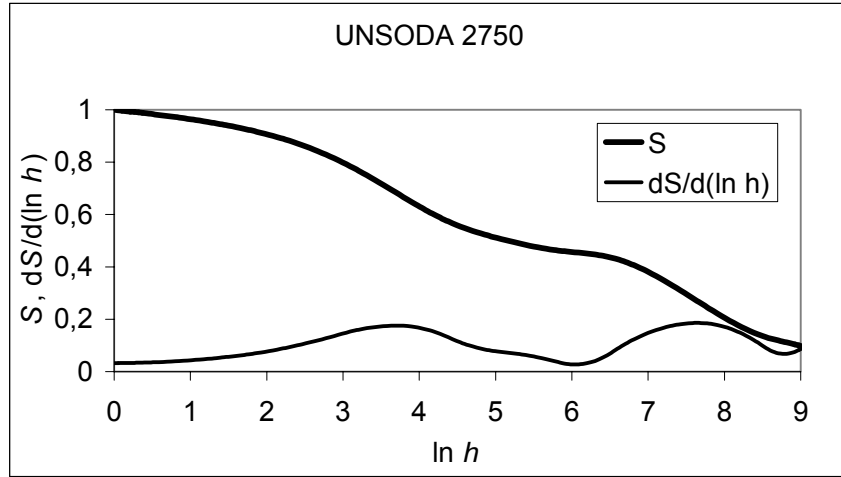

Fig. 1. Soil water retention curve *S(h)* and its derivative d*S/*d(ln *h*) for UNSODA 2750, loam, (E)B hor. *S* is the relative saturation of soil by water, Eq. (3), *h* is the negative pressure head, cm. Separation of matrix from structural domain is at $h_A = 403$ cm

If there exist two or three minima, we consider the minimum minimorum (i.e. the lowest minimum between the peaks) as h_A, see **Fig. 2**. Equation (2) of soil water retention curve and Eq. (3) of relative saturation of soil by water have then the forms (Kutílek, 2004)

$$S_i = \frac{1}{2} erfc \left[\frac{\ln(h_i / h_{mi})}{\sigma_i \sqrt{2}} \right] \qquad (6)$$

$$S_i = \frac{\theta_i - \theta_{Ri}}{\theta_{Si} - \theta_{Ri}} \qquad (7)$$

where $i = 1$ is for matrix pores and $i = 2$ for structural pores. With the principle of superposition, applied already by Othmer *et al.* (1991) and by Zeiliguer (1992) we define
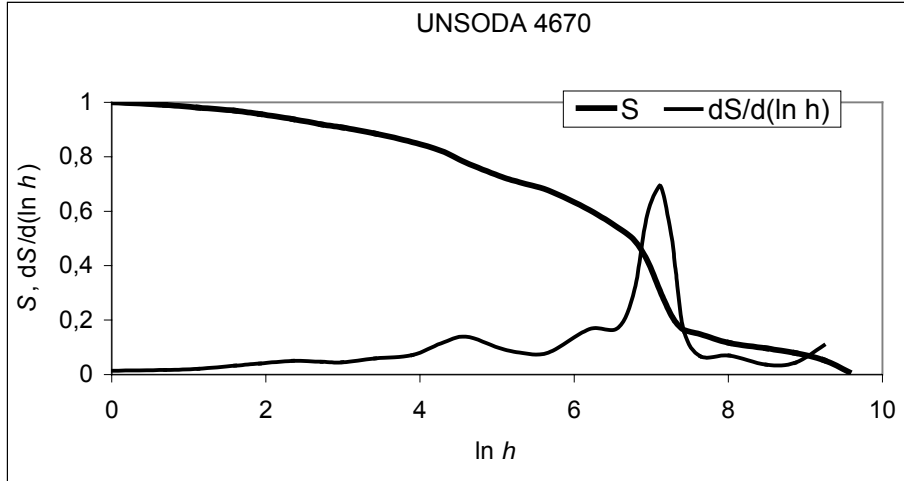
$$\theta = \theta_1 \theta_2 \qquad (8)$$

Fig. 2. Soil water retention curve $S(h)$ and its derivative $dS/d(\ln h)$ for UNSODA 4670, Typic Hapludalf, silt, A1 hor. Separation of matrix from structural domain is at $h_A = 296$ cm

Since coarse micropores of $r > r(h_A)$ would cause instability of aggregates, we assume that the matrix porous system does not contain coarse micropores above h_A. Then

$$\theta_{S1} = \theta(h_A) \text{ and } \theta_{S2} = \theta_{S\text{-}EXPER} - \theta_{S1} \tag{9}$$

For $0 > h \geq h_A$ is

$$\theta_1 = \theta_{S1} \text{ , } S_1 = 1 \tag{10}$$

and θ_2 is obtained by optimization,

$$S_2 < 1. \tag{11}$$

For $h < h_A$ is θ_1 obtained by optimization, $S_1 < 1$. (12) $\theta_{S\text{-}EXPER}$ denotes the saturated water content determined experimentally.

Unsaturated hydraulic conductivity is modified to bi-modal soil in a similar way and

$$K_{R_i} = S_i^{\alpha_i} \left\{ \frac{1}{2} erfc \left[(\ln \frac{h_i}{h_{mi}}) \frac{1}{\sigma_i \sqrt{2}} + \frac{\beta_i \sigma_i}{\sqrt{2}} \right] \right\}^{\gamma_i} \tag{13}$$

The subscripts in parameters α_i, β_i, γ_i reflect the assumption that values of parameters could differ for the two domains. With $K_i = K_{Ri}K_{Si}$ and using the principle of superposition we obtain

65

$$K = K_1 + K_2. \qquad (14)$$

The value of K_{S2} is obtained by optimization and $K_{S1} = K_{S\text{-}EXPER} - K_{S2}$. The procedure allows us to define separately conductivities of the two domains and to separate from the measured K that portion of K_2 which can be considered as preferential conductivity, see **Fig. 4** as an illustrative example.

This procedure differs from the approach of Kosugi and Inoue (1999) who have first constituted two (or generally n) subsystems but finally in evaluating relative unsaturated conductivity they have treated the soil as one system. The consequence was that they did not differ between parameters of subsystems and α, β, γ were common to the whole optimization procedure. The conductivities of matrix domain and of structural domain were not obtained as separate ones.
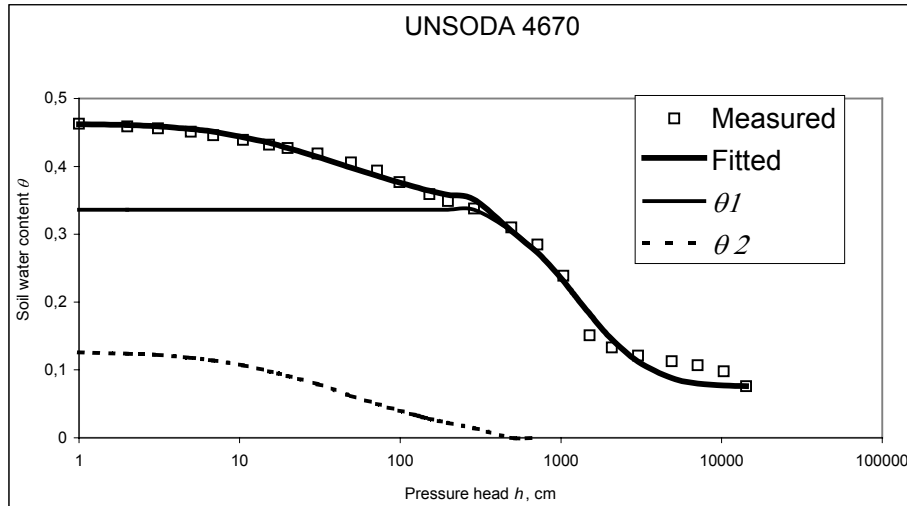

Fig. 3.   Separation of soil water retention curve into the retention curves of matrix (θ_1) and structural (θ_2) domains, Eq. (6) for UNSODA 4670, Typic Hapludalf, silt, A1 horizon

Optimization was performed in following steps: The experimentally determined data of the soil water retention curve $\theta(h)$ are first transformed into $S(h)$ according to Eq. (3). Then, a cubic spline function is fitted resulting in a smooth curve $S(\ln h)$ passing through the experimental data. It is assumed that θ_R is the water content at $h = -15000$ cm. When θ_R was considered as equal to the estimate of hygroscopic coefficient, the parameters were only slightly changed. θ_R was therefore kept equal to the measured water content at $h = -15000$ cm. The curve $\partial S(\ln(h))/\partial \ln(h)$ was calculated from smooth curve $S(\ln h)$. Let us note that the curve is identical to the pore size distribution if h is recalculated to -

equivalent pore radius r. When the model of cylindrical pores is used, then for contact angle equal zero and for tabled viscosity at 20°C is $r = 1490/h$, where r is in μm and h in cm. This very simple type of recalculation is taken as a first approximation. If we knew the dependence of pore shape upon pore size and upon horizons we could proceed to a higher approximation of r.
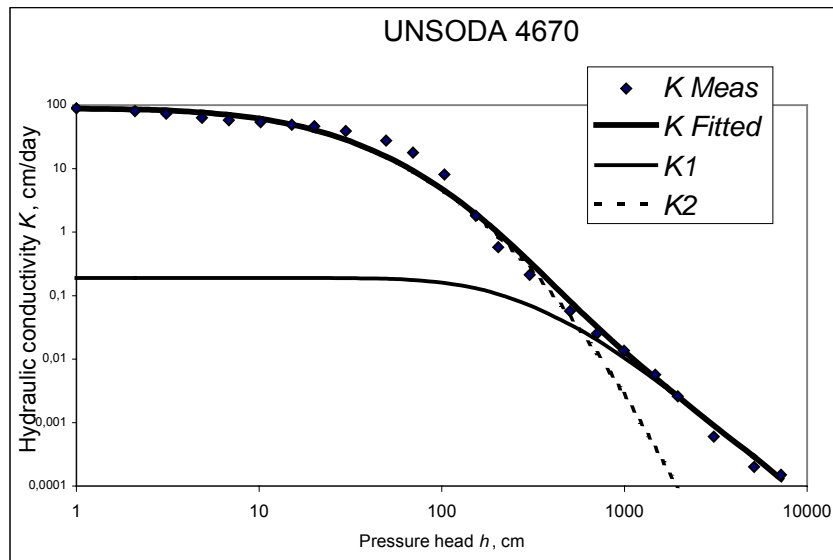

Fig.4. Example of separation from the measured K that portion of K_2 which can be considered as preferential conductivity

The value h_A separating the two principal pore domains was obtained as the minimum between two major peaks on the derivative curve. Next the parameters h_{m1}, h_{m2}, σ_1, σ_2 (Eq. 6) were determined for conditions (8) to (12). The non-linear curve fitting was carried out by conjugate gradient method applied to find the minimum of a function $f(x)$ of n variables (Powell 1977, 1978). The procedure provides a fast rate of convergence. 180 equidistant sample points were read from the smoothed $S(h)$ curve and used in fitting. The optimized parameters h_{m1}, h_{m2}, σ_1, σ_2 enter into Eq. (13) for each of the domains. The optimization was similar to the procedure applied to the soil water retention curve. A smooth curve was plotted through the experimental points by cubic spline. The whole range of conductivity was subdivided into 130 sample points, which were used for fitting the parameters. Saturated conductivity K_{S2} was determined together with parameters α_1, β_1, α_2, β_2 from Eq. (13) by Powell's (1977, 1978) conjugate gradient method for condition (14). We assumed $\gamma = 1$ according to the study of

Kosugi (1999), who found that the value of γ is in majority of instances close to 1 for log-normal distribution.

Materials

The theory was tested on data sets on soil water retention curves and on unsaturated hydraulic conductivity functions obtained from the UNSODA data base (Leij *et al.*, 1996 and Nemes *et al.*, 1999) and on the data sets published by Othmer *et al.* (1991). All soils and their horizons were typical by their bimodality. Soil characteristics relevant to the studied problem are in **Table 1**.

Table 1. Characteristics of soils

Soil code	Soil taxon	Depth [cm]	Soil horizon	Soil texture	Soil structure
UNSODA (Leij *et al.*, 1996, Nemes *et al.*, 1999)					
2750	Bruennli series	0-30	(E)B	loam	n.d.
2751		30-60	Bv	sandy loam	n.d.
2752		60-100	(Sd)BC	loam	n.d.
4660	Typic Dystrochrepts	15-25	Ah	sand	single grain
4661		30-40	Bv	sand	single grain
4670	Typic Hapludalf	20-30	A1	silt	coherent
4671		40-50	Ag1	silt loam	coherent to fine
4672		70-85	Bt	silt loam	Fine to moderate
Othmer *et al.* (1991)					
S 15	Gleyic Hapludalf	15	Ap	Loam	medium subangular
S 60		60	Btv	Loamy silt	medium subangular and blocky

n.d. not determined

Soil water retention curves of both sources, the UNSODA database and of Othmer were determined on undisturbed soil samples in the laboratory. Unsaturated conductivity data were determined in laboratory for the used UNSODA database and in the field by instantaneous method by Othmer.

Results and discussion

Soil Water Retention Curves

Parameters of soil water retention curves, Eq. (6) were determined for conditions (8) to (12). They are in **Table 2**.

Table 2. Parameters of soil water retention curves, Eq. (6) in matrix (indexed by 1) and structural (indexed by 2) domains, separated by pressure head h_A

Soil	z, cm	h_A, cm	Matrix domain			Structural domain		
			θ_{S1}	h_{m1}, cm	σ_1	θ_{S2}	h_{m2}, cm	σ_2
UNSODA								
2750	0-30	403	0.390	2864	1.05	0.217	29	1.36
2751	30-68	344	0.393	4044	1.09	0.122	19	1.88
2752	60-100	384	0.376	3011	1.09	0.099	18	1.71
4660	15-25	15	0.318	64	1.78	0.145	3	0.85
4661	30-40	8	0.326	33	1.06	0.102	3	0.73
4670	20-30	296	0.336	1249	0.81	0.126	47	1.50
4671	40-50	185	0.337	1366	0.92	0.075	59	0.71
4672	75-85	626	0.307	3229	1.15	0.087	140	1.22
Othmer †								
S 15	15	55	0.318	1086	1.48	0.148	6.8	1.20
S 60	60	30	0.35	788	1.63	0.069	10.0	0.94

† Parameters according to Kutílek (2004)

The computed retention curves are very close to the experimentally determined data. The matrix domain is separated from the structural domain by a minimum on the derivative curve h_A, see **Fig. 1** and **Fig. 2**. The value h_A is in very broad ranges extending from 8 cm in B-horizon of sandy Dystrochrept up to 626 cm in B-horizon of silt loam Hapludalf. The equivalent pore radii are from186 μm to 2.4 μm. If sand is excluded, the ranges are 30 to 626 cm, i.e. 50 to 2.4 μm. The value of separation of structural (interaggregate) pores from the matrix (textural) pores is therefore not a fixed value of pressure head, or pore radius. It is in broad ranges, dependent upon the soil taxon, soil horizon, texture and probably upon soil use, too. The classification systems of soil pores by Brewer (1964), Luxmoore (1981), Greenland (1981), Ahuja (1984) and others are based upon fixed boundaries between pore size categories as *eg* macropores, mesopores, micropores, or between transmission and storage pores. Their objectivity is questionable when we consider our results.

There was a small difference between h_A found directly on the derivative curve and h_A optimized together with h_{mi} and σ_i. We preferred then the use of directly determined data from the derivative curves. We have detected an inferior minimum on the derivative curve in 30% of studied soils; the example is in **Fig. 2**. Inferior minimum corresponds in our studied soils to $h = 2$ to18 cm in the domain of structural pores. Its nature cannot be determined without a detailed micromorphologic research. Let us note that Pagliai *et al.* (1989) and Pagliai and Vignozzi (2002) detected this type of secondary minimum at radius equivalent to $h = 3$ to 5 cm ($r = 300$ μm to 500 μm) by direct micromorphologic studies of some soils and their use. We have included those secondary minima into structural domain without attempting for inclusion of hypothetical subclasses in this study.

The values of σ_i and h_{mi} in **Table 2** offer information on pore size distribution in matrix and structural domains. The shape of the pore size distribution is related to σ close to 1 in majority of instances and there is a tendency to obtain the curve slightly more flat in matrix domain of B-horizon. An opposite tendency is in the structural domain of B-horizon. The equivalent mean pore radius is variably changing with depth in matrix domain. It decreases in structural domain of B-horizon of Hapludalfs when compared to A-horizon.

Using the tabled parameters, we plotted the retention curves of the matrix and of the structural domains, example is in **Fig. 3**. If the pressure head is replaced by the equivalent radius r, we obtain the cumulative function of pore size distribution of individual domains.

In **Table 3** we use the equality $\theta_{Si} = P_i$, where P_i is the porosity of the i-th domain. Structural porosity decreases with the depth from A-hor. to B-hor. when it is compared to matrix porosity. Gleyic process contributes to this decrease. Contribution of structural porosity to the total porosity is in ranges from 0.357 to 0.161, and it is decreasing with the depth, too.

When the restrictive conditions (9) and (10) are not applied, we obtain in 50% a slight improvement of computed retention curves, i.e. they are closer to experimental data, but in remaining 50% the error of the computed retention curves increases. The improvement of the retention curve in those 50% of instances does not result in improvement of computed conductivities, quite opposite, se the next chapter. In addition to it, we do not assume that the matrix could contain coarse capillary pores of dimensions of hundreds μm. As we have already mentioned, the coarse pores would cause instability of aggregates and their disintegration into smaller aggregate units.

Saturated Hydraulic Conductivity

Saturated hydraulic conductivity of the structural domain K_{S2} was optimized together with parameters of unsaturated conductivity function. Saturated hydraulic conductivity of the matrix domain $K_{S1} = K_{S-EXPER} - K_{S2}$. The data are in **Table 4**. The values of matrix saturated conductivity are from one and half order of magnitude up to three orders of magnitude lower than saturated conductivity of structural domain, see **Table 3**.

Saturated conductivity of sand is the only one exception. Our results are in agreement with direct measurements of Horn (1994) who obtained saturated conductivities inside of aggregates by several orders of magnitude lower than saturated conductivities of the whole soil.

Table 3. The ratio of saturated water contents θ_i and of saturated hydraulic conductivities K_{Si} in matrix domain (indexed by $i = 1$) and in structural domain (indexed by $i = 2$) of soils. The ratio of structural porosity θ_{S2} to total porosity P

Soil	Depth [cm]	Horizon	θ_{S1}/θ_{S2}	θ_{S2}/P	K_{S1}/K_{S2}
UNSODA					
2750	0-30	(E)B	1.80	0.357	0.0026
2751	30-60	Bv	3.22	0.237	0.0058
2752	60-100	(Sd)E	3.80	0.208	0.0010
4660	15-25	Ah	2.19	0.314	0.049
4661	30-40	Bv	3.20	0.238	0.237
4670	20-30	A1	2.67	0.273	0.0021
4671	40-50	Ag1	4.49	0.182	0.031
4672	75-85	Bt	3.53	0.221	0.0035
Othmer					
S15	15	Ap	2.22	0.318	0.0105
S60	60	Btv	5.20	0.052	0.0067

Unsaturated Hydraulic Conductivity

Unsaturated hydraulic conductivity function $K_i(h)$ of both domains depends upon parameters α, β, γ and upon parameters of the soil water retention curve h_m, σ, see Eq. (13). We assumed that the parameter $\gamma = 1$. Optimization procedure was performed for condition (14) and the data are in **Table 4**. The parameters α_1, β_1 of the matrix domain differ substantially from α_2, β_2 of the structural domain, in matrix domain is $\alpha_1 < 0$ and $\beta_1 > 0$ in majority of instances, while in structural domain is $\alpha_2 > 0$ in majority of instances and β was roughly in 50 % positive and in 50% negative. The opposite sign is for pairs α_1, α_2 or for β_1, β_2 in 65% of instances. All discussed differences in values of parameters are proof that

the shape, connectivity and tortuosity of pores are different in the two domains and that their hydraulics has to be treated separately, as it was proposed in earlier publications (Othmer *et al.*, 1991, Gerke and van Genuchten, 1993). Verwoort and Cattle (2002) studied relationships between the quantified parameters of micromorphology of pores and the parameters α, β of Eq. (5) for monomodal clay soil. Their statement on increasing β with decreasing r is valid for our domains, too, since β is lower in structural domain than in matrix domain. There is an agreement on the mutual relation of α, β. When α is decreasing with the depth in a certain taxon, then β is increasing and vice versa.

Table 4. Parameters of relative unsaturated hydraulic concuctivity, Eq. (13) in matrix (indexed by 1) and structural (indexed by 2) domains

| Soil | z, cm | Measured K_S cm/day | Fitted | | | | | |
| | | | Matrix | | | Structural | | |
			K_{S1}, cm/day	α_1	β_1	K_{S2}, cm/day	α_2	β_2
UNSODA								
2750	0-30	190.08	0.185	-1.94	3.33	189.59	0.024	1.79
2751	30-60	25.92	0.015	-0.53	1.402	25.90	3.44	-0.47
2752	60-100	14.95	0.015	-0.60	1.52	14.87	4.13	-0.56
4660	15-25	625.5	30.87	0.96	0.92	593.88	0.92	-1.83
4661	30-40	1140	218.2	-1.22	2.81	920.2	0.022	0.094
4670	20-30	88.99	0.189	-1.04	2.64	88.80	2.19	-0.64
4671	40-50	12.27	0.368	-0.99	2.50	11.90	0.024	0.98
4672	75-80	2.42	0.009	-0.50	1.26	2.58	2.59	-0.78
Othmer †								
S15	15	11.50	0.12	1.0	2.3	11.38	0.45	0.70
S60	60	15.0	0.10	-0.3	1.4	14.9	-1.0	1.8

† Parameters according to Kutílek (2004)

If we use uniformly $\alpha = 0.5$, $\beta = 1$, $\gamma = 2$ (Mualem, 1976) with two domains of retention curves, we obtain errors of the more than one order of magnitude in certain parts of the $K(h)$ function.

When the restrictive conditions (7) and (8) are not applied in the retention curve, then the optimized $K(h)$ function had greater sum of errors, compared to $K(h)$ function computed for retention curves with conditions (7) and (8).

Conclusions

1. The modified theory on hydraulic functions in a bi-modal lognormal pore size distribution system is well applicable. Eq. (6) of soil water retention curve

with conditions (8) to (12) offers data either identical or with negligible error when the experimental data are taken as reference. Water retention curves of matrix and of structural pores can be plotted separately and the separate porous systems can be identified.

2. The structural porosity is substantially lower than the matrix porosity. However, the separation of both domains occurs at non-constant pressure head h_A with its value in broad ranges from 30 to 626 cm, corresponding to equivalent pore radius from 50 μm to 2.4 μm, if sand is excluded.

3. Matrix saturated conductivities are by one and half order of magnitude up to three orders of magnitude lower than saturated conductivities of the structural domain.

4. The parameters characterizing the unsaturated conductivity function α_1, β_1 of the matrix domain differ substantially from α_2, β_2 of the structural domain. The shape, connectivity and tortuosity of pores are assumed to be different in the two domains.

Acknowledgments

References

7. **Brooks, R.H., Corey A.T:** Hydraulic properties of porous media. Hydrology paper 3, Colorado State Univ., Fort Colins, CO, USA, 1964.
8. **Brutsaert, W.:** Probability laws for pore size distribution. Soil Sci. 101:85-92. 1966.
9. **Burdine, N.T.:** Relative permeability calculations from pore-size distribution data. Trans. Am. Inst. Min. Metall. Pet. Eng. 198:71-77, 1953.
10. **Childs, E.C., Collis-George N.:** The permeability of porous materials. Proc.Royal Soc. London A. 210:392-405, 1950.
11. **Durner, W.:** Predicting the unsaturated hydraulic conductivity using multi-porosity water retention curves. p.185-202 *In* M.Th.van Genuchten, F.J. Leij, and L.J.Lund (ed.) Indirect Methods for Estimating the Hydraulic Properties of Unsaturated Soils. University of California, Riverside, CA, USA, 1992.
12. **Fatt, I., Dijkstra H.:** Relative permeability studies. Trans.Am.Inst.Min.Metall. Pet.Eng. 192:249-255 (quoted acc. to Scheidegger, 1957), 1956.
13. **Gerke, H.H. van Genuchten M.Th.:** A dual-porosity model for simulating the preferential movement of water and solutes in structured porous media. Water Resour. Res. 29:305-319, 1993.
14. **Horn, R.:** The effect of aggregation of soils on water, gas and heat transport. p. 335-361. *In* E.D. Schulze (ed.) Flux Control in Biological Systems, Academic Press, 10, 1994.

15. **Kosugi, K.:** Three-parameter lognormal distribution model for soil water retention. Water Resour. Res. 30:891-901, 1994.
16. **Kosugi, K.:** General model for unsaturated hydraulic conductivity for soils with lognormal pore-size distribution. Soil Sci. Soc. Am. J. 63:270-277, 1999.
17. **Kosugi, K., Inoue M.:** Analysis of soil water movement by using a generalized model for unsaturated hydraulic conductivity (in Japanese) p. 71-72. *In* Proc. 11 Ann. Conf. Joint Research Program, The Arid Land Research, Tottori Un., 1999.
18. **Kutílek, M., Nielsen D.R.:** Soil Hydrology. Catena Verlag, Cremlingen Destedt, Germany, 1964.
19. **Kutílek, M.:** Soil hydraulic properties as related to soil structure. Soil Tillage Res. 75:175-184, 2004.
20. **Leij, F.J., Alves W.J., van Genuchten M.Th., Williams J.R.:** Unsaturated Soil Hydraulic Database. UNSODA. 1.0 User´s Manual. Report EPA/600/R-96/095. Environmental Protection Agency, Ada, OK., 1996.
21. **Leij, F.J., Ghezzehei T.A., Or D.:** Modelling the dynamics of the soil pore-size distribution. Soil Tillage Res. 64:61-78, 2002.
22. **Mualem, Y.:** A new model for predicting the hydraulic conductivity of unsaturated porous media. Water Resour. Res. 12:2187-2193, 1976.
23. **Mualem, Y.:** Modelling the hydraulic conductivity of unsaturated porous media. p. 15-36 *In* M.Th.van Genuchten, F.J. Leij, and L.J.Lund (ed.) Indirect Methods for Estimating the Hydraulic Properties of Unsaturated Soils. University of California, Riverside, CA, USA, 1992.
24. **Mualem Y., Dagan G.:** Hydraulic conductivity of soils: Unified approach to the statistical models. Soil Sci. Soc. Am. J. 42:392-395, 1978.
25. **Nemes, A., Schaap M.G., Leij F.J.:**. Database UNSODA Version 2. CD-R Hydrus −1D, -2D. U.S. Salinity Lab., USDA-ARS, Riverside, CA., 1999.
26. **Othmer H., Diekkrüger B., Kutílek M.:** Bimodal porosity and unsaturated hydraulic conductivity. Soil Sci. 152:139-150, 1991.
27. **Pachepsky, Ya.A., Mironenko E.V., Shcherbakov R.A.:** Prediction and use of soil hydraulic properties. p. 203-213 *In* M.Th. van Genuchten, F.J. Leij, and L.J. Lund (ed.) Indirect Methods for Estimating the Hydraulic Properties of Unsaturated Soils. Univ. of California, Riverside, CA, U.S.A. 1992.
28. **Pagliai, M., Pezzarossa B., Mazzoncini M., Bonari E.:** Effects of tillage on porosity and microstructure of a loam soil. Soil Technol. 2:345-358, 1989.
29. **Pagliai, M. Vignozzi N.:** Image analysis and microscopic techniques to characterize soil pore system. p. 13-38. *In* J. Blahovec, and M. Kutílek (ed.), Physical Methods in Agriculture, Kluwer Academic Publishers, London, 2002.
30. **Scheidegger A.E.:** The Physics of Flow Through Porous Media. Univ. Toronto Press, Canada, 1957.
31. **Tuller M., Or D.:** Unsaturated hydraulic conductivity of structured porous media. A review. Vadose Zone J. 1:14-37, 2002.
32. **Van Genuchten M.Th.:** A closed-form equation for predicting the hydraulic conductivity of unsaturated soils. Soil Sci. Soc. Am. J. 44:892-898, 1980.
33. **Verwoort, R.W., Cattle S.R.:** Linking hydraulic conductivity and tortuosity parameters to pore space geometry and pore size distribution. J. Hydrol. 272: 36-49, 2003.

34. **Walczak R., Zaradny H., van der Ploeg R.R.:** Representation of the soil moisture characteristic by a logarithmic-normal distribution. p. 70-72. *In* J. Šútor (ed). Zbornik čs.-polského seminára Fyzika vody v pode. UHH SAV, Zemplinska Širava 14.-16 Sept. 1982.
35. **Zeiliguer A.M.:** Hierarchical system to model the pore structure of soils: Indirect methods for evaluating the hydraulic properties. p.499-514. *In* M.Th.van Genuchten, F.J. Leij, and L.J.Lund (ed.) Indirect Methods for Estimating the Hydraulic Properties of Unsaturated Soils. University of California, Riverside, CA, USA, 1992.

WHAT CAN WE MEASURE USING ION-SELECTIVE ELECTRODES?

Malinowska Elżbieta

Department of Analytical Chemistry, Warsaw University of Technology, Poland
ejmal@ch.pw.edu.pl

Abstract.

Ion-selective electrodes (ISEs) are one of the biggest groups of chemical sensors, used widely for clinical, environmental, industrial and recently also agricultural analysis. They have been the subjects of widespread interest of analytical chemists for more than 30 years. This is due to the fact that ISEs can provide accurate, rapid and low cost method of analysis. The very important advantage of potentiometric methods employing ISEs is their selectivity and possibility of determination of certain analytes in mixtures without separation of other sample components. Moreover, the analyte is not consumed in the course of the measurements. In this work, beyond the principles of the functioning of ion-selective potentiometric sensors, the overview of their application for the determination of soil electrolytes is presented.

K e y w o r d s : ion-selective electrodes, nutrients, electrolytes, soil.

Introduction

Among standard methods utilized to characterize chemical properties of the soil, the atomic absorption spectroscopy (AAS), flame emission spectroscopy (FES), inductively coupled plasma-mass spectroscopy (ICP-MS) and UV-Vis spectrometry (UV-Vis) are still dominante (see **Fig. 1**).

However, the importance of potentiometric methods, including ion-selective sensors, in determination of nutrient levels in soil arises. This is due to less complex and less time consuming procedures when potentiometric sensors are applied. The very important advantage of potentiometric methods employing ISEs is their selectivity and possibility of determination of certain analytes in mixtures without separation of other sample components. In contrast to many other analytical methods, ISEs are capable of determining ion activities, rather than total concentrations. Moreover, the analyte is not consumed in the course of the measurements and the instrumentation required for potentiometric measurements is dramatically less expensive than in the case of spectroscopic methods.
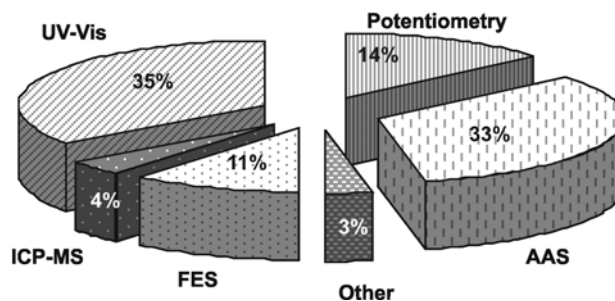
Fig. 1. The contribution of various methods used to measure electrolytes content in soil

Principles of polymeric membrane ion-selective electrodes

Polymeric membrane ion-selective electrodes are in fact relatively simple electrochemical probes that produce a voltage output in response to the activity of selected ions (H^+, K^+, NO_3^-, Na^+, etc.) in aqueous sample phase. The experimental assembly required for ISEs measurements is shown in **Fig. 2**
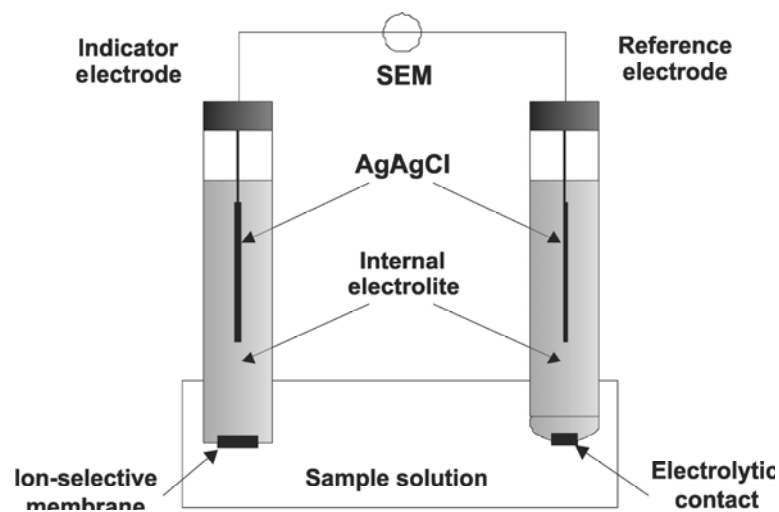

Fig. 2. Schematic representation of the experimental assembly required for potentiometric ion-selective membrane electrode measurements

The measurement principle is simple: two reference electrodes of fixed potential are separated by the ion-selective membrane. The notation of such a cell is:

external reference	aqueous sample	**ion-selective membrane**	*internal filling solution*	*internal reference electrode*

Each vertical line depicts an interface at which a phase-boundary potential can develop. In order to provide stable signals for this cell, all of the interfaces must be well thermodynamically defined. Moreover, a properly designed cell for direct potentiometric measurements should maintain all of these potentials constant, except for the membrane|sample solution interface. Only if this requirement is fulfilled, the variation in the cell potential will be the indication of the activity of the analyte ion in the sample solution.

In practice, the measured potential of an indicator polymeric membrane electrode is measured *vs.* a suitable reference electrode (*eg* Ag/AgCl). Due to the fact that no membrane is ideally permselective, various ionic species can participate in the development of the potential, depending on the membrane selectivity characterized by the selectivity coefficient of the membrane electrode ($K_{i,j}^{pot}$). The resulting cell potential can be expressed by the Nicolsky-Eisenmann equation [14]:

$$E_{w} = E^{0} + \frac{RT}{z_i F} \ln\left(a_i + \sum_j K_{i,j}^{pot} a_j^{z_i / z_j} \right) \tag{1}$$

where: E^{0} is the cell constant (including reference electrode potentials), a_i and a_j are the activities of the analyte and the interfering ions, respectively, z_i and z_j are the charges on these ions, and $K_{i,j}^{pot}$ is the potentiometric selectivity coefficient of the membrane electrode.

For the cell potential to be relatively independent on the interfering ion levels, $K_{i,j}^{pot}$ values should be as small as possible. When the average composition of a given target sample is known, it is possible to estimate so called required selectivity coefficients. Only ISEs of selectivity coefficients lower than the required ones can be considered for measurements in such samples. Typical calibration curve of an ion-selective electrode and most important factors, which are used to characterize working parameters of ISEs (*eg* slope, measuring range, linear range, lowest detection limit and selectivity) are presented in **Fig. 3**.
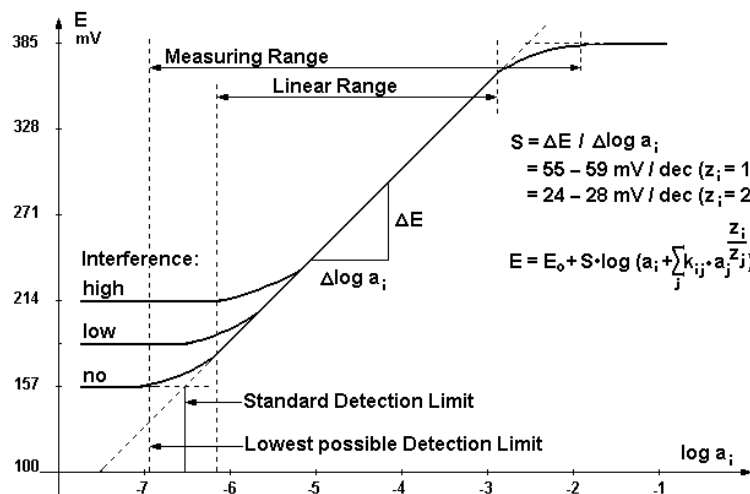
Fig. 3. Typical ISE calibration curve

Depending on the type of membrane, ISEs can be classified as electrodes with solid membrane (*eg* glass membrane or crystal membrane), liquid membrane (based on *eg* classical ion-exchanger), polymeric membrane (with ion-exchanger and neutral or charged carrier) and modified membranes (for gas-sensing or enzyme electrode). The best-known example of ISEs is the glass electrode (pH electrode), which exhibits a wide linear range of the calibration curve (typically 2-12 pH) and excellent selectivity over most common cations (*eg* K^+, Na^+, Ca^{2+}, *etc*). The membrane of glass pH electrode is manufactured as a bulb of typical wall thickness of 0.05-0.2 mm (the optimum thickness is the result of compromise between the mechanical properties and electrical resistance). By changing the glass membrane composition it was possible to fabricate electrodes sensitive to other cations (*eg* Na^+, K^+ or Ag^+), however their selectivity and, as a consequence, applications were rather limited.

Other types of membranes include single crystals of sparsely soluble salt and heterogeneous membranes in which the insoluble salt is incorporated in some suitable inert binder. Insoluble inorganic matererials as: Ag_2S, CuS, CdS, PbS, LaF_3, $AgCl$, $AgBr$, AgI and $AgSCN$ have all been tested as cation exchange membranes, incorporated into an electrode body in the form of single crystal or compressed powder discs. Sensors for the detection of: Ag^+, Cu^{2+}, Cd^{2+}, Pb^{2+}, S^{2-}, F^-, Br^-, I^-, SCN^- and CN^- ions can be constructed from such membranes. The sensitivity to ions of these electrodes arises from the dissolvation equilibria at the membrane surface. The typical measurement ranges of such electrodes lies in the range of $1-10^{-6}$ M.

Polymer membrane electrode technology offers a number of interesting and potentially attractive options for monitoring ions. The key to success in this area is to achieve high degree of selectivity as well as the linear response of sensors in a necessary range of analyte concentrations *via* appropriate membrane chemistries. The selectivity of polymeric membrane electrodes depends on two main factors: the strength of interaction of an analyte ion with an ionophore (ion carrier) that is present in the membrane phase and the relative lipophilicity of tested ions. Due to incredible number of synthetic ionophores that have been designed and synthesized up to now, a great number of ions (inorganic and organic ones) can be measured with ISEs offering sufficient selectivity, reproducibility and detection limits [9,20,21]. Among them there are ISEs suitable for soil macronutrients determination. Moreover, recent publications [6,17], showing the feasibility of shifting the micromolar detection limit to picomolar range, show the chance to apply ion-selective potentiometric sensors for trace metal measurements in relevant environmental matrices.

Ion-selective sensors are also available in miniaturized version. Miniaturized ISEs and ion-sensitive field effect transistors (ISFETs) have several advantages over the classical ion selective electrodes, such as small dimensions of sensors, mass production at low cost, the ability to integrate several sensors on a single electronic chip as well as less consumption of reagents and waste.

Sensors in soil analysis

To characterize the soil quality, various physical and chemical properties have to be determined. There is a large variety of soil sensors described in the literature that can be used for this purpose [3]. Most of them are physical sensors that involve one of the following measurement principles:
- electrical and electromagnetic sensors that measure electrical resistivity/conductivity, capacitance or inductance affected by the composition of tested soil;
- optical and radiometric sensors that use electromagnetic waves to detect the level of energy absorbed/reflected by soil particles;
- mechanical sensors that measure forces resulting from a tool engaged with the soil;
- acoustic sensors that quantify the sound produced by a tool interacting with the soil;
- pneumatic sensors that assess the ability to inject air into the soil.

Such sensors have been used to directly or indirectly assess spatial variability of different mechanical and physical soil properties, including also on-the-go measurements.

The uncontrolled addition of chemical fertilizers can lead to washing out of their excess into surface or ground waters causing serious environmental impact as well as unacceptable production costs. Real time monitoring of nutrient levels in soil would eliminate these unfavorable effects and make it possible to design appropriate irrigation and fertilization management systems. Instrumentation that allows measuring ions directly in the soil is not commercially available at present.

The development of electrochemical sensors for monitoring of various species (ions, gases and biomolecules) in complex samples has been of research interest for resent more than 30 years. Among them ion-selective electrodes have displayed suitable analytical performance (*eg* selectivity, reproducibility etc.) for routine use in "real world" measurements. The best example, proving this statement, is the application of ISEs for clinical analysis. Indeed, instruments incorporating such potentiometric sensors have completely replaced classical spectroscopic techniques in clinical chemistry laboratories for measurements of electrolyte ions (H^+, K^+, Na^+, Ca^{2+}, Mg^{2+}, Cl^-, HCO_3^- *etc*) [18]. These ions as well as NO_3^- and NH_4^+ are the species considered as soil nutrients, and ion-selective electrodes have also been consider as potential tools for their determination starting from the very early stages of their development in 1960-70s. That time mostly ISEs based on glass–type membranes were known, showing sensitivity to very limited number of cations (*ie* H^+, Na^+, Ag^+). Except for pH electrodes, which are routinely used to measure soil pH, the application of other glass electrodes for soil characterization fell down due to their poor selectivities (*ie* for potassium vs. ammonium ions) [15]. A major breakthrough occurred when ionophore-based polymeric membrane ISEs of greatly enhanced selectivities (*eg* using valinomycin as ionophore for K^+-ISEs) were developed [13,19] and made commercially available. Recently, Wang *et al*. [22]. and referenced therein, reported that the batch treatment of soil with $BaCl_2$ replacing salt solution and then the determination of K^+ with ion-selective electrode, directly in soil suspensions, provides a simple, rapid and routine method of determining exchangeable K^+ in soils. The results obtained with the suspension-electrode approach exhibited excellent correlation with those obtained with the filtrate-AAS mode. Ion-selective electrodes have also been used in soil laboratories to conduct NO_3^--Nitrogen standard chemical soil tests.

Whenever soil is sampled for later analysis in the laboratory, certain deviation of the composition can be observed. An ideal solution could be measurements carried out in situ in the soil rather than taking samples. Due to the fast response time and the ability of selective recognition of a given analyte in the mixture of

81

components without sample pretreatment, ISEs are suitable for real time measurements and continuous monitoring of time dependent changes in analyte concentration. Indeed, direct soil chemical characteristics, such as pH or nutrient (*eg* K^+ and NO_3^-) content has been the objective of considerable research. The automation of soil sampling and interfacing with the sensors was the basic concept of those studies. It has been shown that on-the-go soil analysis require rapid and precise soil sampling method, extraction unit and ion measurement systems. The interfacing with the sensors can be achieved by immersing them in extract solutions or using flow injection analysis (FIA) configuration in the case of miniaturized sensors (*eg* ISFETs).

The system consisted of a core-sampling wheel was proposed by Loreto and Morgan for soil pH and nitrate [12]. It was capable of conducting sampling, chemical extraction and measurement of ion concentration using an ISFET in field conditions. While successful attempts were made to measure soil pH, correlations of ISFET response to a conventional nitrate electrode and to laboratory colorimetric analysis felt due to the ISFET's response and calibration drift.

Adsett *et al.* [4] developed a prototype soil nitrate monitoring system with NO_3^- ion-selective electrode. Acceptable results were achieved during laboratory testing, however, field evaluation revealed the need for additional improvement of the sampler and other system units.

Hummel *et al.* [7,8] showed the feasibility of the use of a multi-ISFET sensor chip to measure soil nitrate in a flow injection analysis (FIA) system in manually prepared soil extracts under controlled conditions. Hummel *et al.* have worked also on extraction systems [11,23]. While a mechanical one [11] did not consistently provide soil extracts that could be analyzed by the ISFET/FIA system, laboratory evaluation of an electro-pneumatic soil sampling method [23] for real-time soil sensing was very promising. Recently, research on rapid extraction of nitrate [16] demonstrated that judicious selection of data analysis techniques could provide nitrate measurements in 2–5 s after injection of the extracting solution into the soil core.

A successful automated system for on-the-go mapping of soil pH was developed and tested under field conditions by Adamchuk *et al.* [1]. While travelling across the field, a soil sampling mechanism located in a toolbar-mounted shank scooped a sample of soil from a depth of approximately 10 cm and brought it into firm contact with the sensitive membranes of two flat-surface ion-selective electrodes. After stabilization of the electrode output (typically 5–15 s), a new soil sample was obtained and the electrode surfaces were rinsed at the same time. This method was referred to by the authors as direct soil measurement (DSM). Collins *et al.* [10] modified the soil sampling mechanism by

using a horizontal coring tube, which significantly increased the reliability of on-the-go soil pH mapping. A commercial instrumentation system has recently become available.

The ability to obtain high-resolution maps of soil nitrate and potassium levels at the time of pH mapping could further expand the potential for economic and environmental benefits of site-specific crop management. Preliminary laboratory evaluation of potassium and nitrate ion-selective electrodes showed that it is feasible to use both NO_3^- and K^+ ion-selective electrodes to determine soluble nitrate and potassium contents on naturally moist soil [2]. However, additional research is required both in terms of improving sensor performance and interpretation of the results for site-specific management decisions. According to preliminary field trials, integrated, automated, on-the-go mapping of pH, K^+, and NO_3^- may be used to identify areas of fields with extremely low and high fertility levels and serve as a complimentary data layer for conventional soil sampling programs while significantly reducing the number of laboratory samples required.

Acknowledgements

Summary

It can be envisioned that the combination of recent achievements in the area of chemical sensors (especially that related to the chemical recognition of analytes with appropriate polymeric ion-selective membranes) with breakthroughs in electronics and miniaturization can lead to developments of reliable and selective devices that allow for real-time measurements, in-soil monitoring of electrolytes in time as well as the mapping of soil nutrients in the form of pH, K^+, Ca^{2+}, NH_4^+, NO_3^- or Cl^- ions. The systematic control of these nutrients in soil will allow for an optimisation of the overall crop production process as well as reducing the environmental impact caused by excess of nutrients in the soils.

References

1. **Adamchuk V.I., Morgan M.T., Ess, D.R.:** An automated sampling system for measuring soil pH. Transactions of the ASAE, 42 , 885–891, 1999.
2. **Adamchuk V.I., Lund E., Dobermann A., Morgan M.T.:** On-the-go mapping of soil properties using ion-selective electrodes. In: Stafford, J., Werner, A. (Eds.), Precision

Agriculture. Wageningen Academic Publishers, Wageningen, The Netherlands, pp. 27–33, 2003.

3. **Adamchuk V.I., Hummel J.W., Morgan M.T., Upadhaya S.K.:** "On-the-go sensors for precision agriculture", Computers and Electronics in Agriculture, 44, 71–91, 2004.

4. **Adsett J.F., Thottan J.A., Sibley K.J.:** Development of an automated on-the-go soil nitrate monitoring system. Applied Engineering in Agriculture 15 (4), 351–356, 1999.

5. **Bakker E., Bühlman P., Pretsch E.:** Carrier-based ion-selective electrodes and bulk optodes. 1. General Characteristics. Chem Rev, 97, 3083–3132, 1998.

6. **Bakker E, Bühlmann P., Pretsch E.:** Polymer membrane ion-selective electrodes – What are the limits?' Electroanalysis, 11, 915–922, 1999.

7. **Birrell S.J., Hummel J.W.:** Multi-sensor ISFET system for soil analysis. In: Stafford, J.V. (Ed.), Proceedings of the First European Conference on Precision Agriculture. BIOS Scientific Publishers Ltd., Oxford, UK, pp. 459–468, 1997.

8. **Birrell S.J., Hummel, J.W.:** Membrane selection and ISFET configuration evaluation for soil nitrate sensing. Transactions of the ASAE 43 (2), 197–206, 2000.

9. **Bühlmann P., Pretsch E., Bakker E.:** Carrier-based ion-selective electrodes and bulk optodes. 2. Ionophores for potentiometric and optical sensors. Chem Rev, 98, 1593–1687, 1998.

10. **Collins K., Christy C., Lund E., Drummond P.:** Developing an automated soil pH mapping system. Paper No. MC03-205, ASAE, St. Joseph, Michigan, 2003.

11. **Hummel J.W., Sudduth K.A., Hollinger S.E.:** Soil moisture and organic matter prediction of surface and subsurface soils using an NIR soil sensor. Computers and Electronics in Agriculture 32, 149–165, 2001.

12. **Loreto A.B., Morgan M.T.:** Development of an automated system for field measurement of soil nitrate. Paper No. 96-1087, ASAE, St. Joseph, Michigan, 1996.

13. **Moody G.J., Oke R., Thomas R.B.:** A calcium-sensitive electrode based on a liquid ion exchanger in a poly(vinyl chloride) matrix. Analyst, 95, 910–918, 1970.

14. **Morf W.E.:** The Principle of ion-selective electrodes and membrane transport, Budapest, Akademiai Kiado, 1981.

15. **Mortland M.M.:** Using a glass electrode for estimating exchangeable potassium in soils. Quarterly Bulletin of Michigan Agricultural Experimental Station, 43, 491–98, 1961.

16. **Price R.R., Hummel J.W., Birrell S.J., Ahmad I.S.:** Rapid nitrate analysis of soil cores using ISFETs. Transactions of the ASAE 46, 601–610, 2003.

17. **Püntener M., Vigassy T., Baier E., Ceresa A., Pretsch E.:** Improving the lower detection limit of potentiometric sensors by covalent bonding the ionophore to a polymer backbone, Anal Chim. Acta, 503, 187–194, 2004.

18. **Spichiger-Keller U.E.:** chemical sensors and biosensors for medical and biological applications. Wiley-VCH, Weinheim, 1998.

19. **Stefanac Z., Simon W.:** In-vitro-verhalten von Makrotetroliden in Membranen als Grundlage für hochselektive kationenspezifische Elektrodensysteme. Chimia, 20, 436, 1966.

20. **Umezawa Y.** *et al.*: Potentiometric selectivity coefficients of ion-selective electrodes Part I. Inorganic cations. Pure Appl. Chem., **72**, 1851–2082, 2000.

21. **Umezawa Y.** *et al.*: Potentiometric selectivity coefficients of ion-selective electrodes Part II. Inorganic anions. Pure Appl Chem 74, 923–994, 2002.

22. **Wang J., Scott A.D.:** determination of exchangeable potassium in soil using ion-selective electrodes in soil suspensions. European Journal of Soil Science, 52, 143–150, 2001.

84

23. **Yildirim S., Birrell S.J., Hummel J.W.:** Laboratory evaluation of an electro-pneumatic sampling method for real-time soil sensing. Transactions of the ASAE, in press.

IMPACT OF SATURATED HYDRAULIC CONDUCTIVITY OF SOILS ON NUMERICAL SIMULATION OF SOIL WATER MOVEMENT

Mikulec Vladimir

Institute of Hydrology, Slovak Academy of Sciences, Bratislava, Slovak Republic
mikulec@uh.savba.sk

Abstract

Saturated hydraulic conductivity is the most sensitive input into the physically based numerical models of soil water movement. In presented study was evaluated the impact of saturated hydraulic conductivity, measured by laboratory method of the Falling Head permeameter and field methods of Disc and Guelph permeameter, on mathematical simulation of soil water movement. Values of hydraulic conductivity were measured during growing season of vegetation in 1999 at locality Royal Meadow (Kralovska Luka). Three sets of the hydraulic conductivity values were obtained. Separately for each set of measured values, an average value of hydraulic conductivity for every determined material horizon of studied soil profile was calculated. Owing to these three sets of input values, three variants of simulation of soil water movement, for given locality and time period, were performed. From the results of realized variants of numerical simulation, the water content values in soil horizons 0 – 30, 31 – 60 and 61 – 90 cm were calculated. These values were compared in correspondent horizons. There are also presented values of the water content, obtained from measured values of soil moisture at studied locality during given time interval, in this study. Comparison shows a very good correlation between the values of water content calculated from measured and from modeled values of soil moisture.

K e y w o r d s : hydraulic conductivity, numerical simulation, water content

Introduction

Soil water retention curves (WRC) and values of saturated hydraulic conductivity (K) are basic hydro-physical characteristics of soils. In natural conditions, there are mostly heterogeneous soils that usually demonstrate anisotropy. Therefore, their hydro-physical characteristics also show spatial variability. Applying methods of measurement, only the discrete values of hydro-physical characteristics could be recorded at given point of soil volume. Thus, these discrete values are often used as representative for determined part of soil volume.

Values of K are also heavily influenced by existence of preferential ways of water flow in soil, where the water flows faster than through the regular soil

matrix. Therefore, it is necessary to recognize whether the measured values of K express hydraulic conductivity of soil matrix, or hydraulic conductivity of preferential ways. Only then it is possible to perform correct mathematical simulation (Stekauerova, 1998).

Applied one-dimensional mathematical description of continuous water flow in soil is based on Richards equation. This solution demands, that the soil profile consist of set of roughly homogeneous soil layers. Such homogeneous soil layer can be sufficiently described by average values of measured hydro-physical characteristics (WRC, K).

Material and methods

Studied locality lies at south part of Slovakia, in region of Rye Island (Zitny Ostrov). It is located in Danube inundation, above the hydro power plant Gabcikovo, between inlet channel to the power plant and old riverbed of Danube.

Fig. 1.   Position of examined locality (marked by arrow)

Site of measurement belongs to municipality of Bodiky, and it is called Royal Meadow (Kralovska Luka). Examined locality is a forest ecosystem with predominant poplar vegetation (Novak *et al.*, 1998). Upper soil horizons were classified as loamy, or as a sandy loam. In the depth of 120 cm began a sandy layer, which was in the depth of 150 cm under the soil surface replaced by a deep gravel layer.

Undisturbed soil samples with volume of 100 cm^3 were taken from the measurement site during the growing season of vegetation in 1999. Then, the drainage branches of WRC were determined on hyperbaric device. Values of

K were set using three methods, namely laboratory method of Falling Head permeameter and field methods of Disc and Guelph permeameter (**Fig. 2**).
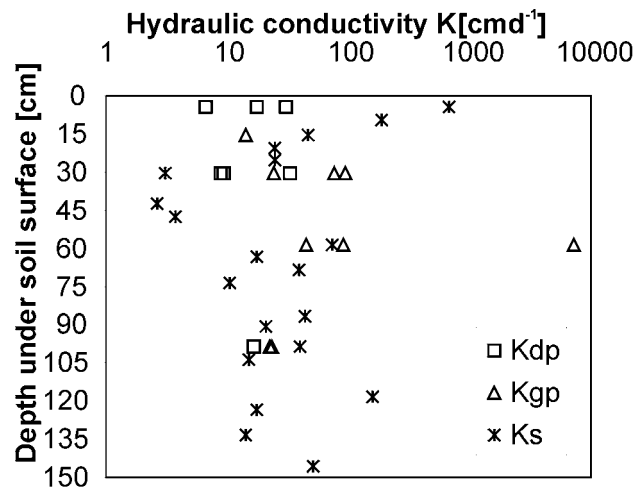
Fig. 2.   Measured values of saturated hydraulic conductivity (K)

Measurements performed with disk permeameter (K_{DP}) represent hydraulic conductivity of soil matrix in state of saturation, or near this state. Values of K_{DP} are usually relatively homogeneous in each particular soil horizon, and also in whole soil profile.

Hydraulic conductivity measured using method of Falling Head permeameter (K_S) reflect mainly vertical conductivity of saturated soil. If preferential ways of water flow are present in such a small volume of soil sample (100 cm^3), then their conductivity is also included in K_S.

Applying Guelph permeameter, the measured values of hydraulic conductivity (K_{GP}) express vertical and horizontal conductivity of saturated soil, including conductivity of preferential ways of water flow, when they influenced the measurement.

Values of K_S and K_{GP} indicate that as deeper are the observed soil horizons, as fewer preferential ways of water flow are there.

Studied soil profile was divided owing to its hydro-physical characteristics (WRC, K) on relatively homogeneous layers, although one of measured values of K_{GP} in 60-cm depth differed in orders from other measured values of hydraulic conductivity. That value was not considered by creating average value of K_{GP} for given soil horizon, because it represented conductivity of preferential ways of water flow in studied soil layer. In applied model, Hydrus-ET (Simunek *et.al.*, 1997), is one-dimensional water flow in soil described by Richards equation. This

88

solution excluded the possibility to take the conductivity of preferential ways of water flow in account. Given problem was overcame by introduction of two (van Genuchten, Wierenga, 1976; Skopp *et al.*, 1981; Chen – Wagenet, 1992a,b) or more domain models (Wilson *et al.*, 1992; Steenhuis *et al.*, 1990), where one domain represented soil matrix (micro-pores) and the other could describe preferential ways in soil (mezo-pores and macro-pores).
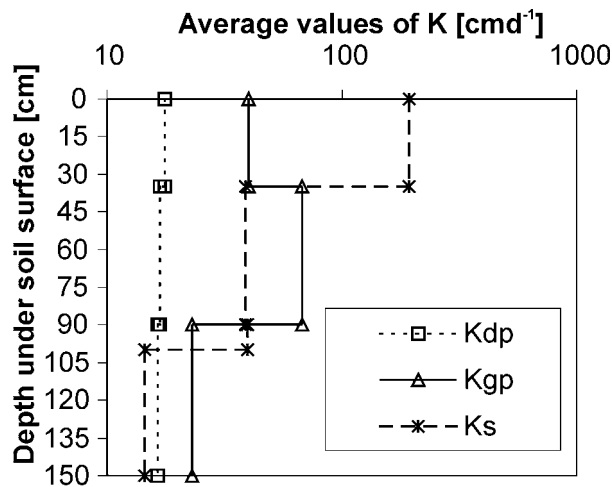
Fig. 3. Average values of saturated hydraulic conductivity (K) in defined material horizons

In determined material layers of soil profile 0 – 35, 36 – 90, 91 – 100 and 101 – 150 cm were defined average hydro-physical characteristics K (**Table 1**; **Fig. 3**) and WRC (**Table 1**). Hysteresis of WRC was neglected and only the drainage part of WRC was used. Course of drainage part of WRC was mathematically approximated according to van Genuchten (1980).

Table 1. Hydro-physical characteristics of soil profile at locality Royal Meadow

Material layer [cm]	Saturated moisture content θ_s [cm^3cm^{-3}]	Field water capacity θ_{pk} [cm^3cm^{-3}]	Residual moisture content θ_r [cm^3cm^{-3}]	Parameter		Average values of K [cmd^{-1}]		
				a [cm^{-1}]	n [-]	K_S	K_{DP}	K_{GP}
0 – 35	0.5474	0.38	0.0684	0.04	1.2971	193.27	17.65	40.15
36 – 90	0.5491	0.35	0.0552	0.05	1.3514	38.90	16.74	67.51
91 – 100	0.5425	0.33	0.0265	0.10	1.1760	39.73	16.46	22.92
101 – 150	0.5231	0.37	0.0484	0.02	1.3827	14.44	16.46	22.92

Owing to used methods of measurement of K, three variants of mathematical modelling of continual change of moisture (θ) in vertical direction, from soil surface to ground water level (GWL), were performed. Monitoring of θ on Royal Meadow, during the studied growing season of vegetation in 1999, was conducted using neutron probe. It was performed in 10-cm intervals from soil surface to GWL.

Monitored values were evaluated owing to availability of soil water for vegetation in Stekauerova and Nagy (2001). Components of water balance in unsaturated zone were quantified using model Global (Majercak and Novak, 1995) in Stekauerova et al. (2001). Set of input data, from which were counted the most correspondent outputs (from models Global and Hydrus-ET) with measured values of θ, was determined in Mikulec (2002).

Initial and boundary conditions

Initial condition for mathematical modelling was given by first measurements of θ at monitored site of Royal Meadow in beginning of the growing season of vegetation in 1999 (Stekauerova et al. 2001).

Upper boundary condition was constituted by climatic characteristics (daily precipitation total [mmday^{-1}], mean temperature [°C], sunshine duration [hours], vapour pressure [hPa] and mean wind velocity [ms^{-1}]) measured at meteorological station of Slovak Hydro-meteorological Institute in Gabcikovo. Upper boundary condition also comprises of phenological parameters (leaf area index [m^{2}m^{-2}], roughness of evaporating surface [m], albedo of surface [cm], root depth [cm] and relative mean water content [%]) of vegetal cover formed by poplar ecosystem.

Lower boundary condition was defined by time series of GWL depth under the soil surface at monitored site. Depth of GWL under the soil surface oscillated during 1999 in interval (192, 258) cm.

Results and discussion

Three methods of measurement of K as the input for mathematical simulation were applied on locality of Royal Meadow for the year 1999. Values of the water content (W) in soil horizons 0 – 30, 31 – 60 and 61 – 90 cm were calculated. Comparison of outputs form mathematical simulation represented by modeled values of soil water content (W_{DP}, W_S, W_{GP}) with values of water content counted from measured series of θ (marked as W_M) can be seen in **Fig. 4**.

Maximal values of W in horizons 0-30 and 31-60 cm were obtained mainly using variant of modelling with values of K_{DP}. Primary reason of such a result

was a low average value of K_{DP}, which was in material layer 0-35 cm roughly 2-times lower than K_{GP} and about 11-times lower than K_S. In material horizon 36-90 cm was K_{DP} around 4-times lower than K_{GP} and somewhere 2-times lower than K_S. Value of K_{DP} was the lowest from all measured values of K. That caused the slowest water flow through modeled horizons of soil, and also brought maximal modeled values of W in soil horizons 0-30 and 31-60 cm in this variant of modelling. Few maximal values of W in soil horizons 0-30 and 31-60 cm occurred also in variant of modelling with K_S, mainly in horizon 31-60 cm. This can be explained with rush change of mean value of K_S from 193.27 cm.day^{-1} in material layer 0-35 cm to 38.9 cm.day^{-1} in material horizon 36-90 cm. Water was accumulated on the boundary between material layers and that caused the increasing of W in modeled soil horizon 31-60 cm. Variant of modelling with K_{GP} in horizons 0-30 and 31-60 cm never achieved a maximal value of W. In this variant vice-versa, were in horizons 0-30 and 31-60 cm acquired all minimal values of W. It was caused by relatively great mean value of K_{GP} in material layer 0-35 cm, which was in next material layer 36-90 cm even greater. In comparison to other variants of measurement of K, was value of K_{GP} in material horizon 36-90 cm the greatest of all. That caused faster water flow through this material layer to deeper horizons of modeled soil profile.

In soil horizon 61-90 cm was also contribution of water from deeper horizons evident. It is obvious mainly in the view of values of W_M (**Fig. 4**). Maximal values of W were no longer achieved by variant using K_{DP}. They were reached mostly applying variant of modelling with K_S. If the position of GWL was high enough, then the maximum was achieved in variant with K_{GP}. Thus the higher position of GWL made sometimes possible for variant with K_{GP} faster water flow in soil layer 61-90 cm, than in variant with K_S. Minimal values of W were again achieved in variant with K_{GP}, excluding mentioned cases with high position of GWL, where minimal values of W were obtained using variant with K_{DP}.
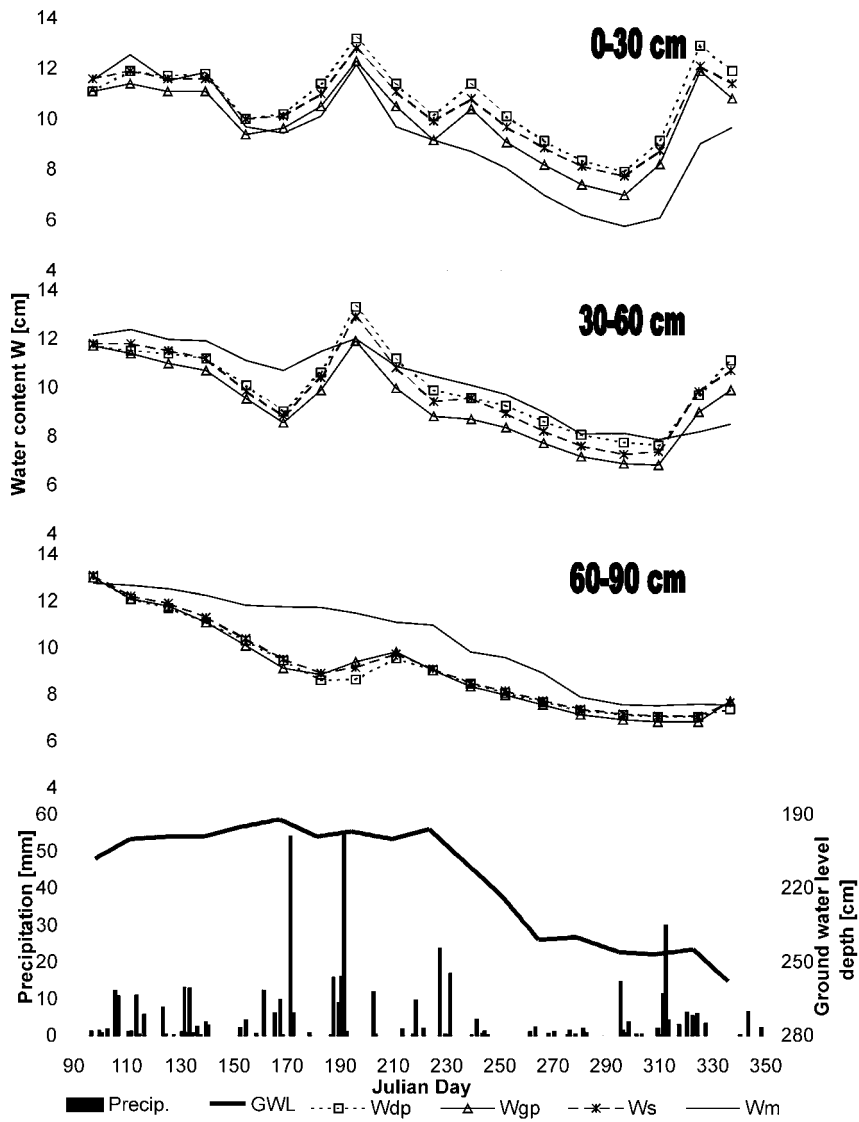
Fig. 4. Time change in water content (W) counted from modeled and measured values of moisture (θ) for growing season of vegetation in 1999 at locality Royal Meadow (In lower part of picture are presented daily precipitation totals and mean daily positions of ground water level)

Correlation between values of W achieved in three variants of modelling and values of W counted from measured values of θ is presented in **Table 2**.

Comparison manifests good correspondence between modeled and measured time series of W in studied soil profile during 1999.

Table 2. Linear correlation between modeled and measured values of water content (W) in studied soil horizons 0–30, 30–60 and 60–90 cm

0-30cm	W_M	W_S	W_{DP}	W_{GP}	30-60cm	W_M	W_S	W_{DP}	W_{GP}	61-90cm	W_M	W_S	W_{DP}	W_{GP}
W_M	1.000				W_M	1.000				W_M	1.000			
W_S	0.898	1.000			W_S	0.811	1.000			W_S	0.905	1.000		
W_{DP}	0.816	0.982	1.000		W_{DP}	0.790	0.990	1.000		W_{DP}	0.892	0.998	1.000	
W_{GP}	0.881	0.998	0.985	1.000	W_{GP}	0.855	0.990	0.973	1.000	W_{GP}	0.907	0.997	0.991	1.000

Conclusions

One-dimensional mathematical modelling of continual change of moisture (θ) in vertical direction, from soil surface to ground water level (GWL), was performed in three variants, owing to applied methods of measurement of saturated hydraulic conductivity (K). Values of K were acquired by laboratory method of Falling Head permeameter (K_S) and by field methods of Disk (K_{DP}) and Guelph (K_{GP}) permeameter, during growing season of vegetation in 1999 at locality Royal Meadow. The drainage branches of soil water retention curves (WRC) were determined on hyperbaric device. Owing to measured hydrophysical characteristics (K, WRC); the studied soil profile consists of set of roughly homogeneous soil layers. Therefore, it was possible to use calculation based only on Richards equation. Numerical simulation of water flow in unsaturated zone of soil was performed on model Hydrus-ET.

Maximal values of W in horizons 0-30 cm and 31-60 cm were obtained by variant of modelling with K_{DP}. Reason of such a result was a low average value of K_{DP}. This value caused simulation of slower water flow and of greater W_{DP} at output of model, in studied soil layers 0-30 cm and 31-60 cm, than in other two variants of numerical simulation.

In soil horizon 61-90 cm was contribution of water from deeper horizons evident. Maximal values of W were no longer achieved by variant of modelling with K_{DP}, but they were reached mostly in variant with K_S.

Minimal values of W were counted by variant of modelling with K_{GP}, because measuring with Guelph permeameter gave in majority of cases bigger values of K than other applied methods. Thus, the modeled water flow was faster in this variant, than in other performed variants of modelling.

Value of K is the most important input to physically based models of water flow through porous media. All presented variants of modelling gave a good information about real state of W in studied soil profile. But still, it is necessary to choose the appropriate method of measuring of K because of wide range of natural conditions. It is also essential to know which method of measurement of K is suitable for used mathematical description of water flow in selected numerical simulation. Only then is the quantity of various numerical simulations used correctly.

References

1. **Chen C., Wagenet R.J.:** Simulation of Water and Chemicals in Macro-pore Soils. Part 1. Representation of the Equivalent Macro-pore Influence and its Effect on Soil Water Flow. J. Hydrol., 130, 1 – 4, p. 105 – 126, 1992a.
2. **Chen C., Wagenet R.J.:** Simulation of Water and Chemicals in Macro-pore Soils. Part 2. Application of Linear Filter Theory. J. Hydrol., 130, 1 – 4, p. 127 – 149, 1992b.
3. **Genuchten M.Th., van Wierenga P:** A Closed–Form Equation for Predicting the Hydraulic Conductivity of Unsaturated Soils. Soil Sci. Soc. Am. J. 44, p. 892 – 898. 1980.
4. **Genuchten M.Th., van Wierenga P.J.:** Mass Transfer Studies in Sorbing Porous Media. I. Analytical Solutions. Soil Sci. Soc. Am. J., 40, 4, p. 473 – 480. 1976.
5. **Majercak J., Novak V.:** Global – a Numerical Model for Water Movement in the Soil Root Zone. Research Report, IH SAS, Bratislava, Slovak Republic, 75 p. 1995.
6. **Mikulec V.:** Determination of Applicability of a Group of Input Data Sets for Numerical Simulation of the Soil Water Movement in the Unsaturated Zone at the Locality Bodiky. X. Poster Day IH and GPI SAS, Bratislava, CD-ROM, p. 294 – 303, 2002.
7. **Novak V., Sutor J., Majercak J., Simunek J., Genuchten M., Th.:** Modelling of Water and Solute Movement in the Unsaturated Zone of the Rye Island (Zitny Ostrov) Region, South Slovakia. IH SAS, Bratislava, Slovakia, 73 p., 1998.
8. **Simunek J., Huang K., Sejna M., Genuchten M., Th., Majercak J., Novak V., Sutor J.:** The HYDRUS-ET Software Package for Simulating the One – Dimensional Movement of Water, Heat, and Multiple Solutes in Variably Saturated Media. U.S. Salinity Laboratory, USDA, ARS, Riverside, California, USA and IH SAS, Bratislava, Slovakia, 184 p. 1997.
9. **Skopp J., Gardner W.R., Tyler E.J.:** Solute Movement in Structured Soils: Two – Region Model with Small Interaction. Soil Sci. Soc. Am. J., 45, 5, p. 837 – 842, 1981.
10. **Steenhuis T.S., Parlange J.Y., Andreini M.S.:** A Numerical Model for Preferential Solute Movement in Structural Soils. Geoderma, 46, 1 – 3, p. 193 – 208. 1990.
11. **Stekauerova V.:** Determination of Saturated Hydraulic Conductivity in Various Horizons of Structural Soil. Acta Hydrologica Slovaca, 1, p. 123 – 129. 1998.
12. **Stekauerova V., Majercak J., Sutor J.:** Quantification of Water Balance Components in Soil Unsaturated Zone. Acta Hydrologica Slovaca, 2/2, p. 183 – 190. 2001.
13. **Stekauerova V., Nagy V.:** Impact of Climatic Conditions on Water Supply for Plants in Localities Bac and Bodiky. Acta Hydrologica Slovaca, 2/1, p. 58 – 63, 2001.
14. **Wilson G.V., Jardine P.M., Gwo J.P.:** Modelling the Hydraulic Properties of a Multiregion Soil. Soil Sci. Soc. Am. J., 56, 6, p. 1731 – 1737. 1992.

MECHANICAL PROPERTIES OF AGRICULTURAL GRANULAR MATERIALS

Molenda Marek, Horabik Józef

Institute of Agrophysics, Polish Academy of Sciences, Lublin, Poland
mmolenda@demeter.ipan.lublin.pl

Introduction

Recent decades have brought increased number of processes and operations involving granular materials that resulted in a growing need for new theory and technology. This was accompanied with growing interest in investigations of physical properties of granular materials. Elaboration of effective design methods of technological processes requires detailed knowledge of physical properties of the processed material as well as proper understanding of their interrelations with construction materials. Development and refinement of methods for determination of physical properties of granular materials is becoming particularly important. Despite unquestionable progress in development of measurement methods mechanical properties of granular materials measured in various laboratories can vary greatly. A significant source of the wide range of results is due to the large number of measurement methods and a lack of standard experimental procedures. Moreover some influencing factors such as moisture content, bulk density, packing structure and load history remain out of control that contribute to observed variability.

Granular materials of biological origin constitute a coherent group of materials distinguished by large deformability of particles and strong dependence of their mechanical properties on moisture content. Contrary to materials of mineral origin, moisture penetrates inside grain, leading in some cases to qualitative changes in physical properties.

Airflow resistance – method and materials

Corn, soybeans, red wheat and white wheat were conditioned to three moisture content levels using air at 20°C/55%, 20°C/65%, and 20°C/75% (R.H.). The moisture content was determined using the oven method and the test weight using the Winchester cup. The samples were screened according to USDA-GIPSA procedures and the percentage of fines, splits, or broken kernels determined as appropriate. Ergun's [2] equation was used to predict the airflow

resistance of corn, white wheat, red wheat, and soybeans at three moisture content levels, and two packing densities.

The system used for measuring airflow resistance comprised a cylindrical PVC pipe with a diameter of 0.25 m and a height of 0.49 m. Air was introduced through a plenum in the bottom of the cylinder. The differential static pressure was measured at 0.05 m above the bottom of the cylinder and 0.4 m above. The static pressure was measured using a variable reluctance differential pressure transducer (Validyne DP103, Northridge, CA) with a diaphragm with a maximum pressure rating of 1370 Pa and an accuracy of ±0.25% full scale. The flow rate was measured using a hot wire anemometer (Alnor Model 2106, Shoreview, MN) and the pressure drop across a nozzle.

Airflow resistance – results

To obtain a high bulk density a "sprinkle" filling method was used. Grain was transferred using a scoop to a hand held sieve shaken above the top of the grain column. Kernels were evenly dispersed over the area of the column and formed denser bedding. Loose filling was accomplished using a funnel that was kept within 2 cm of the grain surface during filling and was termed centric. In this case the grain during filling formed a conical sloping surface with the vertex directed upward and the grains tending to rest with their long axis along a line of the formed cone. Bulk density differences were achieved by filling the chamber using the sprinkle and centric method. Sprinkle filling resulted in a bulk density that was 2.6 to 11.5% greater than the initial test weight. Centric filling resulted in a bulk density that was slightly greater or less than the test weight determined using the Winchester cup method. The largest amount of packing occurred with grain at the medium moisture content level, except for the corn. Bulk density strongly influenced properties of granular material.

Method of filling test apparatus with wheat that resulted in an increase in density (decrease in porosity) considerably increased the airflow resistance (see **Fig. 1**). The effect of grain orientation that would be typical in storage bins was negligible, less than 10% in airflow resistance.

Strength properties – methods and materials

A great deal of work has been done to develop a usable theory of gravity flow of granular materials. The most widely accepted approach was developed by Jenike and published in 1961 [3]. The author further refined the approach, but his original testing method and interpretation is still the basis of many codes of

practice and later investigations by other researchers. Jenike method (also termed as direct shear test) gives as a result of determination the parameters of internal friction (also termed strength parameters) – cohesion (c), angle of internal friction (φ_c) and effective angle of internal friction (φ_c).
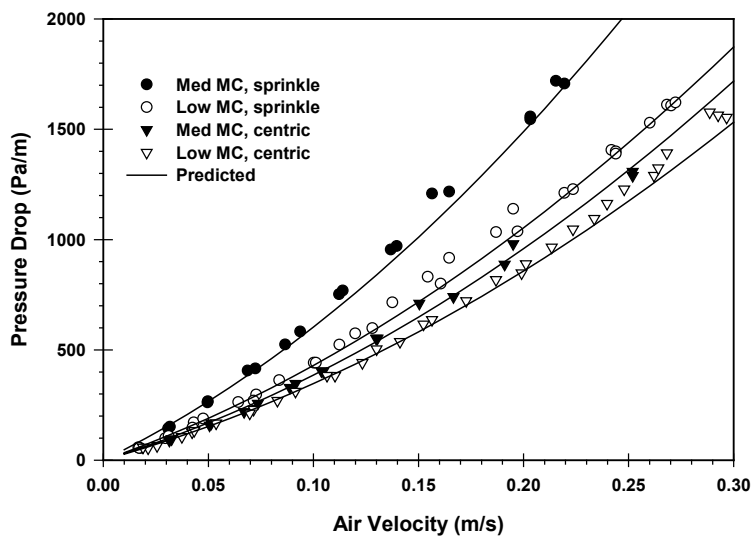
Fig. 1. Measured and predicted pressure drop versus air velocity for soft red wheat at the low (10.5%) and medium moisture content (12.7%) sprinkle versus centric filling [4].

Strength properties – results

In our project [4] the method of sample deposition was found to have significant influence on both force-displacement characteristics and coefficient of internal friction. Stress history had considerable influence on the rate of friction force increase. The angle of internal friction of cereals was found to be influenced by the initial orientation of non-spherical grain in the test specimen. The maximum change in the angle of internal friction for wheat was found of approximately 4 degrees.

Granular materials of plant origin differ from mineral materials in strong susceptibility to moisture changes as well as in deformability of particles. With the moisture content increase of cereals the angle of internal friction increased in a range from 22° in the case of 10% m.c. oats up to 35° for 20% in m.c. wheat. The lateral to vertical pressure ratio decreased with an increase in moisture content and was found in the range from 0.30 in the case of 20% in m.c. corn up to 0.49 for 10% in m.c. oats. Effect of deformability of grain brings difficulties in

testing of strength of cereal grain of increased moisture content. For such a material stress-strain curve did not level until relatively high displacement. For direct shear test on wet grain (up to 20% of m.c.) the shear path had to be elongated up to 0.1 displacement-to-sample diameter ratio (as compared to 0.05 – Eurocode 1 [1] recommended).

Flowability – method and materials

Flowabilily is a measure of the quality of granular product that influences its end-use value for some materials used in the chemical, mineral, pharmaceutical and food industries. Variation in flowability of ingredients is a significant source of errors during the weighing and proportioning, resulting in non-uniformity in the finished product.

The concept of flow function may be explained by theoretical experiment as follows. Let us consider a cylindrical sample of material compacted under major stress, σ_1, in container with frictionless walls (see **Fig. 2**). After completing compaction the container is removed and vertical compressive load required to just crush the sample is measured; that is equal to unconfined yield strength of the material, σ_c.

The experiment may be repeated for several values of consolidating pressure and pairs of σ_1, σ_c, are obtained. A plot of σ_1 against σ_c is termed flow function for the considered material.
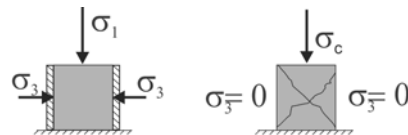
Fig. 2   Unconfined yield strength σ_c.

Flowability – results

Two groups of food powders: cereal powders and non-starch powders were tested for flowability (maximum consolidation pressure of 100 kPa) [5]. The first group comprised coarse flour, semolina, wheat groats, pearl barley groats and oatmeal; the second group comprised icing sugar, table sugar, potato flour, powdered milk and table salt. The flow functions of all tested materials took values characteristic for free flowing and easy flowing materials. The tendency, known for mineral powders, that material with larger particles flow easier was confirmed for examined food powders. Flowability of wheat meal was tested with

increasing content of fines (particles of size from 0.1 to 0.2 mm). Addition of 25% of fines resulted in a higher than twofold increase in flow function (see fig.3). Content of fines was also found to influence significantly compressibility of the meal. In uniaxial test basic material reached maximum vertical pressure at strain of 0.05, while the material containing 25% of fines reached maximum stress at a strain of 0.07.
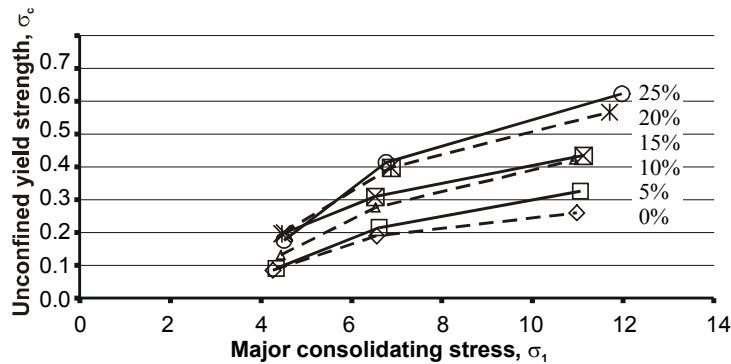
Fig. 3. Flow functions sc(s1) of six samples of wheat meal containing various amount of fines

Conclusions

Previous work had indicated that Ergun's equation would not be applicable to grain aeration due to packing effects within the bin. However, research has indicated that packing can be estimated using granular mechanics models and changes in porosity of grain bulks could be estimated. The overall error using Ergun's equation was less than 10 Pa/m, when the pressure drop was less than 250 Pa/m. If all data was included up to a pressure drop of 1,000 Pa/m the standard error averaged 40 Pa/m. The effect of grain orientation that would be typical in storage bins was negligible, less than 10% increase in airflow resistance. However, the fill method and resulting bulk density increased the airflow resistance by an order of magnitude. Ergun's equation, with an appropriate model of porosity variation during storage, could be utilized for the design and analysis of grain aeration systems.

Direct shear tests performed with 21cm in diameter shear box have shown that the method provided for accurate and reproducible results of the strength parameters of grain. For testing of wet grain (up to 20%), however, shear path had to be elongated up to 0.1 sample diameter (as compared to 0.05 recommended by Eurocode 1) to achieve steady state flow conditions in shear zone. Triaxial compression tests with 15 cm in diameter sample of wheat performed on the same

grain have shown that results of both methods were consistent, thus direct shear test can be recommended as equivalent to triaxial compression method for testing wheat grain and seeds of similar geometrical and chemical structure.

The flow functions of all tested food powders took values characteristic for free flowing and easy flowing materials. Content of fines in wheat meal was found to influence strongly flowability and compressibility of the material. Addition of 25% of fines (particles of size from 0.1 to 0.2 mm) resulted in a higher than twofold increase in flow function.

References

1. **Eurocode 1:** Basis of design and actions on structures. Part 4. Actions in silos and tanks. DD ENV 1991-4: 1996.
2. **Ergun S.** Fluid flow through packed columns. Chemical Engineering Progress 48: 89-94, 1952.
3. **Jenike A.W**.: Gravity flow of bulk solids. Bulletin of the University of Utah 52(29), 1961.
4. **Molenda M., M.D. Montross, S.G. McNeill, J. Horabik**: Airflow resistance of seeds at different bulk densities using Ergun's equation, submitted to Transactions of the ASAE, 2004.
5. **Stasiak M., M. Molenda**: Mechanical properties of agricultural granular materials. Res. Agr. Eng., 50(1): 6-10, 2004.

EVOLUTION OF GASES FROM SOIL IRRIGATED WITH PURIFICATED WASTEWATER

Nosalewicz[1] Magdalena, Stępniewska[2] Zofia

[1]Institute of Agrophysics, Polish Academy of Sciences, Lublin, Poland
m.nosalewicz@demeter.ipan.lublin.pl
[2]Catholic University of Lublin, Poland

Introduction

Irrigation of soil with municipal wastewater after mechanical and biological cleaning can be treated as a third step of their purification. However the irrigation with substantial doses of the wastewater can induce anoxic conditions in soil what, can cause emission of the radiatively active trace gases such as methane and nitrous oxide.

Nitrous oxide (N_2O) is one of the greenhouse gases playing important role in destroying the ozone layer (Chang *et al.* 1987; Cicerone 1987). Nitrous oxide is 300 (mass basis) times more radiatively active than CO_2 at absorbing infrared radiation (Rodhe, 1990).

Atmospheric concentrations of N_2O have been increasing at a rate of 0.2-0.3% per year (Kroeze 1994) during the last century. Agricultural soils are among the largest sources of anthropogenic N_2O and N_2O emission from agricultural land. The emission varies from 0.03% to 2.7% of the total nitrogen (N) fertilizer applied (Eichner, 1990). Increasing atmospheric content of N_2O gives cause for serious environmental concern.

Artificially drained organic soils contribute to an important degree to the atmospheric load of N_2O (Maljanen *et al.* 2003). Irrigation of soils with substantial doses of the wastewater can induce anoxic conditions in which nitrate (NO_3^-) and nitrite (NO_2^-) are converted to dinitrogen gas (N_2). Intermediate in the process of denitrification is nitrous oxide which most is emitted from wastewater treatment systems (Schalk-Otte *et al.* 2000). N_2O can also be produced from nitrification in aerobic conditions (Williams *et al.* 1992).

Methane is the second most important greenhouse gas after CO_2 and contributes to the global warming in about 20% (Bouwman 1990). CH_4 in the atmosphere has a lifetime of about 12 years, and its concentration is increasing in the atmosphere at the rate of about 0.8% y^{-1}. The increase of CH_4 is a cause of considerable concern because CH_4 plays an important role in atmospheric chemistry and radiation forcing (Gilbert *et al.* 1995). CH_4 has a global warming

potential of about 24.5 times higher as relative to CO_2 and is responsible for approximately 25% of anticipated warming (IPCC 1995).

Soil production of CH_4 is associated with wetlands, flooded rice production, termites' activity, landfills and areas of gas production. About 40% of annual CH_4 emissions are produced in the soil (Mosier *et al.*, 1991). Methanogenesis is affected by many physical and biochemical factors, such as soil pH, redox potential, organic matter content, temperature and soil moisture content (Yu *et al.* 2001).

The two principal mechanisms that remove atmospheric CH_4 are reaction in the troposphere and CH_4 oxidation by bacteria in soil. The amount of about 700 Tg of methane is annually consumed in soils.

The aim of the study was to investigate the rate of methane and nitrous oxide evolution from fields irrigated with municipal wastewater after second step of purification in the wastewater treatment plant.

Materials and methods

The experimental fields were located in the valley of Bystrzyca river, with a peat muck soil (Eutric Histosol). The fields of a surface 0.8 ha were prepared in order to obtain three treatments with different plant: Populus alba and Populus nigra, Salix americana and Salix viminalis, and mix of grasses (with Alopecurus pratensis, Phalaris arundinacea, Festuca pratensis as dominating grass species).

The basic characteristics of soil Eutric Histosol material: 32.9 % organic C, pH 7.37 in KCl and particle size fraction: 4% (0-0.1 mm), 55% (0.1-0.02 mm) and 41% (<0.02 mm).

Determination of evolution of the trace gases was perfumed on the fields with mix of grasses irrigated 10 times during the vegetation season with 600 and 1200 mm of wastewater per year. A single wastewater dose was 60 and 120 mm for lower and higher irrigation level, respectively. The irrigation wastewater contained in average 25 mg NO_3-N dm^{-3}, and 30 mg of total N dm^{-3} while the average content of total phosphorus was 5 mg dm^{-3} of which 4.8 mg dm^{-3} constituted phosphate P (Kotowski *et al.* 1999).

The evolution of the gasses from the soil surface was measured with a chamber (5.7 dm^2 in the cross section) technique. After the soil surface was covered with the chambers, periodical air sampling for gas chromatographic analysis followed the increase of the concentration of methane, nitrous oxide and carbon dioxide with time. Each time two samples of the atmosphere were taken within the time interval 30 and 60 minutes after the soil surface has been covered with the chambers.

Moreover, soil air was sampled from the depths of 10 and 50 cm and analysed for oxygen, carbon dioxide, methane and nitrous oxide content. Simultaneously redox potential at the same depths was measured.

Results and discussion

The results are presented for a flooding cycle performed in 6.08-12.08.1997.

Irrigation caused a decrease of oxygen content in soil air, which was related to the irrigation wastewater dose and the depth within the soil profile. The observed decrease in the content of oxygen was accompanied by decreases of soil redox potential and increases in the content of carbon dioxide, nitrous oxide and methane (**Fig. 1** … **Fig. 5**).
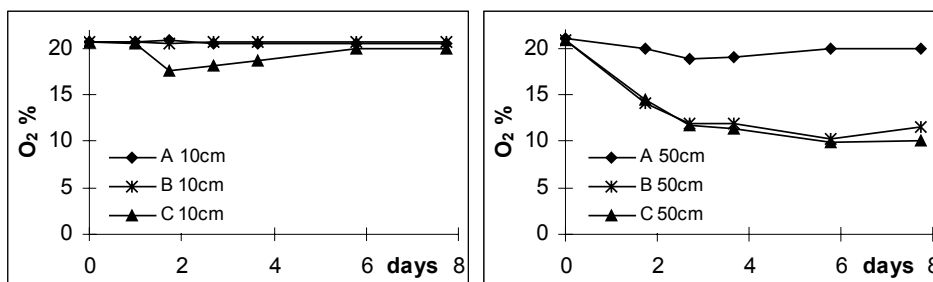
Fig. 1. The changes of oxygen content in soil air at a depth of 10 and 50 cm in the fields irrigated with wastewater (A- control, wetting by precipitation and ground water; B - 60 mm single dose; C- 120 mm double dose)

Oxygen content in the soil air changed much more distinctly at a depth of 50 cm as compared to the depth of 10 cm (**Fig. 1**). Oxygen concentrations decreased during first days of the flooding cycle and then tended to increase. Not always, the original level was reached during the observation period. Minimum concentrations of oxygen did not drop below 17% at a depth of 10 cm and below 8% at a depth of 50 cm. The concentrations of oxygen are similar at a depth of 50 cm for lower and higher irrigation doses.

Redox potential during a single flooding cycle dropped from initial 500-600 mV down to 170 mV at a depth of 10 cm and even below 0 mV at a depth of 50 cm (**Fig. 2**). Differentiation between the irrigation doses was distinct for a depth of 10 cm where return to the higher Eh values was much more rapid for the lower irrigation dose.
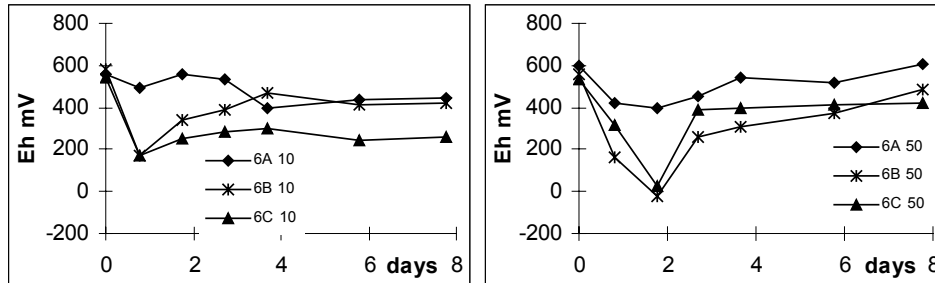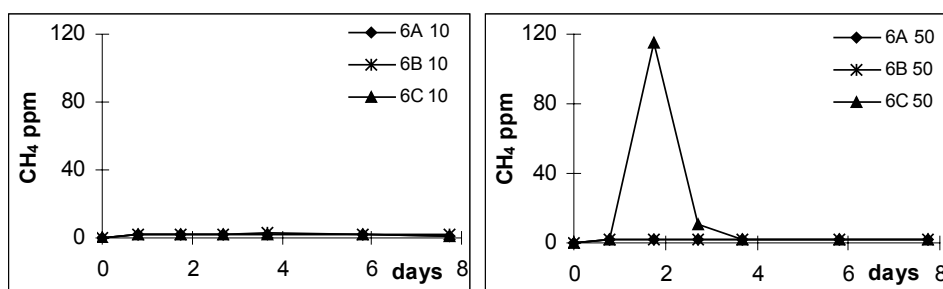
Fig. 2. The changes of redox potential at a depth of 10 and 50 cm in the fields irrigated with wastewater. Explanations as in **Fig. 1**

Carbon dioxide content at a depth of 10 cm ranged from 0.1 to 0.3% in the control and low dose treatments and increased distinctly only in the high dose field up 1.5% (**Fig. 3**). At a depth of 50 cm the control carbon dioxide concentration was within 1.0 - 1.5 intervals while that for the flooded treatments were close to each other and increased until 6% during the entire measurement period comprising first 6 days after application of irrigation.
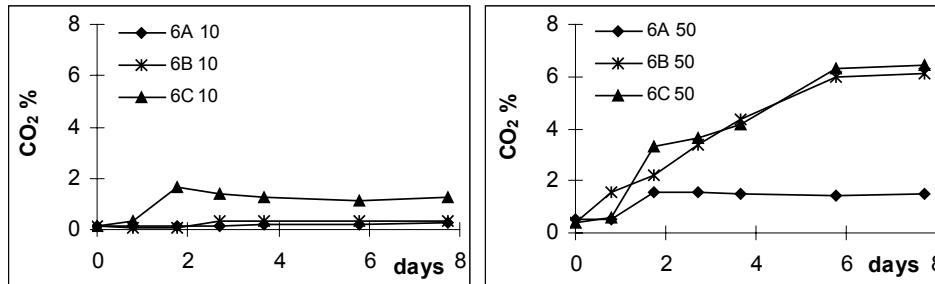
Fig. 3. The changes of carbon dioxide content in soil air at a depth of 10 and 50 cm in the fields irrigated with wastewater. Explanations as in **Fig. 1**
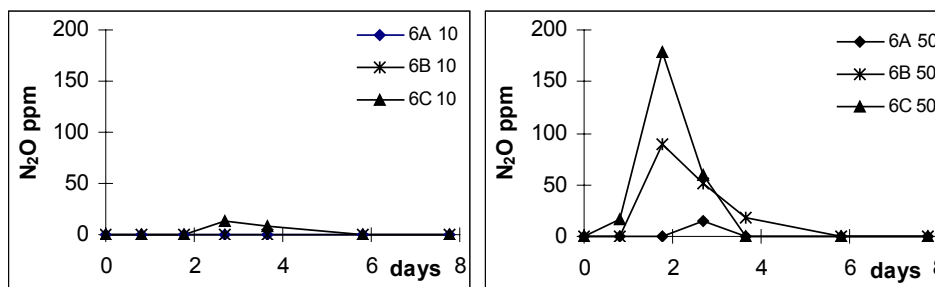
Fig. 4. The changes of nitrous oxide content in soil air at a depth of 10 and 50 cm in the fields irrigated with wastewater. Explanations as in **Fig. 1**

104

Nitrous oxide within the surface horizon increased distinctly above the control level only in the high dose treatment reaching 14 ppmv after three days from the flood onset (**Fig. 4**). For 50 cm depth maximum values were observed after two days from the application of the flooding and reached 90 ppmv for low water dose and 180 ppmv for the higher one.

Fig. 5. The changes of methane content in soil air at a depth of 10 and 50 cm in the fields irrigated with wastewater. Explanations as in **Fig. 1**

Methane concentrations increased distinctly above the atmospheric level only in the high dose treatment at a depth of 50 cm where it reached about 110 ppmv after two days from the beginning of flooding (**Fig. 5**).
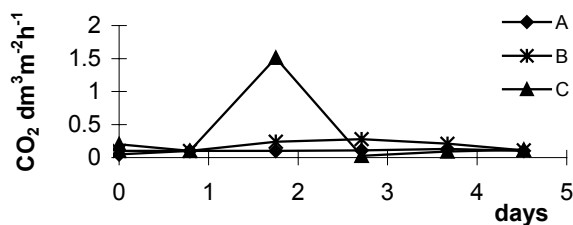
Fig. 6. Surface fluxes of carbon dioxide from the fields irrigated with wastewater. Explanations as in **Fig. 1**

The flux of carbon dioxide from the soil surface to the atmosphere (**Fig. 6**) reached after 2 days a maximum equal to 1.5 $dm^3 m^{-2} h^{-1}$ (what corresponds to about 36 dm^3 CO_2 m^{-2} day^{-1}). This rate is comparable with the highest values reported in the review of Gliński and Stępniewski (1985) for diurnal respiration of different soils and more than two times higher as the maximum value reported by Watanabe *et al.*. (1997) for grassland treated with cattle and swine excreta.

The flux of nitrous oxide from the soil surface did not exceed the level of 0.015 $dm^3 m^{-2} h^{-1}$ (or 20 mg N $m^{-2} h^{-1}$) i.e. it was by about two orders of magnitude lower than that of carbon dioxide (**Fig. 7**). In diurnal terms, it reached the level 0.36 $dm^3 m^{-2} d^{-1}$ corresponding to the loss of 0.48 g N_2O-N $m^{-2} d^{-1}$ or 4.8 kg N_2O-N $ha^{-2} d^{-1}$. This value is pretty high as compared to the values reported in the literature.
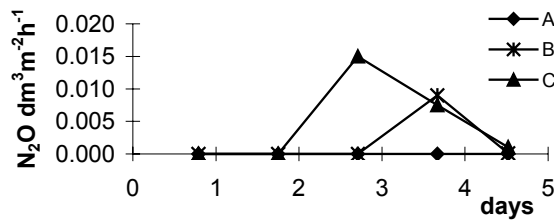
Fig. 7. Surface fluxes of nitrous oxide from the fields irrigated with wastewater. Explanations as in **Fig. 1**

For instance in the rice paddy fields in China the N_2O fluxes from the soil surface were usually ranging from 0.005 to 0.5 mg N $m^{-2} h^{-1}$ (Xu *et al.* 1997). The values reported by Watanabe *et al.* (1997) for a grassland soil after surface application of cattle and swine excreta range from 0.1 to 1.0 mg N $m^{-2} h^{-1}$ but are still at least 20 times lower as compared to our data. The average amount of nitrate nitrogen incorporated in our experiment with the irrigation wastewater to the soil was about 1.5 g m^{-2} for lower irrigation dose and 3 gm^{-2} for the higher dose (15 and 30 kg of NO_3-N ha^{-1}, respectively). Thus, the contribution of denitrification in the total nitrogen balance was substantial reaching about 16% of the incorporated nitrate nitrogen.
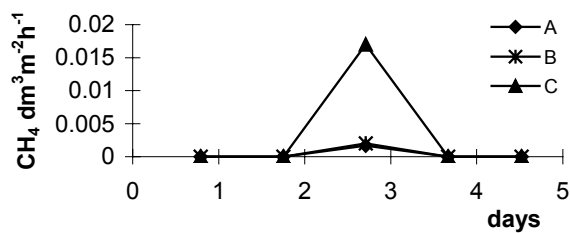
Fig. 8. Surface fluxes of methane from the fields irrigated with wastewater. Explanations as in **Fig. 1**

106

The amount of methane diffusing from the soil surface to the atmosphere was of the same order of magnitude as that of nitrous oxide (**Fig. 8**). The maximum value 0.017 $dm^3 m^{-2}h^{-1}$ corresponds to 0.012 mg CH_4 $m^{-2}h^{-1}$. It should be noted that the review concerning rice paddy fields in China (Cai 1997) gives the interval of the methane flux from in the range from 0.2 to 76 mg CH_4 $m^{-2}h^{-1}$. Our values are much lower indicating that the methanogenesis in this experiment was not advanced.

Conclusions

Irrigation of soil with high doses of nitrate abundant municipal wastewater can lead to intensive denitrification contributing to 16% of the incorporated nitrates. The irrigation cycles induce a temporal drop of soil redox potential, and a decrease of oxygen content in soil air and an increase of carbon dioxide, methane and nitrous oxide content in it. The evolution of methane was of the same order of magnitude as that of nitrous oxide.

References

1. **Chang C., Cho C.M., Janzen H.H.:** Nitrous oxide emission from long term manured soils. Soil Sci. Soc. Am. J. 62: 677-682. 1998.
2. **Cicerone R.J.:** Changes in stratospheric ozone. Science, 237, 35-42, 1987:
3. Rodhe H.: (1990): A comparison of the contribution of various gases to the greenhouse effect. Science, 248, 1217-1219.
4. **Kroeze C.:** Nitrous oxide and global warming. The Science of the Total Environment 143, 193-209, 1994.
5. **Eichner M.J.:** Nitrous oxide emissions from fertilized soils: summary and available data. J. Environ Qual, 19, 272-280, 1990.
6. **Maljanen M., Liikanen A., Silvola J., Martikainen P.J.:** Measuring N_2O emissions from organic soils by closed chamber or soil/snow N_2O gradient methods. European Journal of Soil Science, 54, 625-631, 2003.
7. **Schalk-Otte S., Seviour R.J., Kuenen J.G., Jetten M.S.M.:** Nitrous oxide (N_2O) production by *Alcaligenes Faecalis* during feast and famine regimes. Wat. Res., 34, 7, 2080-2088, 2000.
8. **Williams E.J., Hutchinson G.L., Fehsenfeld F.C.:** NO_x and N_2O emissions from soils. Global Biogeochem Cycles, 6, 351-388, 1992.
9. **Bouwman, A.F.:** Soils and Greenhouse Effect. Wiley Chichester.UK, 25-32, 1990.
10. **IPCC** (Intergovernmental Panel On Climate Change). Climate Change 1995. The supplementary report to the IPCC Scientific Assessment. (Ed J.T. Houghton, B.A. Callander & S.K. Varney) Cambridge University Press, Cambridge, 1995.
11. **Gilbert B., Frenzel P.:** Methanotrophic bacteria in the rhizosphetre of rice microcosms and their effect on porewater mathane concentration and methane emission. Biol. Fertil. Soils, 20, 93-100, 1995.

12. **Mosier A., Schimel D., Valentine D., Bronson K., Parton W.:** Methane and Nitrous oxide fluxes in native, fertilized and cultivated grassland. Nature, 350, 330-332, 1991.
13. **Yu K.W., Wang Z.P., Vermoesen A., Patrick W.H., Van Cleemput O.:** Nitrous oxide and methane emissions from different soil suspensions: effect of soil redox status. Biol Fertil Soils, 34, 25-30, 2001.
14. **Cai Z.C.:** A category for estimate of CH_4 emission from rice paddy fields in China. Nutrient Cycl. Agroecosyst. 49, 171-179, 1997.
15. **Gliński J., Stępniewski W.:** Soil Aeration and its Role for Plants. CRC Press, Boca Raton, Florida, USA, 1985.
16. **Kotowski M., Stępniewska Z., Saczuk M., Kotowska U., Pasztelan M.:** Acta Agrophysica, 22, 93, 1999.
17. **Watanabe T., Osada T, Yoh M., Tsuruta H.:** N_2O and NO emissions from grassland soils after the application of cattle and swine excreta. Nutrient Cycl. Agroecosyst. 49, 35-39, 1997.
18. **Xu H., Xing G. X., Cai Z.C., Tsuruta H.:** Nitrous oxide emissions from three rice paddy fields in China. Nutrient Cycl. Agroecosyst. 49, 23-28, 1997.

SEMI-SCALE TESTING OF HYGRIC PERFORMANCE OF MULTI-LAYERED SYSTEMS OF POROUS MATERIALS USING THE TDR MEASURING TECHNOLOGY

Pavlík Zbyšek, Černý Robert

Czech Technical University in Prague, Faculty of Civil Engineering, Department of Structural Mechanics, Prague, Czech Republic
cernyr@fsv.cvut.cz

Abstract

A new approach to the assessment of hygric performance of multi-layered systems of porous materials is presented in the paper. A sufficiently large representative volume of the studied structure is exposed to difference climate conditions very close to reality in a semi-scale experiment. In the investigated structure, monitoring of moisture and temperature fields is carried out employing sophisticated measuring technology adjusted to the conditions of semi-scale experiments. The application of the semi-scale method is illustrated on the example of an interior thermal insulation system on the basis of hydrophilic mineral wool applied on two common building envelopes, namely brick wall and calcareous marly limestone wall. The measured results give evidence that the hygrothermal function of both tested building envelopes is satisfactory, because the thermal insulation material remains dry during the most critical part of the year. The obtained data demonstrate the possibilities of semi-scale experiments at the verification of newly designed building structures as well as at the calibration of mathematical models solving the problems of coupled moisture and heat transport.

Introduction

Determination of hygrothermal performance of the systems of building materials can be done basically in two different ways. The first possibility is to experimentally determine thermal and hygric parameters of particular materials applied in the tested building structure in laboratory conditions. From these basic material tests the necessary data for the subsequent process of computational analysis of the tested building structure is obtained, where the tested building structure can be loaded by real climatic conditions. The second way how to describe the hygrothermal behaviour of the whole building structure is to measure thermal and hygric parameters directly in the tested construction. In these tests, moisture content, relative humidity and temperature fields are monitored mostly. The measurements can be applied directly on real buildings or on so-called test houses.

In this paper, a semi-scale measuring and simulating technology for investigation of hygrothermal performance of building materials their multi-layered systems developed recently [1] is employed for the analysis of hygrothermal functionality of a contact interior thermal insulation system on the mineral wool basis. The designed sophisticated technology called NONSTAT is a certain halfway step between laboratory measurements and the measurements directly on a real building in real climatic conditions. In the semi-scale experiments, the thickness of the specimens of building envelopes is the same as in the practical application on building site. The applied exterior climatic data correspond to the reference year data, for the interior climate common data for the respective type of houses are chosen.

Semi-scale measuring system - nonstat

NONSTAT (see [1] for more details) is a climatic chamber system (**Fig. 1**), which consists of two climatic chambers for simulation of climatic conditions and a connecting tunnel for placing the analyzed specimen.

Fig. 1. The climatic chamber system

It can be used for measuring hygric and thermal field variables in the tested structure and monitoring moisture and heat transport in the structure caused by climatic loading. For monitoring moisture content and temperature, special sophisticated devices developed in Poland by Easy Test, Ltd. are used. The sensors for moisture content measurements work on the TDR (Time-Domain Reflectometry) principle [2,3], the precision of these sensors in moisture content reading is ± 2 % in the range of relative moisture content 0-100 %. Temperature is measured by resistance thermometers with accuracy ± 0.8 °C in the range from – 20 °C to 70 °C [4]. For measuring relative humidity, temperature, heat flux and air velocity, the measuring technique from Ahlborn is used [5]. The accuracy of particular sensors is as follows: capacitive relative humidity sensors are applicable in the range of humidities 5-98 % with accuracy ±2 %, temperature sensors have accuracy ± 0.4 °C in the temperature range from –20 °C to 0 °C and ± 0.1 °C in the range from 0 °C to 70 °C, accuracy of heat flux sensors is ± 5 % from the measured value and the precision of air velocity sensors is ± 0.01 m/s in the range of air flow velocities from 0.1 to 2.0 m/s. A computer, including the climatic data entry into the exterior climatic chamber, operates the whole measuring system.

Basic idea of the designed thermal insulation system, its composition and properties

The application of interior thermal insulation systems on building envelopes is not a natural solution but sometimes there is no other option available. A typical example is a historical building, where the facade has to be kept in its original appearance mostly, and the exterior insulation systems are excluded for that reason. In that case the development of such an insulation system would allow to prevent moisture damages and to upgrade the thermal properties of the envelope as the only reasonable option.

A common solution to this problem consists in placing a vapor barrier just under the internal plaster on the surface of the insulation layer, so that both the insulation layer and the load bearing structure are protected against water vapor. However, this is a solution, which can perform well on the theoretical level only. In the practice, it is very difficult to avoid mechanical damage of water vapor barrier placed in such an inappropriate way. A sole nail or hook driven into the wall for instance if hanging up a painting can damage the proper function of the barrier. In addition, even in the case that the barrier would perform without mechanical damage, the absence of water vapor removal from the interior through the envelope in the winter period, when the air ventilation in the interior is usually

limited, can lead to an undesirable increase of relative humidity in the interior and to the worsening of the internal microclimate.

The mechanical damage of water vapor barrier can be avoided by placing the barrier between the thermal insulation material and the load bearing structure. However, the amount of water condensed in the insulation layer would be in this case for certain time period of year relatively high. It is naturally possible to use such a thermal insulation material, which cannot be damaged by long-term water exposure, but the presence of water will always have a negative effect on the thermal insulation properties of the material. In the climatic conditions of North and Middle Europe the danger of liquid water generation is concentrated to winter months mostly. Therefore, the worsening of thermal insulation function would occur just in the winter period of year when it is absolutely undesirable.

An alternative to the application of traditional water vapor barriers is using a vapor retarder instead, which permits a part of water vapor to diffuse further to the load bearing structure. Then, even if the retarder is placed between the thermal insulation layer and the load bearing structure, the amount of condensed water in the thermal insulation layer is lower, and the structure is not damaged because it is exposed to such a water vapor flux only, that can be transported through it without condensation.

The requirements to the thermal insulation layer in the above arrangement are quite high. It should have a low thermal conductivity in dry state, and the thermal conductivity even should not increase too much if moderate presence of liquid water appears. In addition, the material should have a high capability of liquid water transport because it is supposed to redistribute the condensed water backward to the indoor room as fast as possible in order to maintain a sufficiently low moisture level and corresponding sufficiently good thermal insulation properties of the layer.

The application of capillary active or hydrophilic materials as a dehumidification method is a big innovative step in the building insulation/renovation technology and offers the possibility to develop new solutions for old, long-lasting problems, where expensive traditional renovation methods fail. The first attempts in this direction were done by Häupl *et al.* [6], where calcium silicate plates were used as capillary active thermal insulation.

In this paper, a newly developed interior thermal insulation system designed on the basis of principles and fundamentals given above, is investigated. In the first test, the designed system was applied on the brick wall 450 mm thick. The MU hydrophilic mineral wool boards 80 mm thick (Rockwool, SA) were used as the thermal insulation. The boards were fixed on brick wall using B2 water vapor retarder on the cement basis (Karlomix, Ltd.) having good gluing properties. The thickness of retarder layer was 10-15 mm (**Fig. 2**). The exterior and interior

renders were not used on the tested building structure because of their supposed low effect on the hygrothermal performance of the system.
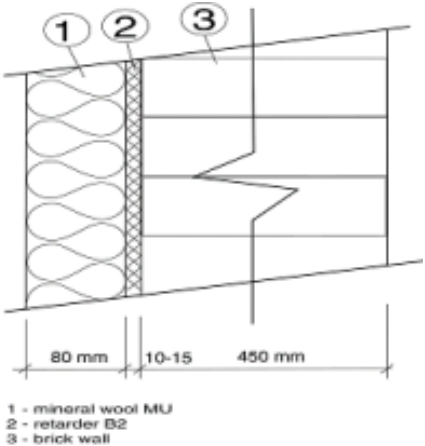

Fig. 2. Application of the insulation system on the brick wall

In the second experiment, calcareous marly limestone wall again 450 mm thick was used. The boards of DU material developed also by Rockwool SA were used as thermal insulation. Compared to MU, this thermal insulation material presents a more advanced step in the development of hydrophilic mineral wool materials for application in interior thermal insulation systems. The DU boards of 100 mm thickness have dual density (hard and soft layer) because of their two functions, mechanical and thermal insulating.
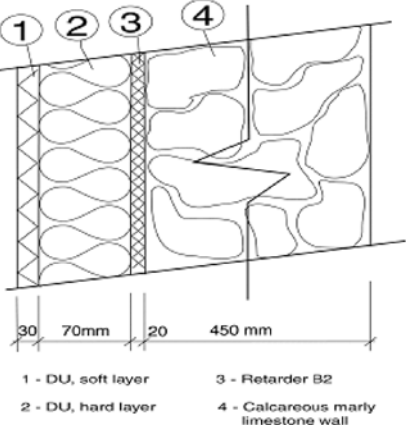
Fig. 3. Application of the insulation system on the calcareous marly limestone wall

The hard layer has the thickness of 30 mm, the soft layer with the main thermal insulation function is 70 mm thick. The mineral wool boards were fixed on the bearing structure also by water vapor retarder B2 (Karlomix, Ltd.) on cement basis with the thickness of 20 mm (**Fig. 3**).

Mechanical and hygrothermal properties of materials involved in the tested building envelope are in details described in [7,8].

Measuring technology, sample arrangement, difference climate conditions

In our measurements, the sensors for determination of moisture content, temperature, relative humidity, airflow velocity and heat flux were used. The accuracy of the relative humidity sensors was tested individually using saturated salt solutions with specified relative humidity. The TDR sensors were also individually calibrated to obtain their particular reference travel times t_{ref} and characteristic probe lengths l_p [2]. In this calibration, the travel times for water t_w and benzene t_b experimentally determined for each sensor were used. Taking into account the basic equation used in time-domain reflectometry measurements [2]

$$\sqrt{\varepsilon_a} = \frac{c\Delta t_m}{2l_p} \tag{1}$$

we obtain

$$\sqrt{\varepsilon_w} = \frac{c}{2l_p}\left(t_w - t_{ref}\right) \tag{2}$$

$$\sqrt{\varepsilon_b} = \frac{c}{2l_p}\left(t_b - t_{ref}\right) \tag{3}$$

where ε_w is the dielectric constant of water, ε_b the dielectric constant of benzene, ε_a the apparent dielectric constant of measured material, Δt_m the time interval between reflections points identifying the beginning and the end of the sensors rods, t_w the travel time reading from calibration in water, t_b the travel time reading from calibration in benzene. Using the above equations, the reference time t_{ref} and the characteristic probe length l_p were determined in the following form:

$$t_{ref} = \frac{\sqrt{\varepsilon_w} * t_b - \sqrt{\varepsilon_b} * t_w}{\sqrt{\varepsilon_w} - \sqrt{\varepsilon_b}} \tag{4}$$

$$l_p = \frac{c}{2} * \frac{t_w - t_b}{\sqrt{\varepsilon_w} - \sqrt{\varepsilon_b}} \tag{5}$$

Then, the apparent dielectric constant of measured material was obtained as

$$\sqrt{\varepsilon_a} = \frac{c}{2l_p}\left(t_{probe} - t_{ref}\right) \tag{6}$$

The volumetric moisture content was then determined using the following equation [9]:

$$\theta = \frac{\sqrt{\varepsilon_a} - 0.819 + 0.168 * \rho - 0.159 * \rho^2}{7.17 + 1.18 * \rho} \tag{7}$$

where ρ is the bulk density of the material.

The process of sample preparation can be divided in two phases: installation of the probes to the samples, and positioning of the sample into the tunnel between the climatic chambers.

In the tested structure, the sensors for monitoring moisture content, temperature and relative humidity are placed to beforehand-bored holes. The upper part of the bore opening is closed by silicon sealing. The probes for monitoring moisture content measure properties of moist material, therefore it is necessary to fill up back the bored hole by the powder of the same material to avoid air gaps between the rods of the probe and the material.

For a proper setting of initial conditions, it is necessary to achieve first near-steady-state conditions in the wall between the chambers, where there are simulated inside and outside climatic conditions. The heat flow, which is the most important parameter in this respect, is measured by Ahlborn probes. It is necessary to fix the heat flow probe on the specimen without any air layer, therefore the face of the wall has to be grinded down. The heat flux sensors are then spot glued on frontal side of measured construction and the space between the sensor and the wall is filled with conducting gel to prevent from forming air space.

After positioning all sensors, the prepared sample is placed into the connecting tunnel, which is then connected by sleeve connectors between climatic chambers. The sample, placed into the connecting tunnel, has to be thermally and waterproof insulated from the tunnel wall in order to achieve one-dimensional heat and moisture transport in the tested structure. For that reason, the lateral faces of the sample are insulated using extruded polystyrene boards in

combination with mineral wool and provided with a water- and water vapor-proof coating.

When the climatic chambers are connected, real climatic conditions in both climatic chambers are simulated. In the chamber, which should simulate interior climatic conditions in common residential houses, the constant temperature and relative humidity is set up. In the chamber, simulating exterior climatic conditions, real climatic data for temperature and relative humidity are used, in our case we have chosen climatic data for the test reference year (TRY) for Munich, Germany [10].

Measurements on the brick wall

The measurements were performed using the technology described above. In **Fig. 4** placing of the sensors in the tested structure is shown, which was done with respect to the possible condensation zones. The measurements were first performed continuously for 65 days on non-insulated brick wall to achieve steady state conditions in the structure. The boundary conditions in the chambers were as follows: internal temperature 21°C, internal relative humidity 50 %, external temperature 2°C, external relative humidity 90 %. The temperature initial conditions in the brick wall were the same as the conditions in the laboratory, i.e. 22°C, the initial relative humidity was higher than in the laboratory, typically between 70 % and 90 % due to the fact that the brick wall was freshly walled. After 65 days of measurement, there was applied the thermal insulation system, which applicability was tested for the most unfavorable external climatic conditions, i.e. for the winter period. The boundary conditions for temperatures and relative humidities on the external side were chosen according to the data for TRY Munich, the measurements began with the climatic data for January 1. The internal climate was the same as for the non-insulated brick wall. The measurements on insulated structure were performed for 62 days. Typical experimental results for the insulated structure are shown in **Fig. 5** – **Fig. 10**. Moisture content, relative humidity and temperature were monitored in the tested structure, airflow velocity was measured in the warm climatic chamber and heat flux was monitored both on exterior and interior surface of the tested structure.
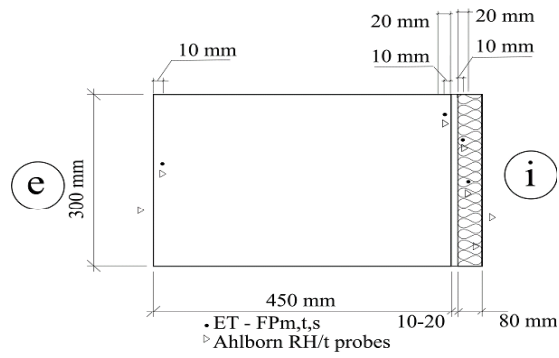
Fig. 4.   Positions of the sensors in the tested insulation system applied on the brick wall
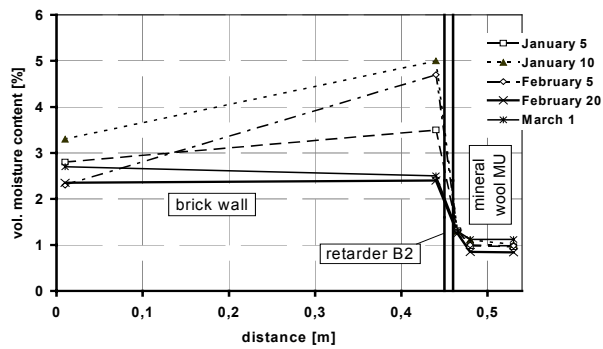

Fig. 5.   Volumetric moisture content profiles in the insulated brick wall
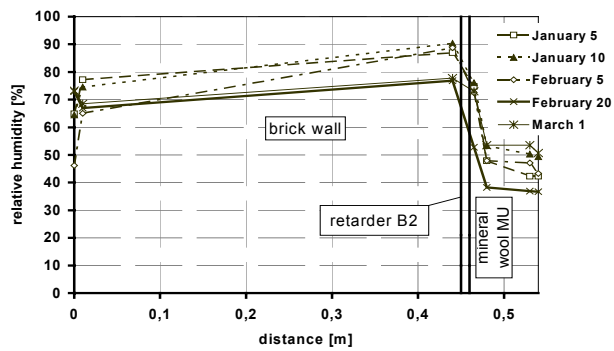

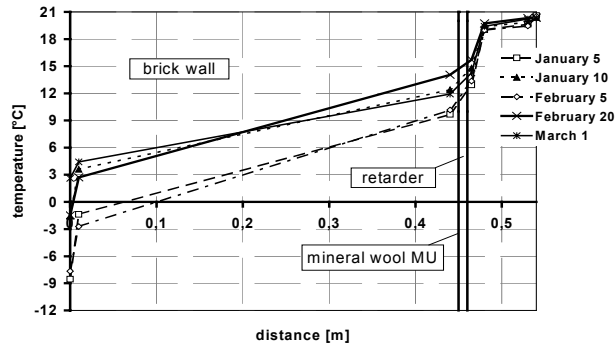**Fig. 6.**   Relative humidity profiles in the insulated brick wall

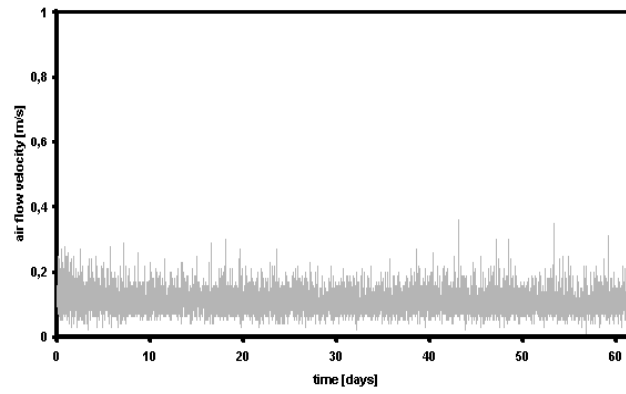**Fig. 7.** Temperature profiles in the insulated brick wall

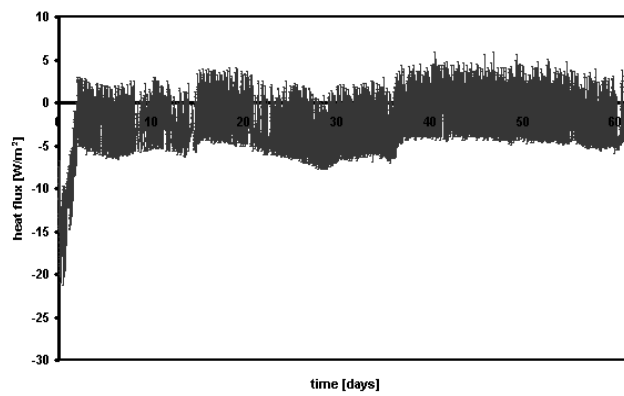**Fig. 8.** Airflow velocity in the warm climatic chamber in the experiment with the brick wall
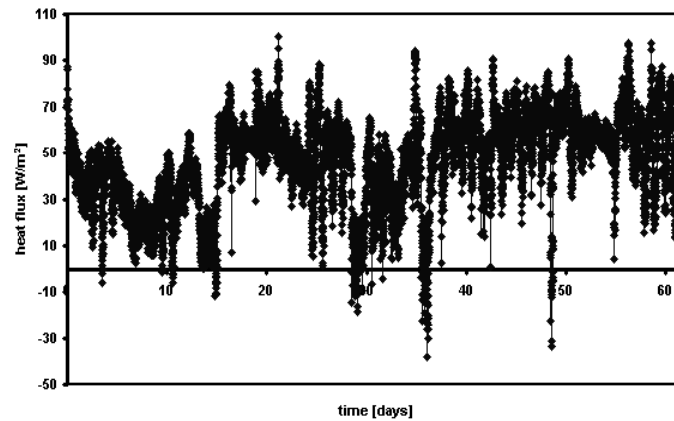

Fig. 9. Heat flux on the interior surface of the tested structure (mineral wool)

118

Fig. 10. Heat flux on the exterior surface of the tested structure (brick wall)

Measurements on the calcareous marly limestone wall

The scheme of the tested structure and the sensors positioning is shown in **Fig. 11**. The boundary conditions for temperatures and relative humidities on the external side were chosen according to the data for TRY Munich, the measurements began with the climatic data for December 1. So, the freshly walled structure was loaded by very unfavourable climatic conditions and the most unfavourable case of application of thermal insulation system was simulated. Internal climate was the same as for the brick wall; internal temperature 21 °C, relative humidity 50 %. The measurements were first performed on non-insulated structure for 38 days. After that, the climatic chamber system was disconnected and the tested insulation system was applied. Measuring of insulated structure was performed for 55 days, hence the most critical part of the year from the point of view of unfavourable climatic conditions was simulated. Typical experimental results are shown in **Fig. 12 – Fig. 17**. Volumetric moisture content profiles, relative humidity profiles and temperature profiles in the insulated structure, heat fluxes on structure surfaces and air flow velocity in the warm climatic chamber are given in a series of times.

Discussion

In the first test of functionality of the designed interior thermal insulation system applied on the brick wall, the measured results have shown, that the

119

relative humidities in the brick wall decreased with time during the analyzed winter period. After 50 days of climatic loading these achieved values around 75% (**Fig. 6**) and no overhygroscopic moisture was observed (**Fig. 5**).
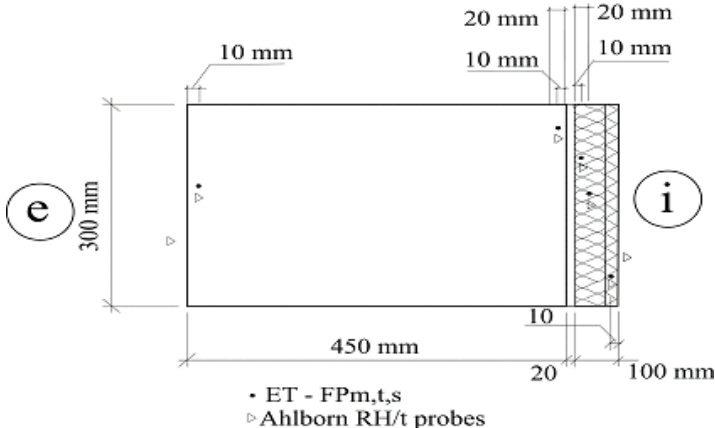

Fig. 11. Positions of the sensors in the tested insulation system applied on the calcareous marly limestone wall
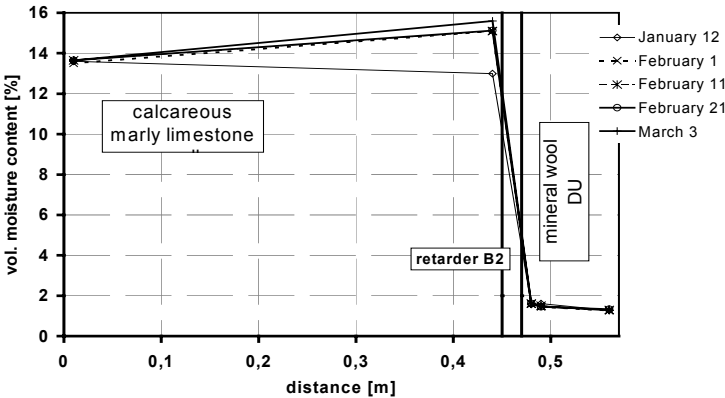

Fig. 12. Volumetric moisture content profiles in the insulated calcareous marly limestone wall

The relative humidities in the thermal insulation layer were significantly lower. Apparently, the hydrophilic thermal insulation layer exhibited a very positive effect on the hygrothermal behavior of the wall even in the most critical part of the year from the point of view of water condensation. Also, the water vapor retarder exhibited a good function in controlling the water vapor transport from the interior to the exterior through the bearing structure.
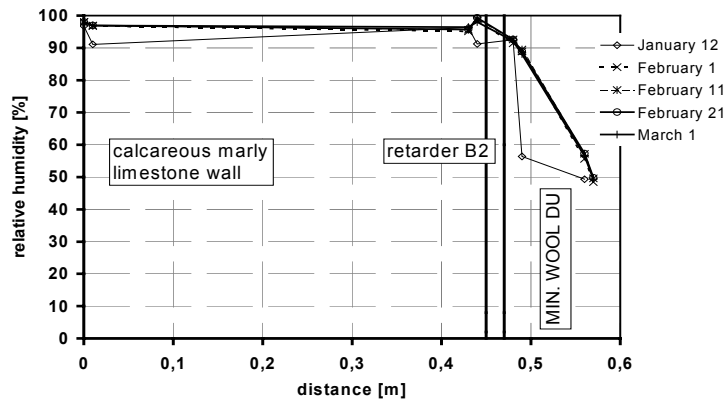
120

Fig. 13. Relative humidity profiles in the insulated calcareous marly limestone wall
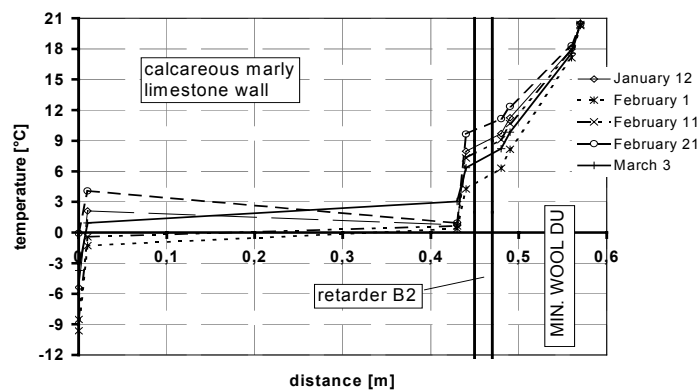

Fig. 14. Temperature profiles in the insulated calcareous marly limestone wall

In the case of application of the developed interior thermal insulation system on the calcareous marly limestone wall, the results were not very prospective. The overhygroscopic moisture was present in the whole limestone wall during the whole studied time period (**Fig. 12**), and only in the thermal insulation layer it was missing, the relative humidity being between 90 % and 50 % (**Fig. 13**). This clearly shows a bad performance of the water vapor retarder that had the water vapor diffusion resistance factor too low, which allowed too much water vapor to be transformed into the load bearing structure. In a combination with the relatively high water vapor diffusion resistance factor of calcareous marly limestone and the initial water condensation after sudden application of boundary conditions, this failure of water vapor retarder resulted in the bad performance of the whole system.
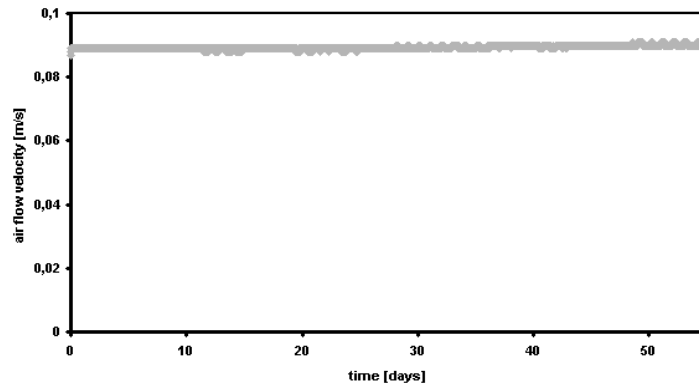
Fig. 15. Airflow velocity in the warm climatic chamber in the experiment with the calcareous marly limestone wall
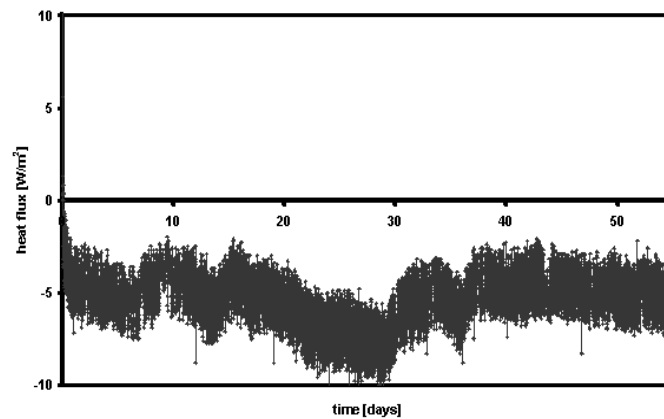

Fig. 16. Heat flux on the interior surface of the tested structure (mineral wool DU)

However, it should be noted that the worst possible case chosen in the semi-scale experiment with the calcareous marly limestone wall will very unlikely occur in the practice. The application of a severe combination of initial and boundary conditions, where initially the sample is at room temperature, and on one of its ends there is applied suddenly temperature close to 0 °C, which is maintained then for several months, was in fact very artificial, so that this case can be considered as only theoretical.

In measuring airflow velocity in the warm chamber, significant differences were observed for measurements with the brick wall (**Fig. 8**) and the calcareous marly limestone wall (**Fig. 15**). While for the brick wall, the air flow velocity

varied with time in the range from 0 to 0.3 m/s, for the calcareous marly limestone wall it was practically constant, 0.09 m/s. As the conditions in the warm chamber were supposed to be constant for both two studied cases and for the whole measuring time, the only probable reason for the observed differences is that there was a small damage of the sealing in the warm chamber during the measurements with the brick wall. This damage caused certain convective heat transfer between the chamber and the exterior, which has led to the increase of air flow in the chamber.
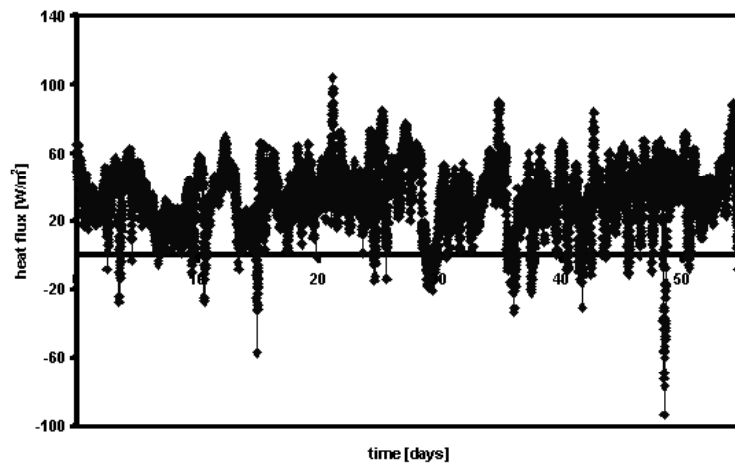

Fig. 17.   Heat flux on the exterior surface of the tested structure (calcareous marly limestone wall)

Fig. 18 – **Fig. 19** show that the air exchange with the surroundings affected the temperature in the warm chamber only slightly. However, the relative humidity varied approximately from 30% to 50%, which was a consequence of the low relative humidity in the surrounding laboratory (typically around 30%). Nevertheless, the changes in relative humidity in the warm chamber were still realistic from the point of view of interior conditions in most living houses in Czech Republic so that the obtained results are representative. The course of the heat flux with time on the internal surface during the measurements with the brick wall (**Fig. 9**) was also found to be kind of strange. The probable reason was not very good fixing of the sensor on the surface of the wall, which was done using a glue. Therefore, in the second experiment with the calcareous marly limestone wall conducting gel was used for fixing the sensor together with the glue that was applied on the corners only. This solution was apparently more successful.
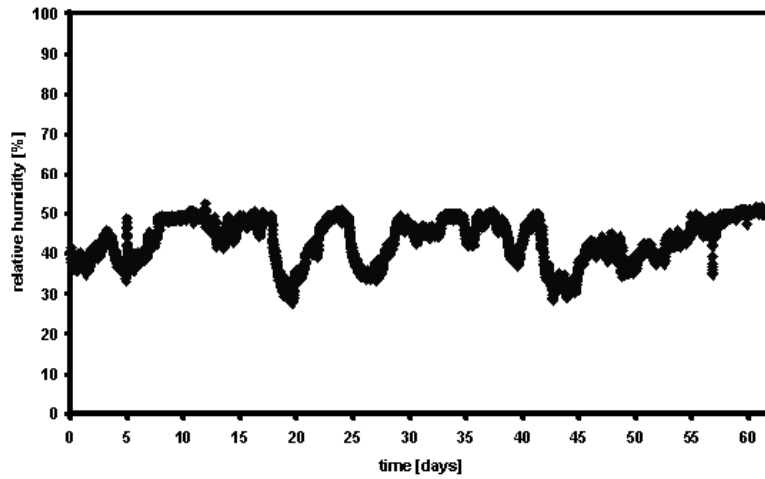
123

Fig. 18. Relative humidity history in the interior climatic chamber in the experiment with the insulated brick wall
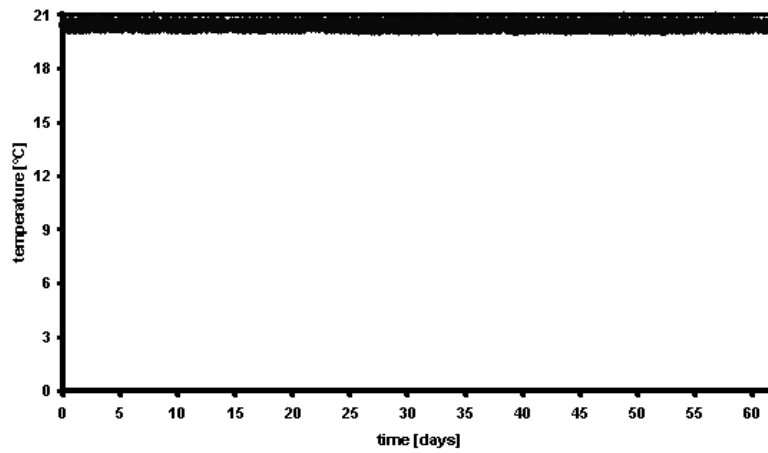

Fig. 19. Temperature history in the interior climatic chamber in the experiment with the insulated brick wall

Conclusions

The analysis of hygrothermal performance of the designed interior thermal insulation system with hydrophilic thermal insulation in semi-scale conditions have

clearly documented the usefulness of such treatment in the process of designing new building envelopes and their technological solutions. It has also proved its applicability in the process of verification and calibration of mathematical models solving the problems of coupled moisture and heat transport.

The measured results showed a very good function of the hydrophilic thermal insulation material, which remained dry during the most critical part of the year in both studied cases. They also revealed a critical role of the water vapor retarder, which should have the water vapor resistance factor high enough to moderate water vapor transport from the interior to the load bearing structure and to prevent from condensation there. From this point of view, the applied water vapor retarder was suitable for the brick wall but it failed for the calcareous marly limestone wall. The experiment with the calcareous marly limestone wall also well illustrated the necessity to handle stonewalls very carefully during their reconstructions.

References

1. **Pavlík Z., Pavlík J., Jiřičková M., Černý R.:** System for Testing the Hygrothermal Performance of Multi-Layered Building Envelopes. Journal of Thermal Envelope and Building Science, 25, pp. 239-249, 2002.
2. **Plagge R., Roth C.H., Renger M.:** Dielectric soil water content determination using time-domain reflectometry (TDR). In: A. Kraszewski (ed.), Proc. of Second Workshop on Electromagnetic Wave Interaction with Water and Moist Substances at the 1996. IEEE Microwave Theory and Techniques Society International Microwave Symposium in San Francisco, pp. 59-62, 1996.
3. **Plagge R., Grunewald J., Häupl P.:** Application of time domain reflectometry to determine water content and electrical conductivity of capillary porous media. Proceedings of the 5th Symposium of Building Physics in the Nordic Countries, C. E. Hagentoft, P. I. Sandberg (eds.). (Goteborg: Vasastaden AB), pp. 337-344, 1999.
4. **Easy Test** – Soil Water Monitoring Device brochure, Easy Test Ltd., Lublin, 2000.
5. **Ahlborn Mess- und Regelungstechnik**, Operating Instructions Term Type 5500-3. Otto E. Ahlborn, Holzkirchen 2000.
6. **Häupl P., Grunewald J., Fechner H.**: Moisture behaviour of a "Gründerzeit" – house by means of a capillary active calciumsilicate inside insulation. In: Proceedings of the Building Physics in the Nordic Countries, pp. 225-232, Göteborg 1999.
7. **Jiřičková M., Černý R.**: Thermal and Hygric Properties of Mortars and Water Vapor Retarders for Interior Thermal Insulation Systems. In: 11th Symposium for Building Physics, TUD Dresden, vol. 1, pp. 319-328, 2002.
8. **Jiřičková M., Černý R.:** Hygrothermal Properties of Various Types of Mineral Wool Based Thermal Insulation Materials. In: CTU Reports: Contributions to Experimental Investigation of Engineering Materials and Structures. Prague: CTU, pp. 1-11, 2001.

9. **Malicki M.A., Plagge R., Roth C.H.:** Improving the calibration of dielectric TDR soil moisture determination taking into account the solid soil. European Journal of Soil Science, 47, pp. 357-366, 1996.
10. **Grunewald J.:** DELPHIN 4.1 - Documentation, Theoretical Fundamentals, TU Dresden, Dresden 2000.

COMPARISON OF SOIL PARTICLE SIZE DISTRIBUTION FROM LASER DIFFRACTION AND SEDIMENTATION METHODS

Ryżak Magdalena, Walczak Ryszard T.

Institute of Agrophysics, Polish Academy of Sciences, Lublin, Poland
mryzak@demeter.ipan.lublin.pl

Introduction

Particle size distribution is one of the most fundamental soil characteristics, which directly affects many physical and chemical soil properties. On the base of particle size distribution one can estimate other soil properties such as: water retention and water conductivity coefficients in saturated and unsaturated zones [1,2,6,7,10,11]. For over 100 years particle size distribution has been used to describe similarities and differences between soils. According to Loveland and Whalley [9], the classification of soils in terms of particle size stems from the work of Atterberg [3]. Nowadays, about 400 methods are known, used for measuring particle size distribution [9]. The most frequently used are sieve, pipette and areometer methods. Pipette and areometer methods are also known as sedimentation methods. All the above mentioned methods are imperfect and time consuming. An alternative for measuring the particle size is laser diffraction method. This method does not yield identical particle size distribution with sieve and sedimentation methods, which were used before [4,5]. Each of these methods is based on different principles and assumptions, and uses different approximations. Results from laser diffraction method and the sieve and sedimentation methods cannot be directly compared because the laser diffraction method underestimates sand and clay fractions and overestimate the silt fraction.

The objective of our study is to determine the equations of regression, which make possible to compare particle size distribution from sedimentation and laser diffraction methods.

MATERIALS AND METHODS

Institute of Agrophysics PAS disposes Malvern Mastersizer 2000 which measures particle size in a large range: 0.02–2000 μm (in liquid or air dispersion) on the base of laser diffraction method.The angle at which the light is scattered by a particle is inversely proportional to the size of the particle. The theory of Mie, which describes an interaction between laser light and particles, is used to convert

data from laser light diffraction to particle size distribution. This theory requires knowledge of the refractive index of the material tested. We used refractive index n_r=1.577 and absorption index n_i=0.1 for the optical model calculation. In this paper we presented 22 soils samples, which were analyzed using laser diffraction method. We used distilled water as a dispersant and 4 minutes of ultrasound (of maximum power) to obtain good dispersion. In order to compare results from laser diffraction method particle size distribution of 22 soil samples were measured using areometer method with application of Cassagrande with Prószyński modification.

Results and discussion

Particle size distribution of 22 soils determined by areometer and laser diffraction methods are presented in **Table 1** below.

Table 1. Particle size distribution of 22 soils determined by areometer and laser diffraction methods

| Soil No. | Percentage of particular fractions (%) | | | | | |
| | Measured by areometer | | | Measured by laser diffraction | | |
	Sand	Silt	Clay	Sand	Silt	Clay
1	54	40	6	47	50	3
2	56	40	4	47	50	3
3	56	35	9	47	50	3
4	72	24	4	57	40	3
5	78	19	3	62	36	2
6	31	60	9	38	59	3
7	13	75	12	17	77	6
8	13	75	12	17	77	6
9	14	81	5	18	76	6
10	14	80	6	18	76	6
11	20	75	5	20	74	6
12	14	77	9	18	77	5
13	33	42	23	14	70	16
14	34	41	25	13	72	15
15	28	47	25	12	74	14
16	33	39	28	14	65	22
17	43	33	24	20	68	12
18	15	57	28	13	75	13
19	87	11	2	77	22	1
20	92	7	1	82	18	1
21	90	9	1	81	18	1
22	94	4	1	88	11	1

Comparison of results obtained for soil samples using areometer and laser diffraction methods were presented below (**Fig. 1**) in textural groups. The same soil sample measured these two methods can belong to two different groups of soil in dependence from applied method.
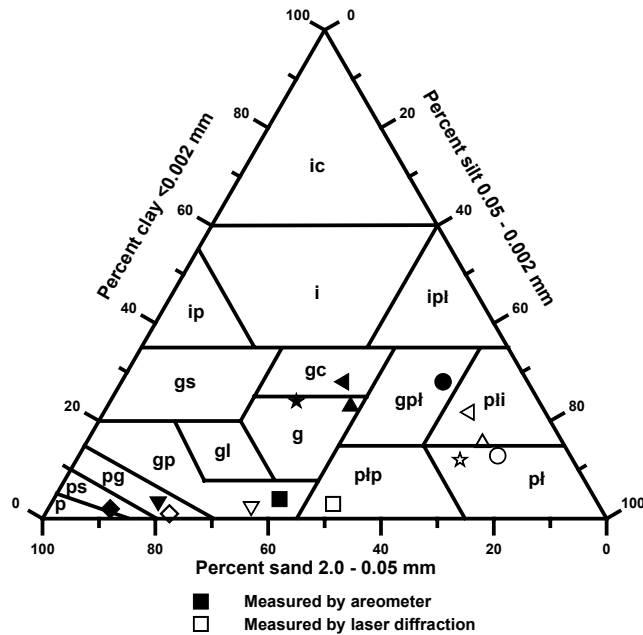

Fig. 1.   Results obtained for soil samples using areometer and laser diffraction methods in textural groups

On the **Fig.1**: ic – heavy clay, i – clay, ip – sandy clay, ipł – silty clay, gs – medium loam, gc – heavy loam, gpł – silty loam, płi – clayey silt, g – loam, gl – light loam, gp – sandy loam, pg – loamy sand, ps – slightly loamy sand, p – sand, płp – sandy silt, pł – silt.

Results from laser diffraction method and the sieve and sedimentation methods are not identical and cannot be directly compared. For example one soil sample can be classified as heavy loam (on the base of areometer method) while the same sample can be classified as clayey silt (on the base of laser diffraction method). Laser diffraction method underestimates sand and clay fractions and overestimates the silt fraction.

We obtained the equations of regression on the base of 22 soil samples, which permit to compare results from areometer and laser diffraction methods. Relations between sand, silt and clay fraction obtained from these methods are presented below.
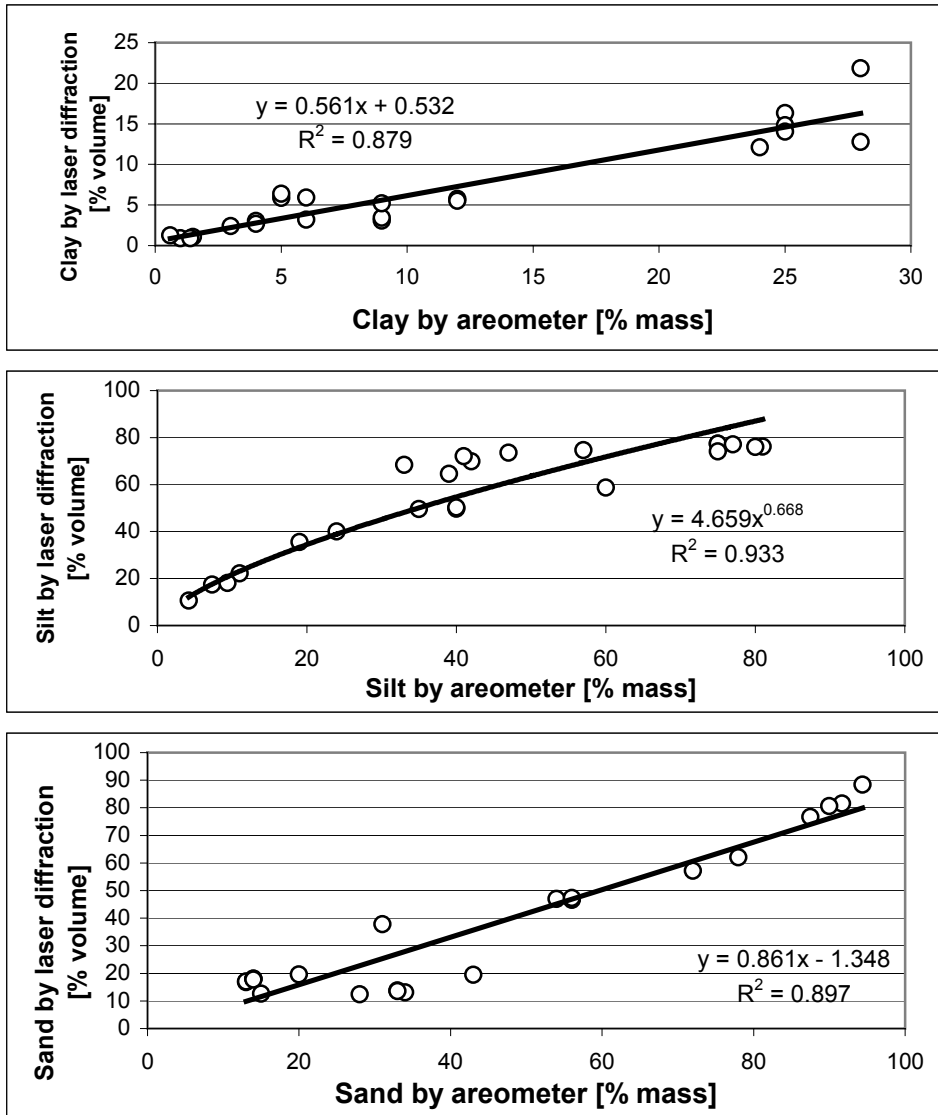
Fig. 2. Relations between fractions of sand, silt and clay obtained by areometer and laser diffraction methods for 22 soil samples.

In order to check the equations of regression presented in **Fig. 2** in this paper we used set of data from Kasza's [2] measurement, which were presented in **Table 2** (columns I and II).

Table 3. Set of data from Kasza's [2] measurements and data obtained from regression equations (columns III) and relative error of the calculated values (i.e., the difference between measured (column II) and predicted values (column III) expressed as the percentage of the measured value).

Soil No.	I Measured by laser diffraction by Kasza [2]			II Measured by areometer by Kasza [2]			III Data calculated from regression equations for Kasza's [2] soil samples			IV Relative error %		
	Sand	Silt	Clay	Sand	Silt	Clay	Sand	Silt	Clay	Sand	Silt	Clay
1	16	76	8	20	60	20	16	72	12	20	−20	40
2	20	70	10	19	56	25	15	69	15	21	−23	40
3	14	76	10	17	59	24	13	71	14	24	−20	42
4	18	72	10	23	56	21	18	69	12	22	−23	43
5	20	70	10	24	56	20	19	69	12	21	−23	40
6	25	66	9	28	52	20	23	65	12	18	−25	40
7	30	61	9	32	49	19	26	63	11	19	−29	42
8	17	72	11	27	49	24	22	63	14	19	−29	42
9	18	72	10	27	52	21	22	65	12	19	−25	43
10	26	64	10	28	50	22	23	64	13	18	−28	18
11	25	65	10	27	54	19	22	67	11	19	−24	50
12	32	60	8	34	49	17	28	63	10	18	−29	41
13	28	62	10	32	50	18	26	64	11	19	−28	64
14	20	70	10	27	55	18	22	68	11	19	−24	64
15	34	56	8	39	43	18	32	57	11	18	−33	64
16	24	66	10	30	46	24	24	60	14	20	−30	42
17	22	67	11	31	45	24	25	59	14	19	−31	42
18	23	67	10	24	55	21	19	68	12	21	−24	37
19	22	70	8	19	58	23	15	70	14	21	−21	39
20	20	70	10	27	51	22	22	64	13	19	−25	41
21	20	71	9	38	45	17	31	60	10	18	−33	41
22	24	67	9	30	52	18	24	65	11	20	−25	39
23	40	52	8	58	29	13	45	44	8	22	−52	38

For the purpose of conversions of data from laser diffraction method into areometer method (as were measured before) the relationship between these two methods were less than satisfactory.

Conclusions

1. Results from laser diffraction method and the sieve and sedimentation methods are not identical and cannot be directly compared.
2. Equations of regression presented in this paper permit to compare results from laser diffraction and areometer methods. These equations are imperfect and ought to be treated as preliminary and constituting an announcement of further research on more extensive soil material.
3. Laser diffraction method has many advantages: short time of analysis, small sample required for measurement, analysis is independent of the particles density and results are presented at a continuous particle size distribution curves.
4. Laser diffraction method can be very useful when we obtained satisfactory correlation between laser diffraction and sedimentation methods, which are accepted as an international norm for particle size analysis of soils.

References

1. **Arya L.M., Leij F.J., Shouse P.J., Van Genuchten Martinus Th.:** Relationship between the Hydraulic Conductivity Function and the Particle – Size Distribution. Soil Sci. Soc. Am. J., 63:1063-1070, 1999.
2. **Arya L.M, Paris J.F.:** A physicoempirical model to predict the soil moisture characteristics from particle – size distribution and bulk density data. Soil Sci. Soc. Am.J., 45: 1023-1030, 1981.
3. **Atterberg A.:** Die Klassification der humusfreien und der humusarmen Mineralboden Schwedens nach der Konsistenzverhaltnissen derselben. Int. Mitt. Bodenkd, 6, 27-37, 1916.
4. **Buurman P., Pape Th. and Muggler C.C.:** Laser grain – size determination on soil genetic studies. 1.practical problems. Soil Science, Vol.162 No.3, 1997.
5. **Eshel G., Levy G.J., Mingelgrin U., Singer M.J.:** Critical evaluation of the use of laser diffraction for particle – size distribution analysis. SSSAJ 68: 736 – 743, 2004.
6. **Gupta S.C., Larson W.E.:** A model for predicting packing density of soils using particle - size distribution. Soil Sci. Soc. Am. J Vol 43, (758-764), 1979
7. **Jaynes D.B, Tyler E. J.:** Using soil physical properties to estimate hydraulic conductivity Soil Science Vol.138, No.4, 1984
8. **Kasza I.:** Laser method for granulometric studies of loamy, silty and clayey deposits (in Polish) Przegląd Geologiczny 40(5), 323-325, 1992.
9. **Loveland P.J, Whalley W.R.:** Particle size analysis. In Smith K.A, Mullins C.E.: Soil and environmental analysis. Physical methods. Marcel Dekker, Inc., 2001.
10. **Sławiński C.:** The influence of soil physical parameters on the water conductivity coefficient value (model research)(in Polish). Acta Agrophysica, 90, 5-75, 2003.
11. **Walczak R.T.:** Model research on the relation between water retention and solid phase parameters (in Polish). Problemy Agrofizyki, 41, 5-69, 1984.

VERIFICATION OF DIELECTRIC MIXING MODELS ON THE BASE OF TDR MEASUREMENTS

Skierucha Wojciech, Malicki Marek A.

Institute of Agrophysics Polish Academy of Sciences, Lublin, Poland
skieruch@demeter.ipan.lublin.pl

Introduction

The increasing popularity of Time Domain Reflectometry (TDR) technique in the dielectric determination of soil water content (Or and Wraith [16], Topp *et al.* [21] implies the necessity of verification of the dielectric mixing models. The commonly used models describing the soil dielectric constant as the mixture of solid matter, water and air are: α model (Birtchak [2], Bohl *et al.* [3], Steru [20]), the model proposed by *de Loor* [4] and empirical models (Malicki and Skierucha [15], Malicki *et al.* [14], Skierucha [18], Topp *et al.* [21]).

The soil water content sensor used in TDR method and presented schematically in **Fig. 1**, consists of two parallel metal rods (or three metal rods applied by Heimovaara [12], Wright and Or [24], Zegelin *et al.* [25]) of the length *L*, inserted into the tested soil [10,11,15]. The time, *t*, for the electromagnetic (EM) wave to cover the distance *L* may be calculated as the sum of propagation times along the individual soil phases (Kraszewski [13]):

$$t = t_s + t_a + t_w \tag{1}$$

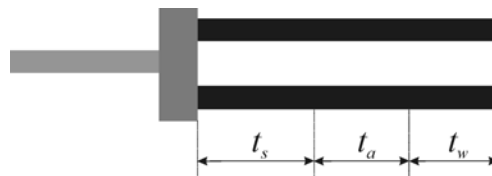where the indexes *s*, *a* and *w* stand for solid, gas and water phases, respectively.

Fig. 1.   TDR interpretation of soil as a tree phases medium in dielectric mixing model α

In most practical conditions the velocity of EM wave propagation, *v*, in the soil may be presented as:

$$v = \frac{c}{\sqrt{\varepsilon}} = \frac{2L}{t} \tag{2}$$

133

where c is the velocity of light in free space, ε is the soil dielectric constant. The total propagation time, t, of EM wave can be expressed by dividing it into elementary propagation times along the solid, water and air phases of the soil expressed by (1) by means of (2):

$$t = t_s + t_a + t_w = \frac{2L\sqrt{\varepsilon}}{c} = \frac{2L_s\sqrt{\varepsilon_s}}{c} + \frac{2L_a\sqrt{\varepsilon_a}}{c} + \frac{2L_w\sqrt{\varepsilon_w}}{c} \qquad (3)$$

with: L_s, L_a, L_w are idealized by the presented model parts of the probe inserted into an elementary soil phase. Rewriting to last two elements of the Eq. (3), multiplying by the elementary cross-section S and then dividing by the whole volume of soil in the cylinder defining the sphere of influence of the TDR measurement method gives:

$$\sqrt{\varepsilon} = \sqrt{\varepsilon_s}\frac{V_s}{V} + \sqrt{\varepsilon_a}\frac{V_a}{V} + \sqrt{\varepsilon_w}\frac{V_w}{V} = \sqrt{\varepsilon_s}(1-\phi) + \sqrt{\varepsilon_a}(\phi-\theta) + \sqrt{\varepsilon_w}\theta \qquad (4)$$

or using the parameter α, which summarizes the geometry of the medium with relation to the applied electric field (Roth *et al.* [17]):

$$\varepsilon = \left((1-\phi)\varepsilon_s^{\alpha} + (\phi-\theta)\varepsilon_a^{\alpha} + \theta\varepsilon_w^{\alpha}\right)^{\frac{1}{\alpha}} \qquad (5)$$

which is the 3-phase dielectric mixing model α, expressing the square root of the apparent dielectric constant of soil in the terms used by soil scientists: ϕ – soil porosity and θ – volumetric water content. Whalley [23] presented the similar discussion.

Following Birchak *et al.* [2], Alharthi and Lange [1] assumed $\alpha = 0.5$, which gives the Eq. (4). After introducing adsorbed water as a forth phase Dobson *et al.* [7] determined α by regression data for different frequencies (ranging from 1.4 to 18 GHz) and soil types (ranging from sandy loam to silty clay) and obtained $\alpha = 0.65$. The four-phase dielectric mixing model α, accounting for the adsorbed to soil solid phase bound water has the following form:

$$\varepsilon^{\alpha} = (1-\phi)\varepsilon_s^{\alpha} + (\phi-\theta)\varepsilon_a^{\alpha} + (\theta-\theta_{bw})\varepsilon_w^{\alpha} + \theta_{bw}\varepsilon_{bw}^{\alpha} \qquad (6)$$

where water exists in two phases: as free water, w, like capillary water and bound water, bw, like molecular or film water. Generally the α-model of soil dielectric mixture may be presented as follows:

$$\varepsilon^{\alpha} = \sum_i V_i \varepsilon_i^{\alpha} \qquad (7)$$

134

where V_i is the volumetric concentration of i-th phase and ε_i is the dielectric constant of this phase.

The four-phase model proposed by *de Loor* [4,5] and used by Dirksen and Dasberg [6] and Dobson and Ulaby [7] is:

$$\varepsilon = \frac{3\varepsilon_s + 2\theta_w(\varepsilon_w - \varepsilon_s) + 2\theta_{bw}(\varepsilon_{bw} - \varepsilon_s) + 2\theta_a(\varepsilon_a - \varepsilon_s)}{3 + \theta_w\left(\dfrac{\varepsilon_s}{\varepsilon_w} - 1\right) + \theta_{bw}\left(\dfrac{\varepsilon_s}{\varepsilon_{bw}} - 1\right) + \theta_a\left(\dfrac{\varepsilon_s}{\varepsilon_a} - 1\right)} \tag{8}$$

where the indexes s, w, bw and a refer to solid phase, water, bound water and air, respectively. This model describes heterogeneous mixture where foreign granules with dielectric constant ε_i are imbedded in a homogeneous and isotropic dielectric with dielectric constant ε. The imbedded foreign granules in Eq. (8) represent free water, bound water and air. The host medium is the solid phase.

The empirical models $\varepsilon(\theta)$ and $\varepsilon(\theta,\rho)$, where ρ is the soil bulk density, form the formula of the appropriate regression curves [14,15,18,21]. The formula (9) presented below and discussed in Skierucha [18] will be used in this paper as the reference:

$$\varepsilon = \left(0{,}573 + 0{,}582\rho + (7{,}755 + 0{,}792\rho)\,\theta\right)^2 \tag{9}$$

where $\rho\,[\text{g/cm}^3]$ is the soil bulk density.

The verification of the discussed 3-phase and 4-phase models is presented in the following sections.

Material and methods

Sixteen mineral soils of different texture, volumetric water content and bulk and particle density were investigated (**Table 1**).

The following variables were measured: dielectric constant, ε, bulk density, ρ, particle density, ρ_s, and gravimetrically determined volumetric water content, θ. Dielectric constant, ε, was determined using TDR (LOM/m from *Easy Test, Ltd.* [8]). The remaining variables were measured with the application of standard methods.

The solid phase dielectric constant, ε_s, was calculated from the formula (derived from the formula (5)):

$$\varepsilon_s = \overline{\varepsilon_s} = \frac{1}{n}\sum_i^n \left(\frac{(\varepsilon(\theta = 0))^\alpha - \phi_i}{1 - \phi_i}\right)^{\frac{1}{\alpha}} \tag{10}$$

135

where $\alpha = 0,5$.

The solid phase dielectric constant was calculated on the base of three-phase model α applied to all soil samples from **Table 1** fitting the exponential function to the experimental data.

Table 1. Selected properties of the investigated mineral soils, where ρ [gcm^{-3}] is the soil bulk density, ρ_s [gcm^{-3}] is the soil particle density

No	Localization	Soil type (FAO)	Level (depth in cm)	Bulk density (gcm^{-3})	Particle density (gcm^{-3})	Texture % (FAO)		
						Sand	Silt	Clay
1	Parana. Brazil	Haplic Ferrasol	Ah (0-10)	1.27÷1.60	2.62	82	6	12
2	Parana. Brazil	Haplic Ferrasol	Bws (120-140)	1.31÷1.77	2.67	72	8	18
3	Grunewald. Germany	Haplic Luvisol	Bt (90-120)	1.35÷1.55	2.53	2	75	23
4	Grunewald. Germany	Haplic Podzol	Bhs (30-45)	1.21÷1.60	2.54	88	10	2
5	Elba. Italy	Chromic Luvisol	Ah (0-20)	1.34÷1.64	2.63	46	31	23
6	Elba. Italy	Chromic Luvisol	Bt (150-180)	1.33÷1.73	2.65	35	31	34
7	Elba. Italy	Luvic Calcisol	Ah (0-20)	1.25÷1.68	2.57	50	26	24
8	Elba. Italy	Luvic Calcisol	Btk (80-100)	1.14÷1.52	2.53	26	28	46
9	Werbkowice	Haplic Chernozem	Ap (0-20)	1.18÷1.40	2.28	2	52	46
10	Parana. Brazil	Rhodic Ferrasol	Ah (0-10)	1.01÷1.37	2.88	4	16	80
11	Parana. Brazil	Rhodic Ferrasol	Bws (140-160)	1.04÷1.24	2.88	3	16	81
12	Ohlendorf. Germany	Haplic Luvisol	Bt (60-80)	1.31÷1.62	2.70	2	75	23
13	Ohlendorf. Germany	Arenic Cambisol	C (70-120)	1.59÷1.70	2.63	98	2	0
14	Markuszów	Orthic Podzol	Bh1 (40-60)	1.58÷1.80	2.64	85	12	3
15	Czesławice	Orthic Luvisol	Ck (150)	1.25÷1.61	2.48	0	68	32
16	Janów Lubelski	Eutric Cambisol	Bh (20-30)	1.14÷1.53	2.43	1	31	68

For dry soil ($\theta = 0$) only solid and air phases are present, therefore knowing the porosity of the most dry soil from the tested samples it is possible to estimate the ε_s as the average of all tested mineral soil samples according to Eq. (10).

This extrapolation gives the average value of dielectric constant soil solid phase equal to 4.72, which is in agreement with the published data (Dirksen and Dasberg [6], Friedman and Robinson [9]). The detailed statistics of the performed calculations are in **Fig. 2**.

It is assumed that for each soil type there is a transition water content value, θ_{WP}, which makes the distinction between soil water as bound or free. This water content can be determined from the empirical formula (Wang and Schmugge [22]) as:

$$\theta_{WP} = 0,0674 - 0,00064 \cdot SAND + 0,00478 \cdot CLAY \qquad (11)$$

where *SAND* and *CLAY* are percents of sand and clay in the tested soils. The index *WP* stands for wilting point as Wang and Schmugge [22] correlated the transition water content with the wilting point water content.
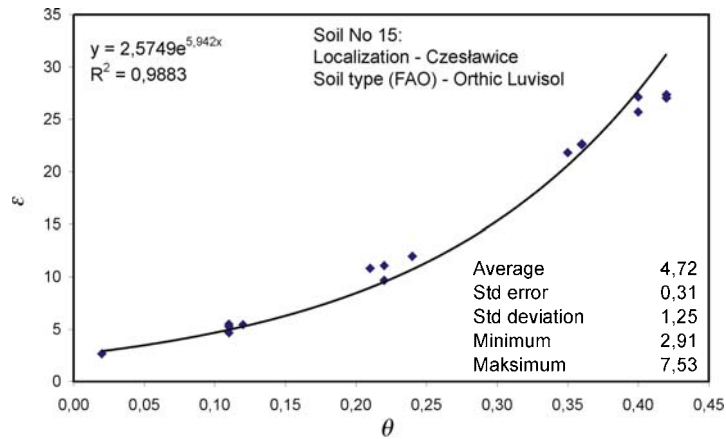
Fig. 2. Determination of the dielectric constant of soil solid phase using extrapolation and three-phase soil dielectric mixing model α.

Further discussion concerning 4-phase models assumes:

- If $\theta > \theta_{WP}$, the soil dielectric constant is represented by the 3-phase models, that is the formula (5) for the α-model, and the formula (8) for the *de Loor* model at $\theta_{bw}=0$.

- If $\theta \le \theta_{WP}$, the soil dielectric constant is represented by the 4-phase models, that is the formula (6) for the α-model, and the formula (8) for the *de Loor* model, at $\theta_{bw} = \theta$ and $\varepsilon_{bw} = \varepsilon_s + (80,2 - \varepsilon_s)\dfrac{\theta_{bw}}{\theta_{WP}}$, where ε_s is the soil solid phase dielectric constant, according to (10) for $\alpha = 0,5$.

Results and discussion

The relation between the soil dielectric constant, ε, and soil water content, θ, is presented in **Fig. 3**. It comes that for water content below 0.3 the values calculated from the empirical model (9) are higher than the measured ones. This is particularly evident for samples with high clay content (**Table 1**, no. 10, 11 and 16), *ie* for clay content more than 60%. High clay content is positively correlated with the amount of bound water surrounding soil solid particles (Or and Wraith [16]). These particles of water have the dielectric constant lower than that of free water. Therefore the model (5) is not adequate for clayey soils.

The value of dielectric constant of bound water, ε_{bw}, increases with the distance from the solid particles. Dirksen and Dasberg [6] confirmed this for soils of high specific surfaces.
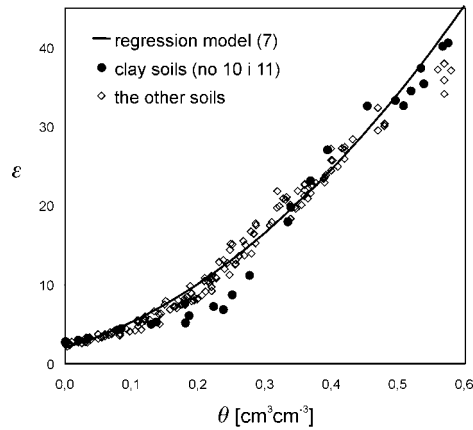
Fig. 3. Relation between the soil relative dielectric constant, ε, and soil volumetric water content, θ, for the investigated mineral soils; the solid line represents the empirical model (9) calculated for the average bulk density of the soil samples 1.42 [gcm^{-3}]

The comparison of ε values calculated from the 3-phase model (5) and measured by TDR device is presented in **Fig. 4**. There are two distinct ranges of ε, below and above the transition value of $\varepsilon_{TDR} \cong 15$, and this distinction generally does not depend on the value of the parameter α.
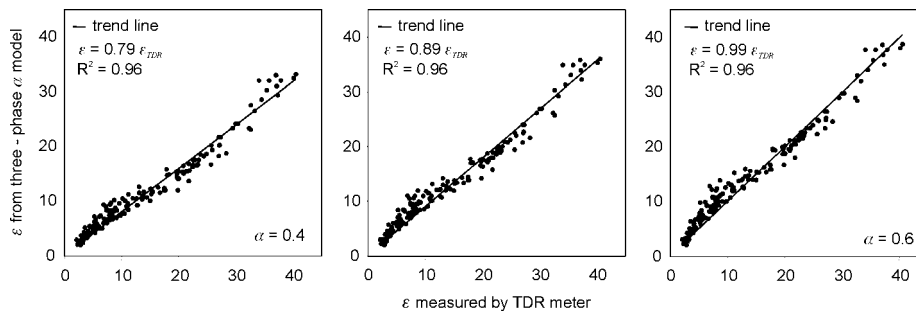
Fig. 4. Comparison of soil relative dielectric constants of the investigated soil samples measured by TDR method (horizontal axis) and calculated from 3-phase model α (5) for different values of α parameter.

Below the transition value, the soil dielectric constants calculated from the model are higher than the measured ones. For each α parameter the distribution of data is similar (R^2=0.96), the slope of the trend line is near 1 for α=0.6. For ε greater than the transition value, the 3-phase α model generates numbers close to the measured ones.

The empirical regression model (9), accounting for the soil density, does not eliminate the characteristic decline of data around the transition value of ε, although it makes it smaller (**Fig. 5**). The inclusion of soil bulk density to the empirical model of $\varepsilon(\theta)$ significantly increases the accuracy of TDR soil water content determination (Malicki *et al.* [14], Skierucha [18]).
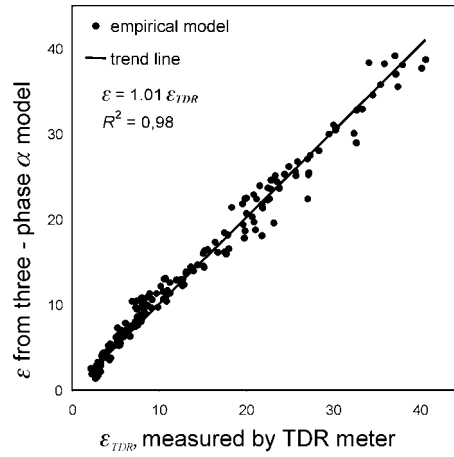

Fig. 5. Comparison of the soil dielectric constants measured by TDR method (horizontal axis) and calculated by the empirical model (9) accounting for soil bulk density

The 4-phase models (6) and (8) account for the presence of soil bound water, θ_{bw}, the magnitude of which can be expressed as:

$$\theta_{bw} = x \cdot S \cdot \rho \tag{12}$$

where x[m] is the distance from the solid phase surface and S[m^2/g] is the soil specific surface depending mainly on the soil clay content. According to Or and Wraith [16] and Sposito [19] the bound water is formed by no more than 3 monomolecular layers of water, where the single layer thickness is 3×10^{-10}[m]. The dielectric constant of the bound water is lower than that of capillary water because of hindering effect of solid phase induced to water dipoles. The relation between the bound water dielectric constant and the distance from the solid phase surface is unknown.

139
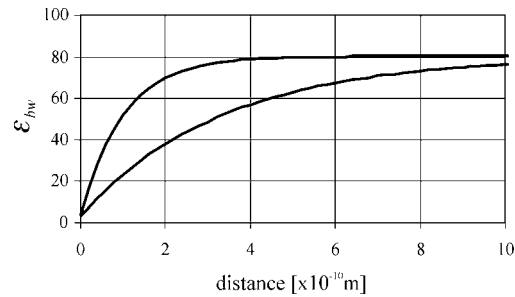
Fig. 6. Values of dielectric constant of bound water, ε_{bw}, related to the distance, x, from the phases interface

Or and Wraith [16] assume the exponential function, similar to the presented below (**Fig. 6**):

$$\varepsilon_{bw} = 80,2 - 77 \cdot e^{-kx} \tag{13}$$

where k is the parameter influencing the change of ε_{bw} with the distance of water particles from the phases interface.
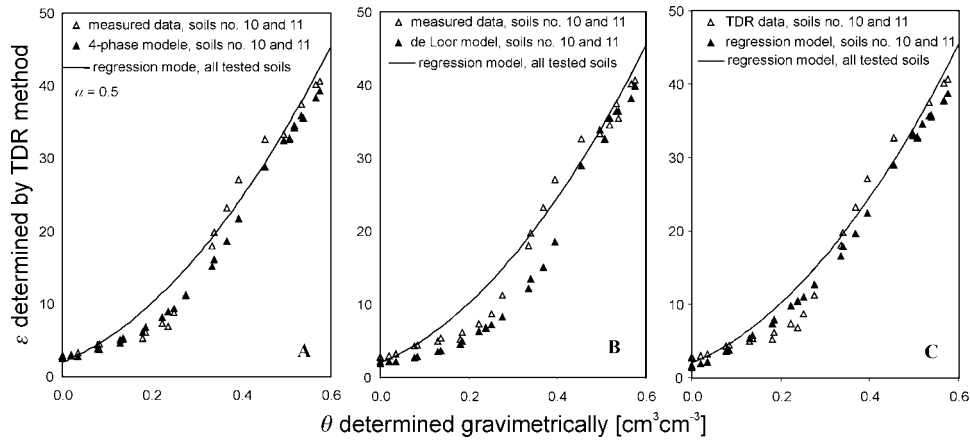

Fig. 7. Effects of the 4-phase models for the investigated clay soils (Table , no. 10 and 11): A – for model α, B - for *de Loor* model and C – effect of regression model (9) accounting for soil bulk densities, the solid line represents model (9) for $\rho = 1,42$ [gcm^{-3}]

To verify the observations concerning the influence of bound water on the $\varepsilon(\theta)$ relation the soils 10 and 11 (**Table 1**) are examined. They have the highest clay content from among the investigated soils and the transition water content is distinct on the $\varepsilon(\theta)$ curve (**Fig. 3**). The value of transition water content, θ_{WP}, is calculated from the formula (11) presented after [22]. The assumptions presented

earlier in the "Material and methods" section are applied to 4-phase models (6) and (8) for two selected soils (**Fig. 7**). The regression model shows higher values as compared to the measured ones for water contents below 0.35 (**Fig. 7C**).

The data calculated from the modified 4-phase models follow the measured data in the range where the regression model produces higher values. In the range of $\varepsilon < 15$ the 4-phase models work in agreement with the TDR measured data. Better correlation is achieved after application of α model than the model of *de Loor*. For all tested soils the values of ε produced by 4-phase modified α model as compared to the TDR measured ones are presented in **Fig. 8**.
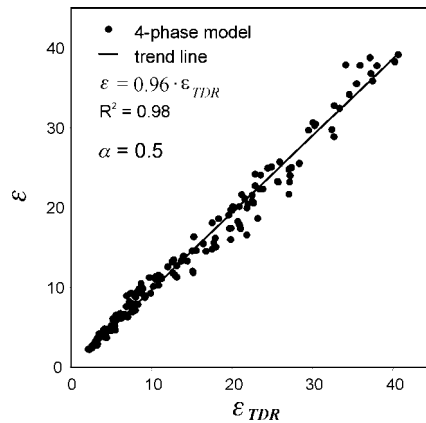
Fig. 8. Comparison of the analysed soil dielectric constant measured by TDR method (horizontal axis) and calculated from the 4-phase model α

Scatter of data in **Fig. 8** is comparable with that from the empirical model (9) accounting for the soil bulk density.

Conclusions

– Effect of bound water on the dielectric mixing model can be accounted for if clay content is known.
– The modified model α with the clay content as the corrective parameter of bound water works equally well as the regression model with soil bulk density as the corrective parameter.

References

1.   **Alharthi A., Lange J.:** Soil water saturation: dielectric determination. Water Resour. Res. 23(4), 591-595. 1987.
2.   **Birchak J.R., Gardner C.G., Hipp J.E., Victor J.M.:** High dielectric constant microwave probes for sensing soil moisture. Proc. of the IEEE. 62:(1):93-98. 1974.
3.   **Bohl, H., Roth K.:** Evaluation of dielectric mixing models to describe the $\theta(\varepsilon)$ relation. Symposium in Evanston. Sept. 8-9, 1994.
4.   **de Loor G.P.:** Dielectric properties of heterogeneous mixtures. Appl. Sci. Res. B3: 479-482. 1964.
5.   **de Loor G.P.:** Dielectric properties of heterogeneous mixtures. BCRS (Nederland Remote Sensing Board) rep. No. 90-13. TNO Physics and Electronics Lab., The Hague. 1990.
6.   **Dirksen C., Dasberg S.:** Improved calibration of Time Domain Reflectometry soil water content measurements. Soil Sci. Soc. Am. J. 57:660-667. 1993.
7.   **Dobson M.C., Ulaby F.T., Hallikainen M.T., El-Rayes M.A.:** Microwave dielectric behavior of wet soil - Part II: Dielectric mixing models. IEEE Transactions on Geoscience and Remote Sensing. GE-23:35-46. 1985.
8.   **Easy Test:** Soil water status monitoring devices. Instytut Agrofizyki PAN, Lublin. 2004.
9.   **Friedman S.P, Robinson D.:** Particle shape characterization using angle of repose measurements for predicting the effective permittivity and electrical conductivity of saturated granular media. 38(11), 1-11. 2002.
10. **Gardner C.M.K, Bell J.P., Cooper D., Dean T.J., Hodnett M.G.:** Soil Water Content. Soil Analysis – Physical Methods (edited by Smith K.A., Mullins C.E.). Marcel Dekker, Inc. New York. 1-73. 1991.
11. **Heimovaara T.J.:** Design of triple-wire Time Domain Reflectometry probes in practice and theory. Soil. Sci. Soc. Am. J. 57: 1410-1417. 1993.
12. **Heimovaara T.J.:** Frequency domain analysis of time domain reflectometry waveforms, 1-Measurements of complex dielectric permittivity of soils. Water. Res. Res., 30:189-199. 1994.
13. **Kraszewski A, Kulinski S, Matuszewski W:** Dielectric properties and a model of biphase water suspension at 9.4 GHz. Journal of Applied physics. Vol. 47, No. 4: 1275-1277. 1976.
14. **Malicki, M., Plagge A.R., Roth C.H.:** Reduction of soil matrix effect on TDR dielectric moisture determination by accounting for bulk density or porosity. European Journal of Soil Science, Vol. 47, No. 3, 357-366. 1996.
15. **Malicki M.A., Skierucha W.:** A manually controlled TDR soil moisture meter operating with 300 ps rise-time needle pulse. Irrigation Science. 10:153-163. 1989.
16. **Or D., Wraith J.M.:** Temperature effects on soil bulk dielectric permittivity measured by time domain reflectometry: A physical model. Water Res. Res., 35, No.2: 371-383. 1999.
17. **Roth, K., R. Schulin, H. Flühler, Attinger W.:** Calibration of Time Domain Reflectometry for water content measurement using a composite dielectric approach. Water Resources Research. 26:2267-2273. 1990.
18. **Skierucha W.:** The dependence of the propagation velocity of electromagnetic wave in the soil on the soil selected properties. PhD Thesis. Instytute of Agrophysics Polish Academy of Sciences, Lublin (in Polish). 1996.
19. **Sposito, G., Prost R.:** Structure of water adsorbed on smectites. Chem. Rev., 82, 553-572. 1982.

142

20. **Steru, M.:** Electrical control of water content of materials (in French). Measures & Contrôle Industriel. 24:33-38. 1959.
21. **Topp G.C., Davis J.L., Annan A.P.:** Electromagnetic determination of soil water content: measurements in coaxial transmission lines. Water Resources Research. 16:574-582. 1980.
22. **Wang J.R., Schmugge T.J.:** An empirical model for the complex dielectric constant of soils as a function of water content. IEEE Trans. Geosci. Remote Sensing. GE-18:288-295. 1980.
23. **Whalley W.R.:** Considerations on the use of time-domain reflectometry (TDR) for measuring soil water content. Journal of Soil Science. 44:1-9. 1993.
24. **Wright J.M., Or D:** Temperature effects on soil bulk dielectric permittivity measured by time domain Reflectometry: Experimental evidence and hypothesis development. Water Res. Res., 35, No.2: 361-369. 1999.
25. **Zegelin S.J., White I., Jenkins D.R.:** Improved field probes for soil water content and electrical conductivity measurement using Time Domain Reflectometry. Water Res. Res., 25, No.11: 2367-2376. 1989.

TDR SOIL WATER CONTENT, SALINITY AND TEMPERATURE MONITORING SYSTEM – DESCRIPTION OF THE PROTOTYPE

Skierucha Wojciech, Wilczek Andrzej, Walczak Ryszard T.

Institute of Agrophysics Polish Academy of Sciences, Lublin, Poland
skieruch@demeter.ipan.lublin.pl

Abstract

The study presents two electronic devices developed in the Institute of Agrophysics: an upgraded version of a portable moisture meter of porous media, working on the Time Domain Reflectometry principle of operation and a data logger intended to monitor physical and chemical parameters of soil, equipped with the wireless communication and internet access. These devices are compatible with the TDR probes developed in IAPAS and used in many research institutions all over the world. Due to the flexible interfaces of the presented data logger system it can be an element of the complex measurement systems not only for the measurement of soil water content, temperature and salinity but also other physico-chemical properties of soil environment.

Introduction

Selective measurements, without destructive interference to the measurement process and measured medium from unpredictable reasons are easy for interpretation but practically hard to accomplish [3]. The unwanted sources of error when identified can be eliminated by application of a physically good model of the observed process or by empirical correction based on reference measurements. A lot of measurement errors happen during the wire-transmission of an analog signal from the sensor equipped by an appropriate transducer, converting the usually non-electrical signal to its electrical representation, to the measuring unit. To avoid wire-transmission errors modern measurement systems combine the measuring unit with the sensor-transducer element in the form of a smart transducer or smart sensor. Smart sensors [7] are equipped with microcontrollers or digital signal processors capable to convert the measured signal to the digital form, performing individual calibrations and necessary corrections. Thus most of the data processing is completed at the sensor and the command and data communication with it usually performed in wireless way.

The main reasons for the development of automatic measurements systems are: the requirement objective readouts, without the unwanted interference from error sources including the influence of an experiment operator and economical

144

reasons. The integral part of such a system is a data logger for autonomic data collection and storing. The recent development of telecommunication and associated electronics gives the new tools and means for the idea of automatic measurement of environmental physical and chemical properties, especially low power converters of non-electrical signals to easy for processing electrical signal, powerful microcontrollers integrated with analog-to-digital and digital-to-analog converters, timers, digital interfaces and abundant non-volatile memory.

The presented study shows the potential of the MIDL (Multi Interface Data Logger) data logger, its functional features and the function in the automatic measurement system of physical and chemical parameters of soil and ground. The system has been developed in the Institute of Agrophysics in Lublin, Poland, as the direct answer for the need to collect data from ion-selective electrodes that measure the concentration of selected ions in the soil (Research Project 2 P04G 032 26 financed by the State Committee for Scientific Research). Also, the measurement devices developed, produced by the Institute of Agrophysics and used by a number of scientific soil laboratories [2,9] need a modern and hardware as well as software compatible data logger. The detailed description of functional and technical parameters of this system as well as the details of start procedures is presented in [4,5,6].

The MIDL – Multi Interface Data Logger follows up-to-date trends of electronics and informatics offering the users many features superior to the ones that have the old D-LOG data logger [2].

It has been assumed that the MIDL data logger should provide:
- Ethernet 10Base-T Internet communication features,
- radio communication in the non-licensed 433MHz frequency band [74],
- supply by an external power source 6-12VDC,
- limited power consumption below 2W in the continuous work mode,
- communication interfaces for monitoring and configuration the device by means of a PC compatible computer, ie serial RS232C and infrared (IRDA) wireless digital data transmission,
- serial RS232C and RS485 work interfaces for connecting measurement devices,
- 4-bit output parallel port in TTL standard (to be compatible with the old measurement devices developed in the Institute of Agrophysics),
- user accessible universal connector for MMC (MultiMedia Card) memory card with the capacity up to 128MB memory,
- internal temperature sensor and real time clock,
- limited power consumption in the standard in the standard work mode, ie the energy used from 12VDC power source during 90 days should not exceed 2Ah, when the total script execution time is 3.6hours (including

0.33hours of RS232C or RS485 operation), the total radio communication – 7hours, the total time of the device in the watch mode (with the radio access periods of minimum 2seconds) – 2000 hours.

- temperature range of work –25°C to 85°C.

Fig. 9. Multi Interface Data Logger (in the middle between TDR soil water content, salinity and temperature meters) in the configuration for the measurement of 16 TDR FP/mts probes

The picture with the prototype MIDL data logger system controlling two TDR meters, each with a multiplexer for connecting up to 8 TDR FP/mts probe in presented in **Fig. 9**.

Functional description

MIDL data logger consists of two functional versions, *ie* MASTER and SLAVE. The both versions are built on the base of the same hardware; SLAVE uses the whole hardware features while MASTER only the part of it. The functional features are distinguished by software automatically identifying the version.

MIDL can operate in various modes and **Fig. 10** presents the most complex mode where the system consists of a number of MASTER devices controlled by via Internet by PC compatible computers.

MASTER modules are wireless transceivers (receivers and transmitters) of signals from Internet to radio signals between PC and the addressed SLAVE module. The wireless radio link works according to the accepted assumptions in

146

the non-licensed frequency band of 433 MHz [11]. The SLAVE modules together with the connected measurement devices (by means of the serial interface RS485) are complete data acquisition systems. Each of them contains all the elements necessary to control the measurement process by the connected probes, store the collected data and communicate with the MASTER device to transmit the whole or a part of the storage memory to the PC, *ie* a separate supply source, microcontroller, real time clock and abundant (up to 128 MB) nonvolatile memory.
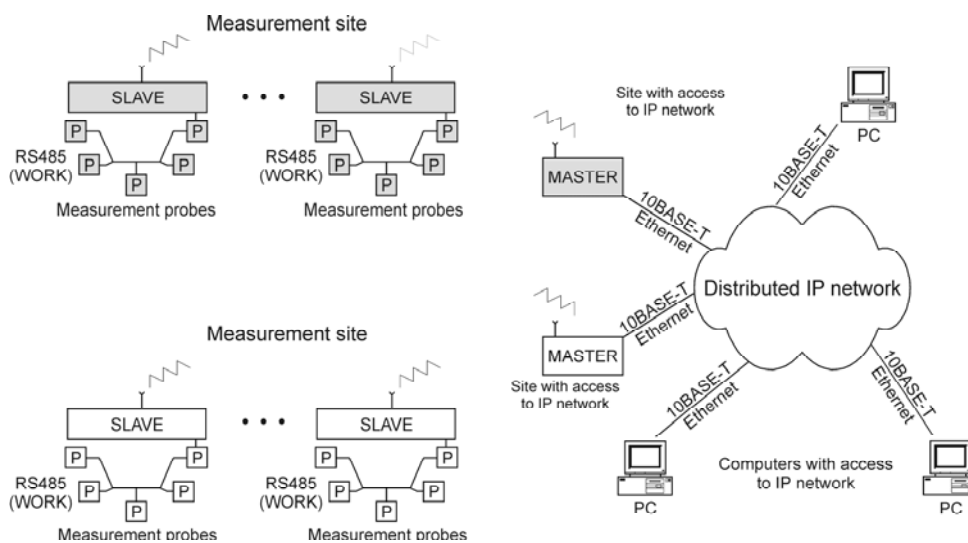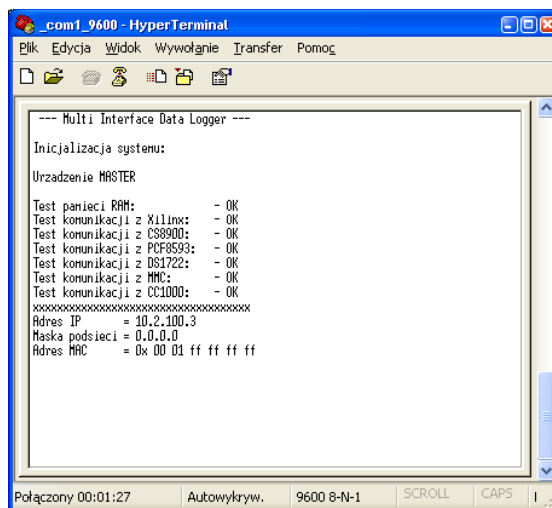
Fig. 10. Example setup of devices for soil and ground physico-chemical parameter monitoring system using wireless communication

The access to MASTER and SLAVE devices is possible from any place accessible by the IP network and in case of Internet network – from any place in the world. The devices are protected by unique Internet addresses and access passwords. The range of the applied radio link is limited to about 500 meters in the case when there are no physical obstacles between the transmitting and receiving antennas. The applied radio link in built from commercially available, completely assembled and tested electronic modules [1]. During transmission and reception they consume small power (about 100mW), they can be completely disconnected for a defined period to save power and quickly connected again. The communication speed is 9600 bits per second, and in case of large file transmission, *ie* above 1MB, is not economical due to limited energy in the supply battery. Another considered solution is to provide each SLAVE module with

GPRS modem that enables much more fast connection with the Internet network. The basic drawback to apply GPRS modems is that they consume much more power than the presently applied 433 MHz modules. However it is possible to program the transmitting and receiving modems for short-time work, *ex* 10 minutes during 24 hours, to transmit the collected data to the base station (PC computer). Such a solution would guarantee large amount of data transmission and battery saving, which is a fundamental assumption of the presented data logger system. The described service of "wireless Internet" is presently provided by majority of mobile telecommunication providers.

MIDL system handling

The detailed description of MIDL system handling, including the description of user interface accessible from an WWW Internet browser, is presented in the Operation Manual [4].

Fig. 11. Serial RS232C port terminal window with the MIDL system initial tests

After switching on the system performs checking of its basic functional elements and the tests results are transmitted by the RS232C configuration interface. The tests results can be checked after connecting RS232 cable between the configuration interface and PC compatible computer. Then the user should run any RS232C terminal program on PC computer (*ex* Hyper Terminal in Microsoft Windows system), switch on the power supply and the computer display will present the tests results (**Fig. 11**).

148

All test communicates must be positive for the correct operation of the MIDL data logger. The window contains also network configuration parameters that are necessary to know for establishing connection with the system.

Configuration of basic parameters of the MIDL system

The correct operation of the system needs initial configuration of the Internet link. The configuration parameters are included in a system file "server.ini" located on the MMC memory card. This file may be placed in the MIDL data logger in three ways:
- writing on the MMC card by means of an universal read/write device dedicated for MMC memory cards, connected to a PC computer, inserting the card into the slot in the MIDL device (MASTER or SLAVE) and switching on the power supply,
- accessing the cart in the device slot by WWW site,
- accessing the cart by means of FTP protocol to send the "server.ini" file by Internet.

Before accessing the card by WWW browser or FTP client the device must be connected to the computer by means of IP network.

System files

There is a number of file types in the MMC memory card. From a WWW site it is possible to access script files ("*.scr" file extension) and output data files ("*.txt" file extension). All files on the MMC memory card are accessible by FTP client or by reading the card in the universal card reader read/write device:
- files with „*.htm", „*.css", „*.js" extensions – files of graphical user interface used by a WWW browser,
- files with „*.scr" extensions – device executable script files,
- files with "*.txt" extension - output data files generated by executable scripts,
- files with "*.ini" – system files with the device configuration parameters.

The format and command of the executable script files are presented below.

Executable script files

Files with „*.scr" extension treated by the device as executable script files.

Table 2 below presents an example script file with commands that: fix the SLAVE RS232C serial port transmission speed to 9600 baud, give a name to the

output data file where the data from the addressed sensor will be stored, send a command to the serial RS485 interface with the address activating the individual sensor, format the data received from the sensor and setting the SLAVE device into the sleep mode for a given period of time. The beginning of the script is marked by [beg] and the end by [end] directives.

Table 2. An example of the executable script file

```
[beg]
port(9600)
filename("RS485t.txt")
outp(RS485,"Command sent to the work interface RS485 \n\r")
fprintf("Result of the measurement received by RS485: ")
inp(RS485,14,4000)
sleep(120)
[end]
```

When the defined period of time, when the device is in the sleep mode, terminates, the script file executes from the beginning.

The script commands for autonomic, cyclic control measurements by the SLAVE device are presented in **Table 3**.

Table 3. Script file commands

Command	Description
`port(baudrate, databits, stopbits, paritychecking);`	Setting parameters of the serial port
`outp(port, "data");`	Sending data by the working interface
`inp(port, length, wait);`	Receiving data from the working interface
`filename("name");`	Setting the file name where the data received from working interfaces will be stored
`sleep(sec);`	Bringing the MIDL into the sleep mode for defined number of seconds
`fprintf("format");`	Introduction of additional formatted data into the output file

Each sensor connected to the SLAVE module should "understand" the script commands. This requires that each sensor is provided with an appropriate hardware and software interface. Therefore the term "sensor" means a device converting the analyzed signal (*ex* temperature, pressure, electrical conductivity, etc.) into the corresponding electrical signal.

Such a sensor integrated with a decision-making element, computation and communication facilities forms a smart sensor [8,10]. Smart sensors must be also identified and have means for storing individual calibration data.

The presented data logger system for collecting physical and chemical parameters of soil environment represents modern trends in the development of measurement systems that is manifested by low power consumption, high capacity of storage memory and possibility to control the measurement process from any place in the world using Internet connection or application of wireless radio connection in the case when the access to the monitored object is limited. Traditional sensors and measurement devices, such as soil thermometers, reflectometric soil water content meters, soil tensiometers for water potential measurement, rain-gauges and others may be easily equipped with not expensive, intelligent communication interfaces enabling identification, addressing as well as hardware and software compatibility with the presented MIDL data logger. The system was designed in modular way for future modifications following the progress in the metrology of non-electrical quantities and the general technological development.

New prototype version of FOM/mts soil water content, salinity and temperature measurements

The device presented in **Fig. 12** is the new generation of TDR soil water content, salinity and temperature meter constructed in the Institute of Agrophysics.

For compatibility reasons it uses the same probes as the ones developed some years ago and used in many research laboratories all over the world [2]. The meter has memory capable to store about 1000 data points that can be labeled for identification. The operation of the meter is by a five-pushbutton keypad that controls the display by means of user-friendly software. A small lithium-polymer rechargeable battery commonly used in mobile telephones supplies the device. It can be optionally equipped with the Global Positioning System (GPS) for giving longitude and latitude coordinates of the meter for localization. This feature is fundamental in application in precision agriculture.

New version has the following features:
– accuracy and resolution not worse than FOM/mts from Easy Test,light handheld enclosure,
– ability to register and store up to 1000 labelled readings,
– real time clock,

– operates with Easy Test TDR probes with different cable lengths (from 1.5 to 9.5 m),

Fig. 12. Prototype of a handheld soil water content, salinity and temperature meter constructed with the application of modern components

– keyboard and LCD display (160x128 dots) with user friendly operating software,
– optionally equipped with GPS module for localization,
– connection by USB interface with PC compatible computer for data transfer,
– lithium-polymer (without memory effect enabling charging at any time) battery supply.

FP/m, FP/mts - Field Probe for moisture, temperature and salinity of soil

FP is a Time-Domain Reflectometry (TDR) probe for momentary or semi-permanent installation (**Fig. 13**). Thin-wall PVC body of the probe provides ultimate low heat conductivity, thus allowing avoiding the parasite "thermal bridge" effects on distribution of soil water content in the probe's sensor vicinity. Through a preaugered pilot hole it can reach any depth without destroying either the soil structure or disturbing the heat and mass transport in the soil. For semi-permanent installation the probe can be inserted horizontally through a sidewall of a soil pit or slantwise (**Fig. 14**), from the soil surface. The probe installed once may be left intact in the soil for as long as necessary, then drawn out at the end of the experiment.

Fig. 13. FP/m, FP/mts - Field Probe for water content, temperature and salinity of soil developed in the IAPAS, Lublin

FP/m is a probe for *in situ* field measurement of the soil water content whereas FP/mts is its version for simultaneous measurement of water content, temperature and salinity (electrical conductivity) of the soil from the same sampling volume.

Both probes are suitable for periodic measurements at random and/or fixed locations, where instantaneous profiles of water content, temperature and salinity are to be determined by readings taken at various levels of the soil profile. Each of them may also be applied as a mobile probe (FP/m/m or FP/mts/m) for momentary measurements in surface layer of the soil, by walking over the field and inserting the probe in the soil surface layer at chosen sites. The shortest available probe is 15 cm long. Its support pipe has not any bending. To place the probe at 5 – 15 cm depth it can be inserted horizontally through a sidewall of a shallow soil pit. The longest possible probe is 400 cm long (probes longer than 150 cm are delivered as a kit to be assembled by the user). In order to install FP in the soil, a pilot hole has to be preaugered from the soil surface, deviated out of vertical of an appropriate angle, *a*.
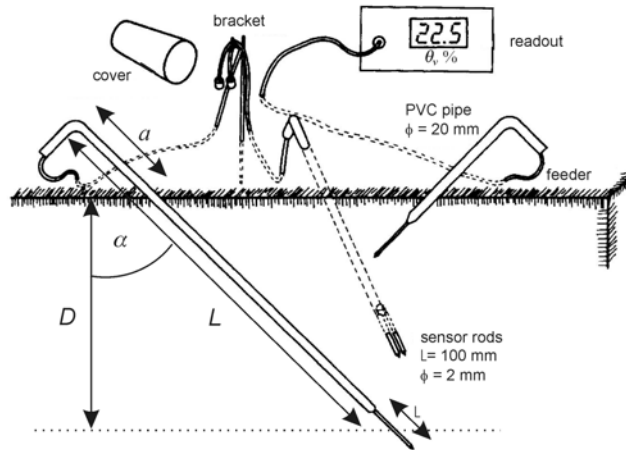
Fig. 14. The principle of installation of the FP-type probes. In order to minimize disturbances in the soil structure the probes are inserted into the soil via pilot holes, circularly distributed over the soil surface. The holes run slantwise and converge along a chosen vertical line. The cables are buried below the soil surface to protect them against the UV sun radiation as well as against rodents.

The shortest available probe is 15 cm long. Its support pipe has not any bending. To place the probe at 5 – 15 cm depth it can be inserted horizontally through a sidewall of a shallow soil pit. The longest possible probe is 400 cm long (probes longer than 150 cm are delivered as a kit to be assembled by the user). In order to install FP in the soil, a pilot hole has to be preaugered from the soil surface, deviated out of vertical of an appropriate angle, *a*. The probe length, *L*, and the depth, *D*, the sensor rods are meant to reach in the soil profile (the installation depth) are related as follows:

$$L = \frac{D}{\cos\alpha} - 5 + a \qquad (14)$$

where: *L*, *D* and *a* in cm and α is the out of vertical deviation angle. The length, *L*, is distance between the base of the sensor rods and the bending point of the plastic support pipe and *a* is length of the part of the probe body sticking out the soil surface. Different combinations of *L*, *a* and α allow to reach the intended deepth, *D*. Suggested magnitude for a is 30°.

The approximate region of influence of the FP probe, defined as a solid beyond of that changes in water content do not markedly affect readings of water content is presented in **Fig. 15**.
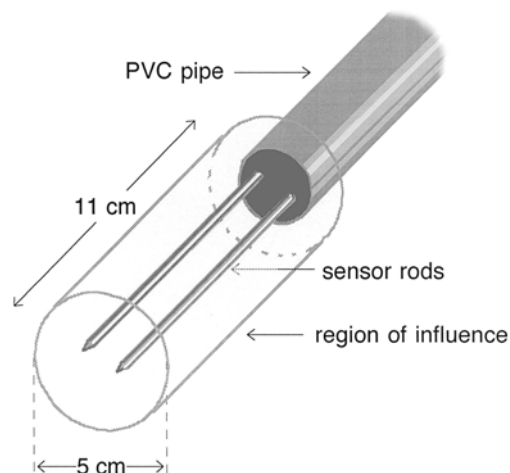
154

Fig. 15. Approximate region of influence of the FP probe, defined as a solid beyond of that changes in water content do not markedly affect readings of water content

Features of the FP probes for soil water content, salinity and temperature measurement developed in IAPAS, Lublin:

 − Sensor: a section of a transmission line made of two, 100 mm long parallel stainless steel rods having 2 mm diameter and separated by 16 mm
 − Sensor support: a section of a PVC tube having 2 cm outer diameter and optional length (15 cm - 150 cm or longer) dependent on the intended depth of the sensor installation
 − Cable length: 6 m from the sensor to the BNC terminating connector
 − Region of influence: a cylinder having approximated diameter of 5 cm and height of 11 cm, circumferenced around the sensor rods.

Summary

The new TDR soil moisture meter is a light, handheld device equipped with a clock, a large amount of memory capable to store thousands of measured values while powered from a single charging of a small battery. A graphical display unit is used for presenting the signals reflected from a TDR sensor, displaying the measured values of moisture, electrical conductivity and temperature. The operation of the device is controlled by software user interface by means of a keyboard. A user can select the variable to measure (moisture, temperature or electrical conductivity in all combinations), give names to each collected data point for identification in the memory, connect the meter to PC compatible

computer by a standard USB connection and monitor the state of battery. Also the meter is equipped with the GPS unit for geographical localization with the accuracy of ± 5m.

The MIDL (Multi Interface Data Logger) is a functional device for controlling the operation of various measurement devices and store the collected data in a memory, which is in the form of a standard Multi Media Card (MMC). The access to data collected from the connected sensors and the configuration data is possible by the radio interface, serial interface or Internet by means of the Internet browser. The device executes the commands in cyclic way controlling the measurement process by means of serial interface. It has very low power consumption and one of the executable commands sets a sleep mode of the device and then, after the programmed delay the device wakes up to continue operation. Each MIDL data logger has a unique number to identify in the Internet network and for the construction of widespread measurement networks with global access.

The requirements to have the objective data without the unwanted interference to the measured process from the experiment operator and the economical reasons are the main factors of the development of automatic data acquisition systems. This is especially important in field measurements with variable atmospheric conditions and other reasons making the access to the measured sites are hard to accomplish. The integral part of such a system is a data logger for monitoring the complex natural or industrial processes. Data loggers collect and store information from the sensors for further processing. They are only input devices even if the measurement process needs some conditioning of the sensors to get the response. The measured process should not be influenced by the measurement system, which is the case of the real time acquisition systems applied for the control. The progress of automatic measurement is closely related to the development of electronics and communication. The development of mobile communication enables to finance other branches of electronics, especially sensors of non-electrical signals integrated with data conversion electronics, microcontrollers equipped with analog signal conversion as well as wireless data transmission systems.

References

1.   **Chipcon Smart RF CC1000** - Single Chip Very Low Power RF Transceiver (http://www.chipcon.com/files/CC1000_Data_Sheet_2_2.pdf), 2004.
2.   **Easy Test:** Soil water status monitoring devices. Instytut Agrofizyki PAN, Lublin. 2004.
3.   **Malicki M.A.:** Methodical aspects of water status monitoring in selected biological materials (in Polish). Acta Agrophysica, 19, Lublin 1999.

4. **MIDL:** Data logger for field monitoring of soil and ground physical and chemical parameters. Operation Manual (in Polish). Institute of Agrophysics Polish Academy of Sciences, Lublin, 2004.

5. **MIDL:** Data logger for field monitoring of soil and ground physical and chemical parameters. Technical Manual (in Polish). Institute of Agrophysics Polish Academy of Sciences, Lublin, 2004.

6. **MIDL:** Data logger for field monitoring of soil and ground physical and chemical parameters. Start-up Manual (in Polish). Institute of Agrophysics Polish Academy of Sciences, Lublin, 2004.

7. **Skierucha W.:** Temperature effect on soil dielectric permittivity: description of laboratory setup and applied software (in Polish). Acta Agrophysica. 72:125-133. 2002.

8. **Skierucha W., Wilczek A.M, Walczak R.T.:** Application of smart sensors in the measurement of soil physical parameters. Research in Agricultural Engineering, Vol. 50, (3), 96-102, 2004.

9. **Walczak R.T., Sławiński C.:** Study and modelling the mass and energy transfer in agrophysics (in Polish). Eksploatacja i Niezawodność. 4, 6-15. 2000.

10. **Wiczer J.:** Connectivity: smart sensors or smart interfaces. ISA 2001 Emerging Technologies Conference, Huston, TX, Sept. 10-13, 2001.

11. **Wilczek A., Mazurek W., Skierucha M.:** Application of wireless communication in automatic monitoring of temperature in soil profile (in Polish). Acta Agrophysica 93:123-133, 2003.

CALIBRATION OF TDR INSTRUMENTS FOR MOISTURE MEASUREMENT OF AERATED CONCRETE

Sobczuk Henryk, Suchorab Zbigniew

Institute of Environmental Protection Enginnering, Faculty of Environmental Engineering,
Lublin Univetsity of Technology, Poland
h.sobczuk@fenix.pol.lublin.pl

Abstract

Moisture appearing in the building barrier is a normal phenomenon and practically inevitable in our climatic zone. Anyhow, large amounts of water occurring in barriers are disadvantageous from as well construction as hygienic-sanitary causes. Water penetrating the pores of building materials is one of the biggest problems during winter. When it occurs in highest levels, freezing and thawing many times, it causes material disintegration and decrease of its bearing parameters. Too much moisture in building structure during wintertime causes also decrease of its insulating parameters, which leads to indoor temperature decreases and generates extra expenses for heating. All disadvantages mentioned above indicate the need to elaborate an easy and possibly low-invasive method for measurements of moisture in porous media. For measurements of building materials moisture levels we propose using of TDR method. TDR (Time Domain Reflectometry) is a well developed and commonly used method for measuring of moisture levels in soils. There are some factors causing difficulties with precise measurements of water content in the materials. The most important problem seems to be the fact that dielectric constant of mineral material may vary in values depending on kinds of material, which may lead to need to callibrate measuring instruments to obtain serious results for exact material.

The major aim of this article is to present TDR measuring method as a tool to measure changes of water content in building materials, propose a way of calibration for measurement needs and presenting data and calibration curves for aerated concrete block as a commonly used building material. The formulas and curves are established basing on gravimetrical experiments with constant measurements of TDR signal propagation in blocks of aerated concrete. We had prepared calibration curves for most popular kinds of aerated concrete in Polish building market: 400 (kg/m^{-3}), 500 (kg/m^{-3}), 600 (kg/m^{-3}), 700 (kg/m^{-3}) and it is possible to use them in measurements of moisture profiles in the buildings. Application of other probes constructions may enable adoption of this method for building materials – much harder than soils and aerated concrete, but it is necessary to find a proper calibration method that will make it possible to measure most of common materials in Polish building market. This paper seems to be an approach to this extensive topic.

K e y w o r d s : TDR method, aerated concrete, building materials, calibration curves, calibration formulas.

Introduction

Moisture appearing in a building barrier is a normal phenomenon and practically inevitable in our climatic zone. But, unfortunately in high amount it is disadvantageous from construction and sanitary point of view. Water, which penetrates pores of building materials, is one of the biggest problems during the winter season, when it occurs in highest level. Freezing and thawing many times, causes material disintegration and decrease of its bearing parameters. It also creates a very good environment for biological life development like mould that not only decreases the durability of the material but also spoils indoor microclimate in stricken rooms [5]. Too much moisture in the building structure during wintertime also causes a decrease of its insulating parameters, which leads to indoor temperature decrease and generates extra expenses for heating. All the disadvantages mentioned above indicate the need to elaborate an easy and possibly low-invasive method for measurements of moisture in porous building material.

For measurement of building materials moisture we apply TDR method. TDR (Time Domain Reflectometry) is a well developed and commonly used method for measuring of moisture levels in soils. It enables quick, precise and, relating to soils, non-ivasive way compared to the gravimetrical method. TDR methology allows continues observation of dynamics of moisture in porous media. Also, gravimetrical examinations demand separation of an extract of the whole material and using TDR enables *in-situ* measurements.

Measurement of moisture content in the examined porous medium relays on the estimation of propagation time of electromagnetic signal in metal rods of a probe introduced in such a system. Time of propagation is linearly dependent on the dielectric constant of the medium, which in turn directly depends on water content in the porous material. Relative dielectric constant (apparent permittivity) of mineral material ranges between 1 and 4 and relative dielectric constant of water equals about 80. In the mentioned range the dielectric constant depends on the water content (for real porous media). Knowing the value of dielectric constant we can estimate the water content (cm^3 cm^{-3}) in the place where the probe was set [2,4].

Unfortunately, there are some factors causing difficulties with precise measurements of water content in the material. The most important problem seems to be the fact that the dielectric constant of mineral material may vary in value depending on kinds of material, which may lead to a need to calibrate measuring instruments to obtain exact results for specific material.

We apply TDR methodology to examine water content in building materials. Both soils and building materials are the porous media that consist of three

phases: solid, liquid and gas. But, in comparison to soils, there is one major difficulty for TDR measurements of moisture changes in building materials – they are hard with a dense structure. For these materials we need to find a proper technique of installation of TDR probes. This technique may demand drilling of special holes for rods of the probes. But it seems to be easy to examine soft building materials such as aerated concrete and a majority of heat insulating materials.

The major aim of this article is to present the TDR measuring method as a tool to measure changes of water content in building materials, suggest a calibration method for measurements and to present data and calibration curves for aerated concrete block as a commonly used building material.

Theoretical bases

According to a popular model of porous media as a mixture of a three-phase it will be assumed, that relative dielectric constant (ε_{TDR}) of three-phase medium is linearly dependant on dielectric constants of particular phases [4]:

$$\varepsilon_{TDR} = \phi_s \varepsilon_s + \phi_g \varepsilon_g + \theta \varepsilon_l \tag{1}$$

where: ε_{TDR} – relative dielectric constant of three-phase medium, ε_s, ε_g, ε_l – respectively, dielectric constants of phases: solid, gaseous and liquid, ϕ_s, ϕ_g – respectively, volumetric content of solid and liquid phase, θ – volumetric water content

Assuming that dielectric permittivity of the gaseous phase in the porous medium is always constant and equals 1. Dielectric permittivity of mineral material varies in a relatively small range between 1 and 4 [2]. We can assume, that relative dielectric constant of three-phase medium depends mainly on water content with the dielectric constant about 80.

Using the above approximation we can establish water content in a porous medium basing on measurement of its relative dielectric constant.

The most popular calibration equation for water content estimation in a porous medium was proposed in 1980 by Topp, where water content, expressed in volumetric moisture θ (cm^{3}cm^{-3}) was dependent on the relative dielectric constant of the medium:

$$\theta = \frac{-530 + 292\varepsilon - 5.5\varepsilon^2 + 0.043\varepsilon^3}{1000} \tag{2}$$

where: θ – volumetric water content in examined porous material [m^3/m^3], ε – relative dielectric constant, determined using following equation:

$$\varepsilon = \left(\frac{ct_p}{2L} \right)^2 \tag{3}$$

where: c – electromagnetic wave velocity in vacum ($3 \cdot 10^8$ m s^{-1}), t_p –propagation time of pulse through probe rods placed in porous medium (s), L – lenght of rod of the probe (m).

This equation allows quick and efficient measurement of water content in soil. But results obtained using it seem to have big measurement error [4] about 0,15 to 0,05 (cm^3 cm^{-3}). This error is often a result of differences of the density of solid material.

A good improvement of this callibration method is Malicki's (1994) equation, which contains not only the relative dielectric constant but also bulk density of the material (ρ):

$$\theta = \frac{\left(\varepsilon^{0,5} - 0.819 - 0.168\rho - 0.159\rho^2 \right)}{7.17 + 1.18\rho} \tag{4}$$

where ρ is the bulk density of the mineral material (Mg m^{-3}).

This equation gives results with a smaller error margin, which balances between -0.03 and 0.03 (cm^3 cm^{-3}).

The calibration methods mentioned above are empirical ones. The idea of measurement is based on checking the time of propagation of the electromagnetic pulse in the rods of the probes placed in a porous medium, and then using correct formulas to determine water content in the examined material.

Another calibration method is the gravimetrical one, which is based on determining calibration curves and formulas that represent relation between water content and the time of pulse propagation or dielectric constant.

The advantage of the laboratory method over the empirical ones is that it includes specificity of the examined material. The dielectric constant of mineral material varies between 1 and 4 and these variations may falsify moisture contents readout. Preparation of calibration curves gives the possibility to connect real water content and signal propagation in exact three-phase material in a form of a calibration formula.

Methodology

Most of literature about TDR methodology is connected with soils. We observe lack of suitable studies on using this method for building materials. That is why we decided to prepare calibration curves for them. As a material to

measure we chose cellular concrete as a commonly used material in Polish building industry (relatively cheap, with suitable construction and heat parameters). Cellular concrete is also a relatively soft material, so we had no problems with introducing classic TDR probes in its porous structure without any special arrangements.

For measurements we used TDR equipment by a Lublin producer "Easy Test". We prepared a set of cellular concrete samples produced at the area of Lublin province. For measurements we used the following densities of material: 400, 500, 600 and 700 (kg m^{-3}), as typical for Polish market. Dimension of each sample was 3×3×12 (cm) (**Fig. 1**). Next, the samples were dried at the temperature of 105°C and weighed until no observable weight loss, which was a confirmation that we have no water content in the prepared sample.
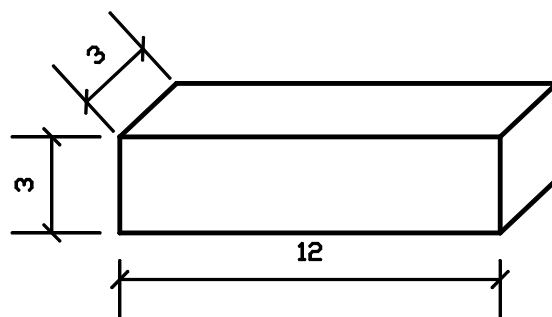
Fig. 1.   Sample of cellular concrete prepared for calibration
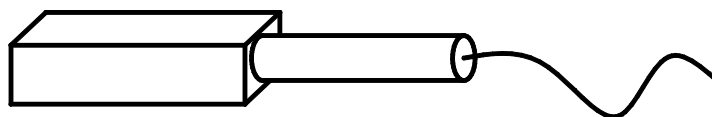
Fig. 2.   TDR probe introduced into a sample of cellular concrete

In the samples prepared in such a way we introduced TDR probes (**Fig. 2**.) and measured the time of signal propagation in the examined medium. Then we dripped them regularly (2 hour periods) with water until reaching a point of total saturation, still weighing and checking the time of propagation with TDR equipment.

Basing on the measurements mentioned above we collected a set of data on relations between the time of signal propagation (ps) in the rods of TDR probes

and water content in the material they were introduced into. We used the above data to estimate calibration curves for measurements of moisture changes in blocks of cellular concrete. Assuming that water density ρ equals 1 (g cm^{-3}) we estimated that the volume of water inside the pores of cellular concrete V_w (cm^3) is numerically equal to their mass. That's why water content θ (cm^3 cm^{-3}) in this material is a relation between the volume of water filling the pores of the examined sample V_w and its total volume V_c (cm^3):

$$\theta = \frac{V_w}{V_c} \tag{5}$$

Using the data of signal propagation velocity in the rods of the probes for different water contents we prepared calibration curves presented below:
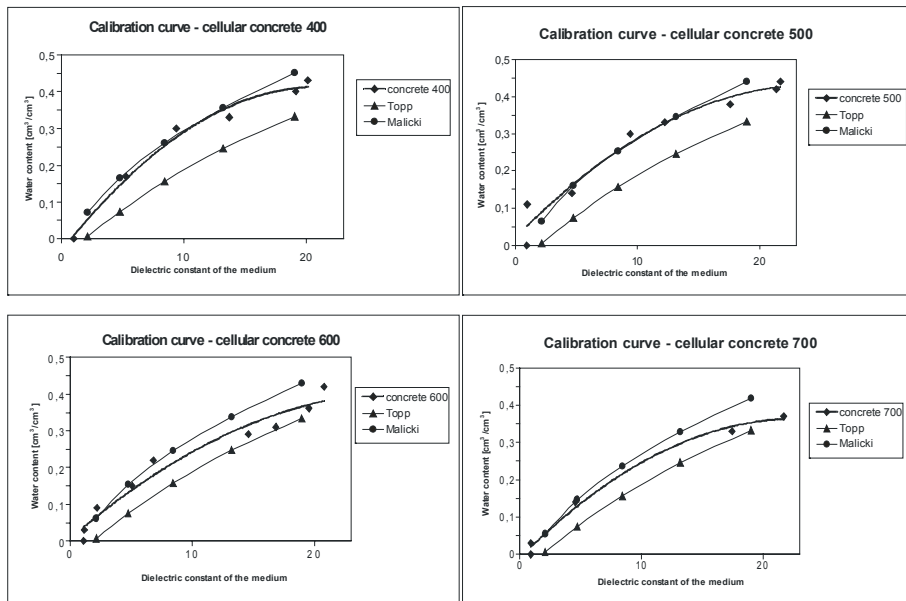
Fig. 3. Calibration curves for moisture changes in cellular concrete according to laboratory measurements and empirical formulas of Topp and Malicki.

On the base of the above curves showing relations between water content and time of propagation (exactly the dielectric constant) we established the following formulas to determine water content in real materials:

$$\theta_{400} = -0,001\varepsilon^2 + 0,0426\varepsilon - 0,0337 \qquad (\text{cm}^3 \text{ cm}^{-3}) \tag{6}$$

$$\theta_{500} = -0,0007\varepsilon^2 + 0,0336\varepsilon + 0,0202 \qquad (\text{cm}^3 \, \text{cm}^{-3}) \qquad (7)$$

$$\theta_{600} = -0,0005\varepsilon^2 + 0,0287\varepsilon + 0,0068 \qquad (\text{cm}^3 \, \text{cm}^{-3}) \qquad (8)$$

$$\theta_{700} = -0,0007\varepsilon^2 + 0,0329\varepsilon - 0,0105 \qquad (\text{cm}^3 \, \text{cm}^{-3}) \qquad (9)$$

Table 1. Relation between time of electromagnetic signal propagation in TDR probes inside cellular concrete and water content of the medium according to empirical formulas by Topp (2), Malicki (4) and data obtained by laboratory measurements

Cellular concrete	T_p	Dielectric contant	Water content according to Topp equation		Water content according to Malicki equation		Water content according to laboratory measurements		Water content according to formulas (6,7,8,9)
	(ps)		(m³m⁻³)	(m³m⁻³)	(%)	(m³m⁻³)	(%)	(m³m⁻³)	(%)
	694	1	-	0.01	1	0	0	0.01	0
400	2547	13.7	0.25	0.36	36	0.33	33	0.36	36
	3011	19.1	0.33	0.44	44	0.4	40	0.42	42
	671	1	-	0	0	0	0	0.05	5
500	1484	4.6	0.07	0.16	16	0.14	14	0.16	16
	2409	12.2	0.23	0.33	33	0.33	33	0.33	33
	3207	21.7	0.37	0.48	48	0.44	44	0.42	42
	709	1.1	-	0.01	1	0	0	0.04	4
	1009	2.1	0.01	0.06	6	0.09	9	0.07	7
600	1793	6.8	0.12	0.21	21	0.22	22	0.18	19
	2827	16.9	0.3	0.4	40	0.31	31	0.35	35
	3139	20.8	0.35	0.45	45	0.32	32	0.39	39
	660	0.9	-	-	-	0	0	0.02	2
	1479	4.6	0.07	0.14	14	0.14	14	0.13	13
700	2096	9.3	0.17	0.25	25	0.31	31	0.23	23
	2875	17.4	0.31	0.39	39	0.33	33	0.35	35
	3208	21.7	0.37	0.46	46	0.37	37	0.37	37

Relations between the dielectric constant and water content for both empirical formulas by Topp and Malicki and also laboratory calibration data are presented in **Table 1.**

Conclusions

TDR measurements technology is a method that gives a lot of possibilities to determine changes of moisture in building barriers. It is significant in designing energy-saving buildings and also in expertises of moist and heat status in the existing constructions. Unfortunately, for building materials, the use of this method is restricted because of the lack of literature and technical problems connected with probes application.

We propose adoption of TDR technology for measurements of changes of moisture for soft building materials such as insulation materials (mineral wool,

polystyrene) and blocks of cellular concrete. Cellular concrete, because of its heat parameters is a very popular construction material in the Polish building market, that is why using of above mentioned technology seems to be worth interesting.

Application of other probe types may enable adoption of this method for building materials that are much harder than soils. It is only necessary to find a proper calibration method that will make it possible to measure most of common materials in the Polish building market. This paper is an approach to this extensive topic.

References

1. **Mojid M.A., Cho H.:** Response of the core and shield rod soft time-domain reflectometry probe to transverse soil-water content heterogeneity. Journal of Hydrology 262, 21 – 27, 2002.
2. **Noborio K.:** Mesurement of soil water content and electrical conductivity by time domail reflectometry: a review. Computers and Electronics in Agriculture, 31, 213 – 237, 2001.
3. **Robinson D.A., Gardner C.M.K., Cooper J.D.:** Measurement of relative permittivity in sandy soils using TDR, capacitance and theta probes: comparison, including the effects of bulk soil electrical conductivity. Journal of Hydrology 223, 198 – 211, 1999.
4. **Schapp M.G., de Lange L., Heimovara T.J.:** TDR calibration of organic forest floor media. Soil Technology, 11, 205 – 217, 1996.
5. **Ważny J., Karyś J.:** Ochrona budynków przed korozją biologiczną. Arkady, 2001.

MEASUREMENT AND APPLICATION OF SURFACE AREA TO CHARACTERIZE SOIL MATERIALS

Sokołowska Zofia

Institute of Agrophysics, Polish Academy of Sciences, Lublin
zosia@maja.ipan.lublin.pl

Introduction

Solid phase of a soil is a mixture of different inorganic constituents as nonporous materials of different size and shape, porous materials with microcapilares or pores and phyllosilicates with the interlayer structure, as well as organic species, mainly organic matte. Different kind of the surface area may be found in soil. The *geometric* surface area is calculated on the data of shapes and dimension of representative soil particles. The *internal surface area* - surface of inter walls of the microcapillares (the term "internal surface" is usually restricted in its application to those cavities, which have an opening to exterior of the grains). The *external surface are*a is defined as the sum of geometric and internal surface area. The *interlayer surface area* - the surface of interlayers walls of minerals type montmorillonite. The *total surface area* - the sum of the surface area of the external, internal and the surface area of organic matter.

Specific surface area of a soil sample is combined surface area of all the particles in the sample, as determined by some experimental technique and expressed per unit mass of the sample. As its definition implies, term specific surface area is an operational concept.

The method of determining the surface area of textured solids, including soil materials, is based on the adsorption of any of number of gases (Gregg and Sing 1978, Ościk 1982). To understand the way, in which measurements of the adsorption of gases or vapours can be used to obtain information about surface area and porosity, it is necessary to deal briefly the concept of the adsorption isotherm.

In the present paper we shall consider the application of the physical adsorption of gases to the estimation of the specific surface area of soils.

Physical adsorption of gases on solid

When a solid is exposed in a closed space to a gas at some definite pressure, the solid begins to adsorb the gas or vapour. The term *adsorption* appears to have

been introduced by Kayser (in 1881) to connote the condensation of gases on free surfaces, in contradistinction to gaseous *absorption* where the molecules of gas penetrate into the mass of the absorbing solid. The term *sorption* proposed by McBain (in 1909), embraces both types of phenomena, adsorption and absorption.

The adsorption is a consequence of the field force at the surface of the solid (the adsorbent), which attracts the molecules of the gas (the adsorbate). The forces of attraction emanating from a solid may be of two main kinds, physical and chemical, and they give rise to physical adsorption and chemisorption respectively. The physical adsorption is also called as van der Waals adsorption. Those bringing about physical adsorption always include dispersion forces (which are attractive in nature) and short-range repulsive forces, and in addition there may be forces due to permanent dipoles within the adsorbed molecule. The process of physical adsorption is reversible, the heat of adsorption is low, and the thickness of adsorbed layers may be a few molecular diameters of a gas molecule. In the present paper we are concerned with physical adsorption.

The amount of gas adsorbed per gram of solid N, depends on the equilibrium pressure p, the temperature T, and also on the nature of the gas and solid. This function at a constant T is called the adsorption isotherm when p increases, and when p decreases - the desorption isotherm. The adsorption N may be measured in any suitable units *ie* grams or milligrams, moles or millimoles, and cm^3 (N.T.P.).

The adsorption isotherm is the most popular expression of adsorption data. The isotherm naturally start at the origin of the co-ordinates and they end is at a nearly of the saturated vapour. No simple interpretation can be given to the main part of the curve. The beginning part of the isotherm is use to obtain the surface area, and the end part to pore structure in a solid body. The volume of liquid which is adsorbed a nearly saturated vapour by 1 gram of adsorbent is called the pore volume of the adsorbent.

In many instances an algebraic expression of the adsorption isotherm is more convenient than its graphic presentation. A few equations have been found to reproduce a large number of experimental isotherms. A number of different theories have been proposed for the interpretation of adsorption data. The best known and probably the most frequently used theory, is that proposed by Brunauer, Emmett and Teller (BET). It leads to the equation called the BET equation, which has proved remarkably successful in the calculation of specific surface area from the isotherms of type II.

The BET equation describes localised multilayer adsorption on a homogeneous surface of an adsorbent:

$$N = \frac{N_m x C_{BET}}{(1-x)[1+(C_{BET}-1)x]}$$

where: $x = p/p_0$ is the relative pressure of a vapour, N – the amount of adsorbed vapour, and C_{BET} is a constant.

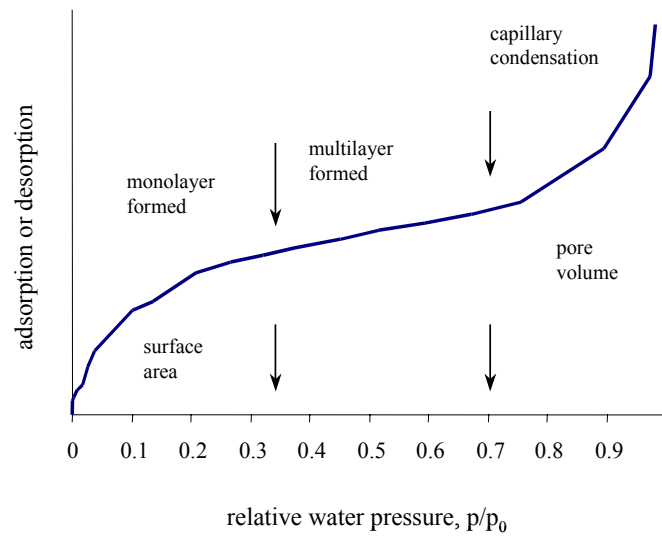The range of validity of BET equation does not always extend to relative pressure as high as 0.30 or 0.5.

Fig. 1. The adsorption isotherm, type II of BET classification

Methods of surface area measurements

The principal physical methods for measuring specific surface area of soils or soil constituents are electron microscopy and X-ray diffraction (the crystallographic or geometric surface area). The majority of chemical methods are based on measurement of adsorption of polar and nonpolar gases or vapours. The adsorbable compounds used to determine specific surface area are chosen on the basis of their molecular properties. Polar adsorbates are water vapour, ethylene glycol or ethylene glycol monoethyl and they used to measure the total surface area. Typical nonpolar adsorbates are nitrogen, argon, krypton and they are used to measure the external surface area. Nitrogen is commonly used as the adsorbate because it interacts weakly with a broad array of surface functional groups and therefore permits for the determination of exposed area of soil.

Calculation the specific surface area from adsorption data

The surface area of soil samples was evaluated from adsorption-desorption isotherms in the BET range of relative water vapour pressures, using the Brunauer-Emmett-Teller (BET) method. The first step in the application of the BET method is to obtain the monolayer capacity (N_m). The second step is to calculate the surface area.

The monolayer capacity from BET plot

The first step in the application of the BET method is to obtain the monolayer capacity (N_m) from the BET plot in the range of relative pressures $0 < p/p_0 > 0.35$:

$$\frac{x}{N(1-x)} = \frac{1}{C_{BET} N_m} + \frac{(C_{BET}-1)}{C_{BET} N_m} x$$

where $x = p/p_0$ is the relative pressure of water vapour, N is the amount of adsorbed water vapour, and C_{BET} is a constant.

If $x/N(1-x)$ is plotted against p/p_0, a straight line should result with the slope $s = (C_{BET}-1)/N_m C_{BET}$ and the intercept $i = 1/N_m C_{BET}$. Solution of the two above equations gives N_m and C_{BET} - $N_m = 1/(s+i)$ and $C_{BET} = (s/i)+1$.
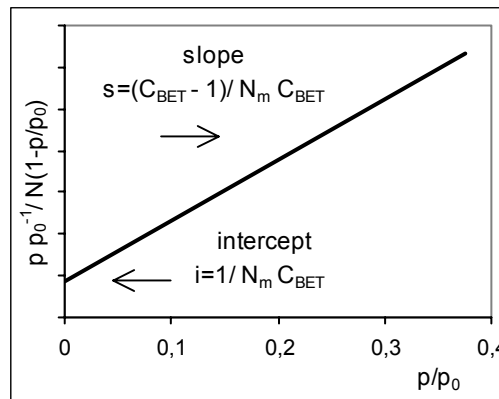
Fig. 2. Calculation of the value N_m (monolayer capacity) from BET plot

Calculation of the surface area

The second step is to calculate the surface area from the dependence:

$$S = N_m \times M^{-1} \times L \times \omega,$$

where: L is the Avogadro number (6.02×10^{23} molecules per mole), M is the molecular weight of gas or vapour (gram per mole) and ω is the molecule cross-sectional area for gas or vapour (m^2 for molecule).

Results

Studies of the surface chemistry of solids frequently involve determinations of specific surface area. Many investigators have attempted to measure surface area as means of describing better the soil materials under study or understanding better a particular process or reaction.

Surface area is significantly related to various chemical and physical properties of soils (Churchman *et al.* 1991, Feller et al. 1992, Sokołowska *et al.* 1993, Petersen *et al.* 1996, Theng *et al.* 1999, Sokołowska *et al.* 2004). The relationships between the specific surface area and some physical and chemical properties of mineral soils are presented in **Table 1**. The values of the correlation coefficient higher than 0.5 were typed in bold.

Table 1. Correlation coefficients of linear regression between the specific surface area obtained from water vapour and nitrogen adsorption data and selected properties of soils, obtained from the data for 482 soil samples.

	Soil fraction, %		OM, %	CEC, cmol·kg^{-1}	Exchangeable cations, cmol·kg^{-1}				
	<0.02	<0.002			H	Ca	Mg	K	Na
soils formed from loess									
S(N$_2$)	0.419	**0.705**	**-0.550**	**0.589**	**-0.555**	**0.570**	**0.646**	-0.197	0.263
S(H$_2$O)	**0.701**	**0.976**	0.395	**0.936**	-0.309	**0.906**	**0.920**	0.098	**0.738**
soils formed from clay									
S(N$_2$)	**0.720**	**0.656**	**-0.503**	**0.542**	0.062	0.400	**0.641**	0.312	**0.553**
S(H$_2$O)	**0.627**	**0.832**	-0.068	**0.579**	-0.178	0.357	**0.891**	**0.666**	0.480
soils formed from silt									
S(N$_2$)	**0.547**	**0.679**	-0.251	0.067	0.268	0.007	**0.612**	0.030	-0.125
S(H$_2$O)	**0.696**	**0.875**	**0.865**	**0.535**	0.084	0.478	**0.901**	0.303	0.270
soils formed from loam									
S(N$_2$)	**0.805**	**0.792**	-0.332	**0.666**	-0.011	**0.606**	**0.712**	0.019	0.479
S(H$_2$O)	**0.936**	**0.902**	0.018	**0.667**	0.203	**0.568**	**0.838**	0.171	**0.559**
soils formed from sand									
S(N$_2$)	**0.561**	**0.641**	0.491	0.425	0.278	0.404	**0.521**	0.191	0.049
S(H$_2$O)	**0.589**	**0.770**	**0.607**	**0.700**	0.358	**0.655**	**0.751**	0.252	0.146

Abbreviation: CEC - cation exchange capacity; OM - organic matter.

For mineral soils there exist a linear relationship between specific surface area and the content of the granulometric fractions and the cation exchange capacity. For the clay fraction the correlation coefficient is very high. Similarly, a strong correlation exists between surface area and CEC. **Fig. 3** and **Fig. 4** give an example illustrating the dependence between the surface area of the alluvial soils and the content of clay fraction and CEC.
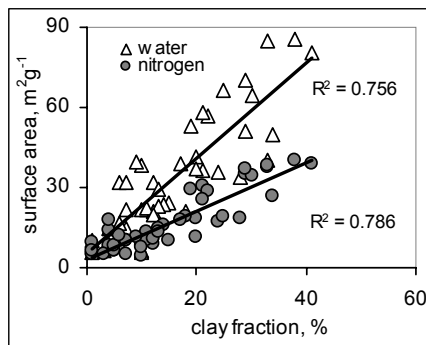

Fig. 3. The relationship between the surface area and the percent of clay content
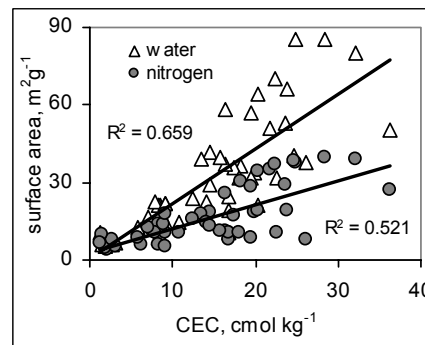
Fig. 4. The relationship between the surface area and the cation exchange capacity (CEC)

The surface area is a function of the content and size of mineral particles, as well as the content and quality of organic compounds (**Fig. 5**).
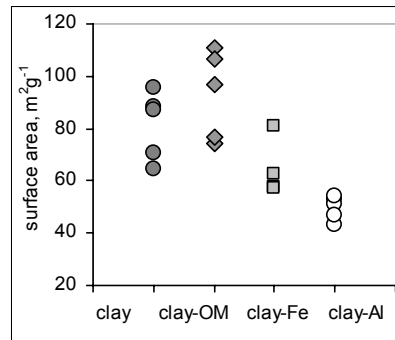
Fig. 5. Surface area of soil clay fraction - from loess soils (abbreviation: black circles - the original clay, diamonds, squares and white circles - clay without organic matter, Fe and Al compounds, respectively)

The method of determination of the surface area of textured solid, including soil material, is based on the adsorption of gases or vapours, and on the

application of the Brunauer-Emmet-Teller (BET) isotherm equation (Gregg and Sing 1978; Ościk 1982; Sing 1982).
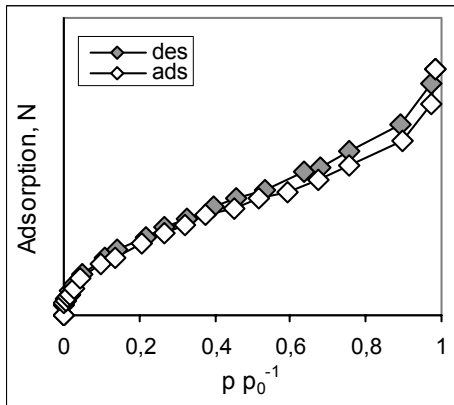
Fig. 6. Example of the water vapour adsorption data: original adsorption-desorption isotherm. $p \cdot p_0$ – relative pressure
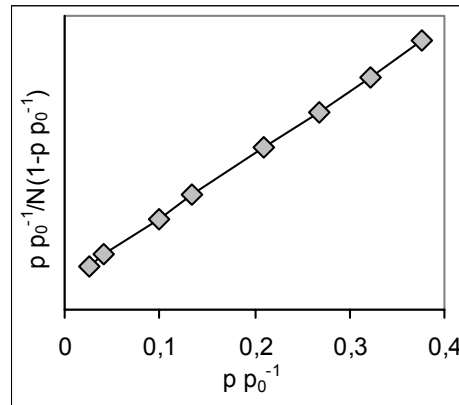
Fig. 7. The BET plot of the water vapour sorption isotherm

Fig. 6 shows a typical adsorption isotherm of water vapour on mineral soil and **Fig. 7** - the isotherm in the coordinates transformed according to the BET equation.
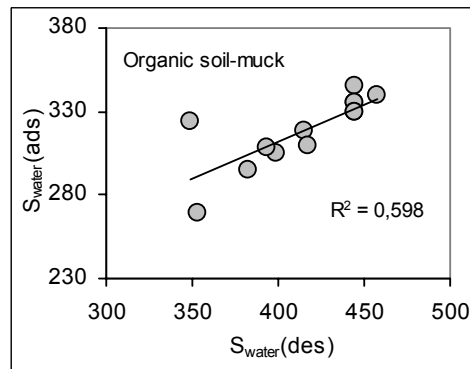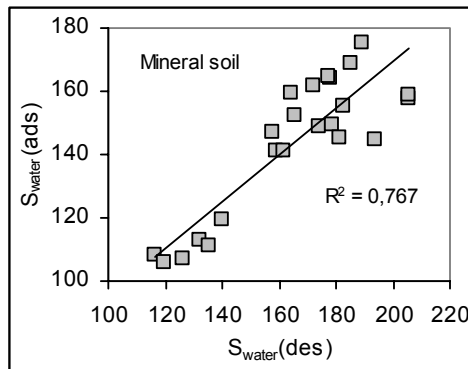

Fig. 8. Relationships between specific surface areas obtained from adsorption and desorption of water vapour

For an ideal adsorption process on an ideal adsorbent the adsorption is reversible, *ie* the adsorption isotherm coincides with desorption one. In the case of real adsorbents, the upper branch of the curve corresponds to desorption, while

172

the lower branch (**Fig. 6**) indicates the adsorption. The explanations advanced for the fact that many adsorbents resist variation in the amount they have adsorbed. Adsorption hysteresis is very common. Generally, hysteresis loop is connected with the character of adsorbent and adsorbate and with the interaction potential between them.
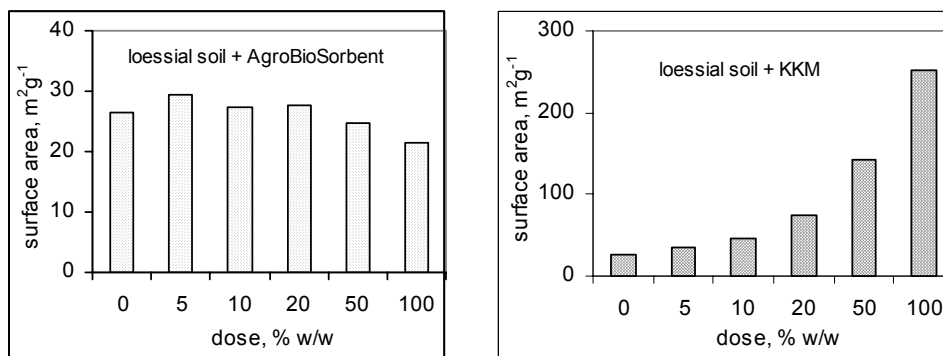

Fig. 9. Specific surface area of the loessial soil with AgroBioSorbent and keratin-bark-urea compost

Fig. 8 shows relations between the values of the surface area obtained from adsorption and desorption isotherms of water vapour in mineral and organic soil.

The surface area may be used as a parameter, which characterizes various soils and soil processes. Surface area changes can result from several interacting factors that include clay minerals, organic matter, farming practice and soil type.

Fig. 10. Average surface area of soil samples from the organic farming and conventional system

Fig. 9 and **Fig. 10** illustrate relation between specific surface area and farming practice.
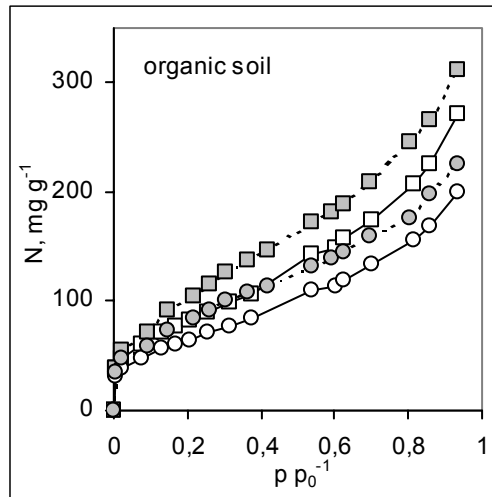
173

Fig. 11. Exemplary sorption (white symbols) and desorption (black symbols) isotherms of the water on the muck; weakly (circles) and strongly (squares) transformed mucks

The term adsorption presently used in the physical chemistry for mineral adsorbents and soils, is not adequate for organic soils. In the latter case the term sorption is more appropriate. The water vapour sorption on peat-moorsh soils indicates that the sorption (saturated) and desorption (drying) processes run independently in the full range of the relative pressures.
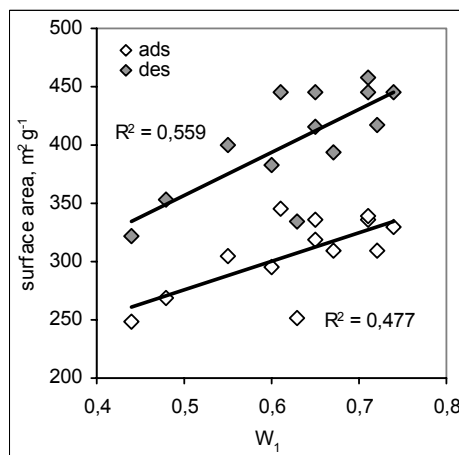
Fig. 12. The BET surface area obtained from sorption and desorption data. W_1- the water holding capacity index of muck

174

The sorption-desorption isotherm does not exhibit the hysteresis loop (**Fig. 11**).

The BET surface area of the organic soils locates in high ranges of surface areas of mineral soils (**Table 2**). Generally, the value of the surface area obtained from sorption (adsorption) and desorption data are different (**Fig. 12**).

Table 2. Surface area of selected organic materials

No.	Organic material	Surface area (m^2/g)	Experimental data/technique
1	Mucks and peats:	average value:	water vapour
	Z_1	345	sorption, BET eq.
	Z_2	345	
	Z_3	347	
	Fibric	349	
	Mesic	342	
	Humic	351	
2	Florida peat	0.61	nitrogen
	Houghton muck	0.73	adsorption, BET
	Soil humic acid, freeze-dried	18	eq.
	Soil humic acid, oven-dried	0.70	
3	Mucks:	average value:	water vapour
	W_1 od 0.41 do 0.50	258.9ad 338.8de	sorption, BET eq.
	W_1 od 0.51 do 0.60	299.9ad 390.8de	
	W_1 od 0.61 do 0.80	311.9ad 406.8de	
	W_1 od 0.71 do 0.80	328.7ad 441.2de	
4	peat	1.5	nitrogen
	muck	0.8	adsorption, BET
	cellulose	2.3	eq.
5	humic acid from podsol	238	water vapour
	humic acid from chernozem	201	sorption, BET eq.
	humic acid from muck soil	220	
6	wheat roots dried at 25^0C:		water vapour
	original	334	sorption, Aranovitz
	cutting	391	eq.
	ground	390	
7	potato starch	259.7ad 368.7de	water vapour
	starch extrudates	214.4-341.3ad 327.2-347.2de	sorption, BET eq.

Explanations: 1 - Sapek B. *et al.*: Proc. VIII Inter.Peat Congr., Leningrad, 1988, Section IV, 288-294; 2 - Chiou C.T.: Environ. Sci. Technol., 1990, 24, 1164-1166; 3 - Sokołowska Z. *et al.*: Acta Agrophysica, 2000, 26, 41-49; 4 - Księżopolska A.: PhD thesis, IA PAN, Lublin 1996; 5 - Szatanik-Kloc A.: PhD thesis. IA PAN, Lublin 2000; 6 - Jamroz J. *et al.* Inter. Agrophysics, 1999, 13, 451-455

Adsorption of gases or vapours and surface area depends on nature of the soil solids. Various kinds of the polar and nonpolar functional groups have been identified in mineral and organic soil constituents. The most important are the carboxylic-, phenolc-, hydroxylic- groups. These groups create primarily hydrogen bonding or van der Waals forces or π-bonding. Several polar functional groups serve as sorption sites for water molecules. Because of a high dipole moment and the ability to form hydrogen bonds, water can be form a quite complex adsorbed layers that can exhibit different properties depending on the kind of surface functional groups binding water molecules. The hydratation or coordination reactions between surface cations and water molecule also influence adsorption of water vapour. Chiou *et al.* 1990 and Penell *et al.* 1995 pointed out that such polar compound as ethylene glycol (EG), can partition into soil organic matter, hampering its use for measuring reliable specific surface area. For the surface area determined by the EG method, Chiou *et al.* 1990 proposed the term "apparent surface area" and "free surface area" for surface determined by N_2-BeET method. Free surface area corresponds to the interfacial area of a solid, which exist before the adsorption and unequivocally measured by an adsorbate that does not change the structure of the solid.

The peat soils undergo swelling and shrinking and a high degree of volume reduction of the peat when dried has been observed. Also, the thermal treatment of organic soils induced their hydrophobization, which has been reflected by change in the wettability of their surfaces by water vapour.

Fig. 13 illustrates the change of the surface area on muck that was thermally treated at 20^0C and 105^0C and additionally initially subjected for wetting-drying cycle.
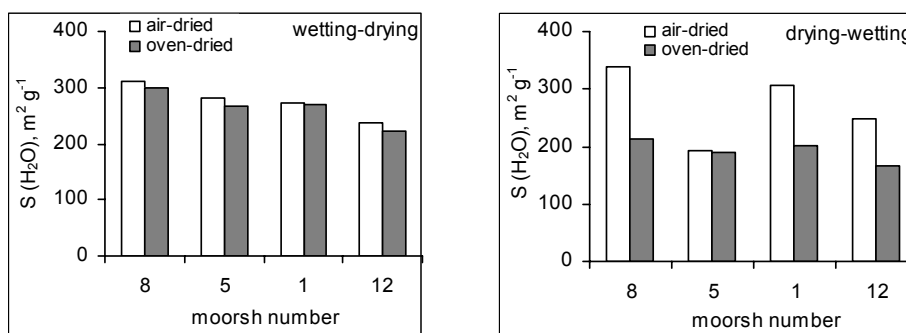

Fig 13.   Relationship between specific surface area, determined for initially wetting-drying and drying-wetting cycles, and temperature of sample drying

176

Conclusions

The adsorption of water vapour and nitrogen, and the surface area depend of the nature of soil solid phase. Different kinds of the polar and non-polar functional groups have been identified in natural organic and mineral soil constituents. The most important are carboxylic-, phenolic-, hydroxylic groups. Nitrogen and sulphur-containing functional groups, such as amino-, imino- and sulphonic acid groups may be also present in smaller quantities. These groups create primarily hydrogen bonding or van der Waals forces. Several polar functional froups are sorption sites for water molecules. Because of a highly specific manner forming quite complex sorbed layer, which can exhibit different properties depending on the kind of the surface functional groups binding water molecules. In the adsorption process of nitrogen the adsorption centers play a smaller role than the porous structure because nitrogen is an inert adsorbate.

It is stress that specific surface area values measured with nitrogen adsorption differ from those measured with the polar adsorbate i.e. water vapour, and care needs to be taken in comparison data obtained using these two methods. The disparity may be to difference in the nature of adsorptive forces involved in sorption polar vs. non-polar molecules. The nitrogen and the watervapour adsorption experiments produce similar values of surface area only in the absence of expandable clay minerals and organic matter.

The surface area may be used as a parameter, which characterize various soils and soil processes.

References

1. **Chiou C.T., J-F Lee, Boyd S.A.:** The surface area of soil organic matter. Envron. Sci. Technol., 24, 1164-1166, 1990.
2. **Churchman G.J., Burke C.M.:** Properties of subsoils in relation to various measures of surface area and water content. J. Soil Sci., 42, 463-478, 1991.
3. **De Kimpe C.R., Laverdiere M.R., Martel Y.A.:** Surface area and exchange capacity of clay in relation to the mineralogical composition. Can. J. Soil Sci., 59, 341-347, 1979.
4. **Feller Ch., Schouller E., Thomas F., Rouiller J., Herbillon A.J.:** N_2 -BET specific surface areas of some low activity clay soils and their relationships with secondary constituents and organic matter contents. Soil Sci., 153, 293-299, 1992.
5. **Gregg S.J., Sing K.S.W.:** Adsorption, surface area and porosity. Acad. Press, London, N.Y., 1978.
6. **Ościk J.:** Adsorption. PWS Ellis Horwood Ltd. Publish. Chichester, 1982.
7. **Pennell K.D., Boyd S.A., Abriola L.M.:** Surface area of soil organic matter reexamined. Soil Sci. Soc. Am. J., 59, 1012-1018, 1995.
8. **Petersen L.W., Moldrup P., Jacobsen O.H., Rolston D.E.:** Relation between specific surface area and soil physical and chemical properties. Soil Sci., 161, 9-21, 1996.

9. **Sing K.S.W.:** Reporting physisorption data for gas/solid systems, with special reference to determination of surface area and porosity. Pure Appl. Chem., 54, 2201-2218, 1982.
10. **Sokołowska Z., Józefaciuk G., Sokołowski S., Urumova-Peszeva A.:** Adsorption of water vapour on soils: The influence of organic matter and the components of iron and aluminum on energetic heterogeneity of soil samples. Clays a. Clay Minerals 41, 346-352, 1993.
11. **Theng B.K.G., Rostori G.G., Santi C.A., Percival H.J.:** An improved method for determining the specific surface areas of topsols with varied organic matter, texture and clay mineral composition. Eur. Soil Sci. J., 50, 309-316, 1999.
12. **Sokolowska Z., Hajnos M., Elias E.A., Alaily F.:** Characteristics of the surface area of Vertisols from the Gezira region in Sudan. Int. Agrophysics, 18, 83-90, 2004.

ASSESSMENT OF THE EFFECT OF GROUNDWATER LOWERING ON THE CAPILLARY RISE IN A SANDY SOIL

Stenitzer Elmar and Gassner Leopold

Institute for Soil Water Management Research of the Austrian Federal Agency
for Water Management, Petzenkirchen, Austria
elmar.stenitzer@relay.baw.at

Abstract

Importance of capillary conductivity in assessing the effect of lowering groundwater depth on the water supply of grassland by capillary rise is demonstrated applying the model SIMWASER using data on soil water regime and grass growth from field experiments in the Drau valley in Carinthia/Austria.

Keywords: gravel, capillary rise, grass yields, simulation model SIMWASER

Introduction

In the Drau valley in Carinthia /Austria in dry summers capillary rise from rather high groundwater levels substantially is contributing to meet the water demand of the grass sward. This high groundwater during summer months is typical for alpine river valleys and is caused by snowmelt in the high mountain regions. Lowering the riverbed downstream of a newly constructed hydropower plant to increase its efficiency was accompanied by declining ground water depths in the valley floor and lower grass yields. Field experiments were run from 1991 to 1995 to test, if and to what amount this measure could have been the reason for the grass yield depressions. In the work presented here the problem concerning the quantification of the capillary rise and it's effect on the grass yield by a simulation model using either measured or estimated hydraulic soil parameters is described.

Material and methods

The study area is situated at the village Baldramsdorf near Spittal/Drau river in the middle reach of the Drau river in Carinthia in Southern Austria (13°27' E, 46°48' N, 560 m above sea level). Mean annual air temperature is 8.5°C and mean annual rainfall amounts to 900 mm. Silty sand soil of alluvial origin and variable depth is underlain by a gravely and stony aquifer. Groundwater depth at

the study site varied between 100 and 200 cm below surface (**Fig. 1**) with the higher levels during summer months reaching near to or even into the sandy subsoil.
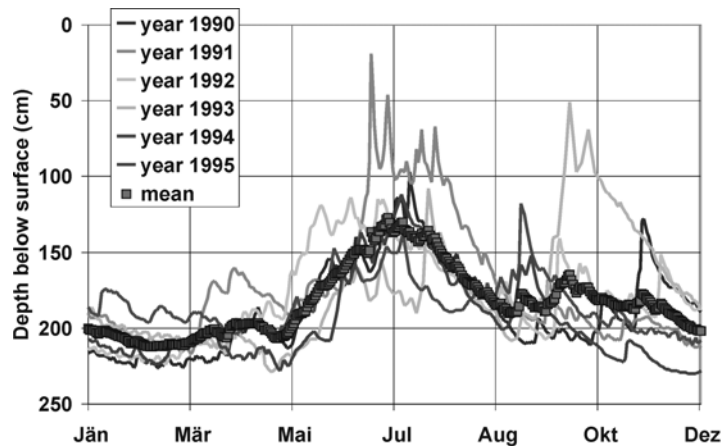

Fig. 1. Groundwater level at study site

Measurements

Soil water suction was measured using calibrated WATERMARK granular matrix sensors and WATERWISE gypsum blocks down to 100 cm depth, while water content was measured by EASYTEST FP/m field probe moisture sensors down to 50 cm, which was assumed to be the main rooting zone of the grassland. These measurements were made systematically three times a week during the growing seasons 1991 – 1995. Hourly measurements of soil water suction by WATERMARK granular matrix sensors and of soil temperature using an automatic "SOIL MASTER STATION" were also made. In 1991 water content occasionally was measured by a Neutron Moisture Meter down to 150 cm depth.

The above mentioned TDR-, gypsum block, granular matrix and temperature sensors were installed into the wall of a soil pit, from which undisturbed soil samples were taken for determination of pore size distribution by pressure plate extractors and capillary conductivity by EASYTEST LOM Laboratory Operated Meter system. Disturbed samples for analysis of grain size distribution, humus and carbonate content were also taken from the soil pit. A self-recording gauge nearby measured ground water depth.

An automatic weather station powered by a solar panel stored hourly values of air temperature, air humidity, wind velocity, global radiation and precipitation. Grass yields were measured by hand harvesting three plots of each 1 square

meter, weighing it in the field, and taking a sub-sample, which then was send to a special laboratory, where dry matter content and feeding value were determined.

Simulation model

For the assessment of the effect of groundwater lowering on capillary rise and thus on grass growth, the simulation model SIMWASER was used. This model is based on the gas exchange of a plant leaf: assimilation (or plant growth) and transpiration (water consumption) are taking place at the same time via the stomata of the leaf. If there is not enough water for full transpiration, stomata will close and assimilation of carbon dioxide will be stopped, and no growth will take place. This relationship between transpiration and assimilation may be defined by the simple formula

$$Pact = Ppot*(Tact/Tpot)$$

Pact = actual photosynthesis [kg CH_2O/m^2,d]
Ppot = potential photosynthesis [kg CH_2O/m^2,d]
Tact = actual transpiration [mm/d]
Tpot = potential transpiration [mm/d]

This means that actual photosynthesis (= actual plant growth) may be derived from it's potential value by the relation of actual to potential transpiration: so if there for example the actual transpiration is only 50 % of it's potential value because of shortage of water in the soil, the actual growth will also be about 50% of the potential growth, which relationship can be found in numerous irrigation trials.

Potential assimilation is derived from air temperature, global radiation, current leaf area and from light response curve of the respective plant. Potential transpiration is calculated from air temperature, global radiation, humidity, wind velocity and stomatal resistance of the crop stand. Actual transpiration is given by the amount of water, which the plant roots are able to withdraw from the rooted soil layers and will depend on current rooting depth and rooting density as well as on current water content in these soil layers, which in the special case is influenced by the amount of capillary rise from ground water. This capillary upward flux as well as the vertical movement between the different soil layers is estimated using DARCY's law as function of the suction gradient and the capillary conductivity in the soil layers. Within the rooted soil layers water extraction by the grass roots is estimated as function of the rooting density, suction gradient between roots and soil and capillary conductivity. A more

181

detailed description of the model is given in Stenitzer 2004, Stenitzer and Murer 2003, Moreno *et al.* 2003.

Hydraulic soil parameters

The hydraulic soil parameters, which are needed to run the model, were derived by combining field and laboratory measurements: "Field pF_curves" of the different soil layers down to 50 cm were available from concurrent measurements of water content by the TDR instrument and of soil water suction by the resistance sensors and were completed in the high pressure regions by laboratory measurements. Hydraulic conductivity at suctions between 100 – 300 hPa had also been measured in the laboratory and were extrapolated by the method of MILLINGTON & QUIRK (Bower and Jackson 1974) for the whole suction range between $0 – 10^7$ hPa. For the soil layers 60 – 100 cm only sporadic water content measurements by the Neutron Moisture Meter were available and were combined with suction heads estimated from depth above groundwater rather than from resistance blocks, the measuring range of which were confined to higher suctions.

No measurements of the hydraulic parameters of the gravely material found between sandy subsoil and groundwater surface were available. But from measured grain size distribution the needed data of a comparable soil could be found from literature (Brülhart 1969), which was used successfully in the calibration run.
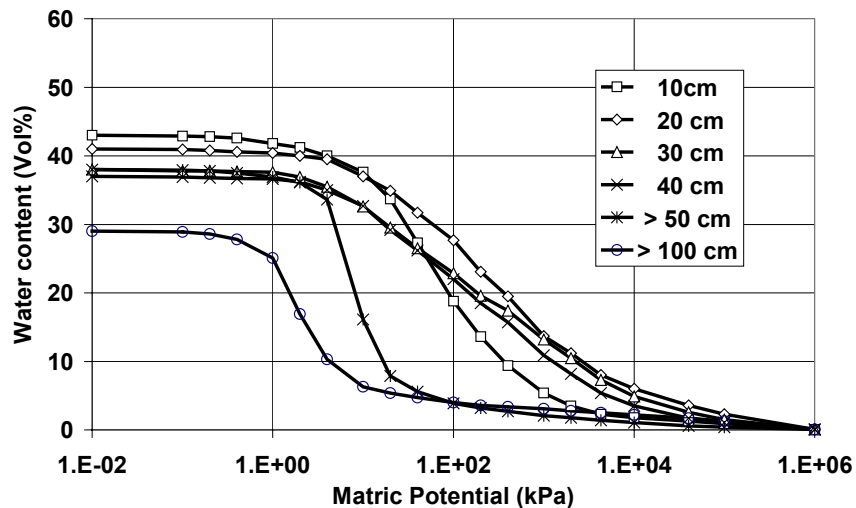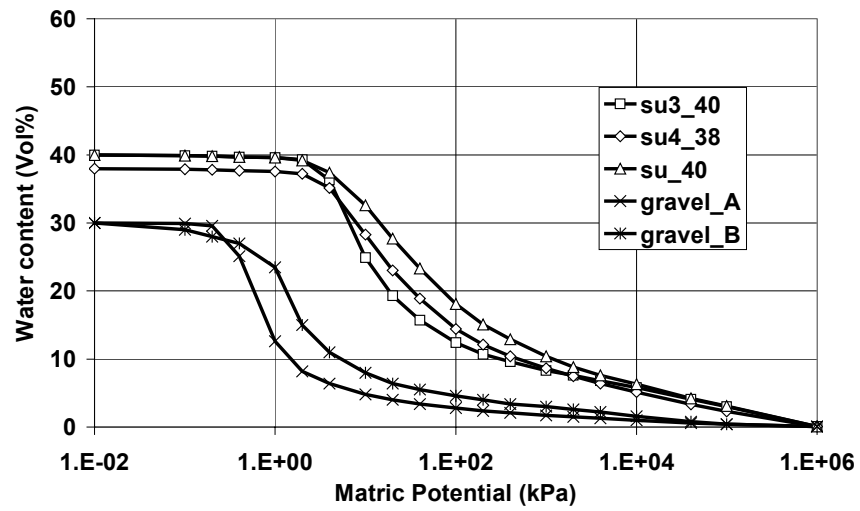

Fig. 2a. pF-curves "calibrated"

182

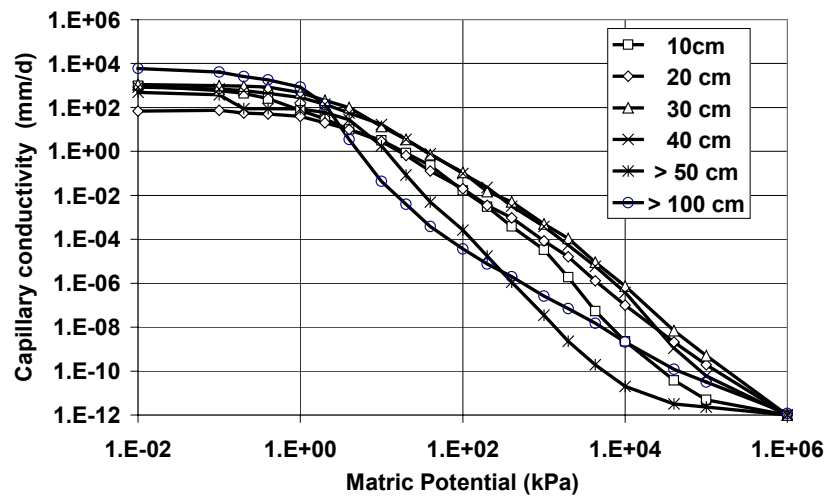**Fig. 2b.** pF-curves "pedotransferfunction"

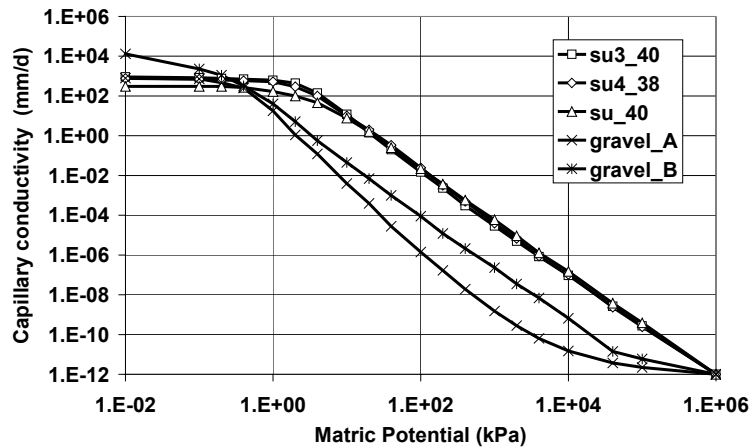**Fig. 2c.** Ku-curves "calibrated"

183

Fig. 2d. Ku-curves "pedotransferfunction"

The effect of lowering the groundwater level upon capillary upward flux and thus on grass yields was simulated with the weather data of the dry year 1994 with only 2 mm rain during second grass growth period from begin of June (first cut May 31st) to second cutting on July 21st. Three different scenarios concerning the hydraulic soil parameters were assumed: the first one was based on measured data, while with the two others pedotransfer functions (PTF) derived from grain size distribution were used. The PTF of the silty sand of top- and subsoil are based on mean values of total pore volume, water content at pF 1.8 and 4.2 and saturated hydraulic conductivity at three density classes given by the DIN 4220 (1998). Two different PTF were used for the gravely underground, both derived from combination of own measurements and literature, the one assuming to be more sandy, the other to be more loamy gravel. Several simulations were run for each of the three scenarios, each one based on different groundwater depth, and calculated capillary rise as well as resulting grass yields was documented.

Results and discussion

Calibration:

Model calibration using hydraulic soil parameters shown in **Fig. 2a** and **Fig. 2c** resulted in good agreement between measured and simulated grass yields (**Fig. 3a**) and in acceptabel coincidence of measured and simulated soil water storage (**Fig. 3b**).
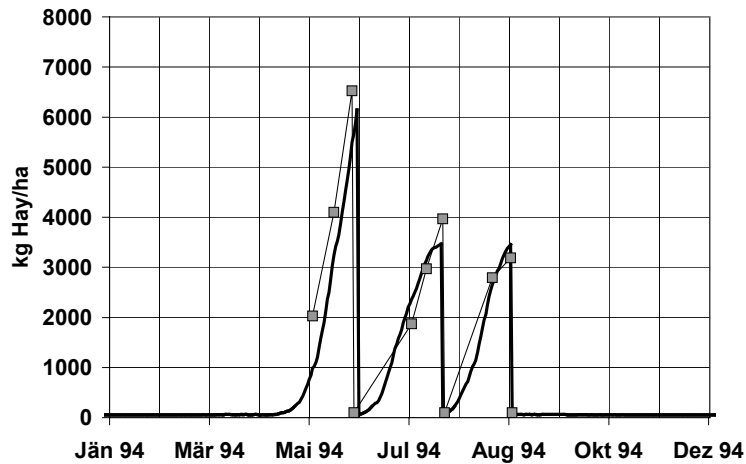
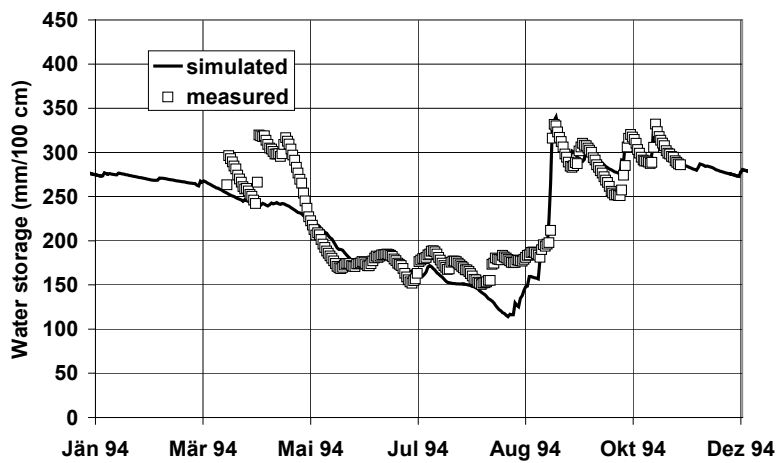**Fig. 3a.** Comparison of simulated and measured hay yield

Fig. 3b. Comparison of simulated and measured water storage 0-100 cm

Scenario simulations:

Simulated capillary rise during dry period in summer 1994 (**Fig. 4a**) as well as simulated hay yield of the total growing season 1994 (**Fig. 4b**) as function of different changes of the mean depth to groundwater show a significant decrease of both the capillary rise as well as of hay yields when the groundwater is lowered

185

only few decimetres. While this relationship is very similar regardless of the differences in the hydraulic parameters of the gravely aquifer, the amount of capillary rise and of hay yield at a given groundwater depth within the range –50 to +30 cm change of groundwater depth are differing very much, thus indicating the need of correct hydraulic parameters of the gravel.
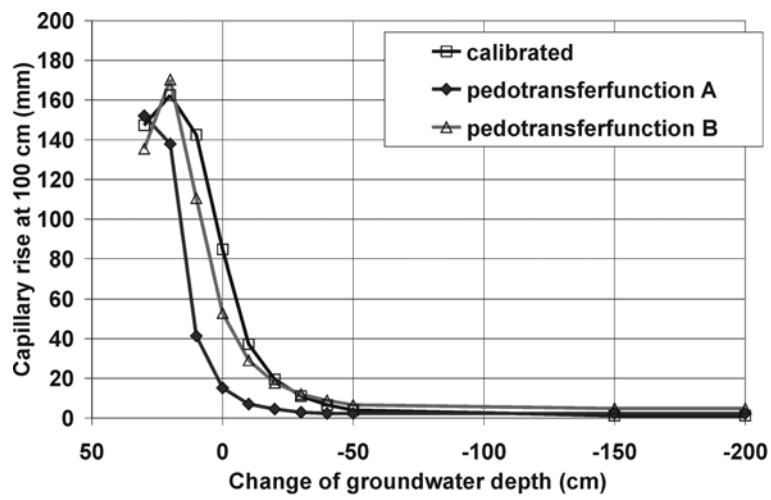

Fig. 4a. Simulated capillary rise during dry period as function of changes in groundwater depth
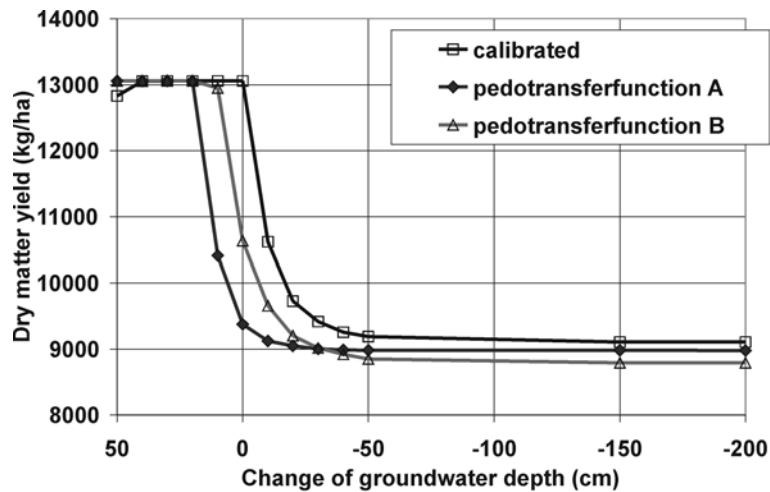

Fig. 4b. Simulated hay yield in 1994 as function of changes in groundwater depth

Because of technical difficulties in obtaining undisturbed samples of gravely soil material and in analysing it's capillary conductivity in the laboratory, some

efforts should be made in developing and testing appropriate water content sensors - *eg* "Open- Ended Coax Probes (Skierucha *et al.* 2004) - to be used in such material.

Conclusions:

In alpine river valleys capillary rise may be essential for grassland growth especially during dry summer periods. Lowering groundwater level by only few decimetres will result in rather high yield depressions in dry summer periods. Quantification of such yield depressions is strongly influenced by the hydraulic parameters of the gravely underground. Only few data on hydraulic parameters of gravely soils are available because of missing field methods suitable for this material. Development of special TDR-sensors to be used in gravely material would highly improve assessment of capillary rise or of deep percolation in very many soil profiles

References

1. **Bouwer H., Jackson R.D.:** Determining soil properties. In: Schilfgaarde J. van (Ed.) Drainage for agriculture. Agronomy Series 17, American Society of Agronomy, Madison, Wisconsin, U.S.A, pp. 611- 672, 1974.
2. **Brülhart A.:** Jahreszeitliche Veränderung der Wasserbindung und der Wasserbewegung in Waldböden des schweizerischen Mittellandes. Eidg. Anst. Forstl. Versuchswes. Mitt. 45, 2: 125-232, 1969.
3. **DIN 4220** Pedologic site assessment –Designation, classification and deduction of soil parameters (in German). DIN-Taschenbuch 187, Beuth Berlin-Wien-Zürich, 1999.
4. **Malicki M.A., Skierucha W.M.:**. A manually controlled TDR soil moisture meter operating with 300 ps rise-time needle pulse. Irrig. Sci. 10, 153-163, 1989.
5. **Moreno F., Murer E.J., Stenitzer E., Fernández J.E., Girón I.F.:** Simulation of the impact of subsoil compaction on soil water balance and crop yield of irrigated maize on a loamy sand soil in SW Spain. Soil & Tillage Research, Vol. 73, 31-41, 2003.
6. **Skierucha W., Walczak R., Wilczek A.:** Comparison of Open- Ended Coax and TDR sensors for measurement of soil dielectric permittivity in microwave frequencies. Int. Agrophysics, 18, 335-362, 2004.
7. **Stenitzer E.:** SIMWASER – A numerical model on soil water balance and plant growth. IKT-Report 5. Institute for Land and Water Management Research, A-3252 Petzenkirchen, Austria, 2004.
8. **Stenitzer E. Murer E.:** Impact of soil compaction upon soil water balance and maize yield estimated by the SIMWASER model, Soil & Tillage Research, Vol. 73, 43-56, 2003.

IN SITU ESTIMATION OF DEEP PERCOLATION IN A DRY AREA BY CONCURRENT MEASUREMENTS OF SOIL WATER CONTENT AND SOIL WATER POTENTIAL

Stenitzer Elmar, Gassner Leopold

Institute for Soil Water Management Research of the Austrian Federal Agency
for Water Management, Petzenkirchen, Austria
elmar.stenitzer@relay.baw.at

Introduction

For sustainable groundwater management, groundwater extraction must be kept below natural groundwater recharge. Quantification of natural groundwater recharge may be assessed either locally from groundwater fluctuations or for the whole catchment area by analysing low water discharge of its outlet. In many cases groundwater fluctuations may be influenced by massive but unknown water extraction and do not reflect natural conditions, and results of analysing low water discharge will not be representative to the area of interest within the whole catchment basin. Physically based simulation models could help to overcome such shortcomings, being able to predict unknown natural ground water recharge from well-known weather-, soil- and cropping- data. Such models have to be validated using measured deep percolation, either from lysimeters or from indirect flux measurements as described in this paper.

Material and Methods

Systematic measurements of soil water content at each 10 cm down to 160 cm by the TDR- method and of soil water suction at 10, 20, 30, 40, 50, 70, 100, 120, 140 and 160 cm depth by calibrated gypsum blocks have been carried out at a natural grassland site on the high terrace of the "Marchfeld plain" east of Vienna since November 2002.

The sensors had been installed at the front wall of an open soil pit by pressing them into the undisturbed soil. During excavation of the pit undisturbed soil samples had been taken at depths representative for 0-40, 40-90 and 90-180 cm, which horizons had been judged to be more or less uniform. Hydraulic conductivity and pore size distribution of these samples, as well as grain size distribution of additional, but disturbed samples were measured in the laboratory.

Fig. 1. Measuring site

Calibration of the WATERWISE gypsum blocks (Richardson & Mueller-Beilschmidt 1988) and WATERMARK Granular Matrix Sensors (Eldredge *et al.* 1993) had been performed by measuring sensor resistances at several pressure levels using suction equipment up to 50 kPa and pressure chambers up to 1500 kPa. **Fig. 2** presents calibration curves of the applied resistance blocks.
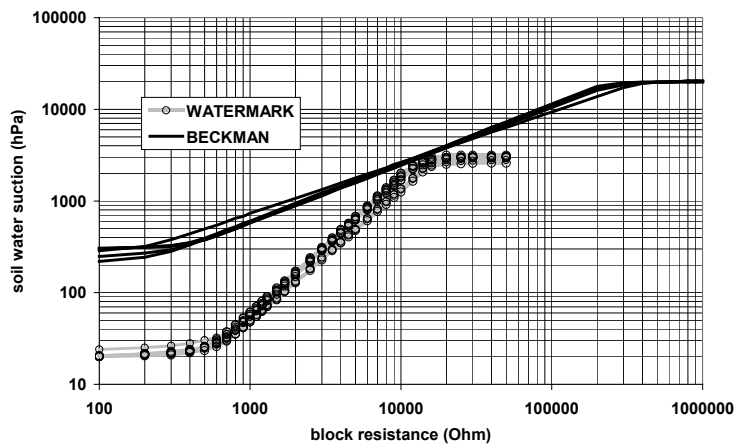

Fig. 2. Calibration curves of resistance blocks

Sensor resistances measured in the field were corrected to 20 °C by an empirical formula (Stenitzer 1993) according to the ambient soil temperatures, which had been also measured at 10, 20, 30, 50, 100 and 160 cm, and resistances were then converted to soil suction using individual calibration curves for each sensor. Combination of these soil water suctions with water contents at same depths yielded field pF-curves (**Fig. 4)**), which were extrapolated in accordance with the laboratory pF-curves of the respective soil horizons.
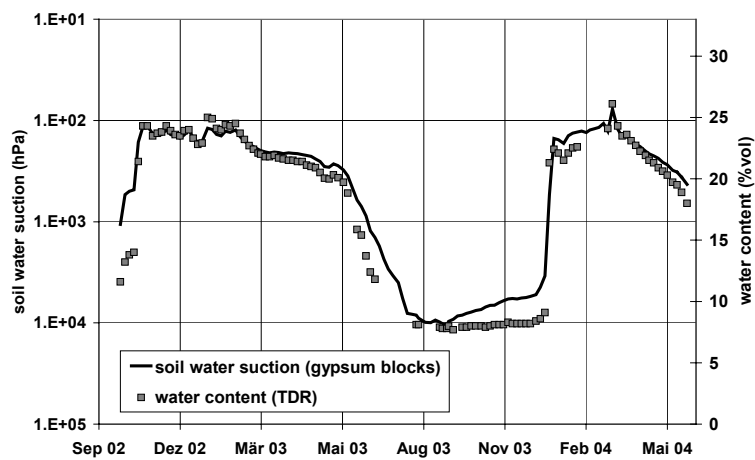
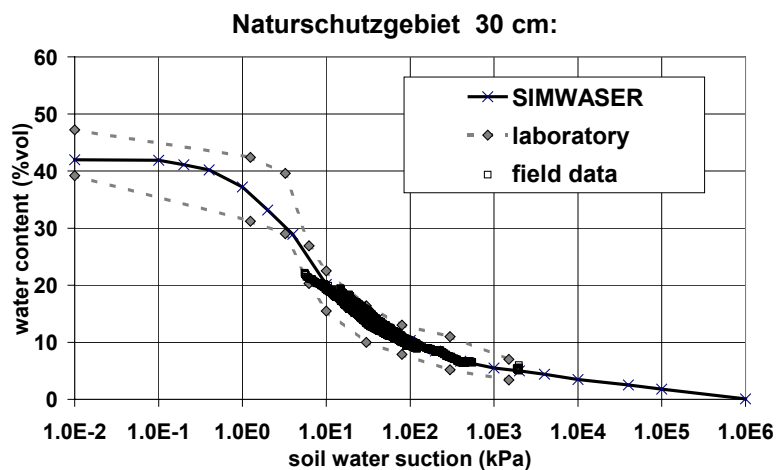**Fig. 3.** Comparison of water content and soil water suction at 70 cm depth

Fig. 4. pF-curve at 30 cm derived from field- and laboratory measurements

Missing water content data were supplemented by data that had been derived by converting measured soil water potential to water contents via the respective field pF-curves (**Fig. 5**).
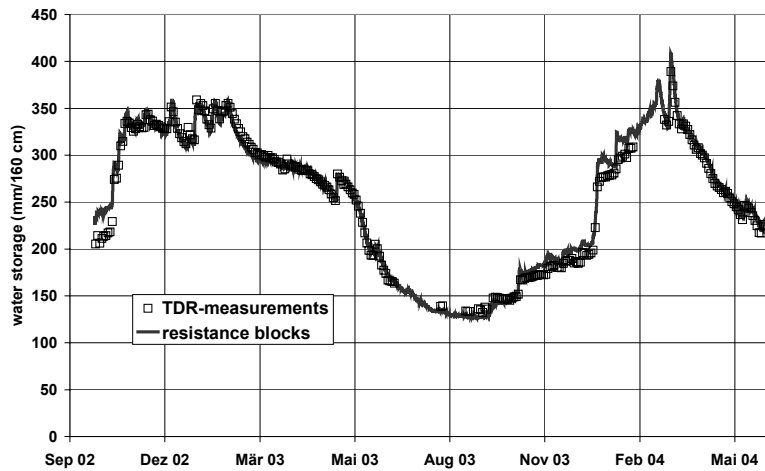

Fig.5. Comparison of profile water storage measured either by TDR or resistance blocks

Capillary conductivity functions for each layer were estimated according to the method of Millington and Quirk (Bouwer and Jackson 1974), by which the shape of the capillary conductivity is derived from the shape of the pF-curve, passing through the saturated hydraulic conductivity measured in the laboratory.
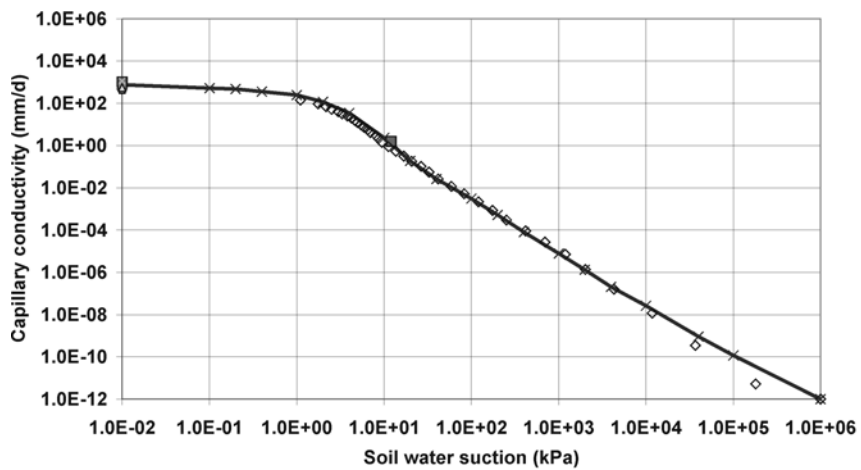

Fig.6. Capillary conductivity function at 160 cm depth

For assessment of the percolation flux at the lower boundary capillary conductivity function of the soil layer at 160 cm was fitted to match both the measured saturated hydraulic conductivity as well as some rough estimation of the mean capillary conductivity at this depth during a drainage period in February 2003 (**Fig. 6**).

Deep percolation and capillary rise were estimated according to Darcy's law, multiplying measured suction gradient between 140 and 160 cm by capillary conductivity at the ambient water content. Calculated accumulated deep percolation was checked during winter periods by comparison with measured decrease of soil water storage, assuming actual evapotranspiration to be 10% of the potential one, which had been calculated from daily weather data using the Penman-Monteith approach (Allen *et al.* 1998).
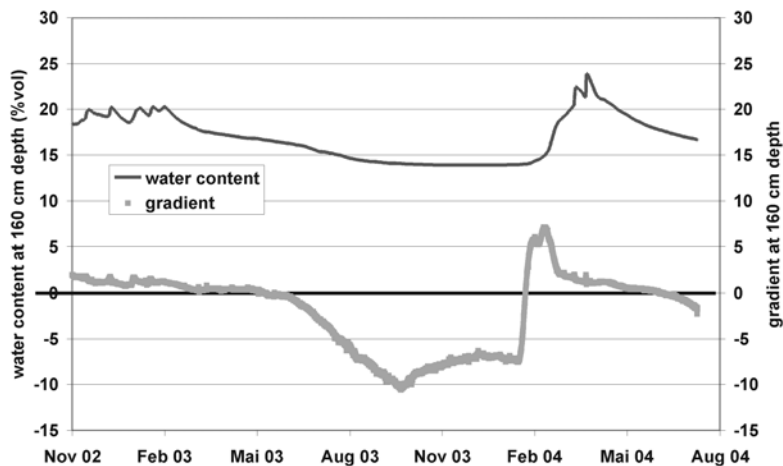

Fig. 7. Water content and gradient at 160 cm depth

Results

Deep percolation was calculated to be 170mm during October 2002 to May 2003 and 230 mm during February 2003 to June 2004; capillary rise took place from June 2003 to end of January 2003 amounting to 40 mm.
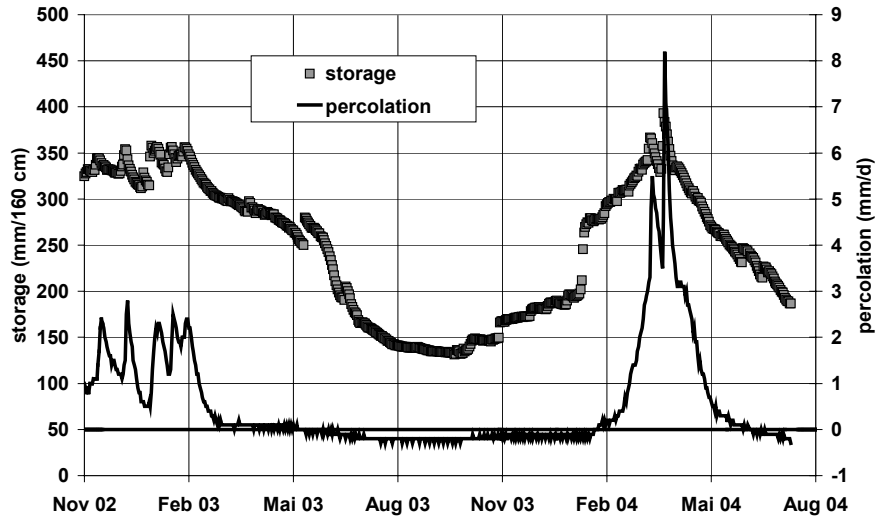
Fig. 8. Profile storage and calculated flux at 160 cm depth

Effective natural groundwater recharge from October 2002 to June 2004 therefore was 360 mm: this is about 38 % of the total precipitation of 947 mm during that period.
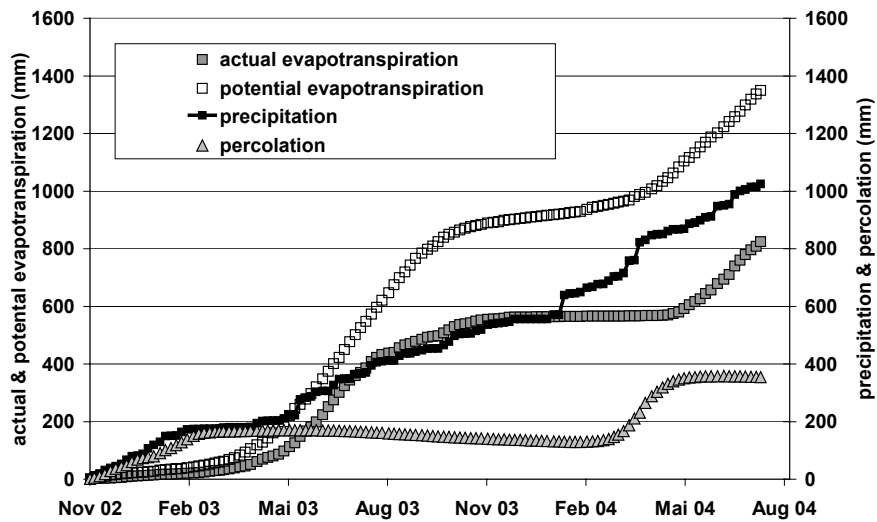

Fig. 9. Accumulated precipitation, actual and potential evapotranspiration and percolation

Examination of the calculated deep percolation by simple soil water balance for selected winter months with negligible evaporation yielded the following correlation:

$$y = 0.9809\,x - 2.1$$

$$r^2 = 0.9344$$

x = (rainfall – evapotranspiration – change in soil water storage)
y = calculated deep percolation

Comparison simple balance to derived percolation amount
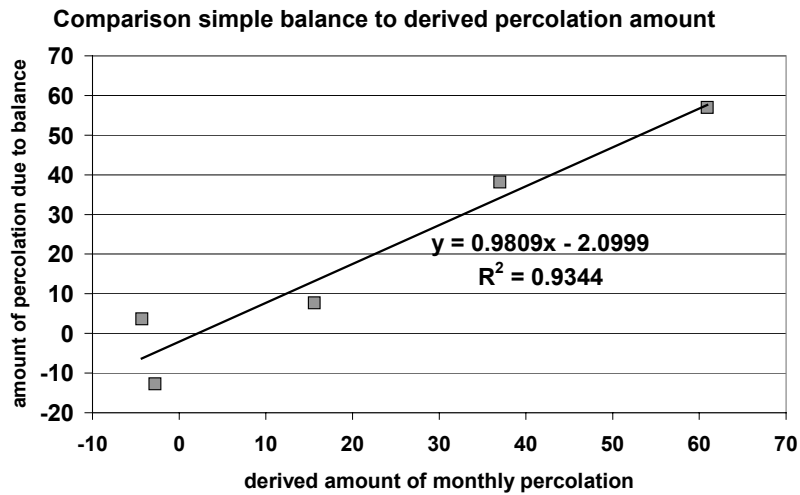
Fig. 9. Relationship between calculated deep percolation and water balance

Conclusion

On condition that good measurements or estimates of the capillary conductivity function of the soil layer at the lower boundary of a soil profile are available, deep percolation may be assessed by continuous measurement of water content and suction gradient at this depth, which should be situated well below the deepest roots. Thus performance of simulation models on soil water balance could be tested, and models could be applied to predict the effects of land use changes upon ground water recharge or to estimate long term ground water recharge of an area of interest.

References

1. **Allen R. G., Pereira L. S., Raes D., Smith M.:** Crop evapotranspiration. Guidelines for computing crop water requirements. FAO Irrigation and Drainage Paper 56. Food and Agricultural Organization of the United Nations. Rome, 1998.
2. **Bouwer H. Jackson R.D.:** Determining soil properties. In: Schilfgaarde J. van (Ed.) Drainage for agriculture. Agronomy Series 17, American Society of Agronomy, Madison, Wisconsin, U.S.A, pp. 611- 672, 1974.
3. **Eldredge E. P., Shock C.C., Stieber T.D.:** Calibration of Granular Matrix Sensors for Irrigation Management. Agron. J., 85:1228-1232, 1993.
4. Richardson, G. Mueller-Beilschmidt P.: Winning with water. Soil-moisture monitoring for efficient irrigation. INFORM, Inc. New York, 1988.
5. **Stenitzer E.:** Monitoring soil moisture regimes of field crops with gypsum blocks. Theor. Appl. Climatol. 48, 159 – 165, 1993.

EFFECT OF ALUMINUM ON MICROPORE SYSTEM OF PLANT ROOTS

Szatanik-Kloc Alicja, Józefaciuk Grzegorz

Instytute of Agrophysics Polish Academy of Sciences, Lublin, Poland
akloc@demeter.ipan.lublin.pl

Introduction

Recent increase of soil acidification due to atmospheric deposition and improper soil nutrition (Dechnik *et al.*, 1990; Ulrich, 1991) increases the actual needs for process studies to evaluate both mechanisms and parameters controlling plant response on acid toxic environments. Aluminum is a major component of acid toxicity in soils (Foy, 1984). Number of studies suggest that the pore system of the root tissue undergo marked alteration under aluminum stress, that is visualized in **Fig. 1**, showing cross sections of no stressed and stressed roots of barley (Szatanik-Kloc and Józefaciuk, 2001).
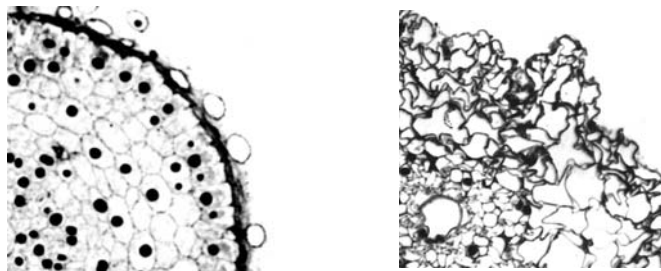
Fig. 1. Cross-section of no stressed (left) and of Al-stressed roots (right)

In the present paper we measured water vapor and nitrogen desorption isotherms for Al stressed roots of barley and wheat, which were interpreted in terms of surface microporosity (nanometers dimensions). Pores of such sizes are important for ions and molecules transport processes (Clarkson, 1991). Anyway, the question whether the pores measured from water desorption are that same as measured by other methods *eg* osmotic permeability (Carpita *et al.*, 1979) or microscopy (Robards, 1970) remains opened.

Materials and methods

Roots of barley Ars and wheat Henika were studied. The plants were grown in a nutrient solution prepared according to Marshner and Romheld (1983). After the plants reached the shooting stage, the pH in some vessels was adjusted to the value of pH=4 and aluminum chloride was added to reach the Al level of 0 (Control), 5 (5Al), 10 (10Al) and 20 (20 Al) mg Al dm^{-3} to induce a strong effect of toxicity (Józefaciuk G. and Szatanik-Kloc A., 2003). All experiments were performed in three replicates.

Water vapor desorption isotherms were measured in triplicate for all root samples using the vacuum chamber about 1 to a few tens of nanometers are detected. During the measurements, temperature was kept constant at 298±0.1 K. The air-dry root samples (*ca* 0.3 g) in weighing vessels were placed in a vacuum chamber over sulfuric acid solutions of stepwise increasing concentrations (decrease of the relative water vapor pressure, p/p_o). The amounts of water present in the samples at a given p/p_o, $a(p/p_o)$, were measured by weighing after 48 h of equilibration, however, at the initial point of desorption 96 h equilibration time was given. The dry mass of the roots (needed for the point of the isotherms at p/p_o=0) was determined after overnight drying of the samples at the temperature of 378 K. The variations in replicated data did not exceed 5%.

Nitrogen desorption isotherms were measured instrumentally at 78 K using Sorptomatic 1990 made by Fisons. Prior to the measurements, to remove all species naturally present and adsorbed to the surface, the samples were heated overnight under vacuum at 70ºC.

Theory

The root tissue is assumed to be a porous solid having a system of capillary shaped pores. The relative water vapor pressure was related to r via Kelvin equation:

$$r = 2 M \sigma \cos\alpha / (\rho \underline{R} T \ln(p_o/p)), \tag{1}$$

where M is molecular mass of water, σ is the liquid surface tension, α is a liquid-solid contact angle (assumed here to be zero), ρ is density of the liquid adsorbate, R is the universal gas constant and T is the temperature of the measurements.

The pore radii calculated in this way should be considered not as absolute values, but rather as "equivalent" ones. Very likely the "real" pores are larger because, before the condensation of water vapor, the walls of these are (pre)covered with a layer of adsorbed water. The thickness of this layer should be

added to the equivalent pore radius to obtain more realistic value. To avoid assumptions on this thickness, further considerations are based on the equivalent pore radii.

The volume v of micropores was taken as the volume of a liquid filling the samples (amount of adsorbed water or nitrogen).

The volume of the condensed water in the root pores at a given water vapor pressure, $v(p/p_o)$, was treated as a sum of pore volumes, $v_i(r_i)$, of the radii $r_i \leq r(p/p_o)$,

$$v(p/p_o) = \sum_{i=1}^{n} v_i(r_i). \tag{2}$$

Dividing the above equation by the total pore volume, v_t, the scaled desorption isotherm, $\Xi_t(p/p_o) = \Xi_t(r(p/p_o))$, can be treated as a sum of fractions of particular pores, $f(r_i)$:

$$\Xi_t(p/p_o) = v(p/p_o)/v_t = \sum_{i=1}^{n} v_i(r_i)/v_t = \sum_{i=1}^{n} f(r_i) = 1 \tag{3}$$

The pore fraction from a given range of sizes can be calculated as:

$$f(r_i) = [\Xi_t(r_{i+1}) - \Xi_t(r_i)]. \tag{4}$$

Calculations were performed using experimental desorption data from $0.32 \leq p/p_o \leq 0.98$ range i.e. for pore radii range of c.a. $1 \leq r \leq 55$ nm. The minimal $p/p_o = 0.32$ value taken for the calculations corresponds approximately to this relative pressure, below which adsorption takes place mostly in monolayer, so this is difficult to treat it like condensation in pores. Thus the total pore volume was taken as the difference between the volume of the condensed (adsorbed) vapor at maximal relative pressure and the amount of adsorbed vapor at the relative pressure equal to 0.32: $v_t = v(p/p_o=0.98) - v(p/p_o=0.32)$. Because pore radii measured from desorption isotherms cover a broad size range, the pore size distribution functions were expressed on a logarithmic scale. Total pore range was divided onto four logarithmically equal subranges. The pore volume (and a scaled desorption isotherm) values for the boundary points of every subrange were estimated by linear interpolation of desorption data.

The average pore radii in the studied range, Rav, was calculated from the formula:

$$Rav = 1/(2v_t) \sum_{i=1}^{n} (r_i + r_{i+1}) (v_{i+1} - v_i), \tag{5}$$

using all experimental desorption data from $0.32 \leq p/p_o \leq 0.98$ range.

Results and discussion

The experimental water vapor and nitrogen desorption isotherms of the studied roots are presented in **Fig.1**. The isotherms of roots grown in the presence of Al differ from these of Al-free roots. The amount of condensed water on both plant roots decreases after aluminium stress.
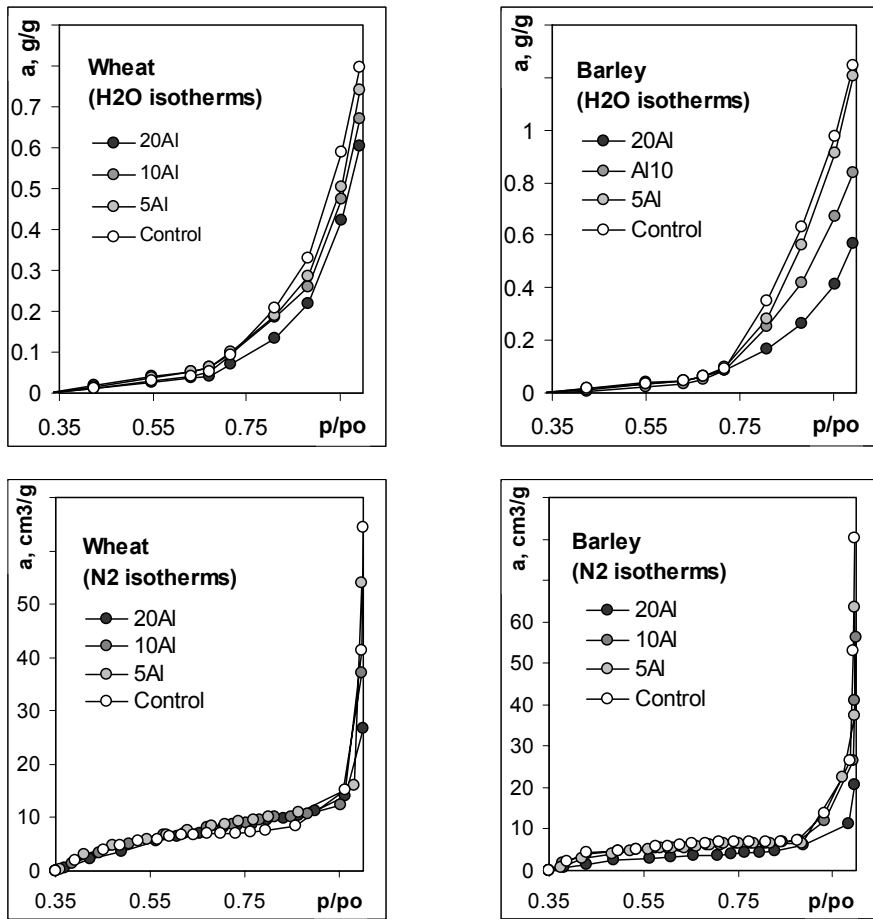

Fig.1.   Water vapor and nitrogen desorption isotherms of the studied roots

Exemplary pore size distribution functions for barley roots are presented in **Fig. 2**. Because pore radii cover a broad size range the pore size distribution functions were expressed on a logarithmic scale. For both plants roots the amount of pores measured both from water and nitrogen desorption decreases with the pore radii increase. No marked differences in the pore size distribution functions were observed at various stress conditions.
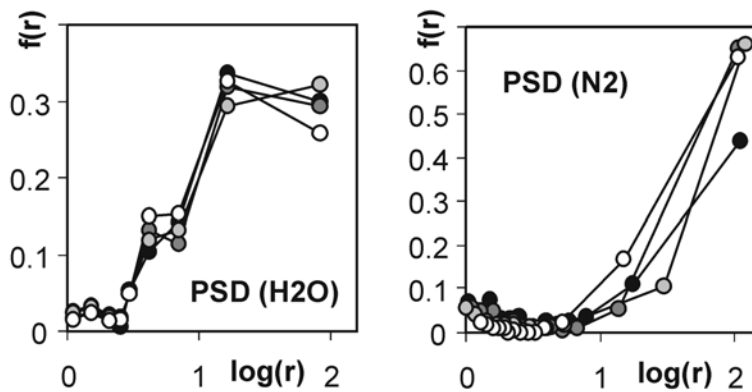

Fig.2.   Micropore size distribution functions of the studied roots calculated from water vapor and nitrogen desorption isotherms (example for barley)

Because of similar pore size distributions, one expects no marked changes in average pore radii, values of which are shown in **Table 1** together with data of pore volumes. Despite higher relative pressures were applied in nitrogen desorption measurements, markedly higher pore volumes are measured from water vapor desorption.

The nitrogen desorption method requires prior evacuation and heating of the sample, which thins water films and brings the root tissues closer. The quasi-contact of the root material (*eg* cell walls) can extend over its significant portion that becomes inaccessible for nonpolar (nitrogen) molecules. If the root contains expansible or swelling material it can collapse on evacuation, giving the same effect. Decrease of the amount of small pores may be additionally caused by the molecular sieving effect that differentiates the entrance of various size gas molecules into narrow pores (Volzone *et al.*, 1999) leading to differences in amount of condensed vapor measured with various size adsorbates. The kinetic effects may diminish the amount of nitrogen to a great extent when entrances to larger pores are of nitrogen molecule dimensions. To easily pass such narrow entrance, the thermal energy of the molecule should be similar to the energy barrier of the adsorption field among the entrance walls. At liquid nitrogen

temperature the thermal energy is low and therefore the equilibrium may not be reached within a standard time of the measurement. Larger average micropore sizes measured from nitrogen desorption are due to markedly higher relative input of largest pores fraction. Indeed if the nitrogen entrance to the smallest pores is limited, the larger ones have more effect on the average value.

No tendencies in changes of micropore dimensions can be found, the micropore volumes appear to consecutively decrease with the increase of Aluminum concentration in the growing solution.

Table. 1. Average radii and volumes of micropores of the studied roots depending on the stress conditions

	BARLEY	WHEAT	BARLEY	WHEAT
	H_2O		N_2	
	average pore radius, nm			
Control	25.3	28.9	81.6	70.3
5Al	27.6	33.3	53.2	83.7
10Al	24.0	31.3	58.3	69.8
20Al	28.8	32.1	64.3	50.6
	pore volume, cm^{3}g^{-1}			
Control	1.25	0.80	0.32	0.25
5Al	1.21	0.74	0.23	0.29
10Al	0.84	0.67	0.16	0.22
20Al	0.57	0.60	0.12	0.15

For the authors, at present, this is difficult to attribute the pores of a given radius to particular structural features of the roots anatomical components. Possibly simultaneous electron-microscopic studies could give a better insight into the above problem. However, some (more speculative at present) comparisons may be drawn: The cell walls microfibrils are between 3-30 nm in diameter (Clarkson, 1991) so the pores formed within the microfibrils net can have radii of a few nanometers. Also pores of about 2 nm radius are reported to occur in the (radish and sycamore) apoplast (Clarkson, 1991). Possibly similar pores might have been detected also in the present experiment. The larger pores may constitute intercellular spaces.

Conclusion

Similar patterns of the root tissue alteration seem to occur for roots of wheat and barley. One may expect that the overall damage of the root tissues under the

stress leads to cracking of the material throughout the pores (pore volume decrease) and the remaining no cracked elements have similar porous character (no changes in pore radii).

References

1. **Carpita N., Sabulase D., Montezinos D., Delmer D.P.:** Determination of the pore size of cell walls of living plant cells. Science 205, 144-147, 1979.
2. **Clarkson D.T.:** Metabolic aspects of aluminium toxicity and some possible mechanisms for resistance. w: I.H. Rorison (Ed.), Ecological aspects of the mineral nutrition of plants. Blackwell Sci. Publ. Oxford and Edinburgh, 381-397, 1969.
3. **Clarkson D.T.:** Root structure and sites of ion uptake. In: Y Weisel, A Eshel, U Kafkafi (eds) Plant Roots The Hidden Half. Marcel Dekker Inc NY, pp. 351-373, 1991.
4. **Cresser M., Billett M., Skiba U.:** The effect of acid deposition on soils. in: Acid Deposition, Sources, Effects and Controls. J.W.S. Longhurst Ed. British Lib. Techn. Commun. 169-196, 1989.
5. **Dechnik I., Gliński J., Kaczor A., Kern H.:** Rozpoznanie wpływu kwaśnych deszczy na glebę i roślinę. Problemy Agrofizyki 60, 1990.
6. **Foy C.D.:**. Plant adaptation to acid, aluminum - toxic soils. Comm. Soil Sci. Plant Anal., 19, 959-987. 1988.
7. **Józefaciuk G., Szatanik-Kloc A.:** Changes in specific area and energy of root surface of cereal plants in Al-solution cultures. Water vapor adsorption studies. Plant and Soil 250 (1), 129-140, 2003.
8. **Marschner H., Romheld V.:** In vivo measurement of root-induced pH changes at the soil-root interface: effect of plant species and nitrogen source. Z. Pflanzenphysiol. 111, 249-254, 1983.
9. **Ościk J.:** Adsorpcja, PWN, Warszawa, pp73-81, 110-117. 1979.
10. **Robards A.W.:** Electronmicroscopy and Plant Ultrastructure. McGraw-Hill NY, 1970.
11. **Szatanik-Kloc A., Józefaciuk G., Masłowski J., Muranyi A., Farkas C.:** Changes in the surface properties of the young sieve roots after 24h aluminium stress. International Agrophysics, 15, 201-206, 2001.
12. **Szatanik-Kloc A., Jozefaciuk G.:** Effect of pH and aluminum on surface properties of barley roots as determined from water vapor adsorption. Acta Phys. Plant., 19, 327-332, 1997.
13. **Ulrich B.:** Natural and anthropogenic components of soil acidification. Z. Pflanzenernaehr. Bodenk. 149, 702-717, 1986.
14. **Volzone C., Thompson J.G., Melnitchenko A., Ortiga J., Palethorpe S.R.:** Selective gas adsorption by amorphous clay-mineral derivatives. Clays and Clay Minerals 5, 647-657, 1999.

SPATIAL DISTRIBUTION OF SOME PHYSICAL PROPERTIES IN RELATION TO SOIL COMPACTION

Usowicz[1] Bogdan, Lipiec[1] Jerzy, Ferrero[2] Aldo

[1]Institute of Agrophysics, Polish Academy of Sciences, Lublin, Poland
[2]CNR, Institute for Agricultural and Earth Moving Machines, Torino, Italy
usowicz@demeter.ipan.lublin.pl

Introduction

Soil vineyard is subjected to frequent vehicular traffic for growing operations of vine plants (Bazzoffi and Chisci, 1999; Lisa *et al.*, 2001). The operations can cause adverse consequences (Ferrero and Lipiec, 2000), such as local compaction and damage of structure in topsoil and subsoil under ruts produced by tractors: the negative effects have different intensity depending on the adopted management of the inter-row (Ferrero *et al.*, 2001; Lipiec and Hatano, 2003).

In highly mechanized viticulture the number of tractor passes per year can be up to 22 in traditionally cultivated and 20% less in grass covered vineyards (Lisa *et al.*, 1995). The ruts produced by tractor have almost permanent location within the inter-rows, which usually spaces 2.0-2.7 m. The pressure exerted on the contact surface of the track varies with the slope and the tractor size: in sloping vineyards the soil compaction can be greater beneath the running wheel in the lower than in the upper portion of the inter-row following the contour, owing to tractor's tilt. This uneven spatial distribution of soil compaction can alter air-water conditions and thermal properties that determine heat and energy transfer in the soil medium and, as a consequence, the conditions for plant growth (Bachmann *et al.*, 2001). In hillside vineyard, sloping configuration and shadow of vine rows can enhance this effect. However the effects of machinery traffic on the soil thermal properties in vineyard have received little attention. Better understanding of these effects can be helpful in evaluating the thermo- and hydro-physical conditions and defining admissible traffic intensity, in order to provide optimum conditions for vine growth and to avoid soil physical degradation. Moreover the knowledge of space-time variation of soil properties helps the farmer to adjust management practices according to what is appropriate to site conditions (Plant *et al.*, 2000).

The effects of different management options on the soil temperature should be evaluated together with moisture, porosity and other limiting factors in order to optimise crop growth (Porter and Mc Mahon, 1987).

Soil thermal properties are important factors, which influence the surface-energy partitioning and the heat flux in soil profile (Kimball *et al.*, 1976). So far investigations showed that the thermal properties are significantly influenced by soil water content, bulk density, mineralogical composition and organic matter content (DeVries, 1963) and to a less extent by soil temperature and pressure and humidity of soil air. Direct measurements of the thermal properties are still difficult and expensive because of high spatial variability of soil physical parameters; for this reason indirect methods for their determination based on properties and parameters that only slightly change in time and can be easily measured, are useful. These properties are texture, mineralogical composition, particle density and organic matter content.

Our objective was to assess the effects of crawler tractor traffic across the vineyard slope on spatial distribution of thermal conductivity, heat capacity and thermal diffusivity of soil under permanent grass cover and traditional cultivation.

Methods

In our study we used a statistical-physical model of the soil thermal conductivity (Usowicz, 1992), based on terms of thermal equivalent circuit and of polynomial distribution (Eadie *et al.*, 1989).

The thermal conductivity was calculated according to the equation (Usowicz 1992, 1995):

$$\lambda = \frac{4\pi}{u\sum_{j=1}^{L} \frac{P(x_{1j},...,x_{kj})}{x_{1j}\lambda_1(T)r_1 + ... + x_{kj}\lambda_k(T)r_k}} \qquad (1)$$

where u is the number of parallel connections of soil particles treated as thermal resistors, L is the number of all possible combinations of particle configurations, $x_1, x_2 ,..., x_k$ a number of particles of individual particles of a soil with thermal conductivity $\lambda_1, \lambda_2 ,..., \lambda_k$ and particle radii $r_1, r_2 ,..., r_k$, where $\sum_{i=1}^{k} x_{ij} = u$, $j=1,2,...,L$, $P(x_{ij})$ is the probability of occurrence of a given soil particle configuration calculated from the polynomial distribution:

$$P(x_{1j},...,x_{kj}) = \frac{u!}{x_{1j}!...x_{kj}!} f_1^{x_{1j}}...f_k^{x_{kj}} . \qquad (2)$$

The condition: $\sum_{j=1}^{L} P(X = x_j) = 1$ is also fulfilled. The probability of selecting a given soil constituent (particle) f_i, $i = s, c, g$, in a single trial was based on fundamental physical soil properties. In this case $f_s = 1 - \phi$ (ϕ is the soil porosity) is the content of individual minerals and organic matter, $f_c = \theta_v$ is the liquid content and f_g is the air fraction in a unit of volume.

So far investigations showed that, to calculate the soil thermal conductivity, the conductivities of main soil component could be used (Usowicz, 1992; 1998). They are: quartz, other minerals, organic matter, water and air. Their values of thermal conductivity and relations to temperature are presented in **Table 1**.

Table 1. Values and expressions for parameters used in calculating the thermal conductivity of soils ([b]T in $^\circ$C)

Source [a]	Thermal conductivity parameters [W m^{-1} K^{-1}]	Expression, value [b]
	quartz $- \lambda_q$,	9.103 - 0.028 T
2	other minerals $- \lambda_{mi}$,	2.93
2	organic matter $- \lambda_o$,	0.251
1	water or solution $- \lambda_w$,	0.552 + 2.34$\cdot$10^{-3} T - 1.1$\cdot$10^{-5} T^2
1	air $- \lambda_a$,	0.0237 + 0.000064 T

a) 1. Kimball *et al.* 1976   2. De Vries 1976

The parameters of the model were defined earlier based on empirical data (Usowicz, 1992; 1995). Predicted thermal conductivity was compared with measured data on the Fairbanks sand, Healy clay, Felin silty loam, Fairbanks peat and loam (DeVries, 1963; Usowicz, 1992; 1995). Regression coefficients were close to unity, determination coefficients of the linear regression were high and ranged from 0.948 to 0.994. These figures indicate a good performance of the model in predicting the thermal conductivity. The basic soil data used to calculate thermal conductivity, with this model, were measured in the experimental vineyard. It was assumed that sand fraction consists mainly of quartz, and that, minerals occur mainly in silt and clay fractions. Based on the soil texture and density of the solid components the volumetric content of quartz and other minerals and organic matter was calculated.

The volumetric heat capacity was calculated using empirical formulae proposed by DeVries (1963):

$$C_v = (2.0 x_s + 2.51 x_o + 4.19 x_w) \cdot 10^6 \qquad [\text{J m}^{-3}\text{K}^{-1}] \qquad (3)$$

where: x_s, x_o, x_w [m³ m⁻³] are volumetric contributions of mineral and organic components and water, respectively. The thermal diffusivity α was calculated from the ratio of the thermal conductivity and volumetric heat capacity: $\alpha = \lambda / C_v$.

To analyse and visualise the results in 3D maps GeoEas and GS+ software were used.

Soil and treatments

The experiment was conducted at a site (450 m a.s.l.), with average slope of 18%, representative of the hillside viticulture of Piedmont (N.W. Italy). The climate has cold winter with snow, dry summer with rainstorms: mean annual temperature 11.3°C, mean of the monthly minima (January) –1.6°C and of the maxima (July) 27.3°C. The vineyard, with rows following the contour lines, lies on silt loam soil containing on average 33% sand, 58% silt, 9% clay. Two soil managements of the inter-rows were compared: conventional cultivation (C), that is: autumn ploughing, two tillings in spring and summer, chopping of the herbs on the rows; controlled grass cover by moving and chopping of the herbs 3-4 times per year, herbicide application under the vine rows. Organic matter content was 4.7% and 3.4% in G and C, respectively. Corresponding values for particle density were 2.60 and 2.62 Mg m⁻³. In both treatments a crawler tractor of 2.82 Mg weight and 1.31 m width was used for tillage and chemical operations along the inter-rows across the slope. The width and length in contact with the ground of each track were 0.3 m and 1.4 m, respectively.

The measurements of soil water content and bulk density in each treatment were done in September on four transects (10 m a part) transversal to the inter-rows (2.7 m width). The measuring points were in places corresponding to upper rut, inter-rut and lower rut areas along the slope (**Fig. 1a**). To determine bulk density and water content, soil cores of 100 cm³ were taken from the depths of 1-8, 9-16 and 17-25 cm in four replicates. It was observed that in cultivated soil rut, depth under the lower vs. upper track was more than twice higher, due to greater ground contact pressure in the former as a result of tractor's tilt on the slope. Similar effect was observed in grass covered soil but the differences between the tracks were smaller.

Temperature data were collected at 6 cm and 11 cm depth in three subplots of each treatment, by means of T-type thermocouples and computer datalogger. The sensors were located in transepts transversal to the inter-rows in correspondence of the upper rut of the tractor, in the center and under the lower rut (**Fig. 1b**).
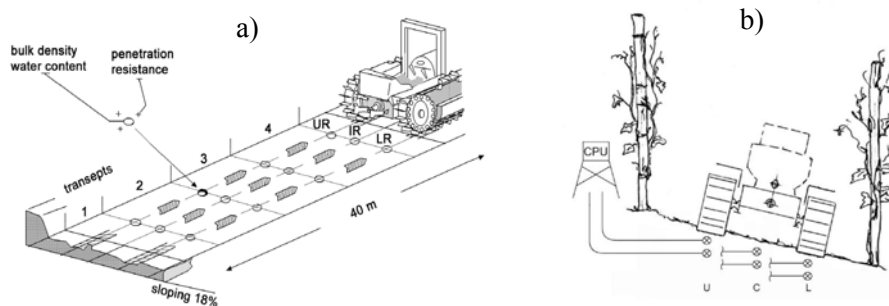
Fig. 1. a) The location of measurements points in the study area of the inter-row: UR – upper rut, IR – inter-rut, LR – lower rut. b) Schematic layout of the vineyard row showing the location of the sensors monitoring the soil temperature: U- under upper track; C- in the central inter-row; L- under the lower track

Air temperature was recorded in the meteorological station situated within the area of the vineyard. Temperatures reading were done hourly (one reading was the average of six measurements taken every 10 minutes).

Results

Figure 2 presents the distribution of bulk density, water content, air content, thermal conductivity, heat capacity and thermal diffusivity of soil along the vineyard slope as characterised by mean value, standard deviation, minimum and maximum values, and variation coefficient for top layer (0-25 cm). The data are from the soil under the centres of the upper rut, inter-rut area and lower rut situated 0.65 m, 1.35 m and 2 m in the inter-row, respectively (**Fig. 1a**). The differentiation of soil bulk density along the slope was greater under grass covered (G) than cultivated (C) soil as shown by standard deviation and minimum and maximum values. In G the density was greater under lower than upper track whereas in C it was similar under both ruts. The differentiation in G is probably a result of earlier tractor passes associated with vineyard management.

Soil water content increased along the slope down in both G and C, to higher extent in the former. The differentiation of soil water content was least in the upper rut and successively increased in the lower rut and inter-rut areas. This uneven distribution of soil water content was associated with both area configuration and shading effect of vine rows and was reflected by in values of soil air content (air-fill porosity) (**Fig. 2**).
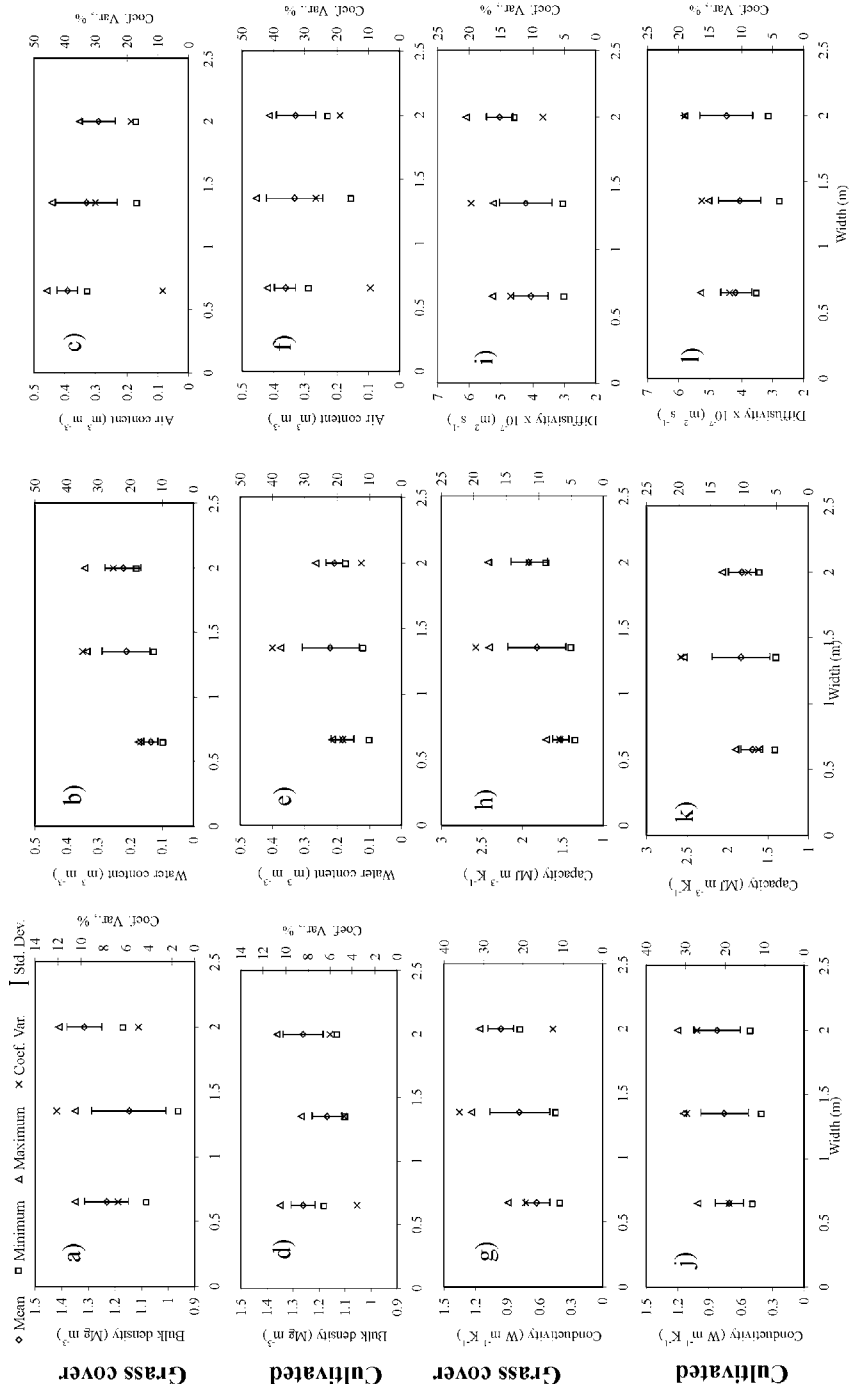
Fig. 2. Statistics of bulk density (a,d), water content (b,e), air content (c,f), thermal conductivity (g,j), heat capacity (h,k) and thermal diffusivity of soil (i,l) in 0–25 cm layer along the vineyard slope of the grass covered and cultivated vineyard

As with particle density, changes in texture within the study area were very tiny. As a consequence, mineralogical composition, estimated from texture, remained unchangeable.

Thus taking this into consideration and results of the earlier studies (DeVries, 1963) we can assume that soil water content and bulk density are main factors affecting differentiation of the thermal properties. Relative effect of soil water content and bulk density was related with kind of soil thermal property. Distribution pattern of heat capacity is largely a reflection of that for water content and much less for bulk density (**Fig. 2b,e,h,k**), whereas comparison of the **Fig. 2a,b,d,e** and **Fig. 2g,j** indicate similar and positive effects of soil water content and bulk density on the thermal conductivity. An increase in bulk density at a given soil water content resulted in higher thermal diffusivity. However, increase in soil water content at given bulk density may increase or decrease thermal diffusivity depending on the occurrence of the characteristic maximum of thermal diffusivity (**Fig. 2i,l**).

The increase of mean values of the thermal properties along the slope down was more pronounced in grass covered than cultivated soil. The values were least in the upper rut and highest in the lower rut. As indicated by standard deviation and minimum and maximum values the differentiation was greater in G than C, mainly in the inter-rut areas. This differentiation in both ruts was lower or similar.

Conclusions

Our research showed that uneven distribution of compaction in the sloping vineyard soil resulted mostly from different loading of the tractor and coupled viticulture machinery whereas that of soil water content – from tillage operations and shading by the vine rows and thus reduced evaporation. The results indicate similar and positive effects of soil water content and bulk density on the thermal conductivity whereas heat capacity is largely a reflection of that for water content and much less for bulk density. An increase in bulk density at a given soil water content resulted in higher thermal diffusivity. However, increase in soil water content at given bulk density may increase or decrease thermal diffusivity depending on the occurrence of the characteristic maximum of thermal diffusivity.

Acknowledgements

References

1. **Bachmann J., Horton R., Ren T., Van der Ploge, R.R.:** Comparison of the thermal properties of four wettable and four water-repellent soils. Soil Scientific Society of America J. **65** pp. 1675-1679, 2001.
2. **Bazzoffi P., Chisci G.:** Soil conservation techniques in vineyards and peach orchards of the Cesena hilly area. Rivista di Agricoltura **33** pp. 177-184. 1999.
3. **DeVries D.A.:** Thermal properties of soils. In: Physics of Plant Environment. (Editor) van Wijk W.R. North-Holland Publ. Co., Amsterdam, pp. 210–235, 1963.
4. **Eadie W.T., Drijard D., James F.E., Roos M. Sadoulet B.:** Statistical methods in experimental physics, PWN, Warsaw, pp. 63–64 (in Polish), 1989.
5. **Ferrero A., Lipiec J.:** Determining the effect of trampling on soils in hillslope - woodlands. International Agrophysics **14** pp. 9-16, 2000.
6. **Ferrero A., Lipiec J., Nosalewicz A. Parena S.:** Conventional tillage or permanent grass cover in hillside vineyards: effects on soil physical characteristics. In: Proceedings of International Conference of Physical Methods in Agriculture, Prague, 27-30 August, pp. 88-92, 2001.
7. **Kimball B.A., Jackson R.D., Reginato R.J., Nakayama F.S., Idso S.B.:** Comparison of field-measured and calculated soil-heat fluxes. Soil Scientific Society of America J. **40** pp. 18-25, 1976.
8. **Lipiec J., Hatano R.:** Quantification of compaction effects on soil physical properties and crop growth. Geoderma 116, 1-2, pp. 107-136, 2003.
9. **Lisa L., Parena S., Lisa L.:** Working times and production cost of grapes in grass covered or tilled vineyards of Piedmont. In: Proceedings of GESCO 8th Meeting, 3-5 July 2000, Vairão (Portugal), pp. 325-330, 1995.
10. **Plant E.R., Pettygrove G.S., Reinart W.R.:** Precision agriculture can increase profits and limit environmental impacts. California Agriculture **54**(4) 66-67, 2000.
11. **Porter M.A., Mc Mahon T.A.:** A computer simulation model for soil temperatures in Australian cereal copping. Soil & Tillage Research **10** pp. 131-145, 1987.
12. **Usowicz B.:** Statistical-physical model of thermal conductivity in soil. Polish Journal of Soil Science, XXV/1, pp. 27–34 1992.
13. **Usowicz B.:** Evaluation of methods for soil thermal conductivity calculations. International Agrophysics **9**(2) pp. 109–113, 1995.
14. **Usowicz B.:** Soil thermal properties software package 2.0. Copyright: Institute of Agrophysics PAS, Lublin, 1998.

NITRATE(V) TRANSFORMATIONS IN SOILS

Włodarczyk Teresa

Instytut Agrofizyki, Polish Academy of Sciences, Lublin, Poland
t.wlodarczyk@demeter.ipan.lublin.pl

Abstract

Nitrate transformation and their circumstances in soils were reviewed. In this paper, the biological processes of nitrate transformation *eg* assimilatory reduction of nitrate, dissimilatory reduction of nitrate, and nitrification (the source of nitrate), the way in which the different interacting processes influence N-nitrate transformation were outline. In this mini-review we have concentrated predominantly on papers concerned with N_2O production. Additionally were shown the main conditions influence on nitrate transformation in the soil.

Introduction

The N atom exists in different oxidation and physical states. Shifts between them are commonly mediated by soil organisms. The ease with which shifts occur in the oxidation states results in formation of different inorganic forms that are readily lost from ecosystem. The NO_3^- form is readily soluble in water and thus subject to leaching and water transport. The NH_4^+-NH_3 forms are subject to volatilisation and fixation both by clays and by soil organic mater (SOM). Nitrogen shortages, therefore, often limit plant productivity. Also, both the gaseous and the soluble phases of this nutrient lead to environmental pollution [88].

Nitrogen in soil

Nitrogen in soil occurs both in organic and inorganic form. Organic nitrogen is in reduced form, some of it as amide nitrogen, relatively easily available to decomposer organisms unless protected mechanically or chemically. Another part of soil organic nitrogen occurs as a constituent of large and often resistant molecules with nitrogen in heterocyclic aromatic rings [120].

Inorganic nitrogen is usually fully reduced, ammonium, or fully oxidised, nitrate. Intermediary oxidation stages also exist but do not accumulate in measurable amounts, except for nitrite under special circumstances. There are

transfers not only between the various soil nitrogen pools, but also between the soil pools and gaseous phase, where nitrogen compounds at different oxidation levels also occur (NH_3, N_2, N_2O, NO) [120].

Only a small part of nitrogen store in the soil is available to plant roots at any given moment. Most is in organic form, usually in large molecule insoluble in water. Organic nitrogen in natural ecosystems originates from dead organisms, plants, and microorganisms. Much of the nitrogen in fresh litter is still in protein form or in decomposition products of proteins, *ie* peptides and amino acids. These substances are attractive substrates for microorganisms, which often can use as a source of carbon as well as of nitrogen.

The decomposition of litter does not mean that litter nitrogen immediately transferred to inorganic nitrogen or transformed into the limited number of low-molecular organic compounds in which it may be available to plant roots and mycorrhizal fungi. Microorganisms do the chemical degradation of the litter, and even if they may produce extracellular enzymes, most take of the nitrogen up themselves. The rate at which the microbial nitrogen is transferred to the available pool depends on the C/N ratio of the substrate and on the death rate the microorganisms [120]. Microorganisms are a major source for N mineralization in soil because of the much lower C:N ratios of bacteria and fungi relative to plant residue. Bacteria have C:N ratio as low as 3.5:1, fungi, of 10 to 15:1. The average soil population is found to have a C:N ratio of 4 to 7:1 [88].

The normal case, however, is that most of the ammonium-liberated stays in the ecosystem, although rapidly removed from the soil solution along one of the following pathways: 1) uptake by plant roots (directly or via mycorrhizal hyphae), 2) uptake by microorganisms, 3) adsorption on the surface of soil colloids (in clay-rich soils partly followed by ammonium fixation in the lattice of certain clay minerals), and 4) chemical binding to organic substances. Any ammonium ions left in the soil solution may leave the soil with percolating water, but this is seldom an important pathway in natural ecosystems [120].

Humus is the term for the soil organic matter, which cannot macroscopically be recognised as plant, or animal remains [63]. The humus is very resistant to degradation, with half-lives varying from decades in some intensively cultivated organic soils to several thousand years for organic matter deep in mineral soils in certain soil types (as measured by radiocarbon dating). The chemical structure of humus is not well defined, even if fractions with different characteristic can be isolated by chemical methods (humic acids, fulvic acids). Much of nitrogen appears to occur in heterocyclic aromatic rings, which together with the size of the molecules may account for the resistance to enzyme degradation. Much of the carbon in the humus may originate from the lignin in plant cell walls, as terpenoid fragments can be obtained from both lignin and humus by chemical treatment.

While many fungi and bacteria either lack lignin-degrading enzymes or produce them in small amounts, wood-degrading fungi of so-called white-rot type decompose lignin-rich plant residues relatively easily. Related soil living fungal species can decompose at least part of the soil humus [120].

The concentration of lignin and other high-molecular polyphenolic compounds appears to be one of the important controlling factors for the rate of organic matter decomposition in the forest soil [12].
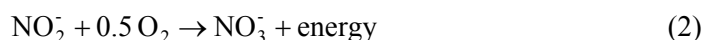
Nitrification

Nitrification is an aerobic process, performed both by autotrophs and heterotrophs in soils.

Autotrophic nitrification is defined as the biological oxidation of NH_4^+ to NO_2^- and NO_3^- in a two-step reaction as presented in the following equations where *Nitrosomonas* performs the first energy yielding reaction:

$$NH_4^+ + 1.5\,O_2 \rightarrow NO_2^- + 2H^+ + H_2O + \text{energy} \tag{1}$$

and *Nitrobacter* the second energy yielding reaction:

$$NO_2^- + 0.5\,O_2 \rightarrow NO_3^- + \text{energy} \tag{2}$$

The chemoautotrophic nitrifiers are generally aerobes that derive their C largely from CO_2 or carbonates but NH_4^+ can originate from mineralization of soil organic material by other organisms or from fertiliser. All organisms in this family are capable of obtaining all their energy requirements for growth from oxidation of either ammonium or nitrite [9].

The bacteria are classified based on whether they oxidise NH_4^+ to NO_2^- (*Nitroso-*) or NO_2^- to NO_3^- (*Nitro*). In most habitats they are closely associated and NO_2^- rarely accumulates [88].

The oxidation of NH_4^+ can be described as:

$$NH_4^+ + 2H + 2e^- + O_2 \xrightarrow{\text{ammonia mono - oxygenase}} NH_2OH + H_2O \tag{3}$$
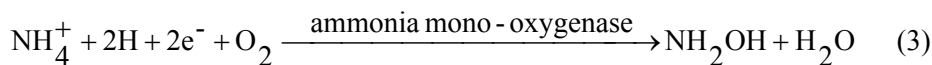
The enzyme ammonia mono-oxygenase has broad specificity and also oxidises propene, benzene, cyclohexane phenol, methanol, and CH_4.

Hydroxylamine is oxidised to NO_2^- as follows:

$$NH_2 + OH + H_2O \xrightarrow{NH_2OH \ \text{oxidoreductase}} HONO + 4e + 4H^+ \tag{4}$$

$$2H^+ + \frac{1}{2}O_2 + 2e^- \xrightarrow{\text{terminal oxidase}} H_2O \qquad\qquad (5)$$
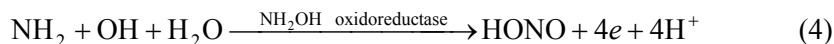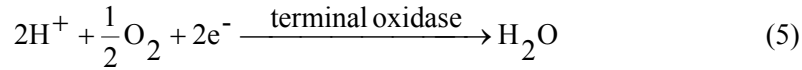
The NO_2^- oxidising bacteria catalyse the reaction:

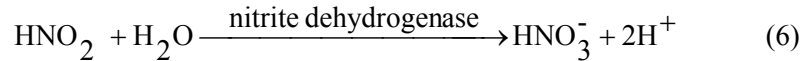$$HNO_2 + H_2O \xrightarrow{\text{nitrite dehydrogenase}} HNO_3^- + 2H^+ \qquad (6)$$

The rate of nitrification in a soil is affected directly and indirectly by many factors, such as temperature, moisture, C/N ratio occurrence of inhibitors of the process itself, or of organic matter decomposition.

The best-known nitrifiers are bacteria of the genera *Nitrosomonas*, which oxidise ammonium to nitrite, and *Nitrobacter*, which oxidise nitrite to nitrate. Both *Nitrosomonas* and *Nitrobacter* are favoured by alkaline to slightly acid soils and are unimportant in strongly acid environments. This does not necessarily exclude them from soils with an average acidity below pH 4.5 [43].

The heterogeneity of a soil means that there may be a large variation in many soil properties, including acidity, between microsites. pH is an important controlling factor, not only for the occurrence of nitrification, but also for any by-products that may be formed. As *Nitrobacter* seems to require somewhat higher pH than *Nitrosomonas*, some accumulation of nitrite may occur under certain circumstances. Gaseous products may also be formed, at different rates under different conditions [120].

It remains to be stated that nitrification is an acidifying process. Under undisturbed conditions, when the nitrate formed is rapidly taken up by roots and reduced back to ammonium and other reduced forms, there is no net acidification [120].

Nitrite accumulates only under conditions where *Nitrobacter* appears to be inhibited while *Nitrosomonas* is not. Typically these conditions are high pH (7.5) and very cold temperatures [18,113].

Assimilatory reduction of nitrate

Soil fixed nitrogen resources may be conserved through both assimilatory and dissimilatory nitrate reductive processes, or they are reduced by dissimilatory reduction. Assimilatory and dissimilatory nitrate reductions both involve the transfer of electrons to nitrogen compounds, but they differ in the ultimate fate of the reduced nitrogen atom.

In the absence of NH_4^+ and organic-N and under conditions where only NO_3^- is available, bacteria, fungi, yeast and algae have first to reduce the NO_3^- [44]. This process is less O_2 sensitive than denitrification and therefore would be

expected to occur under aerobic conditions [90, 74]. The aerobic assimilation of nitrate or assimilatory nitrate reduction is the process of NO_3^--N incorporation into biomass [74]. Some microorganisms reduce NO_3^- to NH_4^+. They use the N in production of biomass (assimilatory reduction), but the process can also serve other purposes (dissimilatory reduction), *eg* as a source of energy or for detoxification of NO_2^-. N_2O can escape during these processes [27,59,103,124].

In nitrate assimilation, the first step is the reduction to nitrite, which is accomplished by the enzyme nitrate reductase. Subsequently, the nitrite is reduced to hydroxylamine by the enzyme nitrite reductase to finally be reduced to ammonia [89]. The net reaction is shown in following equation:

$$NO_3^- \rightarrow NO_2^- \rightarrow [H_2N_2O_2] \rightarrow [NH_2OH] \rightarrow NH_3$$
$$\downarrow \tag{7}$$
$$N_2O$$
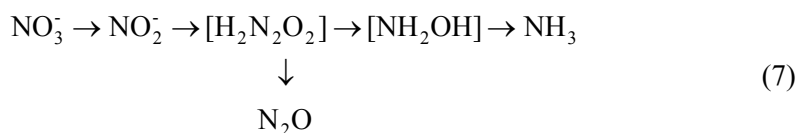
where N_2O rather than N_2 may be produced as a by-product from the indicated intermediate (hyponitrite) [44]. The reaction shown is essentially the same as that which occurs during NO_3^- reduction to NH_4^+ and involves the same precursor of, N_2O again probably hyponitrite [44,74]. This pathway as a nitrous oxide source seems to be significant from studies on forest soils where fungal activity is important. Sextone [106] provided evidence that in an acidic organic coniferous forest soil the N_2O production due to fungal activity may be as much as 40% of the total. Furthermore fungal activity was also suggested by Robertson and Tiedje [95] as an alternate biological nitrous oxide source from forest soil. Finally, certain assimilatory nitrate-reducing yeast has been shown to be able to produce N_2O [60].

Some of the studied nitrate reductases show the existence of an active form and an inactive form that depends on the oxydoreduction conditions of the environment [118]. Under reducing conditions, the enzyme converts into the inactive form. The regulation of the synthesis of the enzyme varies in different species, being constitutive in several species and repressible in others. In *Rhizobium japonicum,* for instance, the assimilatory enzyme is induced in aerobiosis and in the presence of nitrate; meanwhile in anaerobiosis, a dissimilatory nitrate reductase is induced [29]. Both enzymes have different molecular weights and different sensitive to inhibitors [118].

Dissimilatory reduction of nitrate

Dissimilatory reduction is the process through which some microorganisms use the energy generated by the electron transport from an organic or inorganic source to nitrate or to a more reduced nitrogen oxide. This metabolic reduction uses cytochromes mostly as electron donors and occurs with a liberation of dinitrogen as the final product. However, some bacteria lack N_2O reductase, and so produce this gas as a terminal product, or lack nitrite reductase, yielding nitrite as an end product [58].
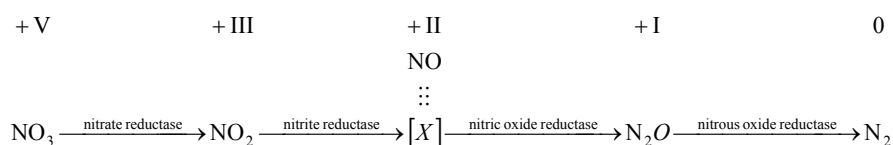
When the dissimilative reduction produces the gaseous dinitrogen or nitrous oxide compounds, the process is termed **denitrification**. However, since reduction, through the metabolic pathway of cytochromes, in some case results in the production of ammonia or nitrite, some authors prefer the more general name of **nitrate respiration** for the process. In other cases, the metabolic pathways do not involve membrane-bound enzymes, cytochromes, or electron transport phosphorylations, and the main product is ammonia. This process is called **fermentative nitrate reduction** [37].

In contrast to assimilatory reduction (nitrogenous compound is incorporated into cellular biomass) for dissimilatory nitrate reduction, the nitrogenous compounds accept electrons in support of cellular respiration. The final products, dinitrogen, nitrous oxide, or ammonium are released from the cell and accumulate in the environment in concentrations far beyond that necessary for biomass synthesis. Three commonly evaluated microbial processes are classed under the tittle of dissimilatory nitrate reduction. These processes can be distinguished by their respective products: a) nitrite, b) ammonium, and c) nitrous oxide and dinitrogen – denitrification.

Biological denitrification is the last step in the N-cycle, where N is returned to the atmospheric pool of N_2. It is an anaerobic process [49].

Biological denitrification is a respiratory process in which N-oxides (electron acceptors) are enzymatically reduced under anaerobic conditions to nitrous oxide and dinitrogen for ATP production by organisms that normally use O_2 for respiration. Most denitrifying organisms are heterotrophic. However, heterotrophic denitrification is the most important processes as a source for N_2O. Nitrous oxide are well documented gaseous products of the heterotrophic denitrifiers [1,11,78].

The process of denitrification (including rhizobial denitrification) can be presented as follows [40]:

$$+V \qquad\qquad +III \qquad\qquad +II \qquad\qquad +I \qquad\qquad 0$$

$$NO$$

$$NO_3 \xrightarrow{\text{nitrate reductase}} NO_2 \xrightarrow{\text{nitrite reductase}} [X] \xrightarrow{\text{nitric oxide reductase}} N_2O \xrightarrow{\text{nitrous oxide reductase}} N_2$$

Nitric oxide (NO) is believed to be either a true intermediate or rapid exchange with an unidentified intermediate.

Anaerobic conditions and the presence of readily oxidisable carbonaceous substrates are necessary for denitrification. Denitrifiers gain carbon for cell growth from the concomitant oxidation of organic molecules [89].

Many microorganisms can use NO_3^- as their primary electron acceptor for obtaining energy from organic compounds when low O_2 availability restricts their metabolism [49]:

$$5(CH_2O) + 4NO_3^- + 4H^+ \rightarrow 5CO_2 + 7H_2O + 2N_2 + \text{energy} \qquad (8)$$
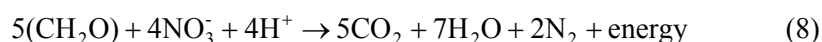
Some microorganisms can obtain energy by using NO_3^- for oxidation of inorganic compounds, eg S^{2-}, Fe^{2+} (autotrophic denitrification). This occurs where NO_3^- diffuses into zone rich in FeS, e.g., sediments in shallow waters [48].

The majority of soil bacteria seem able to denitrify [125,126]. The complete reduction of nitrate proceeds via nitrite, nitric oxide, and nitrous oxide, but not all denitrifiers can carry out the complete reduction from nitrate to N_2. Denitrifying bacteria exhibit a variety of incomplete reduction pathways. The enzymes most commonly missing are nitrate reductase or nitrous oxide reductase; some bacteria produce only N_2, while others give a mixture of N_2O and N_2, and some only N_2O [97,119].

Nitrate reductase of the dissimilatory reduction is a molybdo-iron sulphide protein, but different from the assimilatory enzyme [100,101]. Nitrate reductase has been found to be a membrane-bound enzyme except in *Spirillum iteronii* where is found as a soluble enzyme [47].

Nitrite reductase is the key enzyme that drives the NO_2^- ion toward the synthesis of the gases and NO in contrast with the more economic pathway of ammonia synthesis.

Nitrous oxide reductase is possibly a Cu protein and closes up the recycle of nitrogen by releasing dinitrogen back to the atmosphere [62]. Thus, the function of this enzyme is essential and prevents N_2O from being released into the atmosphere, avoiding the photochemical production of NO; this gas is supposed to be responsible for destroying the atmospheric ozone [33].

Some denitrifiers lack the ability to catalyse the last step from N_2O to N_2 [124].

There has been some doubt if NO is a true intermediate or by product [3] in the process, but a bacterial nitric oxide reductase has recently been characterised: *Pseudomonas stutzeri* loses the ability to denitrify if the genes for this enzyme are blocked [18].

That N_2O is an obligatory intermediate in denitrification is widely accepted [90,129].

N_2O is reduced to N_2 by the labile enzyme nitrous oxide reductase [119]. The reduction can also be carried out by the even more labile enzyme nitrogenase (the enzyme that reduce N_2 to NH_3).

Apart from free living denitrifiers such as *Pseudomonas ssp.*, *Rhizobium ssp.* which live in a symbiotic relationship with leguminous plants have the ability to denitrify. This later process is referred to as rhizobial denitrification [82].

The denitrification process may be performed by N_2-fixers, specifically by *Azospirillum*, and by *Rhodopseudomonas* [2,25]. These species are capable of using nitrate as an electron acceptor, an alternative to oxygen, for generating ATP for nitrogenase activity. Studies with stable isotopes showed that *Rhodopseudomonas spheroides*, strain IL-106, did not directly assimilate nitrate into cell nitrogen, but rather denitrified nitrate to dinitrogen gas which was reutilized via nitrogenase as a source of ammonia for its assimilation [80]. *Rhizobium japomicum* and cowpea strains exhibit substantial rates of denitrification as either free-living or bacteroid cells. *R. triflii, R. leguminosarum* and *R. hedysarum* were able to use nitrate as an electron acceptor, liberating N_2O gas. This liberation was inhibited in the absence of nitrate by aerobiosis or when rich media were used. Similar studies were carried out with nodulated plants, with the aforementioned fast-growing rhizobia, showing that *Rhizobium* in an active denitrifier in symbiosis as well as in the free-living state [25].

Denitrification is usually thought as a bacterial process, but Shoun *et al.* [108] reported that many fungi are capable of evolving N_2O under anaerobic conditions.

Non-denitrifying fungi and bacteria can produce N_2O during the process of **dissimilatory reduction of NO_3^- to NH_4^+.** This pathway, which is regulated by oxygen and unaffected by ammonium, can be a contributing source of N_2O from systems which suffer prolonged anaerobic periods, e.g. in sediments and rice paddy fields [124]. According to Bleakley and Tiedje [15] this pathway of N_2O production is of minor importance. However, with the high activity of these microorganisms coupled with an appreciable NO_2^- accumulation in soil, this pathway may be more important than is generally acknowledged [124].

Some researchers have suggested that soil microbial population dynamics may be more important factor than soil physical and soil chemical factors in explaining the characteristics of nitrous oxide production from soil [1,49,90,104].

Total denitrification fluxes (N_2O plus N_2) are directly proportional to soil **NO_3^- concentrations** when the other important component, a readily metabolizable organic substrate, is also present and non rate-limiting. When a lack of metabolizable organic matter limits potential denitrification, N_2 plus N_2O fluxes do not increase with increasing NO_3^- concentration [102].

Because denitrification is an enzymatically catalysed process, the reaction rate of the process is anticipated to follow some form of Michaelis-Menten kinetics. That is, the rate of nitrate reduction to dinitrogen and nitrous oxide should increase until a saturating concentration is reached. Once enzyme-saturating concentration of the substrate have been reached, two alternatives are generally observed. There can be no effect of the augmented substrate levels or substances may become inhibitory. The latter situation is generally detected when studying denitrification, where augmented nitrate concentration inhibits nitrogen oxide reductases. Nitrate reduction in soil is generally found to be either a zero- or first-order process [121]. For example Bowman and Focht [17] observed first-order kinetics with Coachella fine sand. The Michaelis constant for the latter study was 170 µg nitrate ml^{-1}. Reddy *et al.* [92] measured both first- and zero-order reaction kinetics with flooded soils. Włodarczyk *et al.* [129] incubated 6 loess soils (three Eutric Cambisols and three Haplic Phaeozems) under flooded conditions with a wide range of NO_3^- doses under anaerobic found the soil denitrification activity showed Michaelis-Menten kinetics with respect to soil nitrate content with K_M in the range 50-100 mg NO_3^--N kg^{-1}. Freney *et al.* [45] found that emissions increased by 1 to 2 orders of magnitude following heavy irrigation of a field cropped with sunflower and fertilised with urea. Most of the urea had been converted to NO_3^- at the time of the emission measurements.

Emission are characterized by a 'large' efflux of N_2O following fertilizer application at rates which may be between 1 and 3 orders of magnitude higher than baseline levels. This period typically continues for 5 to 8 weeks following the fertilizer application and is followed by declining rates of emission, which gradually approach baseline levels. The dynamics of these post-fertilization events parallel the presence of free NH_4^+ and NO_3^- within the soil, which is directly accessible to the soil microorganisms. Some researches have found nitrous oxide emissions from soil were significantly higher after amendments with nitrifiable-N sources compared to nitrite fertilizer application. This emphasise that nitrification is an important process for nitrous oxide production under field conditions [20,28]. Indeed, comparisons of different fertilizer forms show, for the same application rate, that nitrous oxide emission is highest after application of anhydrous ammonia [21].

High emissions associated with rainfall/irrigation are favoured when fertiliser is applied simultaneously with, or soon before, the event [57,72,127].

Complete reduction of $2NO_3^-$ to N_2 generates $2OH^-$, which may cause environmental pH to rise [117].

The **influence of aeration** on N_2O emission is complex and dependent on interacting factors. N_2O production and emission is usually greatest when the average soil conditions are such that both aerobic and anaerobic sites are abundant. This has been found in several laboratory studies [42].

Soil is heterogeneous and commonly has both aerobic and anaerobic sites. The oxygen status in soil, which is inversely, proportional to the amount of moisture held there, appears in many studies to be one of the key factors influencing nitrous oxide production. As the free oxygen in soil is depleted, a number of predictable changes in microbial activity occur. When the soil oxygen tension has been reduced to less than 1 percent (v/v), the microbial population appears to shift from being predominantly aerobic to anaerobic. With the development of reducing atmosphere, growth yields decline because the energy yielded per mole of fixed carbon oxidised anaerobically is far less that produced from aerobic respiration. The inverse relationship between the rate of denitrification and O_2 concentration has been demonstrated in many studies [13,24,42].

In aerobic soils denitrification can occur in anaerobic microsites such as in the centre of aggregates [56,84] or in areas of localised high oxygen consumption ("hot spots"), which can be associated with the breakdown of particulate organic material [84]. Furthermore some groups of denitrifiers are able to use simultaneously both oxygen and nitrate or nitrite as electron acceptor. Therefore, denitrification by those organisms can occur under aerobic conditions. **"Aerobic denitrification"** can occur in the presence of significant amounts of oxygen. Those denitrifiers are able to simultaneously utilise oxygen and nitrate or nitrite, even when the dissolved oxygen concentration approaches air saturation. An explanation for the usage of both acceptors might be the presence a rate-limiting step in the transfer of electrons from its substrate to oxygen. The provision of a second electron acceptor, in this case nitrate, would allow it to use an additional branch in the electron transport chain [96,97,129].

In anaerobic respirometry experiments, it was observed that aerobically grown *Thiobacillus pantotropha* began to denitrify immediately when it was supplied with substrate and nitrate. Similarly grown cultures of the other strains required 2 to 4 h to induce their denitrifying enzymes [93]. Oxygen and nitrate electrodes were used to monitor the activity of these cultures, and simultaneous nitrate and oxygen removal in *T. pantotropha* suspension was clearly observed [94]. Oxygen and nitrate electrodes were used to monitor the activity of these cultures, and simultaneous nitrate and oxygen removal in *T. pantotropha* suspension was clearly observed [94]. When grown in batch cultures with acetate as the substrate,

T. pantotropha cultures provided with both oxygen (at a dissolved oxygen concentration of 80% air saturation) and nitrate grew more rapidly than similar cultures, which had only one electron acceptor [93].

Mention must be made of another condition, which can favour low O_2 levels, and hence N_2O production within soils. This is the presence of anaerobic microsites, particularly within heavy textured clay soils, where gaseous diffusion is slowed or restricted. Nitrous oxide emissions are often high from these soils, especially those with a large proportion of anaerobic microsites [23,71]. Such microsites exist where root or soil respiration rates exceed the capacity of the soil to allow adequate gaseous diffusion to or from the microsites. The role of O_2 diffusion in soil for denitrification was described in the model of K. A. Smith [112]. This model calculates concentrations in soil and describes how O_2 diffuses down the profile and into aggregates, and the fraction of the soil volume that is anaerobic. The diffusion of O_2 into aggregates rather than down the soil profile appears to be the main rate-determining step for denitrification in this model. Diffusion of NO_3^- from aerobic to anaerobic sites with subsequent reduction in the later may also occur. In aerobic soil, denitrification and autotrophic nitrification, each with its associated N_2O production may occur simultaneously at spatially distinct microsites [18]. Highest N_2O fluxes are expected under microaerophilic conditions in soil where N_2O reduction to N_2 during denitrification is inhibited by O_2 gas and where nitrifiers are sufficiently limited in O_2 gas supply to also form N_2O [61].

After a heavy rainfall, with the presence of nitrate and suitable carbon sources, significant losses of fixed nitrogen from soil can result from the induction of denitrifiers.

In soils and wastewater, even if well-aerated, anaerobic energy-conserving processes can occur inside aggregates and sewage flocculates in the sequence NO_3^-, MnO_2 and Fe_2O_3 respiration followed by SO_4^{2-} and CO_2 reduction [83].

Soil water content is a major factor determining the rate of denitrification [52,79]. Highest emission are often correlated with very wet soil conditions [4,10,34,51,68,69,75,77,85,116,128]. Such findings reflect the fact that denitrification is an anaerobic process. Increasing denitrification rate with increasing soil water content seems most marked above about 60% WFPS [water-filled pore space] [6,55,67,76,81,123].

Several workers observed highest nitrous oxide fluxes from soil during fluctuating moisture conditions compared to either continuously well-aerated or continuous anaerobic conditions [38,111,115].

Denitrification may cease if the soil remains wet for some time, and higher denitrification rates are observed where soils are going through wetting/drying cycles than where soil water content is constantly high [76]. Groffman and Tiedje

[50] showed that the rate of denitrification did not depend on water content in a simple manner. They dried intact soil cores and found that denitrification rates decreased markedly when water content declined from flooding to field capacity. With further drying the decline was less rapid. However, when water content was increased from dry conditions, the sharpest increase in rate of denitrification occurred at low water content. Others also found that denitrification rates depend on history of the sample [46,65].

During fluctuating soil moisture conditions, drying and rewetting cycles may enhance the availability of soil organic matter and this will also favour denitrification. Drying causes shrinkage and disruption of soil aggregates and exposes organic matter not previously accessible to microbial attack. In addition, death of part of the microbial biomass during drying releases additional available carbon. As a result, upon rewetting there is a characteristic flush of soil microbial activity [87].

Microbial processes in soils are the most important sources of N_2O [49]. Nitrous oxide is produced during denitrification and nitrification. It is an intermediate of the denitrification and a by-product of nitrification.

The amount of nitrous oxide emitted via denitrification is related to the factors, which influence the enzyme production for the several steps in the denitrification sequence. Low pH, high nitrate concentration, low moisture and low availability of oxidisable organic material all tend to increase the **nitrous oxide fraction** in the denitrification products [5]. At saturated moisture conditions or under strictly anaerobic conditions (*eg* poorly drained soils and in sediments) N_2-production is favoured as the principal gaseous product [30,76]. With an increase in aeration to an air-filled porosity of about 10%, denitrification and hence the overall gas production (N_2 plus N_2O) declines but the mole fraction of N_2O trends to increase [66].

Many studies showed that the reduction of N_2O to N_2 is more prone to inhibition by O_2 than reduction of NO_3^- to N_2O, thus the N_2O/N_2 ratio decreases with decreasing O_2 concentration. Thus, the presence of O_2 reduces the activity and delays the synthesis of nitrous oxide reductase relative to nitrate reductase and nitrite reductase, so that the N_2O/N_2 ratio increases with increasing O_2 concentration [13,16,36,39,42,70,110,114,124]. The N_2O/N_2 ratio usually decreases with increasing soil water content and tends to be high when the denitrification rate is low [7,77,98,99,105,123,128].

At low soil water content, N_2O emission is low because microbial activity is low and the O_2 supply is ample so that nitrification goes all the way to NO_3^-, and denitrification rates are low. With increasing water content mineralization rate increases and nitrification increasingly produces N_2O. Also denitrification becomes significant with a high N_2O/N_2 ratio as O_2 diffusion becomes impeded.

At high soil water content gas diffusion is severely hindered, denitrification proceeds increasingly towards N_2 and N_2O emission declines. Thus, soil water content where both denitrification and nitrification can proceed will generally give the maximum emission of N_2O. The range of soil water content is normally 45 to 75% WFPS [49]. The relationship between soil moisture content and N_2O emission rate is also often seen in field studies as an association between corresponding values N_2O emission and water content obtained over a period of time, *eg* season or year and over a wide range of water content levels [35,41,86,109]. This relationship is illustrated by Mosier *et al.* [73] who found N_2O emission from a native short-grass steppe during a summer sampling period to be positively correlated with soil water content in the upper 5 cm. Emission were some 10-fold higher at 18 vol-% (36% WFPS) than at 10 vol-% (20% WFPS). Conrad *et al.* [28] made similar observations at water contents of 10 to 20 weight-%. Maximal N_2O fluxes from soils are reported shortly after irrigation or rainfall [26,28,53,54].

Davidson *et al.* [32] studied N_2O emission in a dry tropical forest. Emissions were higher in the wet season than in the dry season, but addition of water to dry soil caused rapid formation of NH_4^+ from mineralization and large pulses of N_2O emission.

Waterlogged conditions are mostly undesirable in agriculture, except for paddy rice. These fields usually emit only small amounts of N_2O while flooded [22].

The high rates of denitrification that occur when soils pass through wetting/drying cycles also show up as high N_2O emissions [31,87]. When a soil is wetted sufficiently by rain or irrigation water to cause anoxic conditions and to initiate denitrification, N_2O will be produced more rapidly than it is reduced. If the soil dries within 24 to 72 h, insufficient time will have elapsed for the development of nitrous oxide reductase, thereby preventing N_2O reduction to N_2 [26]

Firestone and Tiedje [38] showed that after the onset of anaerobiosis essentially three time periods could be distinguished based upon the response of the native microbial population. In the period from 16 to 33 h following anaerobiosis, 40 to 90% of the gaseous denitrification product is evolved as N_2O. Initially NO_3-reductase production is stimulated and enzyme is produced more rapidly than N_2O-reductase. Thus, N_2O accumulates and can be released into the atmosphere. The moisture conditions which seem to favour N_2O production are, therefore, alternating wetting and drying cycles during which both autotrophic nitrification and denitrification are active but where there is not enough time for substantial levels of N_2O-reducatse to form. The large pulses of N_2O, which

typically follow rainfall or irrigation may exceed, background levels by up to 3 orders of magnitude especially after long periods of dryness [28,107].

It is well established that an increase in soil or sediment NO_3^- concentration leads to an increase in the $N_2O:N_2$ ratio in the product gases. This is attributed to the inhibition of N_2O reductase by NO_3^- [14,38,122,129] this effect is further enhanced at low pH.

N_2O formation, accumulation, and subsequent emission from the soil depend both on its production and its reduction to N_2. The production of N_2O depends on the process rate of denitrification and nitrification and on the relative N_2O production, which is the percentage of the reduction (denitrification: $N_2O*100/[N_2O+N_2]$) or the oxidised (nitrification: $N_2O*100/[NO_2^-+N_2O]$) substrate being transformed into N_2O [8]. Firestone and Davidson [40] suggest that the process rate is the most important factor determining the N_2O production.

Changes in soil **redox potential** are related to changes in oxygen levels. If organic matter is added to soil, oxygen is depleted and the potential drops - at time quite precipitously. This is a microbial reaction, because inhibitors of microbial activity prevent both oxygen depletion and the development of reducing conditions. The occurrence of a variety of microbial processes is related to specific redox potential. Some of these are as follows:

Aerobic carbon oxidation	> 0.2 V
Denitrification	0.15 to 0.2 V
Sulphur reduction	0.1 to -0.2 V
Methanogenesis	- 0.2 to -0.3 V.

Masscheleyn *et al.* [70] reported on N_2O emission from rice paddy soils at various redox potentials, ranging from +500 to -250 mV. Two maximums for N_2O evolution were found, at +400 mV when nitrification was the source, and at 0 mV when N_2O was produced by denitrification.

Kralova *et al.* [64] got similar results in a study on denitrification in a soil suspension amended with NO_3^-. The maximum amount of N_2O was evolved at a redox value of 0 mV, while denitrification rates and N_2 emission continued to increase with lower redox levels.

Smith and Patrick [115] showed that alternate anaerobic-aerobic cycling increased N_2O evolution by a factor of 10 to 20 relative to constant aerobic conditions for soil suspensions amended with NH_4^+. No N_2O evolved during constant anaerobic conditions. The redox potential fluctuated during cycling, but was always lower than the redox potential for constant aerobic, and much higher therefore-constant anaerobic conditions.

224

Włodarczyk [128] studied nitrous oxide emission from Eutric Cambisol observed the highest N_2O evolution at 250 mV.

Nitrification and denitrification are the main microbial processes producing N_2O and NO. Other biochemical oxidation or reduction reactions like N_2-fixation and dissimilatory nitrate reduction may yield some traces of N_2O and NO as well.

References

1. **Abou-Seada M.N.I., Ottow J.G.C.:** Effect of increasing oxygen concentration on total denitrification and nitrous oxide release from soil by different bacteria. Biol. Fertil. Soils 1:31-38, 1985.
2. **Aleem M.I.H.:** Biochemistry of chemolitotrophic nitrogen cycle. In Proc. Int. Symp. Nitrogen and the Environment, Malik, K.A., Mujtaba Naqvi, S.H., and Aleem, M.I.H., Eds. Nuclear Institute for Agriculture and Biology, Faisalabad, Pakistan, 29, 1985.
3. **Amundson R.G., Davidson E.A.:** Carbon dioxide and nitrogenous gases in the soil atmosphere. J.Geochem.Explor.38:13-41, 1990.
4. **Anderson J.C., Levine J.S.:** Simultaneous field measurements of biogenic emission of nitric oxide and nitrous oxide. Journal of Geophysical Research 92:965-976, 1987.
5. **Arah J.R.M., Smith K.A.:** Factors influencing the fraction of the gaseous products of soil denitrification evolved to the atmosphere as nitrous oxide. In Bouwman, A.F. (ed) Soil and the greenhouse effect. Proceedings of the International Conference Soils and the Greenhouse Effect. International Soil Reference and Information Centre (ISRIC). John Wiley and Sons, New York pp. 475-480, 1990.
6. **Aulakh M.S., Rennie D.A., Paul E.A.:** Acetylene and N-serve effects upon N_2O emissions from NH_4^+ and NO_3^- treated soils under aerobic and anaerobic conditions. Soil Biol. Biochem. 16; 351-356, 1984.
7. **Aulakh M.S., Rennie D.A., Paul E.A.:** Gaseous nitrogen losses from soils under zero-till as compared with conventional-till management systems. J. Environ. Qual. 13; 130-136, 1984.
8. **Bandibas J., Vermoesen A., De Groot C.J., Van Cleemput O.:** The effect of different moisture regimes and soil characteristics on nitrous oxide emission and consumption by different soils. Soil Science Vol. 158, No. 2 pp. 106-114, 1994.
9. **Belser L.W.:** Population ecology of nitrifying bacteria. Annu. Rev. Microbiol., 33, 309, 1979.
10. **Benckiser G., Haider K., Sauerbeck D.:** Field measurements of gaseous nitrogen losses from an Alfisol planted with sugar beets. Z. Pflanzenernähr. Bodenk. 149; 249-261, 1986.
11. **Benckiser G., Simarmata T.:** Environmental impact of fertilising soils by using sewage and animal wastes. Fert. Res. 37, 1994.
12. **Berg B.:** Nutrient release from litter and humus in coniferous forest soil – a mini review. Scand. J. For. Res., 1, 359-370, 1986.
13. **Betlach M.R., Tiedje J.M.:** Kinetic explanation for accumulation of nitrite, nitric oxide, and nitrous oxide during bacterial denitrification. Appl. Environ. Microbiol. 42; 1074-1084, 1981.
14. **Blackmer A.M., Bremner J.M.:** Inhibitory effect of nitrate on reduction of N_2O to N_2 by soil microorganisms. Soil Biology and Biochemistry 10; 187-191, 1978.

15. **Bleakley B.H., Tiedje J.M.:** Nitrous oxide production by organisms other than nitrifiers or denitrifiers. Applied Environmental Microbiology 44:1342-1348, 1982.
16. **Bonin P., Gilewicz M., Bertrand J.:** Effects of oxygen on each step of denitrification on *Pseudomonas nautica*. Can. J. Microbiol. 35; 1061-1064, 1989.
17. **Bowman R.A., Focht D.D.:** The influence of glucose and nitrate concentrations upon denitrification rates in sandy soils. Soil Biol. Biochem., 6, 297-301, 1974.
18. **Bouwman A.F.:** Exchange of greenhouse gases between terrestrial ecosystem and the atmosphere 4.5. nitrous oxide In Bouwman, A.F. (ed) Soil and the greenhouse effect. Proceedings of the International Conference Soils and the Greenhouse Effect. International Soil Reference and Information Centre (ISRIC). John Wiley and Sons, New York pp. 100-120, 1990.
19. **Braun C., Zumft W.G.:** Marker exchange of the structural genes nitric oxide reductase blocks the denitrification pathway of *Pseudomonas Stutzeri* at nitric oxide. J.Biol Chem. 266:22785-22788, 1991.
20. **Breitenbeck G.A., Blackmer A.M., Bremner J.M.:** Effects of different nitrogen fertilizer on emission of nitrous oxide from soil. Geophysical Research Letters, 7, 85-88, 1980.
21. **Breitenbeck G.A., Bremner J.M.:** Effects of various nitrogen fertilizer on emission of nitrous oxide from soils. Biology and Fertility of Soils 2;195-199, 1986.
22. **Buresh R.J., Austin E.R.:** Direct measurement of dinitrogen and nitrous oxide flux in flooded rice fields. Soil Sci. Soc. Am. J. 52;681-687, 1988.
23. **Burford J.R., Dowdell R.J., Grees R.:** Emission of nitrous oxide to the atmosphere from direct-drilled and ploughed clay-soil. Journal Science Food Agriculture 32:219-223, 1981.
24. **Burton D.L., Beauchamp E.G.:** Denitrification rate relationship with soil parameters in the field. Commun. Soil Sci. Plant Anal. 16; 539-549, 1985.
25. **Casella S., Leporini C., Nuti M.P.:** Nitrous oxide production by nitrogen-fixing fast growing *Rhizobia*, Microbiol. Ecol., 10, 107, 1984.
26. **Cates R.L., Keeney D.R.:** Nitrous oxide production throughout the year from fertilised manured maize fields. Journal of Environmental Quality 16:443-447, 1987.
27. **Cole J.A.:** Assimilatory and dissimilatory reduction of nitrate to ammonia. In J.A. Cole and S.J. Ferguson (eds.) The nitrogen and sulphur cycles. Cambridge University Press, Cambridge. 306-308, 1988.
28. **Conrad R. Seiler W., Bunse G.:** Factors influencing the loss of fertiliser nitrogen in the atmosphere as N^2O. Journal of Geophysical Research 88:6709-6718, 1983.
29. **Daniel R.M., Grey J.:** Nitrate reductase from anaerobically grown *Rhizobium japonicum*. J. Gen. Microbiology, 96, 247, 1976.
30. **Davidson E.A., Swank W.T., Perry T.O.:** Distinguishing between nitrification and denitrification as a sources of gaseous nitrogen production in soil. Applied Environmental Microbiology 52:1280-1286, 1986.
31. **Davidson E.A.:** Sources of nitric oxide and nitrous oxide following wetting of dry soil. Soil Science Society of America Journal 56:95-102, 1992.
32. **Davidson E.A., Matson P.A., Vitousek P.M., Riley R., Dunkin K., Garcia-Mèndez G., Maass J.M.:** Processes regulating soil emissions of NO and N_2O in a seasonally dry tropical forest. Ecology 74, 130-139, 1993.
33. **Delwiche C.C., Bryan, B.A.:** Denitrification. Annu. Rev. Microbiol., 30, 241, 1976.
34. **Dowdell R.J., Smith K.A.:** Field studies of the soil atmosphere II. Occurrence of nitrous oxide. Journal of Soil Science 25:231-238, 1974.

35. **Duxbury J.M., P.K. McConnaughey.:** Effect of fertiliser source on denitrification and nitrous oxide emissions in a maize field. Soil Sci. Soc. Am. J. 50:644-648, 1986.

36. **Erich M.S., Bekerie A.:** Activities of denitrifying enzymes in freshly sampled soils. Soil Sci. 138: 25-32, 1984.

37. **Fenchel T., Blackburn T.H.:** Bacteria and Mineral Cycling, Academic Press, London. Chapter 5, 1979.

38. **Firestone M.K., Tiedje J.M.:** Temporal changes in nitrous oxide and dinitrogen from denitrification following onset of anaerobis. Applied Environmental Microbiology 38:673-679, 1979.

39. **Firestone M.K., Firestone R.B., Tiedje J.M.:** Nitrous oxide from soil denitrification: Factors controling its biological production. Science 208: 749-751, 1980.

40. **Firestone M.K., Davidson E.A.:** Microbiological basis of NO and N_2O production and consumption in soil. In Andrea, M.O. and Schimel, D.S. (eds) Exchange of the trace gases between terrestrial ecosystems and the atmosphere, pp. 7-22. Report for the Dahlem Workshop on Exchange of Gases between terrestrial Ecosystems and the Atmosphere, Berlin 1989. J. Wiley and Sons, 1989.

41. **Folorunso O.A., Rolston D.E.:** Spatial and spectral relationships between field-measured denitrification gas fluxes and soil properties. Soil Science Society of America Journal 49,1087-1093, 1985.

42. **Focht D.D.:** The effect of temperature, pH and aeration on production of nitrous oxide and gaseous nitrogen - a zero order kinetic model. Soil Sci. 118; 173-179, 1974.

43. **Focht D.D., and Verstraete W.:** Biochemical ecology of nitrification and denitrification. In M. Alexander (ed) Advances in Microbial Ecology. Vol.1. Plenum Press, New York, NY.;135-214, 1977.

44. **Freney J.R., Denmead O.T., Simpson, J.R:.** Nitrous oxide emission from soils at low moisture contents. Soil Biology and Biochemistry 11:167-173, 1979.

45. **Freney J.R., Simpson J.R., Denmead O.T., Muirhead W.A., Leuning R.:** Transformation and transfer of nitrogen after irrigation cracking clay soil with a urea solution. Aust. J. Agric. Res. 36; 685-694, 1985.

46. **Galsworthy A.M. and Burford J.R.:** A system for measuring the rates of evolution of nitrous oxide and nitrogen from incubated soil during denitrification. J.Soil Sci. 29; 537-550, 1978.

47. **Gauthier D.K, Clark-Walker G.D., Garrara W.T., Lascelles J.:** Nitrate reductase and soluble cytochrome c in *Spirillum itersonii*. J. Bacteriol. 102, 797, 1970.

48. **Golterman H.L.:** Influence of FeS on denitrification in shallow waters. Verh. Int. Ver. Theor. Angew. Limnol. 24:3025-3028, 1991.

49. **Granli T., Bøckman, O.:** Nitrous oxide from agriculture. Norw. Agric. Sci. Suppl. 12. p.128, 1994.

50. **Groffman P.M., Tiedje J.M.:** Denitrification hysteresis during wetting and drying cycles in soil. Soil Sci. Soc. Am. J. 52, 1626-1629, 1988.

51. **Groffman P.M., Tiedje J.M.:** Relationships between denitrification, CO_2 production and air-filled porosity in soils of different texture and drainage. Soil Biol. Biochem. 23, 299-302, 1991.

52. **Grundman G.L., Rolston D.E.:** A water function approximation to degree of anaerobiosis associated with denitrification. Soil Sci. 144; 437-441, 1987.

53. **Hansen S., Mæhlum J.E., Bakken L.R.:** N_2O and CH_4 fluxes in soil influenced by fertilisation and tractor traffic. Soil Biol. Biochem. 25; 621-630, 1993.

54. **Hao W.M., Scharffe D., Crutzen P.J., Sanhueza E.:** Production of nitrous oxide, methane, and carbon dioxide from soils in tropical savannah during the dry season. J. Atmos. Chem. 7; 93-105, 1988.
55. **Heinemeyer O., Haider K., Mosier A.:** Phytotron studies to compare nitrogen losses from corn-planted soil by the 15-N balance or direct dinitrogen and nitrous oxide measurements. Biol. Fertil. Soils 6; 73-77, 1988.
56. **Horn R., Stępniewski W., Wlodarczyk T., Walenzik G., Eckhard F.E.W.:** Denitrification rate and microbial distribution within homogenous model soil aggregates. Int. Agrophysics, 8, 65-74, 1994.
57. **Hutchinson G.L., Brams E.A.:** Nitric oxide versus nitrous oxide emissions from an ammonium ion-amended Bermuda grass pasture. J. Geophys. Res. 97; 9889-9896, 1992.
58. **Ingraham J.L.:** Microbiology and genetics of denitrifiers. In Denitrification, Nitrification and Atmospheric Nitrous Oxide, Delwiche, C.C., Ed., John Wiley and Sons, New York, 67, 1981.
59. **Kaplan W.A., Wofsey S.C.:** The biogeochemistry of nitrous oxide: A review. Adv. Agric. Mocrobiol. 3, 181-206, 1985.
60. **Klemedtsson L. Svensson B.H., Rosswall T.:** A method of selective inhibition to distinguish between nitrification and denitrification as sources of nitrous oxide in soil. Biology and Fertility of Soils 6:112-119, 1988.
61. **Klemedtsson L. Svensson B.H., Rosswall T.:** Relationship between soil moisture content and nitrous oxide production during nitrification and denitrification. Biology and Fertility of Soils 6:106-111, 1988.
62. **Knowles R.:** Denitrification. Microbiol. Rev., 46, 43, 1980.
63. **Kononova M.:** Humus of virgin and cultivated soils. In: Gieseking J.E. (ed) Soil components. I. Organic compounds. Springer, Berlin Heidelberg New York, 475-526, 1975.
64. **Kralova M., Masscheleyn P.H., Lindau C.W., Patrick W.H. JR.:** Production of dinitrogen and nitrous oxide in soil suspensions as affected by redox potential. Water, Air, Soil Pollut. 61; 37-45, 1992.
65. **Letey J., Hadas A., Valoras N., Focht D.D.:** Effect of preincubation treatments on the ratio of N_2O/N_2 evolution. Journal Environmental Quality 9:232-235, 1980.
66. **Letey J., Valoras N., Hadas, A., Focht, D.D.:** Effect of air-filled porosity, nitrate concentration, and time on the ratio of N_2O/N_2 evolution during denitrification. Journal Environmental Quality 9:227-231, 1980.
67. **Linn D.M., Doran J.W.:** Effect of water-filled pore space on carbon dioxide and nitrous oxide production in tilled and nontilled soils. Soil Sci. Soc. Am. J. 48; 1267-1272, 1984.
68. **Malhi S.S., McGill W.B., Nyborg M.:** Nitrate losses in soils: effect of temperature, moisture and substrate concentration. Soil Biol. Biochem. 22; 733-737, 1990.
69. **Mancino C.F., Torello W.A., Wehner D.J.:** Denitrification losses from Kentucky bluegrass sod. Agron. J. 80, 148-153, 1988.
70. **Masscheleyn P.H., DeLaune R.D., Patrick W.H.:** Methane and nitrous oxide emissions from laboratory measurements of rice soil suspension - effect of soil oxidation-reduction status. Chemosphere 26; 251-260, 1993.
71. **McKenney D.J., Shuttleworth K.F., Findlay W.J.:** Nitrous oxide evolution rates from fertilised soil: effects of applied nitrogen. Canadian Journal of Soil Science 60:429-438, 1980.
72. **Mosier A.R., Hutchinson B.R.:** Nitrous oxide emission from cropped field. Journal of Environmental Quality 10;169-173, 1981.

73. **Mosier A.R., Stillwell M., Parton W.J., Woodmansee R.G.:** Nitrous oxide emissions from a native short grass prairie. Soil Science Society of America Journal 45; 617-619, 1981.
74. **Mosier A.R., Parton W.J., Hutchinson G.L. :** Modelling nitrous oxide evolution from cropped and native soils. In Hallberg R. (ed) Environmental biogeochemistry. Ecol. Bull. (Stockholm) 35:229-241, 1983.
75. **Mosier A.R., Guenzi W.D., Schweizer E.E.:** Soil losses of dinitrogen and nitrous oxide from irrigated crops in north-eastern Colorado. Soil Sci. Soc. Am. J. 50; 344-348, 1986.
76. **Mulvaney R.L., Kurtz L.T.:** Evolution of dinitrogen and nitrous oxide from nitrogen-15 fertilised soil cores subjected to wetting and drying cycles. Soil Science Society of America Journal 48:596-602, 1984.
77. **Murakami T.N. Owa, Kumazowa K.:** The effects of soil conditions and nitrogen form on nitrous oxide evolution by denitrification. Soil Sci. Plant Nutr. 33; 35-42, 1987.
78. **Myrold D.D., Tiedje J.M.:** Establishment of denitrification capacity in soil: Effect of carbon, nitrate and moisture content. Soil Biol. Biochem. 17:819-822, 1985.
79. **Myrold D.D.:** Denitrification in ryegrass and winter wheat cropping system of western Oregon. Soil Sci. Soc. Am. J. 52; 412-416, 1988.
80. **Nicholas D.J.D.:** Recycling of N_2 and H_2 in a denitrifying photosynthetic bacterium. In Proc. Int. Symp. Nitrogen and the Environment, Malik, K.A., Mujtaba Naqvi, S.H., and Aleem, M.I.H., Eds. Nuclear Institute for Agriculture and Biology, Faisalabad, Pakistan, 93, 1985.
81. **Nugroho S.G., Kuwatsuka S.:** Concurrent observation of several processes of nitrogen metabolism in soil amended with organic materials. 2. Effect of farmyard manure on ammonification, nitrification, denitrification and N_2-fixation at different levels of soil moisture. Soil Sci. Plant Nutr. 38, 593-600, 1992.
82. **O'Hara G.W., Daniel R.M.:** Rhizobial denitrification: a review. Soil Biology and Biochemistry 17:1-9, 1985.
83. **Ottow J.G.C., Glathe H.:** Pedochemie und Pedomikrobiologie hydromorpher Böden: Merkmale Voraussetzungen und Ursachen der Eisenreduktion. Chem. ERde 32:1-44, 1973.
84. **Parkin T.B.:** Soil microsites as a source of denitrification variability. Soil Science Society of American Journal 51:1194-1199, 1987.
85. **Parsons L.L., Murray R.E.:** and Scott Smith Soil denitrification dynamics: Spatial and temporal variations of enzyme activity, populations and nitrogen gas loss. Soil Sci. Soc. Am. J. 55; 90-95, 1991.
86. **Parton W.J., Mosier A.R., Schimel D.S.:** Rates and pathways of nitrous oxide production in a shortgrass steppe. Biogeochemistry 6; 45-58, 1988.
87. **Patten D.K., Bremner J.M., Schimel D.S.:** Effects of drying and air-dry storage of soils on their capacity for denitrification of nitrite. Soil Science Society of America Journal 44:67-70, 1980.
88. **Paul E.A., Clark F.E.:** Soil Microbiology and Biochemistry. (eds) E.A Paul, F.E. Clark. Academic Press, Toronto, 1996.
89. **Payne W.J.:** Reduction of nitrous oxides by micro- organisms. Bacteriological Rewievs 37: 409-452, 1973.
90. **Payne W.J.:** Denitrification. John Wiley, New York. 214, 1981.
91. **Powlson D.S., Saffigna P.G., Kragt-Cottar M.:** Denitrification rates at different soil temperature, water contents, and nitrite concentration. Soil Science. 152; 41-52, 1988.

92. **Reddy K.R., Patrick Jr. W.H., Philips R.E.:** The role of nitrate diffusion in determining the order and rate of denitrification in flooded soil: I Experimental results. Soil. Sci. Soc. Am. J. 42, 268-272, 1978.

93. **Robertson L.A., Kuenen J.G.:** Aerobic denitrification: a controversy reviewed. Arch. Microbiol. 139; 351-354, 1984.

94. **Robertson L.A., Van Kleeff B.H.A., Kuenen J.G.:** A microcomputer-based method for semi-continuous monitoring of biological activities. J. Microbiol. Methods 5; 237-242, 1986.

95. **Robertson G.P., Tiedje J.M.:** Nitrous oxide sources in aerobic soils: nitrification, denitrification and other biological processes. Soil Biology and Biochemistry 19: 187-193, 1987.

96. **Robertson L.A., Kuenen J.G.:** Physiological an ecological aspects of aerobic denitrification, a link with heterotrophic nitrification? Revsbech N.P. and Sorensen, J. (eds) Denitrification in soil and sediment. Plenum press, New York. pp. 91-104, 1990.

97. **Robertson L.A., Kuenen J.G.:** Physiology of nitrifying and denitrifying bacteria. In Rogers, J.E. and Whitman W.B. (eds) Microbial production and consumption of greenhouse gases: methane, nitrogen oxides, and halomethanes. American Society for Microbiology, Washington D.C. 189-235, 1991.

98. **Rolston D.E., Hoffman D.L., Toy D.W.:** Field measurement of denitrification: I. Flux of N_2 and N_2O. Soil Science Society of America Journal 42, 863-869, 1978.

99. **Rolston D.E., Sharpley D.W., Toy, D.W.:** Field measurement of denitrification: 3. Rates during irrigation cycles. Soil Science Society of America Journal 46; 289-296, 1982.

100. **Ruiz-Herrera J., DeMoss J.A.:** Nitrate reductase complex of *Escherichia coli* K-12; participation of specific format dehydrogenase and cytochrome b1 components in nitrate reduction. J. Bacteriol., 99, 720, 1969.

101. **Ruiz-Herrera J., Showe M.K., De Moss J.A.:** Nitrate reductase complex of *Escherichia coli* K-12; isolation and characterisation of mutants unable to reduce nitrate. J. Bacteriol., 97, 1291, 1969.

102. **Sahrawat K.L., Keeney D.R.:** Nitrous oxide emission from soils In Stewart, B.A. (ed.) Advances in soil science volume 4, Springer-Verlag, New York pp. 103-148, 1986.

103. **Scott Smith M., Zimmmerman K.:** Nitrous oxide production by non-denitrifying soil nitrate reducers. Soil Sci. Soc. Am. J. 45:865-871, 1981.

104. **Schmidt J., Seiler W., Conrad R.:** Emission of nitrous oxide from temperature forest soils into the atmosphere. Journal of Atmospheric Chemistry. 6, 95-115, 1988.

105. **Schuster M., Conrad R.:** Metabolism of nitric oxide and nitrous oxide during nitrification and denitrification in soil at different incubation conditions. FEMS Microbiol. Ecol. 101; 133-143, 1992.

106. **Sextone A.J.:** Nitrous oxide and its relationship to denitrification. Agronomy Abstracts. Soil Science Society of America, Denver, Colorado Oct 27 to Nov 1 p.277, 1991.

107. **Sherlock R.R., Goh K.M.:** Initial emission of nitrous oxide from sheep urine applied to pasture soil. Soil Biology and Biochemistry 15: 615-617, 1983.

108. **Shoun H., Kim, D-H., Uchiyama H., Sugiyama J.:** Denitrification by fungi. FEMS Microbiol. Lett. 94: 277-282, 1992.

109. **Skiba U., Hargreaves K.H., Fowler D., Smith K.A.:** Fluxes of nitric and nitrous oxide from agricultural soils in a cool temperate climate. Atmos. Environ. 26A; 2477-2488, 1992.

110. **Smirnov P.M. Kidin V.V., Pedishyus**: Loss of nitrogen by denitrification. Biol. Bull. Acad. Sci. USSR 6; 450-459, 1979.

111. **Smith M.S., Tiedje J.M.:** The effect of roots on soil denitrification. Soil Science Society of America Journal 43:951-955, 1979.
112. **Smith K.A.:** A model of extent of anaerobic zones in aggregated soils, and its potential application to estimates of denitrification. J. Soil Sci. 31; 263-277, 1980.
113. **Smith C.J., Chalk, P.M.:** Gases nitrogen evolution during nitrification of ammonia fertiliser and nitrite transformations in soil. Soil Science Society of America Journal 44:277-282, 1980.
114. **Smith C.J. Wright, M.F., Patrick, W.H. JR.:** The effect of soil redox potential and pH on the redaction and production of nitrous oxide. Journal Environmental Quality 12:186-188, 1983.
115. **Smith C.J., Patrick W.H. JR.:** Nitrous oxide emission as affected by alternate anaerobic and aerobic conditions from soil suspensions enriched with $(NH_4)_2SO_4$. Soil Biol. Biochem.,15, 693-696, 1983.
116. **Smith K.A. and Arah J.R.M.:** Losses of nitrogen by denitrification and emission of nitrogen oxides from soils. Proceedings 299 The Fertiliser Society pp. 1-34, 1990.
117. **Sprent J.I.:** The process of the nitrogen cycle. In The ecology of nitrogen cycle. Cambridge University. Press Cambridge.23-61, 1987.
118. **Stouthamer A.H.:** Adv. Microb. Physiol. 14, 315, 1976.
119. **Stouthamer A.H.:** Dissimilatory reduction of oxidised nitrogen compounds. In A.J.B. Zehnder (ed.) Biology of anaerobic microorganisms. John Wiley & Sons Ltd.,New York, NY. pp.245-303, 1988.
120. **Tamm C.O.:** Nitrogen in Terrestrial Ecosystems. Ecological Studies, Vol.81. (Eds.) W.D.Billigs F. Golley O.L. Lange, J.S. Olson, H. Remmert. Springer-Verlag Berlin, Heidelberg, New York, London, Paris, 1991.
121. **Tate III R.L.:** Process control in soil. In: Soil Microbiology (Eds Robert L., Tate III). John Wiley & Sons inc. New York, Chichester, Brisbane, Toronto, Singapore, (1995).
122. **Terry R.E., Tate R.L.:** The effect of nitrate on nitrous oxide reduction in organic soils and sediments. Soil Science Society of America Journal 44:744-746, 1980.
123. **Terry R.E., Tate R.L., Duxbury J.M.:** The effect of flooding on nitrous oxide emission from an organic soil. Soil Sci. 132; 228-232, 1981.
124. **Tiedje J.M.:** Ecology of denitrification and dissimilatory nitrate reduction to ammonium. In Zehner, J.B. (ed) Biology of anaerobic microorganisms. Wiley, New York pp.179-244, 1988.
125. **Umarov M.M.:** Biotic sources of nitrous oxide in the context of the global budget of nitrous oxide. In A.F. Bouwman (ed.) Soils and the greenhouse effect. John Wiley & Sons Ltd., Chichester. 263-268, 1990.
126. **Umarov M.M., Stepanow A.L.:** Microbial formation and consumption of N_2O in soil. Abstracts, 2nd session, 11th International Symposium on Environmental Biogeochemistry, Salamanca, 1993.
127. **Webser C.P., Dowdell R.J.:** Nitrous oxide emission from permanent grass swards. J. Sci. Food Agric. 33; 227-230, 1982.
128. **Weier K.L., Doran J.W. Power J.F., Walters D.T.:** Denitrification and the dinitrogen/nitrous oxide ratio as affected by soil water, available carbon and nitrite. Soil Sci. Soc. Am. J. 57; 66-72, 1993.
129. **Włodarczyk T. Stępniewski W. Brzezińska M. Stępniewska Z.:** Nitrate stability in loess soils under anaerobic conditions – laboratory studies. J. Plant Nutr. Soil Sci. 167, 693-700, 2004.

130. **Zumft W.G., Kroneck P.M.H.:** Metabolism of nitrous oxide. Revsbech N.P. and Sorensen, J. (eds) Denitrification in soil and sediment. Plenum Press, New York pp.37-55, 1990.

INDEX OF AUTHORS